An ultrasonic study of the elastic properties of the high temperature superconducting compounds

Al-Kheffaji, Ali Rushdi

Award date:
1993

Awarding institution:
University of Bath

AN ULTRASONIC STUDY OF THE ELASTIC PROPERTIES OF THE HIGH TEMPERATURE SUPERCONDUCTING COMPOUNDS

submitted by

Ali Rushdi Al-Kheffaji

for the degree of Doctor of Philosophy

of the University of Bath

1993

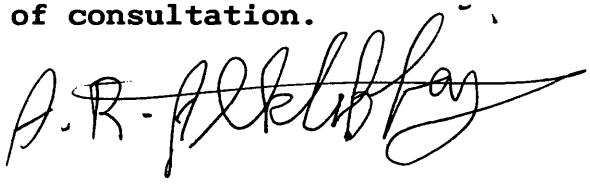

ProQuest LLC
789 East Eisenhower Parkway
P.O. Box 1346
Ann Arbor, MI 48106-1346

In the name of God, most gracious, most merciful

"AND SAY GOD, INCREASE MY KNOWLEDGE"

This work is dedicated to

My father (God bless his soul) for his encouragement and support and who was waiting for the day I finish my degree but unfortunately he didn't live long enough to see it.

My mother for her constant support and love.

My wife Huma.

My brothers Saad and Mohamed.

My sisters Suad, Wedad, Huda, Eman and Jenan.

All my relatives and friends.

ACKNOWLEDGMENT

I would like to express my sincere gratitude to my supervisor, Professor G A Saunders, whose enthusiastic inspiration and valued guidance have led my research period being a pleasant one.

My sincere thanks also goes to Dr. M Cankurtaran who I have benefited alot from his friendship and help, and also to Dr. D Almond for his useful guidance and Dr. P Ford for his kindly help in the writing up of this thesis.

I would also like to thank the technical staff in the solid state research group for the help and the friendly atmosphere they provided especially Bob Draper for his fast and effective reaction in solving any problems, Eddy Lambson for his help in solving any problems with the equipments, Wendy Lambson for polishing the samples and Barry Chapman for his help in the X-ray work and in plotting the figures.

I would like to thank my research colleagues Wang, Fanggao, Haithem, Haider, Parry, Barny, Ian, Sinen, Zul, Sedik and Salleh for a very useful discussions and an enjoyable time. I would also like to thank my friends at Il Bottelino Restaurant for their constant encouragement especially Lino, Raff, Mark Lewis, Norman, Jianfranco, Luciano, Guy, Giuseppe, Andy and Henry.

ABSTRACT

The velocities of longitudinal and shear ultrasonic waves have been measured, using the pulse-echo overlap technique, as functions of hydrostatic pressure and temperature in high temperature superconducting ceramics: the electron doped superconductor $Nd_{1.85}Ce_{0.15}CuO_{4-y}$ and its parent compound Nd_2CuO_{4-y}; $La_{1.8}Sr_{0.2}CuO_{4-y}$ and its parent compound La_2CuO_{4-y}; several $YBa_2Cu_3O_{7-x}$ samples of different density and micro-structural features; $GdBa_2Cu_3O_{7-x}$ in its orthorhombic and tetragonal forms; $Bi_{1.7}Pb_{0.3}Sr_2Ca_{n-1}Cu_nO_{4+2n}$ compounds (where n = 2 or 3).

The ultrasonic wave velocities in these compounds, with the exception of $La_{1.8}Sr_{0.2}CuO_{4-y}$, increase with decreasing temperature. No measurable effect is found near T_c. The results obtained for $YBa_2Cu_3O_{7-x}$ samples showed pronounced thermal hysteresis which has also been observed in the orthorhombic $GdBa_2Cu_3O_{7-x}$ but is absent in its non-superconducting tetragonal phase. Thermal hysteresis is observed in Bi2212 but is absent in the quenched sample and in the Pb doped sample of that compound. The results obtained for $Nd_{1.85}Ce_{0.15}CuO_{4-y}$ show no thermal hysteresis, but there is a marked change in gradient near 220K. The parent Nd_2CuO_{4-y} sample does not exhibit this behaviour, but it does show quite marked hysteresis in the temperature range 200-290K.

ABSTRACT

The $La_{1.8}Sr_{0.2}CuO_{4-y}$ sample shows extreme acoustic mode softening below room temperature with no thermal hysteresis in the temperature range 10-300K. Its parent compound La_2CuO_{4-y} does not show this elastic softening.

The pressure dependences of the ultrasonic wave velocities in ceramic samples of $YBa_2Cu_3O_{7-x}$ show a non-linear behaviour while the behaviour is linear in the very large grained, halide flux grown sample. The results obtained for orthorhombic $GdBa_2Cu_3O_{7-x}$ also show a non-linear behaviour with pressure while the behaviour is linear in the tetragonal phase. The results obtained for $Nd_{1.85}Ce_{0.15}CuO_{4-y}$ and $La_{1.8}Sr_{0.2}CuO_{4-y}$ are found to be linear. The pressure dependences of the ultrasonic wave velocities in the Bi(Pb)2223 compound show a discontinuity in the slope at around 0.03GPa. This behaviour was not observed in the Pb doped and undoped samples of Bi2212 compound. The results obtained for all the samples have been corrected for the effect of porosity using a theoretical model.

$YBa_2Cu_3O_{7-x}$ and $GdBa_2Cu_3O_{7-x}$ compounds are found to be softer than $Nd_{1.85}Ce_{0.15}CuO_{4-y}$ and $La_{1.8}Sr_{0.2}CuO_{4-y}$ compounds. However, the pressure derivatives of the elastic constants in $YBa_2Cu_3O_{7-x}$ and $GdBa_2Cu_3O_{7-x}$ are larger than those of $Nd_{1.85}Ce_{0.15}CuO_{4-y}$ and $La_{1.8}Sr_{0.2}CuO_{4-y}$. Bi-based cuprates are found to be softer than all other high T_c superconducting compounds.

ABSTRACT

The pressure derivatives of the elastic constant of Bi-based cuprates are similar to those of $YBa_2Cu_3O_{7-x}$ and $GdBa_2Cu_3O_{7-x}$ and larger than those of $Nd_{1.85}Ce_{0.15}CuO_{4-y}$ and $La_{1.8}Sr_{0.2}CuO_{4-y}$.

The discrepancy between B_o (the bulk modulus measured ultrasonically at atmospheric pressure) and $B^T(P)$ (the bulk modulus obtained from very high pressure X-ray measurements of lattice parameters) has been resolved by taking the contribution of $(\partial B/\partial P)_{P=0}$ to the high pressure bulk modulus into account.

CONTENTS

CONTENTS

CHAPTER ONE

GENERAL INTRODUCTION

The discovery of new high temperature superconducting compounds has generated renewed scientific interest in the field of superconductivity and raised hopes of the possibility of achieving room temperature superconductivity. This activity has aroused because some of these new compounds, like $RBa_2Cu_3O_{7-x}$ (where R = rare earth elements) and Bi(Tl)-based cuprates, have a transition temperature (T_c) higher than the boiling temperature of liquid nitrogen (77K), while until 1987, the highest T_c known was 23K.

Possible applications of these ceramic perovskite-type materials depend upon a knowledge of their mechanical properties. This can be obtained by measuring the ultrasonic wave velocity propagating through the material and hence calculating the elastic constants. This will give an insight into the elastic response of the material when subjected to some external change. Many scientific and technological advances depend critically on solid state elastic properties, their magnitudes, and their responses to variables like stress and temperature. Elastic constants relate to various fundamental solid state phenomena, such as interatomic potentials, equations of state and phonon spectra. They link

thermodynamically with the specific heat, thermal expansivity, the Debye temperature and Grüneisen parameters. The elastic constants depend only on the velocities of shear and longitudinal waves and the mass density. Using ultrasonic velocity methods, measurements of the changes in the second order elastic constants (*SOEC*) to within 0.1% become possible. This high precision measurement capability permits the use of elastic constants to study the effects on the material of temperature, pressure, mechanical stress, magnetic field, crystallographic transformation and superconducting transition. Hence, elastic constant measurements are of interest in a wide variety of disciplines such as structural design, materials science and experimental and theoretical solid state physics.

One of the major approaches to accurate measurement of the elastic constants of a solid is the pulse echo overlap technique. This technique, which has been used in the present work, consists of the measurement of the transit time of an ultrasonic wave packet as it propagates through a material and undergoes multiple reflections at interfaces with different acoustical properties. In nature, bats use an audiolocation similar to radar. By sending out ultrasonic wave pulses, the bat can locate objects in its flight path from the return time and direction of the echos. In essence,

the pulse echo technique is similar. A short pulse of high frequency ultrasound is introduced into the sample, normal to two flat, parallel faces, and the echo train observed. A radio frequency pulse of about one microsecond duration and with a fast rise time drives the system. The ultrasound is generated by a quartz transducer bonded to the specimen with an adhesive such as silicone grease. The radio frequency pulse (at the resonant frequency of the transducer) is applied across gold electrodes plated on to the quartz and, as a consequence of the piezoelectric effect, a mechanical vibration of the same frequency is launched into the specimen. When this ultrasonic pulse reaches the other end of the specimen, it is reflected back to the transducer-sample interface where once again all but a small fraction is reflected. By the time the first echo reaches the transducer, the radio frequency transmitter has been switched off. At the end of each round trip in the sample, the transducer re-converts a little of the pulse energy into a radio frequency signal. After amplification and detection, this radio frequency signal is displayed on an oscilloscope and a series of echoes of exponentially decreasing amplitude is produced.

Two distinct types of information are made available by using the pulse echo overlap technique. The distance between each successive peak on the echo train represents twice the transit time of the ultrasound pulse across the sample. Therefore, once the sample thickness has been measured, the ultrasound velocity can be obtained as the distance travelled divided by the transit time. The transit time in this work has been measured using a cycle-to-cycle overlap technique which gives a high precision measurements (better than 1 in 10000). This technique is described in detail in chapter four. Another feature is that its amplitude falls away with the distance the pulse travels because the ultrasound is absorbed in the specimen. As a result, the echo pattern decreases exponentially. This absorption is called the attenuation. The measurements of the ultrasonic attenuation provide extensive information about the nature of the material. The dominant interactions leading to damping of the high frequency, elastic waves in solids vary widely and include among others, direct scattering by defects, dislocation damping, heating effects, interaction with lattice (thermal) vibrations and electronic absorption [Saunders (1969)].

CHAPTER ONE

The velocity of sound depends directly upon sample density and elasticity. From measurements of both longitudinal and shear waves propagated along the preferred directions in single crystals, the complete set of elastic constants or moduli can be obtained. These represent the fundamental mechanical properties of a solid well below the yield point: the strains encountered by the solid during the passage of an ultrasonic pulse lie well within the Hooke's law range. The elastic behaviour of solids relates directly to the forces binding the atoms together, and hence the measurement of elastic constants is one of the basic tools in materials science.

The aim of this work is to investigate the elastic and the non-linear acoustic properties of the recently discovered high temperature superconducting ceramic compounds. This investigation has been accomplished by measurements of the temperature and hydrostatic pressure dependences of the ultrasonic wave velocities in these materials. These measurements enable the determination of the elastic constants and their temperature and hydrostatic pressure derivatives.

A brief historical review of the discovery of conventional superconducting compounds together with the discovery of the new high temperature superconducting compounds is

presented in chapter two. Chapter three defines and describes the elastic moduli used most often to characterize the polycrystalline material. Chapter four outlines the experimental techniques employed: details of sample preparation, the principles of the ultrasonic methods and a description of the measurement systems are given.

The crystal structure of the high temperature superconducting ceramic compounds has proved to be a very important factor in the determination of their elastic behaviour as a function of hydrostatic pressure and temperature. Chapter five describes the crystal structure of each of the compounds studied here with the major differences between them.

$Nd_{1.85}Ce_{0.15}CuO_{4-y}$ differs from the other high T_c superconducting compounds by having electrons as the charge carriers. This fact has been established by measuring the thermoelectric power through the sample. The hydrostatic pressure and temperature dependences of ultrasonic wave velocities together with the measurements of the thermoelectric power and the electrical resistance measured for $Nd_{1.85}Ce_{0.15}CuO_{4-y}$ and its parent compound Nd_2CuO_{4-y} are presented in chapter six. The results obtained for the two compounds show the effect of Ce doping on their elastic behaviour.

Chapter seven discusses the results of measurements of hydrostatic pressure and temperature dependences of the ultrasonic wave velocities for $La_{1.8}Sr_{0.2}CuO_{4-y}$ and its parent compound La_2CuO_{4-y}. The temperature dependence of the ultrasonic wave velocity in $La_{1.8}Sr_{0.2}CuO_{4-y}$ shows elastic softening during the cooling process. This elastic softening was also found in the *A15* superconducting compounds [Testardi (1973)]. This similarity in the elastic behaviour gave hope of finding a theoretical explanation for the existence of superconductivity in the copper oxide ceramic compounds along the lines of the well known *BCS* theory.

It is the new high temperature superconducting compounds, $YBa_2Cu_3O_{7-x}$, and with T_c of 90K which has been studied extensively. In this work, the ultrasonic wave velocities propagated through $YBa_2Cu_3O_{7-x}$ samples with different grain sizes and densities have been measured as a function of hydrostatic pressure and temperature. The results, which are discussed in chapter eight, show that the elastic behaviour of this compound varies from sample to sample. Thermal hysteresis has been found in all the samples but, in a different temperature range for different samples. Hysteresis is also found in the pressure dependences of the ultrasonic wave velocities measured in a coarse grained $YBa_2Cu_3O_{7-x}$ sample. All but one of the $YBa_2Cu_3O_{7-x}$ samples

studied here (the halide flux grown sample) show the unusual non-linear behaviour of the pressure dependences of ultrasonic wave velocities.

Chapter nine discusses the results obtained for the orthorhombic and tetragonal $GdBa_2Cu_3O_{7-x}$ compounds. The temperature dependences of the ultrasonic wave velocities in the superconducting $GdBa_2Cu_3O_{7-x}$ sample with the orthorhombic structure show a thermal hysteresis in the same temperature range (200-240K) as that found in $YBa_2Cu_3O_{7-x}$. This effect has been attributed to a structural phase transition. By contrast, the temperature dependences of the ultrasonic wave velocity for the $GdBa_2Cu_3O_{7-x}$ sample with the tetragonal (non-superconducting) structure, shows no thermal hysteresis in the temperature range 10-300K. Both longitudinal and shear ultrasonic wave velocities for orthorhombic $GdBa_2Cu_3O_{7-x}$ have the unusual feature of a non-linear pressure dependence. However, the pressure dependences of the ultrasonic wave velocities in the tetragonal form of $GdBa_2Cu_3O_{7-x}$ are almost linear.

The elastic behaviour of different samples of Bi-based cuprates are investigated by measuring the ultrasonic wave velocities as a function of temperature and hydrostatic pressure. The results obtained will be discussed in chapter ten. Thermal hysteresis has also been observed in different

temperature regions in all the samples studied here. In all of these Bi-based cuprates ceramic samples, the hydrostatic pressure dependences of the ultrasonic wave velocities are linear with the exception of Bi(Pb)2223 samples where a change in slope has been found for both the longitudinal and shear wave velocities as a function of hydrostatic pressure.

Finally, a compilation and discussion of the results obtained for all the samples studied in this work will be presented in chapter eleven together with the conclusions derived from this work.

CHAPTER TWO

THE CONVENTIONAL SUPERCONDUCTORS AND THE DISCOVERY OF THE NEW HIGH TEMPERATURE SUPERCONDUCTING COMPOUNDS

2.1 INTRODUCTION

Superconductivity is the name given to a remarkable combination of electric and magnetic properties which appears in certain conducting materials when they are cooled to extremely low temperatures. Such very low temperatures first became available in 1908 when Kamerlingh Onnes at the University of Leiden succeeded in liquefying helium, and by its use was able to obtain temperatures down to about 1K.

Up to the present time about half of the metallic elements and also a number of alloys and compounds have been found to become superconducting at low temperatures. There are two kinds of superconductor; type-I, type-II. Most of those pure elements which are superconductors exhibit type-I superconductivity, whereas alloys generally exhibit type-II superconductivity. The two types have many properties in common but show considerable differences in their magnetic behaviour.

In this chapter a brief review of the discovery of conventional superconducting compounds will be presented together with the discovery of the new high temperature superconducting compounds.

2.2 HISTORICAL REVIEW

One of the first investigations which Kamerlingh Onnes carried out in the newly available low-temperature range was a study of the variation of the electrical resistance of metals with temperature. It had been known for many years that the resistance of metals falls when they are cooled below room temperature, but it was not known what limiting value the resistance would approach if the temperature were reduced towards 0K. At that time the purest available metal was mercury and, in an attempt to discover the behaviour of a very pure metal, Onnes measured the resistance of pure mercury. He found that at a very low temperatures the resistance became immeasurably small, which was not surprising, but he soon discovered (in 1911) that the manner in which the resistance disappeared was completely unexpected. Instead of the resistance falling smoothly as the temperature was reduced towards 0K, the resistance fell sharply at about 4K, and below this temperature the mercury exhibited no measurable resistance. Furthermore, this sudden transition to a state of no resistance was not confined to the pure metal but occurred even if the mercury was quite impure. Onnes recognized that below 4K mercury passes into

a new state with electrical properties quite unlike those previously known, and he called this new state the "SUPERCONDUCTING STATE".

Further work by Onnes (up until 1913) and other research workers showed that other elements such as lead (T_c = 7.2K) and tin (T_c = 3.7K) showed the same phenomenon. In fact, since its discovery, superconductivity has been found in nearly a quarter of the natural elements. Niobium is found to have the highest critical temperature at 9.2K.

A considerable amount of time passed before physicists became aware of a very distinguishing characteristic of a superconductor, namely, its perfect diamagnetism. In 1933 Meissner and Ochsenfeld found that when a sphere was cooled below its transition temperature in a magnetic field it excluded the magnetic flux. The report of the Meissner effect stimulated the London brothers to propose their equation, which explained the Meissner effect and predicted a penetration depth for how far a static external magnetic flux can penetrate into a superconductor [London (1961)]. The next theoretical advance came in 1950 with the theory of Landau and Ginzburg, which described superconductivity in terms of an order parameter and provided a derivation for the London equation. Both of these theories were macroscopic in character.

In the same year (1950) the isotope effect, whereby the transition temperature decreases when the average isotope mass increases, was predicted theoretically by H Fröhlich (1950) and discovered experimentally by E Maxwell (1950) and co-workers. This effect provided support for an electron-phonon interaction, the "phonon mechanism" of superconductivity.

Due to the economic reasons for cooling and operating at very low temperatures, it was desirable to find superconductors with higher critical temperatures. Hardy and Hulm (1954) reported that the *A15* structure compound V_3Si had a superconducting transition temperature T_c of 17K. Subsequently, Matthias et al (1954) reported a T_c of 18.05K for Nb_3Sn, which also has an *A15* structure. With these discoveries active research on these and similar materials began with the intent both of understanding their properties and of producing materials with higher superconducting transition temperatures for technological applications.

The present understanding of the nature of superconductivity is based on the *BCS* microscopic theory, which was proposed by J Bardeen, L Cooper and J R Schrieffer in 1957 [Bardeen et al (1957)]. This theory involves the formation of bound electron pairs that carry the supercurrent, and an

energy gap that stabilize the superconductive state. The Landau-Ginzburg and London results fit well into the *BCS* formalism.

More recent progress in the latter has brought out a large number of compounds and alloys that are superconducting above 15K. In 1972 The highest transition temperature was approximately 21K in the Nb_3Al-Nb_3Ge alloy system [Matthias et al (1967)]. In 1973 a value of 23.3K had been reached in a niobium-germanium alloy, Nb_3Ge [Gavaler (1973)]. From 1973 until 1986 no further increase in the critical temperature was achieved and the hope for superconductivity at higher temperatures had almost disappeared. Figure 2.1 shows the historical increase in the transition temperature T_c .

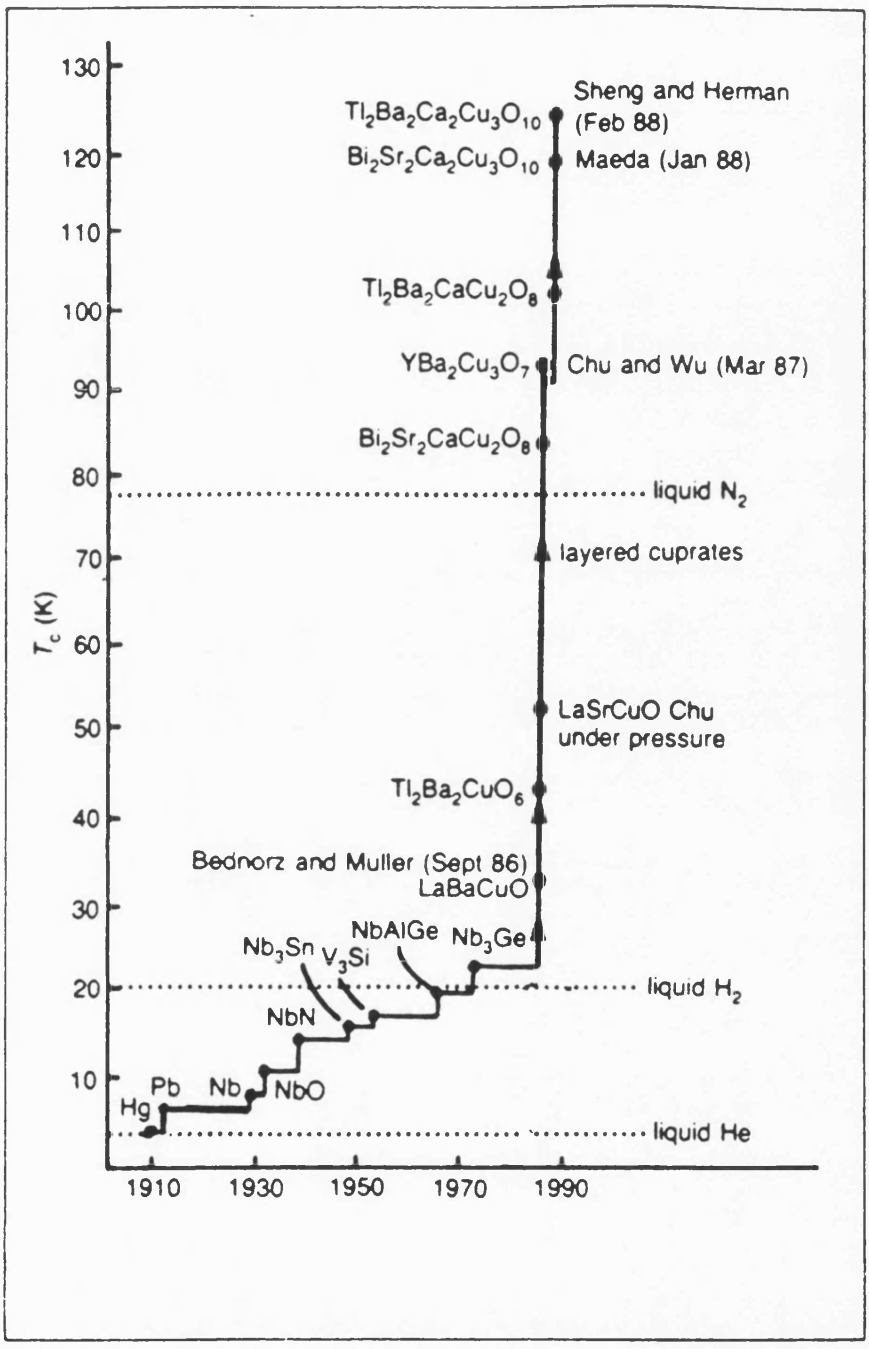

Figure 2.1
The evolution of the superconducting transition temperature with time.

2.3 $La_{2-x}M_xCuO_{4-y}$ COMPOUND (M = Ba, Sr and Ca)

In January 1986, Bednorz and Muller, at *IBM* Laboratories in Zurich, produced a material which was superconducting with a T_c around 30K [Bednorz and Muller (1986)]. It consisted of barium, lanthanum, copper and oxygen and had the formula $La_{5-x}Ba_xCu_5O_{5(3-y)}$. This discovery stimulated new interest in superconductivity, renewing hopes for high temperature superconductivity. Chu et al (1987) increased the critical temperature to 40.2K by applying a pressure of 13kbar to a $La_{2-x}Ba_xCuO_{4-y}$ sample. At the same time Cava et al (1987) found that by replacing the barium with strontium T_c increased up to 36K.

The compound La_2CuO_4 has played a special role in the history of the newly discovered high T_c superconductors. It is the parent compound of the first high temperature superconductor $La_4Cu_5BaO_{5(3-y)}$ found by Bednorz and Müller (1986). The doped La_2CuO_4 family has received particular attention as a fundamental series of high T_c superconductors despite the subsequent finding of new materials with higher T_c . An important reason for this interest has been to search for differences (or similarities) in the physical properties between the new oxide materials and more conventional superconductors.

CHAPTER TWO

Before the discovery of superconductivity in $La_4Cu_5BaO_{15-y}$, the compound La_2CuO_4 was considered to be only an insulator at low temperatures. However, on doping with Ca, Ba and Sr it becomes superconducting above 30K. It is a semiconductor or semi-metal whose transport and magnetic properties are sensitive functions of its oxygen concentration [Bednorz and Müller (1986)]. Cooper et al (1987) found traces of superconductivity in a La_2CuO_{4-y} sample prepared by an amorphous citrate process with an onset temperature around 90K and zero resistivity at around 30K. Grant et al (1987) found that under certain conditions of preparation a superconducting phase was present in their samples. It was observed that the superconductivity was of a non-bulk character, probably induced by a deficiency in La concentration. Subsequently Lang et al (1987) found a structural phase transition from thermal expansion measurements at exactly the same temperatures where superconductivity starts.

Before the advent of the high T_c superconducting oxides, the $A15$ compounds were the most widely studied superconductors with technological applications [Müller (1980)]. In these materials, there is a correlation between phonon softening, giving rise to lattice instability, and T_c enhancement. This is understandable in terms of the BCS theory, as resulting

from the increased electron-phonon interaction. An elastic softening has also been found in the doped La_2CuO_{4-y} compound and this gave rise to the hope that a theoretical explanation for superconductivity in the new materials could be found along the lines of conventional *BCS* theory. However, the problem is still far from resolved and the origin of the high-superconducting transition temperatures remains uncertain.

2.4 $RBa_2Cu_3O_{7-x}$ COMPOUND (R = RARE EARTH ELEMENTS)

Chu and his team at the University of Houston found that by applying pressure to the compound ($La_{1-x}Ba_xCuO_{3-y}$) its critical temperature increased. They attained a value of 40K for the $La_{1-x}Ba_xCuO_{3-y}$ superconductor at 13kbar [Chu et al (1987)]. dT_c/dP of 0.9K/kbar for that compound was much greater than that for any previously known superconductor.

The results suggested that since applying pressure i.e. "squeezing" the atoms produced a greatly enhanced T_c , it would appear likely that a suitable choice of smaller atoms might well produce a greatly enhanced T_c at atmospheric pressure. Chu and his colleagues searched for a suitable combination of atoms. They replaced the lanthanum with yttrium to produce a compound $YBa_2Cu_3O_{7-x}$ which they showed to be a superconductor with a critical temperature of around 90K at atmospheric pressure [Wu et al (1987)].

This big increase in T_c from 40K up to 90K was very important because it was the first superconductor with a T_c above 77K, the boiling point of liquid nitrogen. These superconductors could thus be operated using liquid nitrogen where as previously expensive, difficult to handle, liquid helium had been required.

Thus the discovery of the $YBa_2Cu_3O_{7-x}$ superconductor has started a new era in the field of superconductivity. Cheaper and easier applications of superconductivity now seemed to be real possibility although there are still many problems to be overcome. Scientists continue to try to increase the critical temperature in the hope of finding a superconductor at room temperature.

After the discovery of high temperature superconducting properties in the compound $YBa_2Cu_3O_{7-x}$, a big effort been made to find other high T_c superconducting compounds with a rare earth element substituted for Y. $GdBa_2Cu_3O_{7-x}$ is the second most studied compound of the 123 family (the ratio R:Ba:Cu equal to 1:2:3, where R = rare earth elements). This compound ($GdBa_2Cu_3O_{7-x}$) has similar physical properties to those of $YBa_2Cu_3O_{7-x}$.

2.5 BI-BASED CUPRATES

Since the discovery of ceramic materials exhibiting high superconducting transition temperature, much research on these materials has been carried out. This was part of the effort to discover materials with a T_c higher than that of the widely studied compound $YBa_2Cu_3O_{7-x}$.

Maeda et al (1988) investigated the system CaO-SrO-Bi_2O_3-CuO and found a new superconductor with T_c equal to 110K. The composition was identified to be $BiSrCaCu_2O_x$. Research at many laboratories was immediately focused on this new material. Many researchers were readily able to synthesize a compound with $T_c \approx$ 85K, but were unable to reproduce the result of Maeda et al (1988). The basic structure, however, has been determined by several groups with an approximate composition of $Bi_2Sr_2CaCu_2O_{8+y}$ [Zandbergen et al (1988)].

There are three distinct phases in the series $Bi_2Sr_2Ca_{n-1}Cu_nO_{4+2n}$ but only two of them have aroused particular interest because of their high superconducting transition temperatures. The first one with ideal composition $Bi_2Sr_2Cu_1O_{5+y}$, the Bi2201 (with n=1) with T_c about 20K, the second one having the ideal composition $Bi_2Sr_2CaCu_2O_{8+y}$, the Bi2212 phase (with n=2) with T_c about 80K, the other one with an ideal composition $Bi_2Sr_2Ca_2Cu_3O_{10+y}$, the Bi2223 phase

(with n=3) with T_c about 110K [Maeda et al (1988), Zandbergen et al (1988)]. Much effort has been spent world-wide in making single phase specimens of these materials. Single phase material with the Bi2223 structure can be most successfully synthesized in pure form by partial substitution of lead for bismuth [Takano et al (1988)]. To date the highest value achieved is 125K in compound of thallium, barium, calcium, copper and oxygen, $Tl_2Ba_2Ca_2Cu_3O_{10}$. This compound contains three adjacent Cu-O layers which seemed to suggest that by increasing the number of Cu-O layers, the critical temperature T_c could be raised. However, it was soon found that for the compound containing four Cu-O layers, T_c was only 122K [Ihara et al (1988)] which meant that this idea was not true.

2.6 $Nd_{2-x}Ce_xCuO_{4-y}$ COMPOUND

Great importance has been attached to the discovery [Tokura et al (1989) and Takagi et al (1989)] of $Nd_{2-x}Ce_xCuO_{4-y}$ which is the first of the new high T_c ceramic superconducting materials where the current carriers in the normal state are electrons rather than holes. Superconductivity was achieved in these new materials by a combination of Ce doping and oxygen reduction in the R_2CuO_{4-y} system (R=Pr, Nd and Sm). These new superconductors have the Nd_2CuO_4-type structure, with oxygen deficiency achieved by annealing in a reducing atmosphere. Preparation of a single-phase of these compounds is somewhat a tricky process in comparison with the other high T_c copper oxides. Hall measurements [Tokura et al (1989)] indicate that these materials belong to the family of layered copper oxide superconductors where electrons are the charge carriers above T_c. This behaviour contrasts sharply with that of the previously known high T_c cuprates, which involve holes as the carriers responsible for conductivity. Although the Nd_2CuO_4-type structure is closely related to that of the La_2CuO_4 compound, a significant structural difference between them is that the Cu atoms are octahedrally coordinated by oxygen in La_2CuO_4, but in the R_2CuO_4 materials, the coordination is square planar.

CHAPTER TWO

The origin of the high superconducting transition temperatures in the case of the new ceramic superconductors in general remains uncertain. Many mechanisms [Cava (1990), Rice (1987), (1989) and Emery (1989)] have been put forward but the problem is still far from resolved. There is a considerable interest in finding out what the mechanism responsible for superconductivity in the electron doped $Nd_{1.85}Ce_{0.15}CuO_{4-y}$ material is, and whether it differs from those of the hole type high T_c superconductors.

CHAPTER THREE

ELASTIC PROPERTIES OF SOLID MATERIALS

3.1 INTRODUCTION

Elastic constants relate stress to strain, or force per unit area to relative length change. Stress can be induced by any elastically coupled force: mechanical, thermal, magnetic or electrical. Since solids resist both volume change and shape change, they have at least two independent elastic constants. A low symmetry crystal may have as many as 21 independent elastic constants. The polycrystalline high T_c superconducting compounds studied here are considered to be quasi-isotropic; so their macroscopic elastic constants are assumed usually not to depend on direction. Hence they have been characterized elastically by two independent elastic constants (C_L and C_S). This chapter will define and describe the elastic moduli used most often to characterize polycrystalline material.

3.2 HOOKE'S LAW

Hooke's law states a linear proportionality between strain response intensity (ϵ) and imposed stress (σ)

$$\sigma = C\epsilon \tag{3.1}$$

where C denotes an elastic stiffness modulus. For small strains Hooke's law can be written for particular deformations which can be dilatation, extension or shear (see the next sections). For small strains, Hooke's law can be written inversely

$$\epsilon = S\sigma \tag{3.2}$$

where S is an elastic compliance modulus, and for isotropic media

$$C = 1/S \tag{3.3}$$

Anisotropic media, such as single crystals, textured aggregates or composites, require a more general form of Hooke's law

$$\sigma_{ij} = C_{ijkl}\epsilon_{kl} \tag{3.4}$$

where both stress and strain are symmetrical second rank tensors and C_{ijkl} is a symmetrical fourth rank tensor which has between 2 and 21 independent components depending on the material's elastic symmetry [Ledbetter (1983)].

In this work the compression force will be considered as a negative force and the dilatation or extension will be considered as the positive force. As for the shear force this will always depends on the direction of the shear stress applied.

3.3 COMPRESSIBILITY

All matter (gas, liquid or solid) responds to pressure change and exhibits at least one elastic constant, the compressibility given by:

$$K_T = -(1/V)\left(\frac{\partial V}{\partial P}\right)_T \qquad (3.5)$$

where P, T **and** V **denote the pressure, temperature and volume respectively. Always positive,** K **has units of reciprocal pressure. Gschneidner (1964) suggested that the compressibility "has been measured more than any other elastic property". Bridgman's (1949) pioneering experiments resulted in compressibility values for many solids. Some of Bridgman's experiments determined the linear compressibility,**

$$\kappa_T = (A/l)\left(\frac{dl}{dL}\right)_T \qquad (3.6)$$

where A **denotes the cross sectional area of a rod shaped, hydrostatically pressurized specimen,** l **is the length and** L **the load. For isotropic solids, bulk and linear compressibilities relate according to**

$$K = 3\kappa \qquad (3.7)$$

The constant entropy compressibility

$$K_S = -(1/V)\left(\frac{\partial V}{\partial P}\right)_S \qquad (3.8)$$

where S is the entropy, is obtained under zero heat flow conditions, at high frequencies.

3.4 BULK MODULUS

Rather than compressibility, scientists often use the bulk modulus, (B), to describe a solid's resistance to volume change. For isotropic materials (B) and (K) relate reciprocally:

$$B_T = 1/K_T = -V(\partial P/\partial V)_T \qquad (3.9)$$

B has pressure units, and, herein, elastic constants with pressure units are called elastic moduli. For describing solids, hydrostatic stress, H , is often preferred over pressure, which is a negative stress. Thus,

$$B_T = V(\partial H/\partial V)_T \qquad (3.10)$$

A large bulk modulus usually implies strong interatomic forces, high cohesive energy, high melting point and high elastic stiffness moduli.

3.5 YOUNG'S MODULUS

Engineers find Young's modulus the most familiar elastic constant, as evidenced by its many pseudonyms: extension modulus, tensile modulus, tension modulus, elastic modulus and modulus. Young's modulus in tension or compression are identical, theoretically and experimentally. Some difficulty on this concept arises from engineering Young's modulus measurements using high stress. Since stress affects elastic constants and the stress strain curve shape, the true Young's modulus manifests itself only at very low stress.

Usually defined in terms of a uniaxially stressed rod where both stress (σ_z) and strain (ϵ_z) are measured along the rod axis (z), the Young's modulus (E) is

$$E = \sigma_Z / \epsilon_Z \qquad (3.11)$$

Young's modulus relates to the extensional sound wave velocity in a rod by

$$V_E = (E/\rho)^{1/2} \qquad (3.12)$$

where ρ is the mass density. This relationship provides a simple and accurate method for determining E experimentally at very low stress.

3.6 SHEAR MODULUS

Sometimes called the torsional modulus, rigidity modulus or transverse modulus, the shear modulus (C_S) relates the shear stress (T) to the shear strain (τ):

$$T = C_S \tau \tag{3.13}$$

A cube sheared on one face has a shear strain related to the length change of the face diagonal by

$$\tau = 2\Delta l / l \tag{3.14}$$

In torsion, T is the torsional stress. For isotropic material, shear and torsional C_S' are identical. Both shear and torsion conserve volume but change shape. The bulk modulus describes volume change without shape change.

The shear modulus determines the velocity of a shear-polarized (transverse) sound wave in a plate or of a torsional wave in a rod according to

$$V_S = (C_S / \rho)^{1/2} \tag{3.15}$$

Like Young's modulus, this relationship provides a simple and accurate method for experimentally determining C_S at low stress.

3.7 POISSON'S RATIO

Poisson's ratio, σ , is not an elastic modulus, but a dimensionless ratio of two elastic compliances. Usually defined by a uniaxially stressed rod, Poisson's ratio is the negative ratio of transverse (ϵ_S) and longitudinal (ϵ_L) strains:

$$\sigma = -\epsilon_S / \epsilon_L \qquad (3.16)$$

Theoretically, σ is bounded by -1 and 1/2, but negative σ values are not often observed in quasi-isotropic materials. Thus, in polycrystals σ is bounded practically by 0 and 1/2. A typical value for metals is 1/3, 0.28 to 0.42 being the observed range for most materials. Such σ values mean that a material tends to maintain constant volume during uniaxial deformation. If σ is 1/2, no volume change occurs during deformation.

Another useful interpretation of σ views it as a relative measure of elastic resistance to dilatation and shear, since

$$\sigma = (3x - 2)/[2(3x + 1)] \qquad (3.17)$$

where x is B/C_S . This equation has been used in this work inserting the elastic constants obtained from the ultrasonic measurements. Maximum σ occurs when x is infinite (liquids) and minimum σ when x is zero (incompressible spheres).

3.8 ELASTIC DEBYE TEMPERATURE

The concept of Debye temperature (Θ_D) is useful in describing the thermal behaviour of solids and it plays an important role in the theory of lattice vibrations. In brief, this temperature is a measure of the separation of the low temperature quantum mechanical region, where the vibrational modes begin to be "frozen out", from the high temperature region where all modes begin to be excited according to classical theory. The Debye temperature Θ_D can be obtained directly from heat capacity measurements, and it can be also derived from a set of elastic constants.

A solid in the Debye theory is assumed to behave like a non-dispersive continuum, so the phonons (the quanta of the lattice vibrations) are considered to travel with the same velocity whatever their wavelength and propagation vector are. The maximum frequency of vibration ν_{max} , or the velocity of sound, can be related to a characteristic temperature Θ_D . In practice the velocity is taken equal to the mean velocity of sound and can be computed by integration over the whole velocity surface [Anderson (1963)]. The relation between mean velocity and the characteristic Debye temperature is given by

$$\Theta_D^{el} = \left(\frac{9N}{4\pi V}\right)^{1/3}\left(\frac{h}{k}\right)\left[\int\left(\frac{1}{v_1^3}+\frac{1}{v_2^3}+\frac{1}{v_3^3}\right)\frac{d\Omega}{\pi}\right]^{-1/3} \quad (3.18)$$

where v_i is the ultrasonic wave velocity, h and k are the Planck and Boltzmann constants respectively. N/V is the number of atoms per unit volume. For isotropic materials, such as the high temperature superconducting ceramic compounds, the mean velocity is written as

$$V_m = \left[\frac{1}{3}\left(\frac{1}{V_L^3}+\frac{2}{V_S^3}\right)\right]^{-1/3} \quad (3.19)$$

where $V_L[=(C_L/\rho)^{1/2}]$ and $V_S[=(C_S/\rho)^{1/2}]$ are longitudinal and shear ultrasonic wave velocities respectively. The Debye temperature can then be calculated readily using the following equation

$$\Theta_D^{el} = \left(\frac{9N}{4\pi V}\right)^{1/3}\left(\frac{h}{k}\right)V_m \quad (3.20)$$

3.9 MODE GRÜNEISEN PARAMETERS

The mode Grüneisen parameter is an important tool for investigation of anharmonic effects in solids. The high temperature superconducting compounds can be treated as elastically isotropic solid. By writing the longitudinal and shear wave velocities as V_L and V_S respectively and the vibration frequency ω_i as $q_i V_L$ (or $q_i V_S$) where q_i is the wave vector, the mode Grüneisen parameters of each modes can be defined as

$$\gamma_L = -\frac{d\ln q_i V_L}{d\ln V} \tag{3.21}$$

and

$$\gamma_S = -\frac{d\ln q_i V_S}{d\ln V} \tag{3.22}$$

If we assume that the wave vectors q_i scale as $V^{-1/3}$, then the γ's are independent of the index i and can be written as

$$\gamma_L = \frac{1}{3} + \frac{1}{B^T}\frac{d\ln V_L}{dP} \tag{3.23}$$

and

$$\gamma_S = \frac{1}{3} + \frac{1}{B^T}\frac{d\ln V_S}{dP} \tag{3.24}$$

where P is pressure and B^T is the isothermal bulk modulus. These equations can be rewritten in terms of the pressure derivatives of the effective $SOEC$

$$\gamma_L = -\frac{1}{3} + \frac{B^S}{2C_L}\frac{dC_L}{dP} \tag{3.25}$$

and

$$\gamma_S = -\frac{1}{3} + \frac{B^S}{2C_L}\frac{dC_S}{dP} \tag{3.26}$$

where B^S is the adiabatic bulk modulus. The mean value of the elastic Grüneisen parameter $\bar{\gamma}^{el}$ for an isotropic solid can be obtained from

$$\bar{\gamma}^{el} = \frac{[\gamma_L + 2\gamma_S]}{3} \tag{3.27}$$

These quantities will be used to describe the anharmonicity of the long wavelength acoustic phonons in high T_c superconducting ceramics in the quasiharmonic approximation.

CHAPTER FOUR

ULTRASONIC EXPERIMENTAL TECHNIQUES AND SAMPLE PREPARATION

4.1 INTRODUCTION

The techniques which are available for measurements of the elastic properties of the high T_c superconductors are described and discussed in this chapter. The second order elastic constants ($SOEC$) of a solid body can be determined by measuring the propagation velocities of ultrasonic waves. This is because the velocities of the acoustic phonons in the long wavelength limit are related to the elastic constants of the solid body. Measurement of the transit time (t) of the waves leads to the propagation velocity $V(=2l/t)$ where l is the thickness of the sample under investigation.

In the ordinary pulse echo single ended configuration, illustrated in figure 4.1, an ultrasonic pulse is launched into a sample by means of a piezoelectric transducer bonded to it. The waves which travel through the sample are reflected at the opposite end of it and are detected on return by the same transducer. The pulse also undergos further reflection from the transducer, and then again from the opposite side of the sample and so on. Continuation of these processes will produce an echo train in which the echo heights decrease exponentially with time. This echo train, drawn schematically in figure 4.1, can be displayed on the oscilloscope screen.

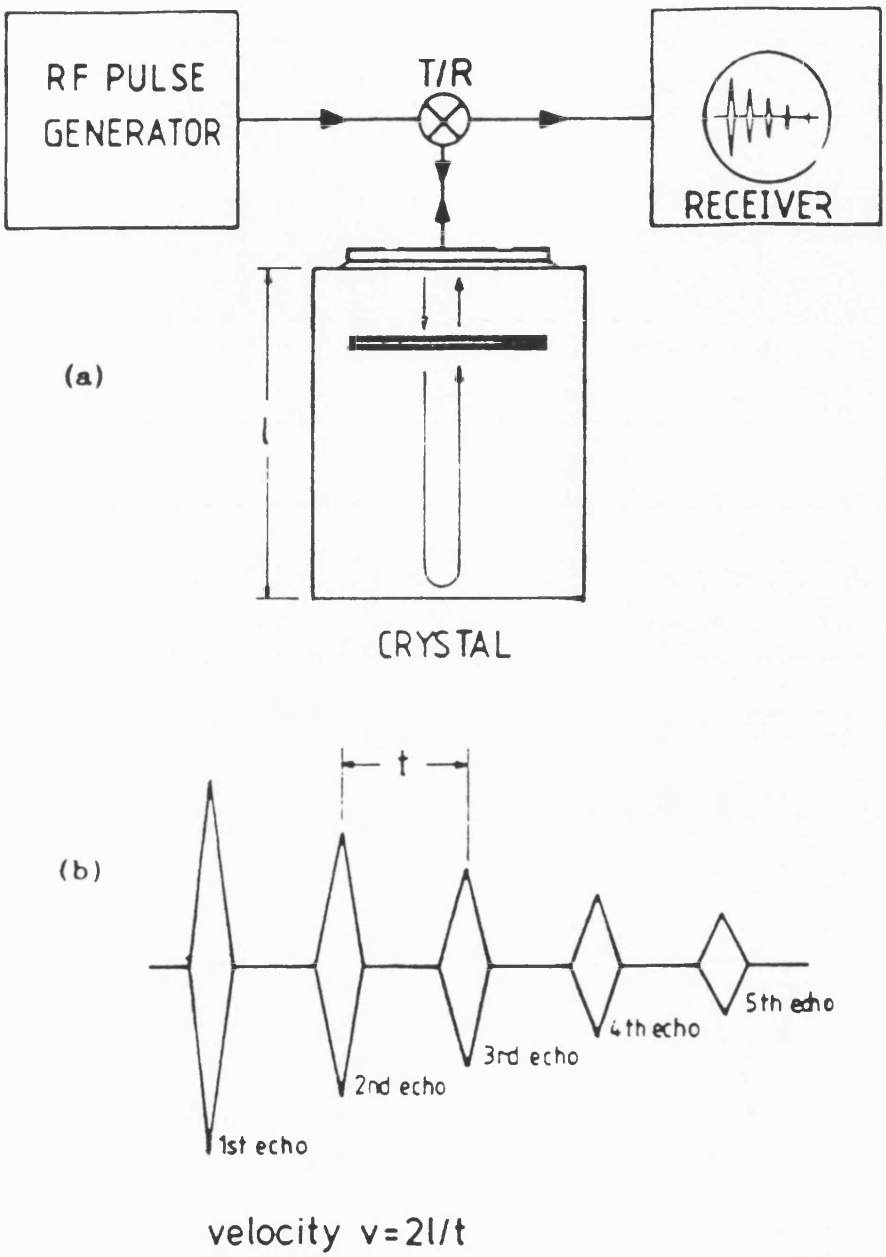

Figure 4.1

Schematic representation of (a) the simple pulse ultrasonic system and (b) envelope of pulse echo train.

The distance between two successive echoes represents the transit time of propagation of the ultrasonic pulse in the sample. However, this method is not sensitive enough to study the effect of temperature and pressure upon the elastic constants because the induced changes in the transit time are relatively small (approximately 1 part in 10^4 and 1 part in 10^3 for the temperature and the pressure experiments respectively). Due to this, another method must be employed to resolve accurately the changes induced in the ultrasonic velocities due to the application of pressure or changes in temperature. The pulse echo overlap method [May (1958), Papadakis (1964), (1966), (1967)] which is used here enables one to measure ultrasonic velocity with high precision (see section 4.4). The basic requirements for this method, i.e. sample preparation and choice of a suitable transducer and bonding material are outlined in this chapter. X-ray measurements performed on the samples are discussed briefly in section 4.5. The dewar system and the closed cycle helium refrigerator used in the experiments to measure the temperature dependences of the *SOEC* are also briefly discussed (see sections 4.6,4.7 respectively). Section 4.8 relates to the hydrostatic pressure system which has been used extensively to measure the pressure dependence of the elastic constants. The use of a manganin coil as a pressure gauge

is explained in section 4.9. The general method of preparing the high temperature superconducting samples which have been studied in this work is described in section 4.10. The possible error sources arising during the experiments are discussed in section 4.11. Finally a technique for correction for the effects of porosity on the elastic properties is explained in section 4.12.

4.2 PIEZOELECTRIC TRANSDUCERS

A transducer is a device used for converting energy from one form to another. Quartz (SiO_2) , as a transducer, plays an important role in the field of ultrasonics where its piezoelectric properties allow the conversion from electrical to mechanical energy, and vice versa, at ultrasonic frequencies. Thus a transducer allows a signal from an electrical circuit to be used to generate a mechanical vibration in the sample. When an electric field is applied, a piezoelectric crystal becomes strained by an amount directly proportional to the electric field strength. Conversely an electric polarisation is produced when a mechanical stress is applied. Due to this phenomenon, a quartz transducer can be used as a transmitter and receiver in an ultrasonic system. When a radio frequency signal from the ultrasonic equipment arrives at the transducer, it causes the quartz transducer to vibrate at its fundamental resonance frequency (here 5 or 10 MHz) and this will lead an ultrasonic plane wave to propagate into the sample. Quartz transducers were used extensively in this work because they have a high electromechanical coupling factor and it show a very small frequency dependence on temperature compared with other piezoelectric materials [Mason (1964)]. In addition they also possess a reasonable mechanical strength so that they

can be thinly cut with high accuracy and retain their piezoelectric properties up to 573°C where a transition from the usual alpha phase (which is piezoelectric) to the beta phase (which is not piezoelectric) occurs. For the present work gold-plated quartz transducers, obtained commercially from Gooch and Housego Ltd., Illminster, England, were used. There were several types but mostly only four of them were used: X-cut 5 and 10MHz (thickness of 572 and 277 μm respectively) and Y-cut 5 and 10MHz (thickness of 392 and 196 μm respectively). X-cut transducers were used to generate and receive longitudinal waves; such a transducer executes a piston-like action when excited by an electrical impulse. The Y-cut ones were used for generating and receiving shear or transverse waves. To differentiate between the X- and Y-cut transducers, the Y-cut transducer is marked by a flat edge (figure 4.2) perpendicular to the polarisation direction. Figure 4.2 includes schematic illustrations of X- and Y-cut transducers. The front face of each transducer has a central gold plated electrode separated by a narrow non-conducting annulus from an outer ring of gold electrode. The outer electrode is used for earthing. The back part of the transducer is completely coated with a thin film of gold and is directly connected to the outer ring of the frontal part by continuity of the gold coating round the edge.

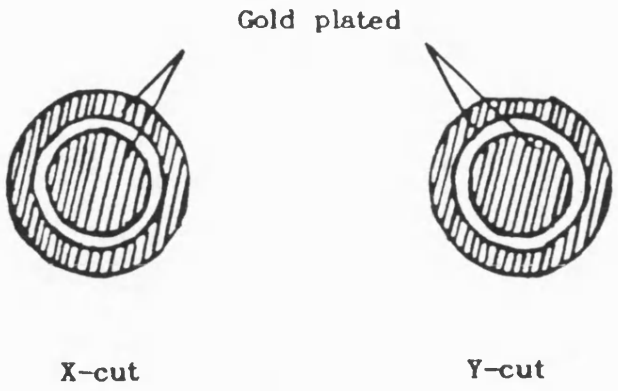

Quartz transducer

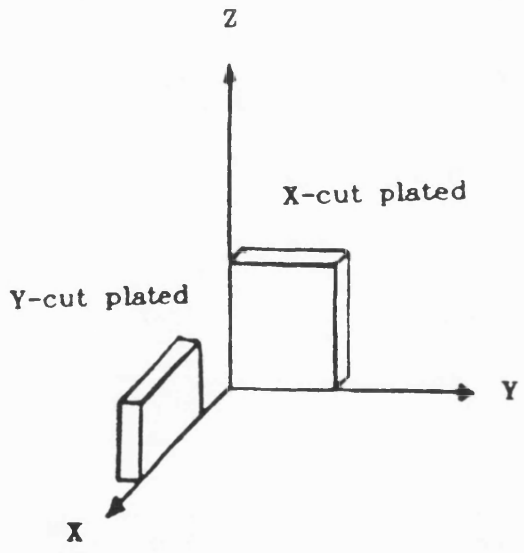

Figure 4.2

The arrangement of X- and Y-cut quartz transducers with respect to the crystallographic axes.

Throughout this work, transducers of diameter 6mm for X- and Y-cut have been used on account of the small surface areas of the samples.

In some instances there were considerable difficulties in obtaining workable echoes using quartz transducers. In these cases lead-zirconium-titanium (which is commonly known as *PZT*) transducers were used. The *PZT* transducer has higher output than quartz for a similar input signal. There are various grades of *PZT* and the grade used in this work was a longitudinal mode *PZT-5A* transducer (Morgan Matroc Limited, Southampton, England).

4.3 ACOUSTIC BONDING MATERIALS

To match the acoustic impedance between the sample and transducer and to insert the acoustic waves into the sample from the vibrating quartz transducer, a bonding agent must be employed between the sample and the transducer as illustrated in figure 4.3. There are different kinds of bonding materials which could be used in ultrasonic experiments [Bateman (1966)]. A good bonding material should not damage or react with either the sample surface or the quartz transducer, and the bonding material characteristics should not change over the specific range of temperature and pressure where the experiment is to be carried out. For instance, in the case of hydrostatic pressure experiments, the bonding agent should be stable and resist erosion when immersed in castor oil or a similar pressure transmitting medium.

The basic requirement for good bonding is that there should be a minimum loss of the acoustic energy. This is normally achieved by using a suitable bonding material as a thin and uniform layer between the surfaces of the sample and transducer. Before making a bond, it is essential that both surfaces to be free from dirt or dust. To achieve this, they have to be cleaned with acetone. Usually a small amount of bonding material is placed on the sample face, the

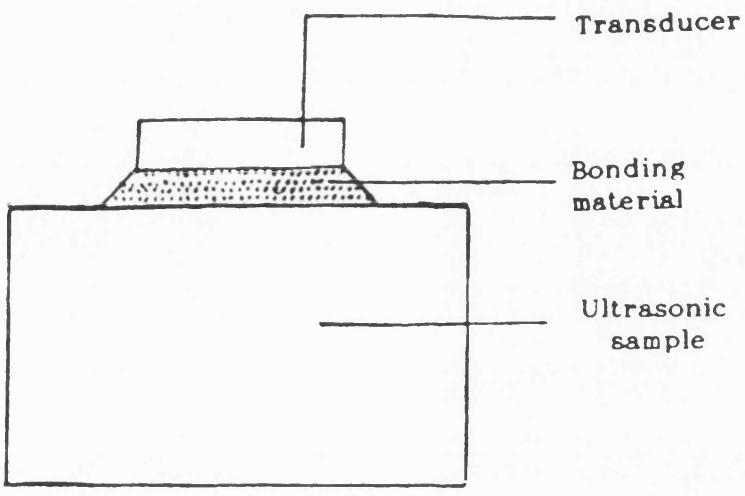

Figure 4.3

Schematic representation of a quartz transducer bonded to an ultrasonic sample.

transducer is then placed over this and gently pressed and rotated. This produces a uniform and thin bond approximately 3 μm thick.

The following three types of bonding materials have been mainly employed in this work:

(A) For ultrasonic measurements made under hydrostatic pressure, a high viscosity resin, Dow Resin *276-V9* (Dow-Corning Corp.) gives excellent bonding in the temperature range -20°*C* to 120°*C*. On pre-heating the Dow Resin to about 50°*C* using a hair-dryer, the bonding substance spreads easily onto the specimen face so that by rotating the transducer onto the sample, a good bond is achieved which enables the transmission of ultrasonic longitudinal and shear waves. Freezing the bond by immersion in liquid nitrogen can make a bond capable of resisting the pressure.

(B) For low temperature measurements (between room temperature and down to 4.2K) Nonaq Stopcock grease (Fisher Scientific Co.) was used successfully. It was necessary to avoid moisture which interacts with Nonaq and can cause a lot of problems at low temperature. To decrease the probability of bond breaking, this bonding material must be always kept in a desicator to reduce the absorption of moisture.

(C) Another type of bonding material which has been used for high temperature work (in excess of 450°*C*) : is Du Pont Thick Film Conductor Composition 9770 (Du Pont UK Ltd.). This was used in measurements of the temperature dependence of dC_{ij}/dP in YBCO sample 2. Unlike other bonding materials, dry bonding of Du Pont is achieved through a heat treatment process [see Salleh (1988) for details] to ensure that both type of waves could be successfully inserted into the sample.

Although the characteristics of the bonding materials used in this work did not change during the pressure and temperature experiments, the calculated sound wave velocities for the samples differ when different bonding materials were used. For example, the longitudinal wave velocity measured at room temperature for the $La_{1.8}Sr_{0.2}CuO_{4-y}$ sample was 4706 m/s ,when Nonaq is used as a bonding agent, but 3977 m/s, when Resin is used. This discrepancy also occurred in all the other samples studied in this work.

4.4 PULSE ECHO OVERLAP SYSTEM

An ultrasonic time-delay measurement system, referred to as the pulse-echo overlap system, was used in this work. This system is a development of that proposed by May (1958) and expanded by Papadakis (1964, 1966, 1967). Essentially it is an extension of the pulse echo single ended system operating by means of overlapping any two, visually selected, intensified echoes on the oscilloscope screen. This provides a precise measurement of the round-trip time of an acoustic wave travelling through the material. The pulse echo overlap technique can be readily used for highly attenuating or thin samples where other methods may be difficult to apply. The block diagram of the pulse echo overlap system is illustrated in figure 4.4. The associated wave forms referred to in the following paragraph are numbered as shown in figure 4.5.

A pulse of 5 or 10MHz frequency (1) is generated by the pulse modulator and receiver unit (*Matec*6600). **A high resolution oscillator set** (*Matec*110) **itself generates a synchronised square wave (2) which is used to power the decade divider and dual delay set** (*Matec*122*A*). **The frequency of this square wave is the same as that of the sine wave produced by the pulse modulator and receiver unit** (*Matec*6600). **The square wave frequency is then reduced in the decade divider and dual delay set** (*Matec*122*A*) **by dividing it by a factor of**

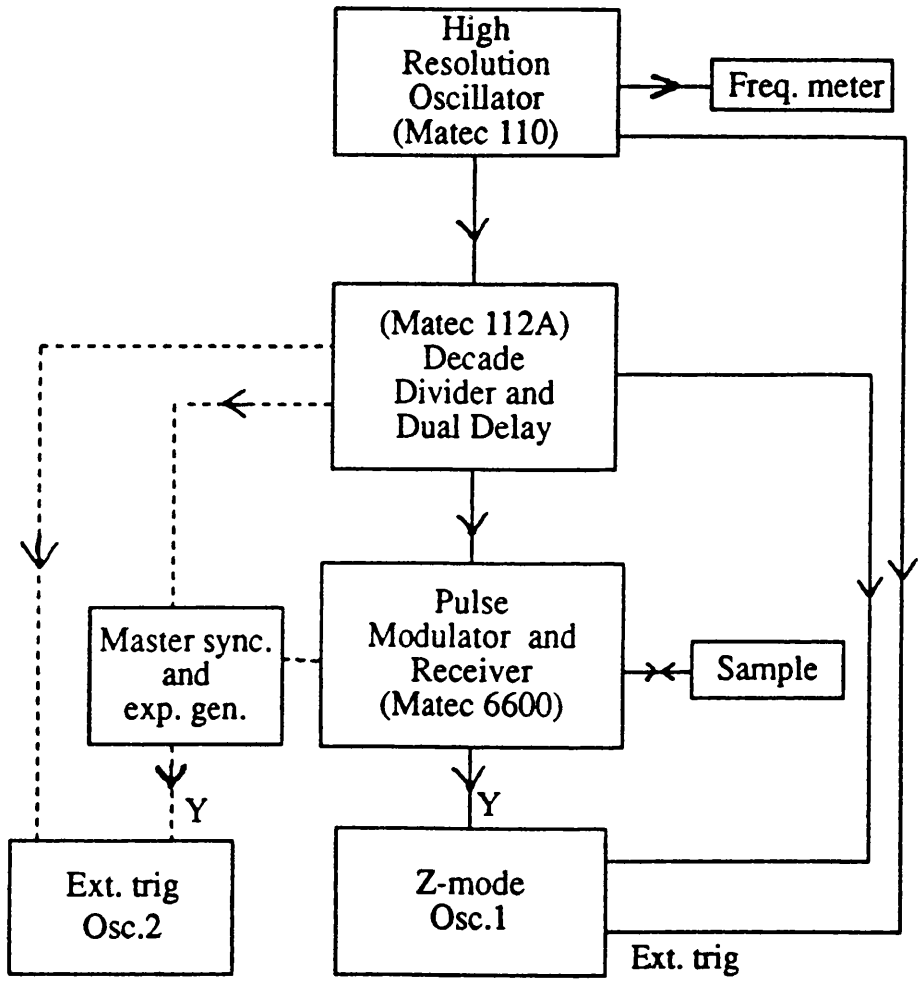

Figure 4.4

Block diagram of the pulse echo overlap system.

(1) Signal Generator.

(2) Master Sync. from High Resolution Oscillator.

(3) Divided Sync. (÷ 10).

(4) Radio Frequency (r.f.) Pulses to Sample.

(5) Radio Frequency Echoes.

(6) Z modulation - Intensification of Echoes 1 and 2.

(7) Video Out.

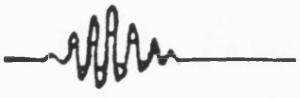

(8) Overlap of Echoes 1 and 2.

Figure 4.5

Schematic of the pulse echo overlap waveforms.

10 (3) in order to trigger the pulse modulator and receiver (*Matec*6600)**. Each triggered pulse creates a radio frequency burst (4) which is in turn transformed by the quartz transducer into a mechanical vibration within the crystal. The successive reflections are then detected by the transducer and amplified by the receiver** (*Matec*6600) **set and the r.f. signals produced by this process are displayed on the oscilloscope (5). For each echo train, the decade divider and dual delay set** (*Matec*122*A*) **produce a pair of square wave pulses (6) which are channelled to the Z-mode of the oscilloscope. By decreasing the oscilloscope brightness, only two intensified echoes are observed on the screen. When the time base of the oscilloscope is roughly set to the value of the echo width, the two intensified echoes are then overlapped on top of each other as seen on the display (8). To ensure that this overlap image remains stationary, the oscilloscope has to be triggered by a high resolution oscillator** (*Matec*110) **with a rate equivalent to the delay between the chosen echoes. Critical adjustment of this equipment enables exact cycle-to-cycle matching within the echoes to be achieved. The transit time measurements have to be consistent and systematic in order to reduce the experimental errors i.e. mismatch of overlapped echoes. In practice a cycle near to the centre of the first echo is**

chosen and overlapped over the equivalent cycle of the second echo. The echo transit time is given by the reciprocal of the oscillator frequency which is read digitally from the frequency meter.

The attenuation of ultrasound can be measured simultaneously with the transit time (as illustrated by dotted line in figure 4.4). As the stress wave, introduced by exciting electrically the quartz transducer, passes through the sample, it loses energy and subsequently successive echoes produce smaller signals. An exponential generator (*Matec* 1204*B*) and a second oscilloscope are adjusted and connected appropriately. The exponential generator produces a calibrated exponential wave curve to fit and match the display of the echo peaks which appear on the second oscilloscope (7 in figure 4.5). A time constant corresponding to the precise fitting of the exponential curve is read from the exponential generator and converted to the attenuation unit *dB* per sec by use of calibration curve provided with the Matec exponential generator instrument.

4.5 X-RAY MEASUREMENTS

After the various heat treatments during sample preparation, X-ray powder diffractometry was performed on the ground-up product, using a Philips PW1820 vertical Diffractometer Goniometer using copper K_α radiation. The X-ray measurements were carried out by Mr. B. Chapman to check that the final samples were of the correct material and single phase, and to determine the lattice parameters for density calculations. Using a facility to cool the sample down to liquid nitrogen temperature, X-ray measurements were also made to determine lattice parameters as a function of temperature and hence the thermal expansion. The diffractometer was estimated (Mr. B. Chapman, private communication) to give an error in 2θ of no more than ± 0.02°, at high θ values this corresponds to an error in lattice parameters of no more than ± 0.002Å.

4.6 THE LOW TEMPERATURE DEWAR SYSTEM

The low temperature cryostat consists of inner and outer dewars as illustrated in figure 4.6a. The outer dewar is suspended from a metal frame. The inner dewar is supported by a stiff spring and connected to the cryostat by a rubber sleeve. To reduce heat conduction to the environment, both dewars are silver plated. Careful alignment of the non-silvered strips down the inner and outer dewars makes

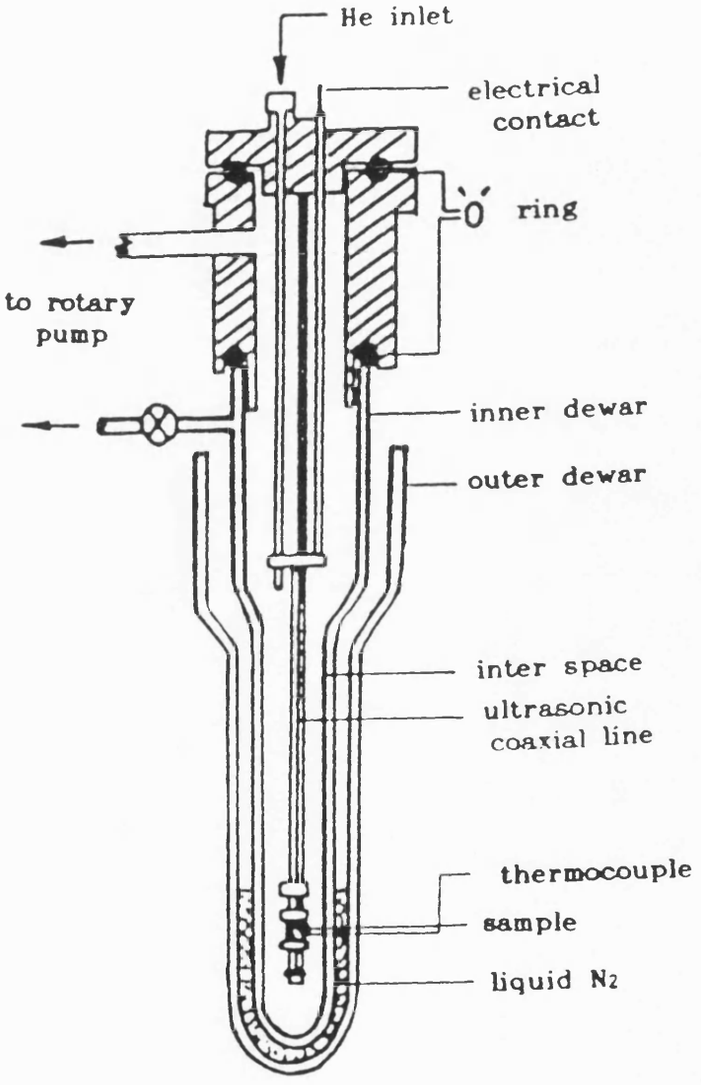

Figure 4.6 (a)

Diagram of low temperature dewar system.

it possible to see the level of the refrigerants in the dewars. The ultrasonic sample holder (figure 4.6b) is held at the bottom of a thin walled stainless steel tube to reduce heat leakage. The sample and its bonded transducer are inserted between two aluminium blocks with the aid of a spring system. The whole system is enclosed in the inner dewar.

To measure the sample temperature, a gold 1% iron-chromel or copper-constantan thermocouple junction is placed near by the sample surface. The temperature, determined to an accuracy of ±0.1K, is displayed digitally on an electronic thermometer (Thor Cryogenics 7010). Before starting any experiment, the inter-space between the double walls of the inner dewar has to be evacuated to approximately 2.7×10^{-4}bar ($27 Nm^{-2}$) and then sealed off by a ground glass tap. This is essential because any heat transferred to the inner dewar after the helium has been transferred will make the helium liquid boil rapidly and change to helium gas which is dangerous because the gas will not have enough space to expand and the dewar may explode. To avoid this, there is a safety valve on the top of the sample holder to release the gas. When the sample holder is in position, the inside of the inner dewar is then vacuum pumped. Vacuum was achieved by a rotary pump and monitored by a Pirani gauge (Edwards

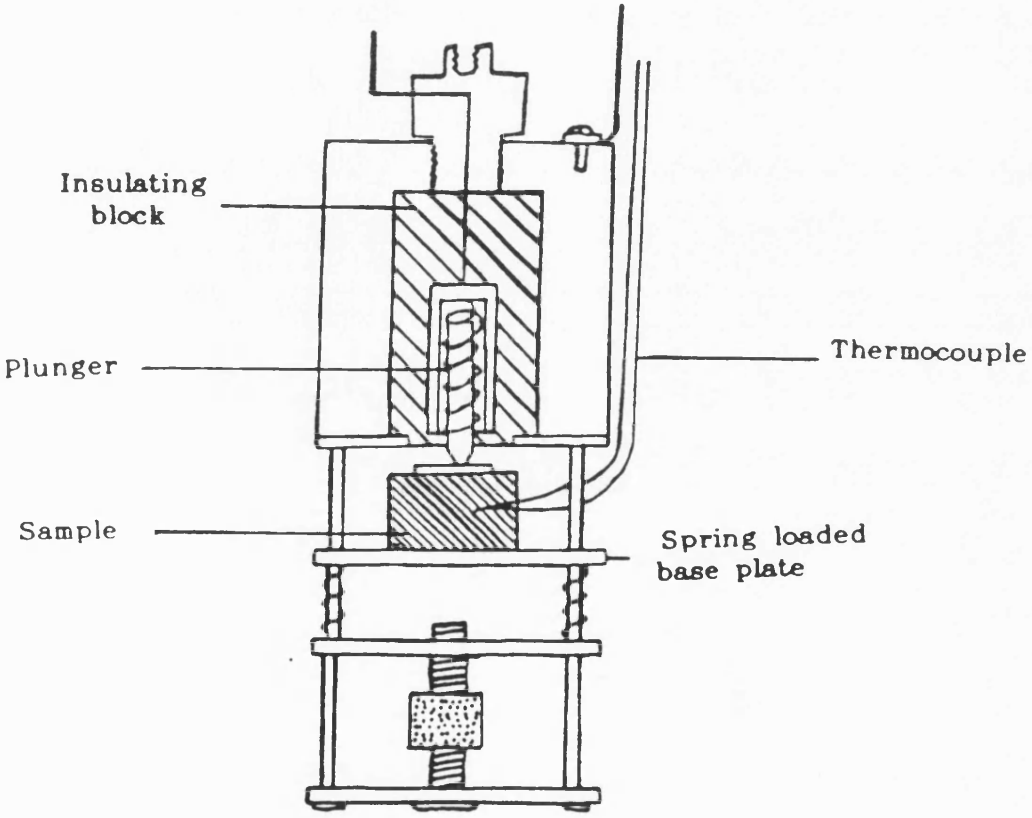

Figure 4.6 (b)

Schematic of low temperature sample holder.

Type *M6A* head). By filling the outer dewar with liquid nitrogen, the ultrasonic sample can be cooled down progressively first near to 77K (which is the boiling point of liquid nitrogen) with a reasonable cooling rate of 0.5K per minute. Liquid helium is then transferred into the inner dewar by a transfer syphon in order to cool the sample down to 4.2K (which is the boiling point of liquid helium). Careful control of the quantity of liquid helium is made to avoid rapid refrigeration which can affect the specimen-bond-transducer junction. The rate of cooling also depends on the vacuum of the inter-space and the inner dewar. In measuring the ultrasonic wave velocities as a function of temperature, the data are taken on both cooling and warming cycles, in order to check the reproducibility of the measurements.

4.7 THE LOW TEMPERATURE CLOSED CYCLE HELIUM REFRIGERATOR

Although most of the low temperature measurements were obtained by using the low temperature dewar system (described in section 4.6), some of the them have been made using a closed cycle refrigerator. The model *22C* Cryodyne refrigeration system (figure 4.7a) provides reliable refrigeration at cryogenic temperatures for long, continuous periods. It consists of a model *SC/SCW* compressor and model 22 cold head (figure 4.7b and figure 4.8). The refrigerator, which uses helium gas as a refrigerant, is designed to interface with many kinds of apparatus that require cryogenic temperatures. At the end of any operating period of the refrigerator, the cold head can be raised to ambient temperature in a relatively short time. A sample holder (figure 4.7c) was fitted at the top of the cold head, so that the ultrasonic wave velocities could be measured down to about 10K. The temperature was controlled to ±0.1K by using a temperature controller model *DRC-91C* (Lake Shore Cryotronics, Inc.) (figure 4.8) which is a microprocessor based instrument which provides analogue control; it is capable of scanning multiple sensor inputs and displaying temperature to better than 0.1K. To obtain reliable cooling rates, the cold head should be at vacuum during the operation of the helium compressor, and that is

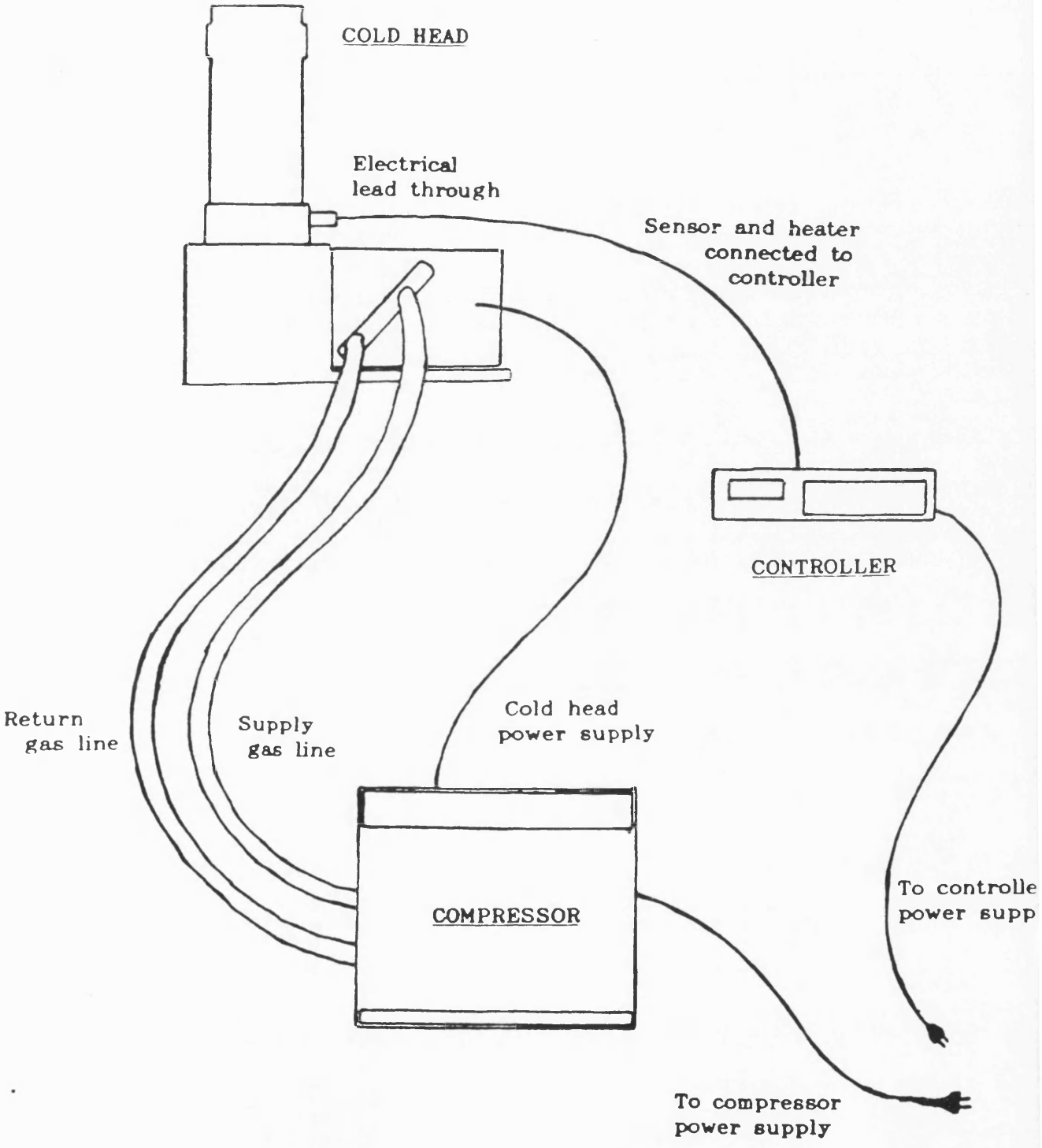

Figure 4.7 (a)

Schematic for the low temperature helium refrigeration system.

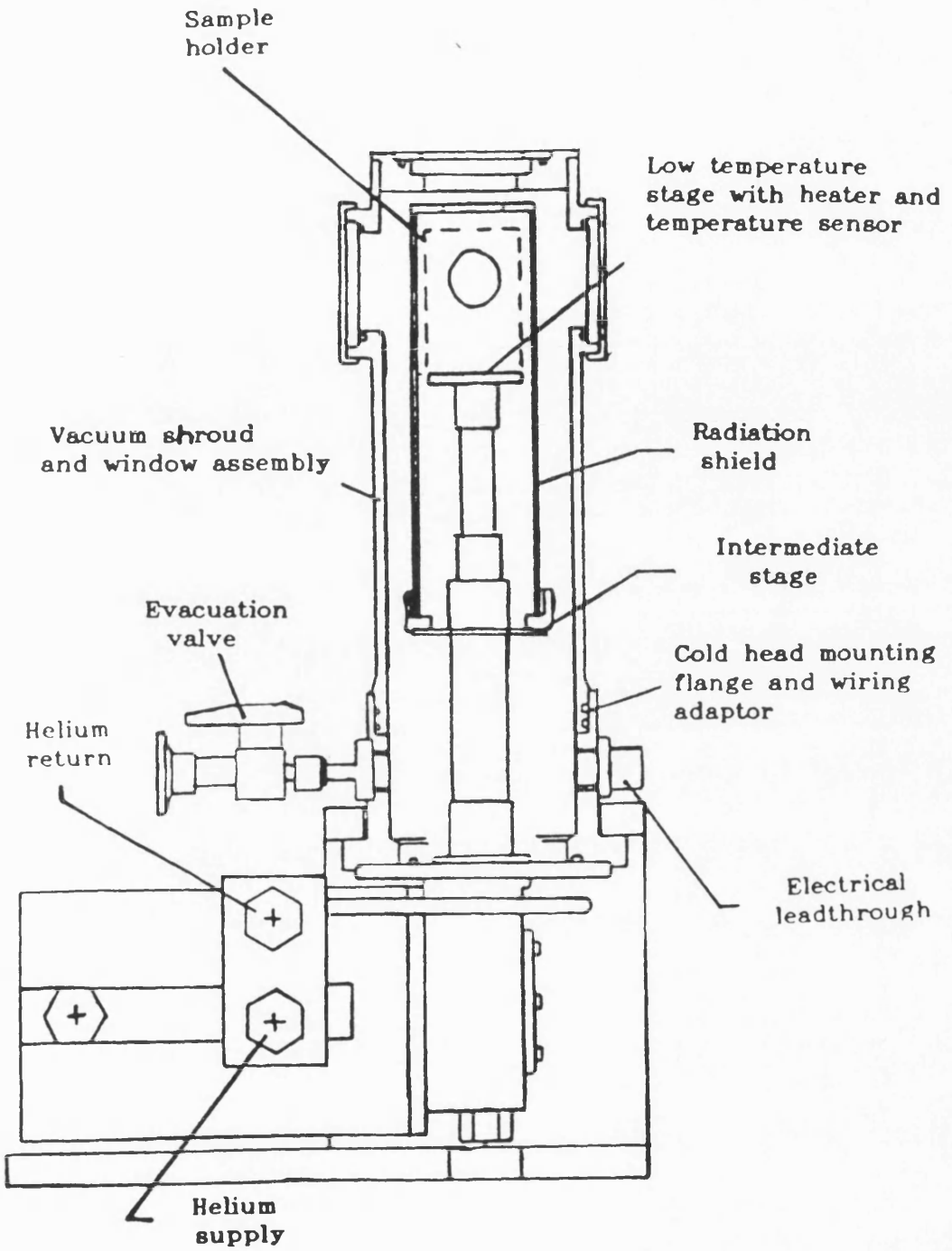

Figure 4.7 (b)

Closed cycle refrigeration system.

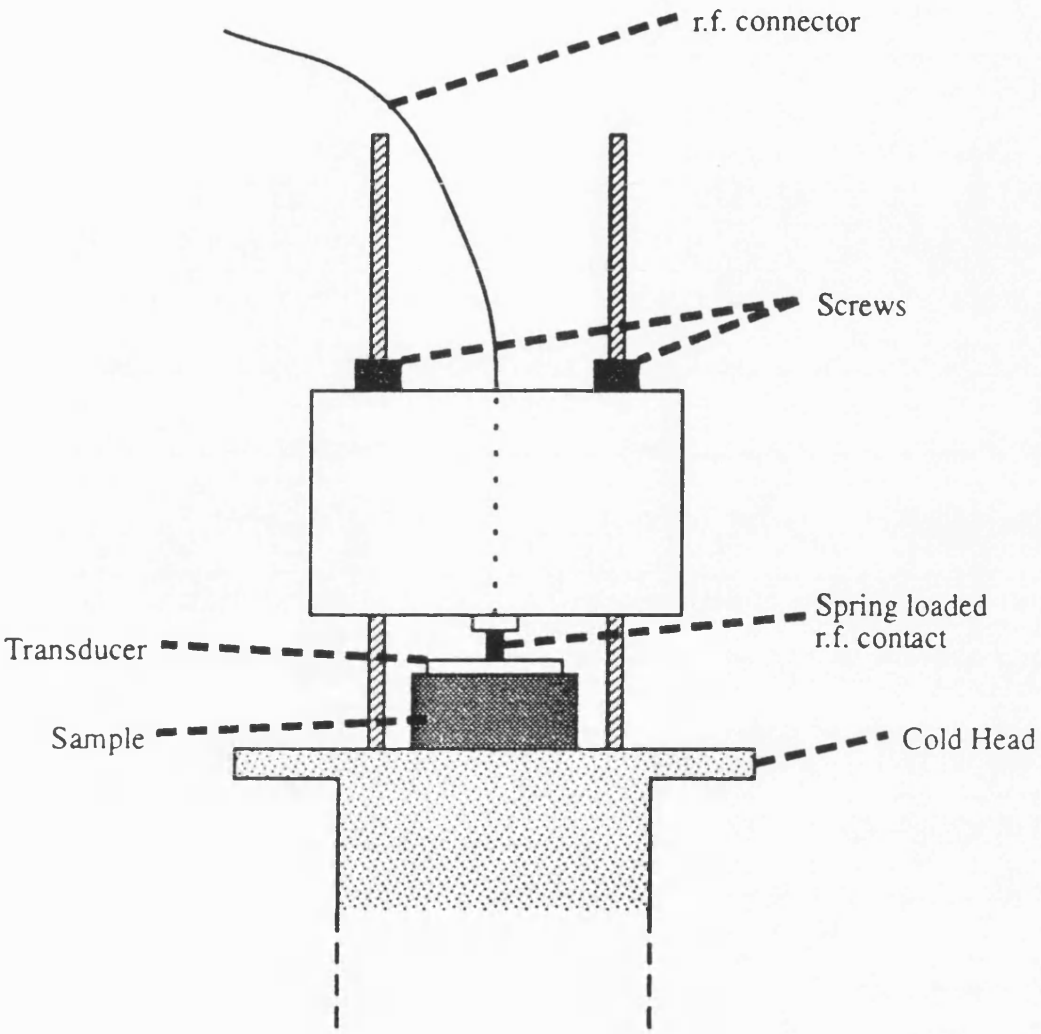

Figure 4.7 (c)

Schematic of the sample holder in the closed cycle refrigeration system.

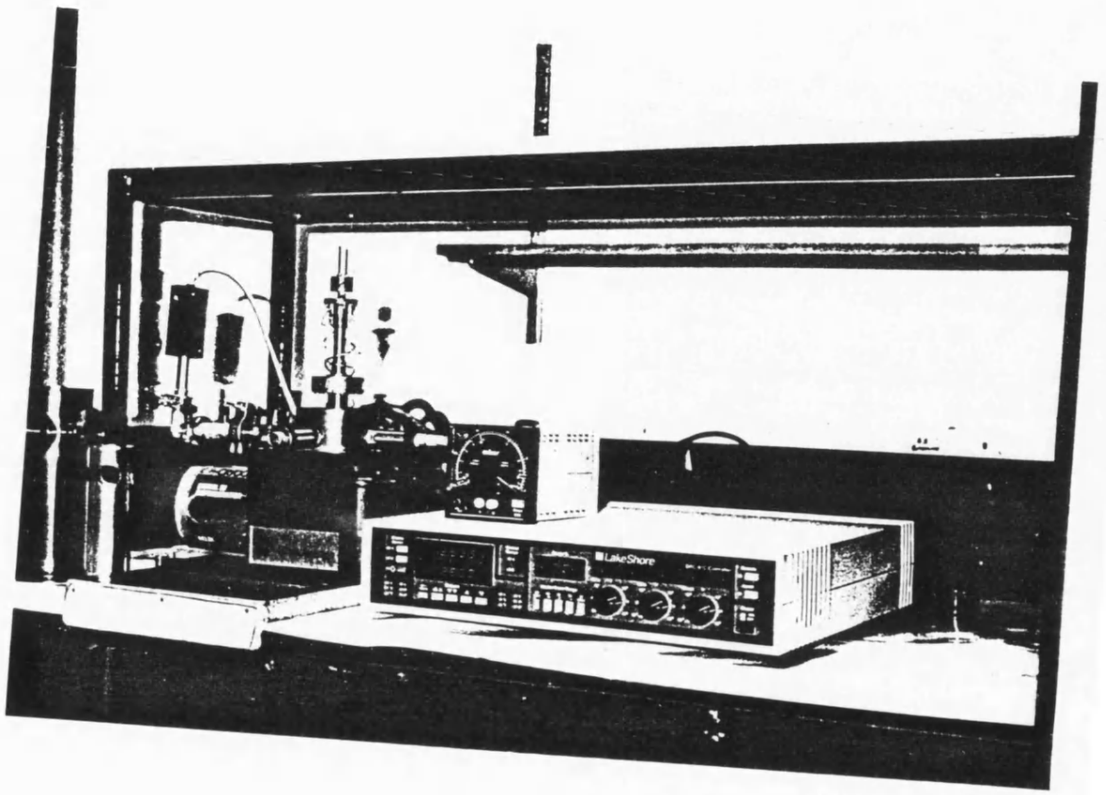

Figure 4.8

The helium closed cycle refrigeration system

achieved to between 10^{-1} and 10^{-2} mbar using a rotary/diffusion pump system (model *H5L2A*, Edwards High Vacuum Ltd., Crawley, Sussex, England).

The helium refrigerator was also used as a cooling system during resistance measurements. The four probe method was employed using copper leads bonded to the sample by silver paint. Thermal equilibrium was maintained by a thin layer of vacuum grease between the sample and the sample holder. The current passed through the sample was stabilized throughout the whole run using a (9818*IEEE*) constant current source (Time Electronic, Kent, England) with accuracy 0.02 with five ranges from 100 μA to 1A. The voltage across the sample was measured by a 5004 digital multimetre (RACAL-DANA Instruments Ltd., England) with resolution of 1 part in 10^{-5} and five ranges from 0.1-1KV. By interfacing the voltmeter, the current source and the temperature controller through an *IEEE* interface with a desk-top computer, the resistance measurements were obtained automatically. This system was used extensively to measure the transition temperature of the high temperature superconductors.

4.8 THE HYDROSTATIC PRESSURE SYSTEM

The effect of the hydrostatic pressure upon the $SOEC$ of the high temperature superconductors was determined using a piston-cylinder pressure system. In this section a brief description of the design and operation of this system is given. The specification of high pressure systems is well documented and has been discussed extensively by many workers [see for example Bradley (1969), Bridgman (1958) and Wentorf (1962)].

The hydrostatic pressure system employed in this work [Brassington (1982)] is a simple piston-cylinder arrangement shown schematically in figure 4.9 and is capable of generating pressures up to 0.2GPa. The pressure cell consists of two pistons which are inserted into opposite ends of the bore (of 25.4mm diameter made along the axis of the thick cylinder) of a cylinder (115mm high and 127mm in diameter). The two pistons and cylinder are made from $EN26$ Nickel alloy Carbon steel. This steel has a Young's modulus of $1.95x10^{11}$ Pa and a linear thermal expansion coefficient of $12x10^{-6}°C^{-1}$. The upper piston is pushed downwards using a 50 tons hydraulic press which is operated by a hand pump (Bishop Lifting Services, Bristol, England) to the fixed lower piston in order to create hydrostatic pressure on the sample within the pressure cell.

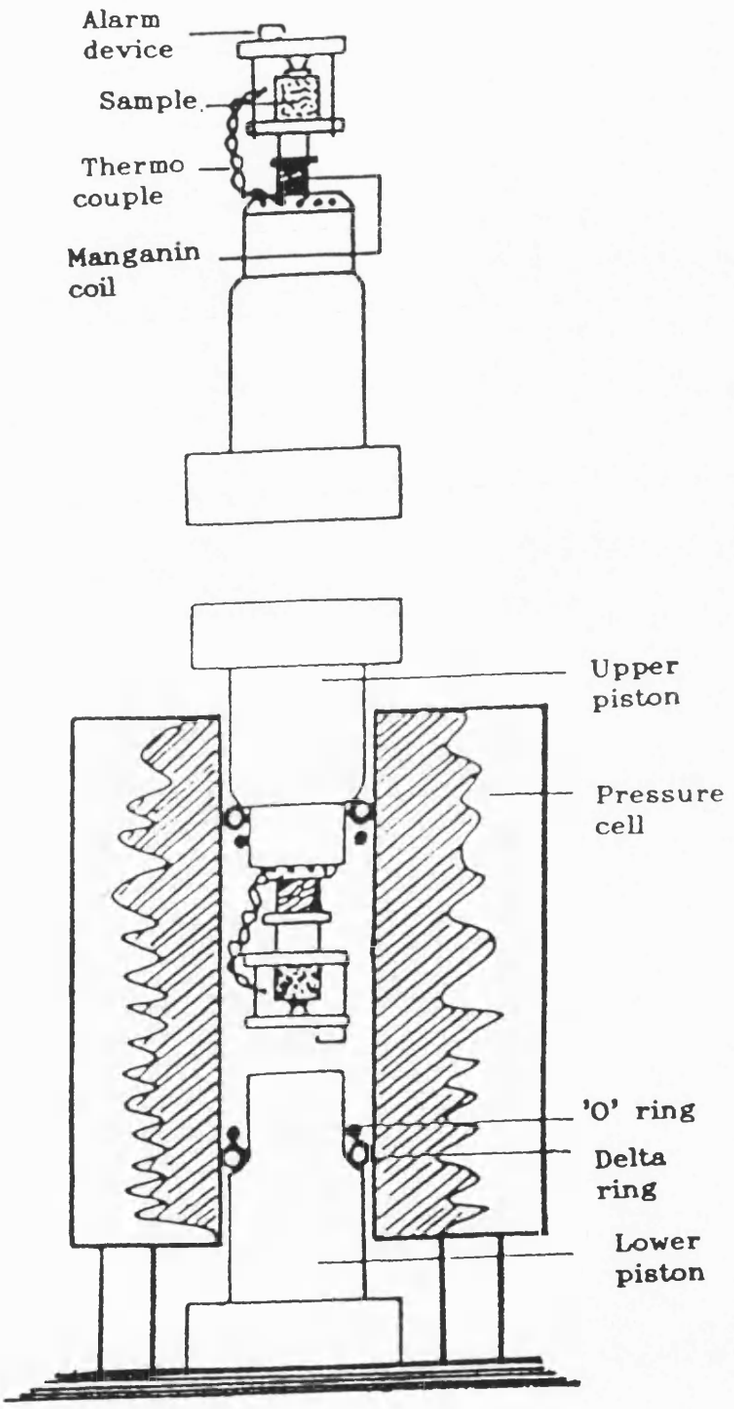

Figure 4.9

Diagram of hydrostatic pressure cell and sample holder.

The sample holder itself (figure 4.9) is constructed onto the upper piston where the manganin coil gauge (see the following section), the thermocouple and the signal input leads are also mounted. A safety alarm device is also included in this system to prevent the sample holder crushing, in case the upper piston is pushed too close to the lower piston. To prevent any oil leakage from the cavity between the two pistons at high pressure, seals between the pistons and the internal cylinder wall are formed by a neoprene O-ring and a p.t.f.e. (polytetrafluoroethylene) ring. There are several conical holes through the upper piston. These holes are filled with beryllium copper plugs insulated with ceramic to avoid any metal contact between the plugs and the sample holder.

The cavity between these two pistons is filled with a fluid which serves as a pressure transmitting medium. Several types of fluids have been identified depending on the range of pressure needed: for pressures less than 0.3GPa, Castor oil is normally employed, Plexol-244 oil for higher pressures up to 1GPa and Silicone fluid (Dow Corning 200/1000 CS) for a combination of high pressures and temperatures. Silicone fluid has a higher boiling point than Castor oil or Plexol-244 oil and does not contain carbon molecules; the other oils cause a black stain on the cylinder and the pistons.

Before taking any data, the pressure of the system is usually increased to a maximum value and held there for about 30 minutes, in order to stabilize the transducer-sample bond and to ensure no leakage in the system throughout the experiment. The pressure is then released and the system is left for another 30 minutes to regain its thermal equilibrium. When the pressure is changed, the temperature inside the cavity alters: an increase in applied pressure by 0.01-0.02GPa results in a significant increase (1°C) in temperature. The pressure is increased usually in steps of about 0.01GPa and the variation of the echo transit time under hydrostatic pressure is measured after 10-15 minutes, to allow the thermal equilibrium of the system to be reached. For safety purposes, the pressure cell is enclosed in a steel cabinet having dimensions 82cm x 79cm x 32cm; the door of which is always kept shut during the experiment.

4.9 MANGANIN COIL AS A PRESSURE GAUGE

For high pressure experiments up to about 10GPa, a manganin coil (Cu-Mn-Ni alloy) can be used as a pressure gauge [Samara and Giardini (1964)] due to the fact that its electrical resistivity is sensitive to changes in pressure. The resistance of manganin wire is nearly linearly dependent upon pressure [Bridgman (1958)]. As a result, this gauge is widely used in piston-cylinder, multi-anvil and other high pressure systems.

The gauge used here consists of 0.1mm diameter manganin wire wound non-inductively on a pyrophyllite core. Pyrophyllite is a soft natural material, which after heat treatment is transformed into a hard ceramic-like substance with reasonable good insulating properties. Each manganin gauge is put through a Bridgman cycle of pressure-temperature seasoning before it is used; the coil is heated to about 200°C for several hours followed by quenching in liquid nitrogen. This process is repeated several times before the final seasoning by pressurising the gauge to the highest operating pressure (0.3GPa) for several hours. This thermal treatment eliminates localised strain regions and hence improves uniformity, while the pressure treatment stabilises the pressure coefficient of resistance [Bridgman (1911)].

The pressure coefficient of resistance of the manganin gauge used to measure the hydrostatic pressure in these experiment is $24x10^{-5}GPa^{-1}$ **[Samara and Giardini (1964)], thus the pressure** P **inside the hydrostatic pressure cell has been calculated using:**

$$P = \frac{(R_P - R_{atm})/R_{atm}}{24x10^{-5}} \qquad (4.1)$$

Here R_P **is the coil resistance at pressure** P **and** R_{atm} **is the coil resistance at atmospheric pressure. The typical resistance of a gauge at atmospheric pressure is about 100 to 120 Ohms. The resistance is measured using a digital multimeter with a sensitivity of 1 part in** 10^{-5} **ohm which in turn leads to the measurement of the applied hydrostatic pressure to a sensitivity of ±0.5%. The temperature coefficient of resistance of a manganin wire is very small** $(10x10^{-6}{}^{\circ}C^{-1})$ **[Wang (1967)], and since the experiment is carried out isothermally, this has a negligible effect upon the hydrostatic pressure measurements.**

4.10 SAMPLES PREPARATION AND CHARACTERIZATION

All but one of the high T_c superconducting samples in this work were prepared in our department; the exception was the sample designated YBCO2 supplied from Aberdeen University. Starting materials were oxide powders obtained from Aldrich Chemical Company Ltd. (Gillingham, Dorset, England) and Johnson Matthey Technology Centre (Reading, England).

The samples were prepared by the usual solid-state reaction method which basically involves mixing the oxide powders and then sintering the mixture at high temperature. The starting materials were as follows:

[1] Y-Ba-Cu-O: Y_2O_3, $BaCO_3$ and CuO.

[2] Gd-Ba-Cu-O: Gd_2O_3, $BaCO_3$ and CuO.

[3] La-Cu-O: La_2O_3 and CuO.

[4] La-Sr-Cu-O: La_2O_3, $SrCO_3$ and CuO.

[5] Nd-Cu-O: Nd_2O_3 and CuO.

[6] Nd-Ce-Cu-O: Nd_2O_3, CeO_2 and CuO.

[7] Bi-Sr-Ca-Cu-O compounds: Bi_2O_3, CaO, $SrCO_3$ and CuO.

[8] (Pb)Bi-Sr-Ca-Cu-O compounds: Bi_2O_3, CaO, $SrCO_3$, PbO and CuO.

The mixture of the oxide powders of desired composition was placed in a ball-mill (with some acetone) and rotated for 3-4 hours to produce very fine grain material; then it

was left in an oven at about $50°C$ to evaporate all the acetone mixed in with it. The mixture was then sintered in a furnace at high temperature, the value of which differs from one compound to another (see table 4.1). After the sintering process the material was ground in a pestle and mortar, and sieved to produce a fine powder (particle size between $250-400\mu m$). This powder was pressed into cylindrical shape pellets (with a diameter about 12.5cm) under a $5tonm^{-2}$ pressure. Finally, the pellets were annealed in oxygen (argon for $Nd_{2-x}Ce_xCuO_{4-y}$ sample) atmosphere at a temperature the value of which also differs from one compound to another (table 4.1), and then cooled down to room temperature with a controlled cooling rate. After the annealing process the samples were mechanically polished to obtain two parallel (to about $10^{-4}rad$) flat faces suitable for ultrasonic measurements.

Many research groups have been working on the effect of the preparation conditions on the superconducting properties since these can be much altered by changing the sintering and annealing temperatures and time or the cooling rate. For example, for a $YBa_2Cu_3O_{7-x}$ sample, Kishida et al (1988) found that changing the annealing temperature by $50°C$ produced a change in T_c by about 4K. Gopalakrishnan et al (1987a) deduced that the change in the cooling rate (from a fast

Table 4.1. Sintering temperature and time, annealing temperature and time and the cooling rate used to prepare the high temperature superconductors, and related compound samples.

Material	Sinter. Temp. (°C)	Sinter. Time (hours)	Anneal. Gas	Anneal. Temp. (°C)	Anneal. Time (hours)	Anneal. Cooling Rate(°C/hour)	Additonal Processes
$YBa_2Cu_3O_{7-x}$ (Y1)	940	48	Oxygen	400	48	20	-
$YBa_2Cu_3O_{7-x}$ (Y2)	960	72	-	-	-	-	This sample was prepared without annealing.
$GdBa_2Cu_3O_{7-x}$ (orthorhombic)	940	48	Oxygen	400	48	20	-
$GdBa_2Cu_3O_{7-x}$ (tetragonal)	940	48	Oxygen	400	48	20	Heated in vacuum at 700°C for 24 hours.
La_2CuO_{4-y}	1000	24	Oxygen	1100	24	20	-
$La_{1.8}Sr_{0.2}CuO_{4-y}$	1000	24	Argon or Nitrogen	1100	24	20	During the sample pressing, polyvinyl acetate dissolved in a minimal quantity of acetone was used as a binder.
Nd_2CuO_{4-y}	950	12	Argon or Nitrogen	950	24	20	After the first sintering, the sample was ground and sintered at 1100°C for 24 hours and then quenched down to room temperature.
$Nd_{1.85}Ce_{0.15}CuO_{4-y}$	950	10	Argon or Nitrogen	1000	12	20	Between the first sintering and the annealing the sample was twice grounded and heated up to 1150°C for 10 hours.
All Bismuth Samples	800	24	Oxygen	840-860	100	20	-

cooling rate to a slow one) after sintering changed the T_c of a $YBa_2Cu_3O_{7-x}$ sample by 23K. For $BiCaSrCu_2O_x$, in contrast, Komatsu et al (1988) found that rapidly cooled samples after annealing showed a higher T_c and sharper superconducting transition, but samples slowly cooled in the furnace after annealing showed a lower T_c and broader transition with a tail.

Most of the samples studied in this work were prepared by annealing in oxygen. However, in the case of $Nd_{2-x}Ce_xCuO_{4-y}$, using argon as an annealing gas produced a superconducting sample while annealing in oxygen did not. The cooling rate after annealing is one very important factor in producing high T_c superconducting samples. The oxygen stoichiometry in these materials is the key factor for the existence of superconductivity. Slow cooling in an oxygen atmosphere gives plenty of time for the oxygen atoms to order in the structure of the material [Gopalakrishnan et al (1987a)].

One of the samples (YBCO2) examined in this work was prepared at Aberdeen University (by Dr. J. Ingrahms). This sample was sintered at high temperature and without annealing in oxygen. It has a particularly high density (about 98%).

4.11 EXPERIMENTAL ERRORS AND CORRECTIONS

In this work there are several possible sources of experimental errors which could affect the overall accuracy of the measurements. These sources will now be discussed individually

(A) MEASUREMENTS OF SAMPLE DIMENSIONS

The dimensions of each ultrasonic sample were measured using a digital micrometer having a resolution of ±0.002 mm. Several measurements were made at different points on the relevant face of each sample and the average value of these measurements was taken as the sample thickness. The standard deviations of these measurements were normally of the order of 0.02%. This typical error contributes directly to the derived velocity and leads to an error of about 0.04% in the resultant *SOEC*.

(B) MEASUREMENTS OF SAMPLE DENSITY

The room temperature densities of all ultrasonic samples were measured by Archimedes' principle. Each value was calculated using

$$\rho_s = \frac{W_a \rho_f}{W_a - W_f} \qquad (4.2)$$

where ρ_s **is the density of the sample,** ρ_f **is the density of the floatation medium used;** W_a **and** W_f **are the weight of the**

sample in air and when immersed in the floatation medium respectively. Samples were weighed using an analytical balance which had a resolution of ±0.1 mg. This procedure enabled the densities to be determined to within 0.1%. From the equation $C_{IJ}(=\rho V^2)$, it can be seen that the error in the density measurement contribute an error directly to the calculated *SOEC*. To obtain a reasonable value for the *SOEC* at any temperature, both the dimensions and density of each sample must be known. This can be achieved by calculating the dimensional changes from the thermal expansion data. The measurements of the changes in the lattice parameters as a function of temperature were made for most of the samples in this work; so that the thermal expansion coefficients could be calculated. However, for some samples these measurements have not been done. Therefore, in general, the room temperature density of each ultrasonic sample has to be used as a reasonable approximation in determining the temperature dependences of the *SOEC*. The corresponding error in density and dimensional measurement contribute a maximum error of about 1% to the *SOEC*.

(C) TRANSIT TIME ERRORS

The largest contribution to the systematic error in the determination of the *SOEC* is due to delays included in transit time measurements from multiple internal reflection within

the transducer and the sample. The accuracy to which the transit time can be measured is limited by factors such as the quality of the bond and the transducer thickness. The time interval between successive echoes increases with transducer thickness. The accuracy can be improved if either a thin transducer or a long sample are used. These two requirements cannot be satisfactorily fulfilled since the samples used in this work are only several mm thick and quartz transducers with fundamental frequencies higher than 10MHz are thin and fragile. Furthermore, attenuation increases rapidly with frequency. Acoustic impedance (the product of density and sound velocity) of both the transducer and the sample are the characteristics that determine the relative contributions of reflections and transmissions of the ultrasonic wave at the sample-transducer interface. Since the physical properties of both media are different, there is an acoustic impedance mismatch between the transducer and the sample. Thus when an ultrasonic wave reaches the transducer and sample interface, part will be reflected and the rest is transmitted. Each portion will undergo multiple reflections in the transducer and sample respectively. The reflection coefficient at the sample-quartz transducer interface can be defined by

$$r_{12} = \frac{\rho_2 V_2 - \rho_1 V_1}{\rho_2 V_2 + \rho_1 V_1} \qquad (4.3)$$

where $\rho_1 V_1$ is the acoustic impedance of the sample, and $\rho_2 V_2$ is the acoustic impedance of the transducer. As a result of the reflection, the received echoes will be time delayed and hence the error of measured transit time is enhanced. In this connection, Kittinger (1977) has provided a procedure to correct the measured transit time. In brief his mathematical computations relate the estimated echo delay δt (in units of the reciprocal fundamental transducer frequency) to the acoustic reflection coefficient. From such calculations the real transit time of an ultrasonic wave can be obtained. In this work, these have been achieved through a computer programme of "TRANS-CORR" [Brassington (1982)] which is based on Kittinger's work. Corrections in practice are of the order of 2 to 5% and lead to an increase in the ultrasonic wave velocity. It is important to note that these corrections take no account of the presence of the gold plated electrode and the acoustic bond material between the transducer and the specimen. However according to Kittinger (1977), those contributions to the apparent echo delay are small.

(D) DIFFRACTION AND NON-PARALLELISM

The piezoelectric transducer can be regarded as a piston source of plane waves. The smaller the transducer the less plane is the wave. So when a small transducer has to be used, the errors in transit time measurement due to the diffraction effects can be significant. This effect has been studied by Truell et al (1969) who concluded that when ultrasonic waves are propagated along two- or four-fold symmetry axes, the transit time error due to diffraction is of order 0.01%, provided the crystal orientation is accurate to within $0.5°$ and the area of the transducer is smaller than that of the sample.

For a sample which is not perfectly parallel the transducer will receive different phases of the wave across its surface. However this error can be reduced to negligible proportions by ensuring the faces of each ultrasonic sample are parallel to better than 10^{-3} radians, which they are here.

(E) PRESSURE DEPENDENCE OF THE *SOEC*

The errors in dC_{ij}/dP at zero pressure can be determined from the error in the gradients of the plot of the change in ultrasonic wave velocities with applied pressure where the corresponding error can be obtained through a least mean square fit computer programme. The hydrostatic pressure itself can be measured within an accuracy of 0.25%. For the longitudinal mode the typical error in dC_{ij}/dP is about 2%.

Since the relative changes of shear ultrasonic wave velocity under hydrostatic pressure are usually considerably smaller than those for the longitudinal mode, the errors introduced are rather larger (≈5%).

4.12 A TECHNIQUE FOR CORRECTION FOR THE POROSITY EFFECTS ON THE ELASTIC PROPERTIES

A correction method has been developed in order to take into account the effects of the porosity on the elastic properties of the ceramic materials under investigation. These ceramics are porous material and the presence of pores has a marked effect on the ultrasonic wave velocity and its pressure dependence. Application of pressure fills the pores with the silicone oil which is used as the pressure transmitting fluid (section 4.8). It is important to determine how much the presence of the oil-filled pores influences the ultrasonic wave velocities, the elastic constants and their hydrostatic pressure derivatives. This is because, to understand theoretically the physical nature of the interatomic binding forces, the most useful quantities to know are the elastic moduli and their pressure derivatives in the non-porous matrix. The solution of the wave equations for propagation under hydrostatic pressure in an isotropic oil-saturated porous medium with a uniform distribution of interconnected pores leads to the following expressions for bulk and shear moduli respectively [Cankurtaran et al (1989a)]:

$$B^m = B^n + \left[\frac{n}{1-n}\right]\frac{(3B^m + 4\mu^n)(B^n - B^w)}{(3B^w + 4\mu^n)} \qquad (4.4)$$

$$\mu^m = \mu^n + \left[\frac{n}{1-n}\right]\frac{9B^n\mu^n + 8(\mu^n)^2 + 6\mu^m(B^n + 2\mu^n)}{(9B^n + 8\mu^n)} \qquad (4.5)$$

Here the superscripts n **and** m **denote the measured moduli in an oil-saturated medium and those of the non-porous matrix respectively. The bulk modulus** B^w **of the silicone oil is 1.0GPa and so its influence is small. For an isotropic material the Lamé constant** μ **is identical to the shear modulus** c_s**.**

The porosity (n**) of the sample under investigation was measured by calculating the theoretical density of the sample from the X-ray measurements and by measuring the actual density of the sample using Archimedes' principle (section 4.11B). For example, the** $Nd_{1.85}Ce_{0.15}CuO_{4-y}$ **sample investigated in this work has a theoretical density of 7330kg/m³ and an experimental density of 6481kg/m³ which gives a porosity of 0.12.**

CHAPTER FIVE

CRYSTAL STRUCTURE OF HIGH TEMPERATURE SUPERCONDUCTING COMPOUNDS

5.1 INTRODUCTION

To understand the mechanisms that bring about the superconducting state in a particular material, it is necessary to know the structure of the compound that exhibits this phenomenon. Single crystal structure studies have been carried out to determine the dimensions of the unit cell, the locations of the atoms in the cell, the electronic charge distribution and the possible presence of atomic irregularities [Akthar et al (1988), Fietz et al (1987), Terada et al (1987), Olsen et al (1988) and Jaya et al (1988)]. X-ray powder diffraction measurements, which can identify a known structure and provide the unit cell dimensions, are useful for checking the quality of the samples [Fietz et al (1987, 1989), Takahashi et al (1987a), Dietrich et al (1987), Aleksandrov et al (1988), Akthar et al (1990) and Ecke et al (1988)]. Neutron powder diffraction has also provided much information about the structural aspects [Howard et al (1989), Pei et al (1990), Izumi et al (1990) and Glazkov et al (1988)].

CHAPTER FIVE

The new high temperature superconducting compounds possess a distorted perovskite structure. In their ideal form the perovskites, which are described by the general formula ABX_3 , consist of cubes made up of three distinct chemical elements (A,B and X) that are present in a ratio of $A:B:X$ 1:1:3 (figure 5.1). The A and B atoms are metallic cations (ions with a positive charge) and the X atoms are non metallic anions (ions with a negative charge). An A cation (the larger of the two kinds of metals) lies at the centre of each cube, the B cations occupy all eight corners and the X anions lie at the midpoint of the cube's 12 edges [Hazen (1988)].

In this chapter an overview of the structure of the high temperature superconducting compounds is given. The structure of the La-M-Cu-O compound (where M = Sr or Ba) and its parent material La_2CuO_4 is presented in section 5.2. The structure of the electron superconductor Nd-Ce-Cu-O together with the structure of the parent compound Nd_2CuO_4 is introduced in section 5.3. In section 5.4 the structure of $RBa_2Cu_3O_{7-X}$ compound (where R = rare earth elements) is presented. Finally in section 5.5 the structure of the Bi-based cuprates and its lead substituted compounds is introduced.

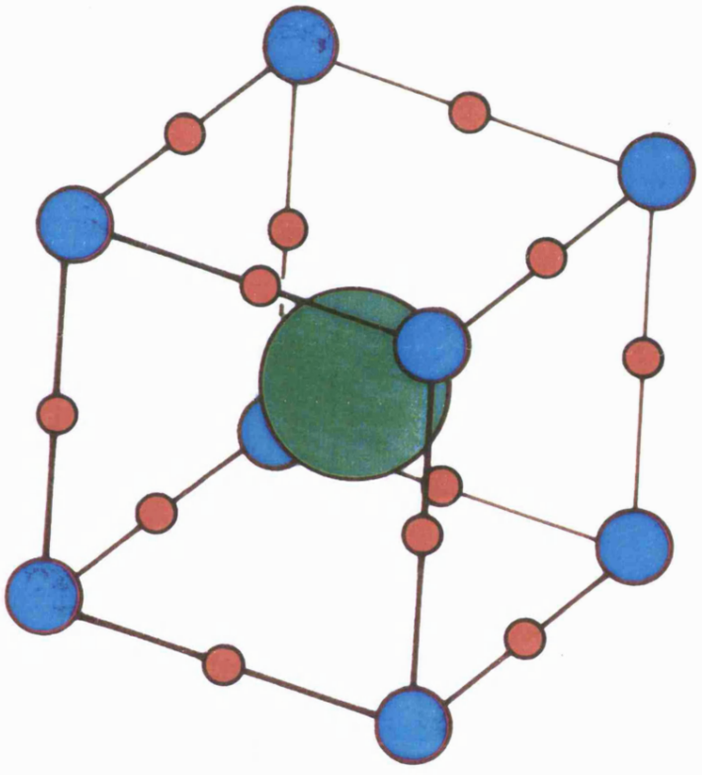

Figure 5.1
The basic structural unit of perovskites is a cube with one larger metallic cation (A) (green) at the centre, eight smaller metallic cations (B) (blue) at the corners and 12 nonmetallic anions (X) (red) at the midpoints of the edges.

5.2 CRYSTAL STRUCTURE OF La_2CuO_4 AND THE DOPED COMPOUND $La_{2-x}Sr_xCuO_{4-y}$

The undoped La_2CuO_4 compound, which forms in an orthorhombically distorted variant of the K_2NiF_4 structure, is non-metallic at low temperatures. The 2:1 La:Cu stoichiometry results in planes of perovskite-like structure with CuO_6 octahedra sharing corners, separated by two layers of *A* atoms, resulting in a highly anisotropic structure [Uchida et al (1987)] (see figure 5.2). La_2CuO_4 itself has orthorhombic symmetry but becomes tetragonal at 500K [Rao (1988)] or at room temperature at the dopant concentrations required to attain bulk superconductivity [Cava (1987c)]. There are reports that this compound can be made superconducting by special post synthesis procedures [Grant et al (1987)], however the superconductivity might not be bulk and the reason for its existence is not yet understood.

In order to introduce charge carriers, and hence obtain superconductivity, it is necessary to partially substitute lanthanum in La_2CuO_4 with a divalent alkaline earth element thus inducing excess positive charge (holes) over and above those in the parent compound. The structure of $La_{2-x}M_xCuO_4$ (where M = Sr, Ba or Ca) is tetragonal at room temperature characterized by sheets of edge sharing Cu-centred O octahedra and La(Sr) atoms forming perovskite layers stacked

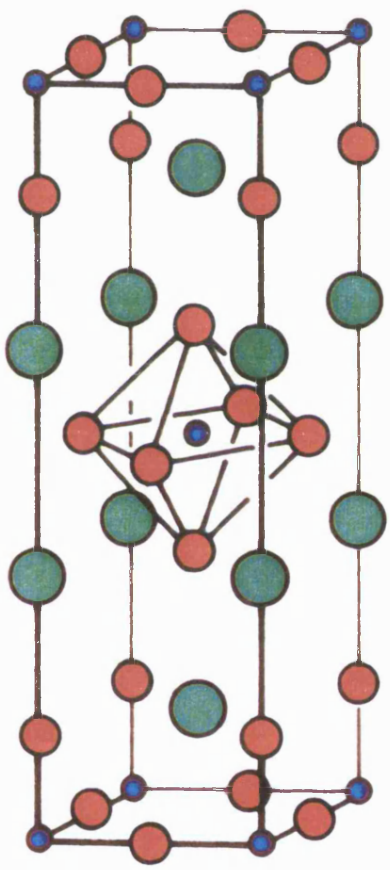

Figure 5.2
The crystal structure of La_2CuO_{4-y}. The colours are as follows: red = O, green = La, blue = Cu. Sr, Ba or Ca substitution occurs on a La site.

along the tetragonal axis [Decroux et al (1987)]. The compound undergoes a structural phase transition from tetragonal to orthorhombic at 255K [Laegreid et al (1990)]. Partial substitution of La in La_2CuO_4 by Ca, Sr or Ba stabilizes the tetragonal structure at room temperature when x is greater than 0.05; superconductivity appears with a T_c increasing until it reaches its maximum at $La_{1.85}Sr_{0.15}CuO_{4-y}$ composition. Kim and Moret (1988a) found that the tetragonal phase is stabilized by pressure and above 1.5GPa (for $La_{1.88}Sr_{0.12}CuO_4$) only the tetragonal phase is found. It was argued that consequently both phases (orthorhombic and tetragonal) are superconducting.

5.3 CRYSTAL STRUCTURE OF THE $Nd_{2-x}Ce_xCuO_{4-y}$ AND ITS PARENT COMPOUND Nd_2CuO_{4-y}

The parent compound Nd_2CuO_{4-y} crystallizes in a tetragonal structure with Cu-O planes and no apical oxygen atoms (figure 5.3). The structural features of the host material Nd_2CuO_{4-y} have already been examined fairly extensively and have been summarized for this type of compounds by Cheong et al (1989).

By doping Nd_2CuO_{4-y} with the tetravalent rare earth cerium yields superconductors with T_c in the 20-30K range. The doped $Nd_{2-x}Ce_xCuO_{4-y}$ compound has an identical structure to that of the undoped parent compound Nd_2CuO_{4-y} [Tokura et al (1989)].

The main structural difference between the $La_{2-x}Sr_xCuO_4$ compound and the $Nd_{2-x}Ce_xCuO_{4-y}$ is the absence of the apical oxygen atoms in the Nd-compound (see figures 5.2 and 5.3).

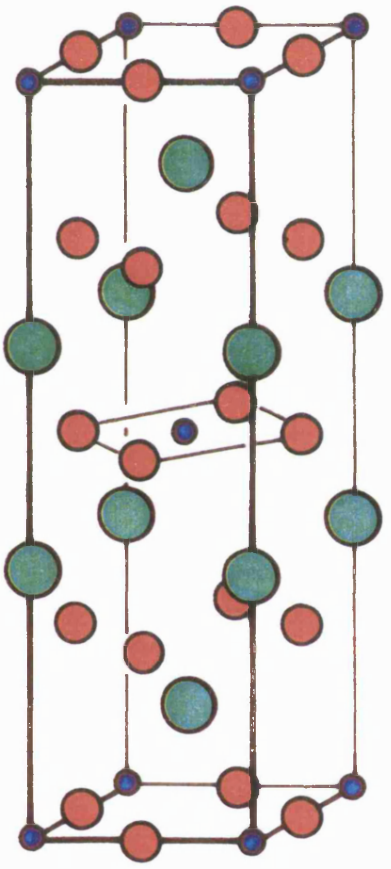

Figure 5.3
The crystal structure of Nd_2CuO_{4-y}. The colours are as follows: red = O, green = Nd, blue = Cu. Ce substitution occurs on a Nd site.

5.4 CRYSTAL STRUCTURE OF THE $RBa_2Cu_3O_{7-x}$ COMPOUND (WHERE R = RARE EARTH ELEMENTS)

The crystal structure of only $YBa_2Cu_3O_{7-x}$ will be considered in this section because, in general, all the other related compounds have the same structural features. $YBa_2Cu_3O_{7-x}$ (figure 5.4) has an orthorhombic structure built up from triple layers of corner sharing polyhedra. Each layer is itself built up from two layers of corner sharing pyramids and of one layer of CuO_4 square planar groups. This structure can in fact be described as an ordered oxygen deficient perovskite in which rows of oxygen atoms parallel to a CuO_2 plane have been eliminated, whereas barium and yttrium ions are ordered in such a way that two barium planes alternate with one yttrium plane along c direction. Superconductivity appears in this compound when $0.5 \leq x \leq 1$.

The compound $YBa_2Cu_3O_{7-x}$ is tetragonal at high temperatures and undergoes a second order phase transition at about 700°C to the low temperature orthorhombic phase [Freitas and Plaskett (1987), Jorgensen et al (1987b), Schuller et al (1987)]. The orthorhombic structure is the superconducting phase of $YBa_2Cu_3O_{7-x}$. The tetragonal phase can be obtained at room temperature by quenching from above the phase transition, and it is found to be semiconducting.

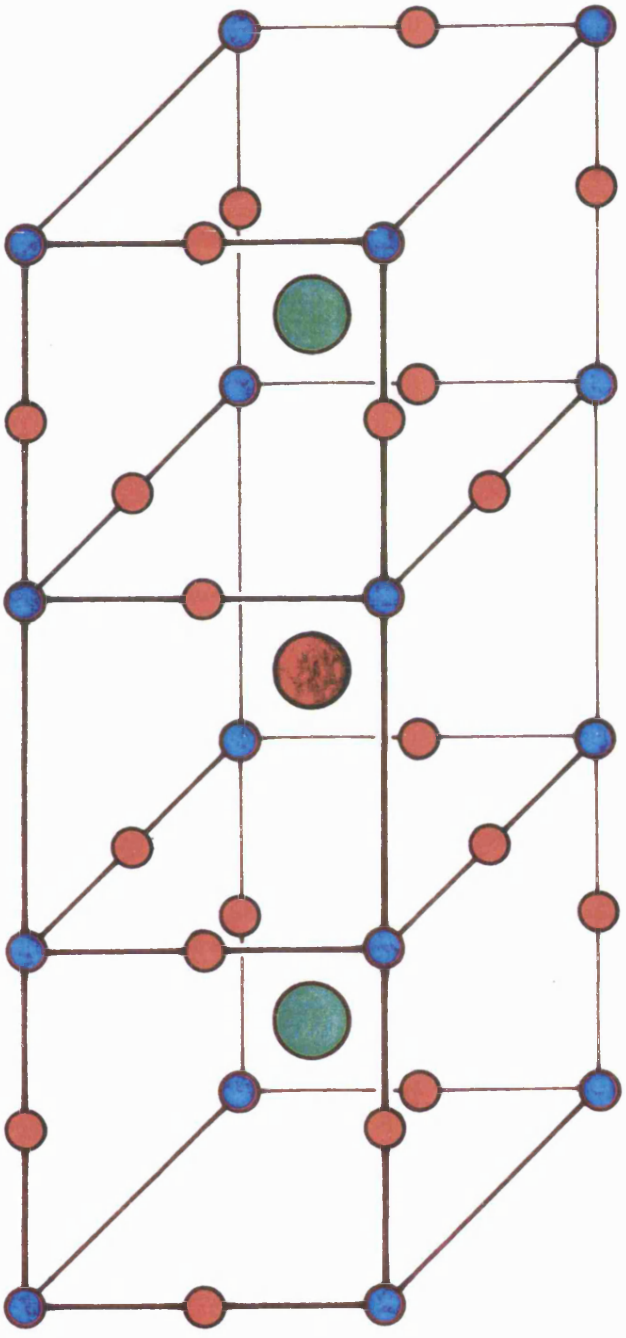

Figure 5.4
The crystal structure of orthorhombic $RBa_2Cu_3O_7$ (where R = Y or Gd). The colours are as follows: red = O, brown = Y or Gd, blue = Cu, green = Ba.

5.5 CRYSTAL STRUCTURE OF THE Bi-BASED CUPRATES AND ITS LEAD SUBSTITUTED COMPOUNDS

Compounds in the series $Bi_2Sr_2Ca_{n-1}Cu_nO_{4+2n}$ including both $Bi_2Sr_2CaCu_2O_{8+y}$, the Bi2212 phase, and $Bi_2Sr_2Ca_2Cu_3O_{10+y}$, the Bi2223 phase, have layer structures containing adjacent pairs of BiO planes which alternate along the c-axis with perovskite-like multilayers. In the n=2 (Bi2212) phase the perovskite-like multilayer is comprised of two copper-oxygen sheets in the form of corner-sharing CuO pyramids separated on the base sides by calcium ions (see figure 5.5). For the n=3 (Bi2223) phase the perovskite-like multilayer is made up of two corner-sharing CuO pyramidal sheets with a planar CuO sheet between them separated by calcium ions [Kanai et al (1989)] (see figure 5.6). In both compounds the Bi_2O_2 layers are comprised of two parallel, planar BiO sheets. The bismuth ion coordination is six: four O in the BiO plane, one O on the adjacent BiO layer, one O on the adjacent apex of a CuO pyramid. These BiO_6 octahedra are strongly distorted having the typical oxygen coordination for Bi^{3+} with three short Bi-O bonds and three much longer Bi-O in the direction of the lone pair electrons. These lone pairs are positioned in the interstice between the pairs of BiO layers leading

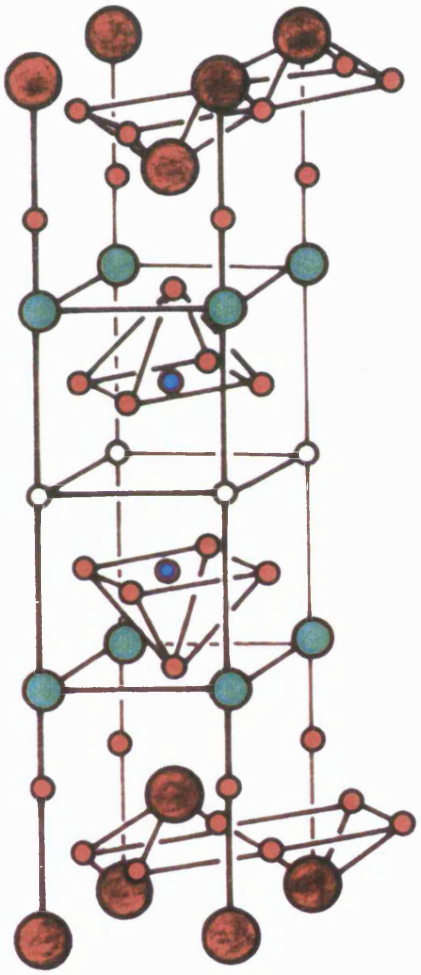

Figure 5.5
The crystal structure of $Bi_2Sr_2CaCu_2O_{8+y}$. The colours are as follows: red = O, open circle = Ca, blue = Cu, green = Sr, brown = Bi. Pb substitution occurs on Bi sites.

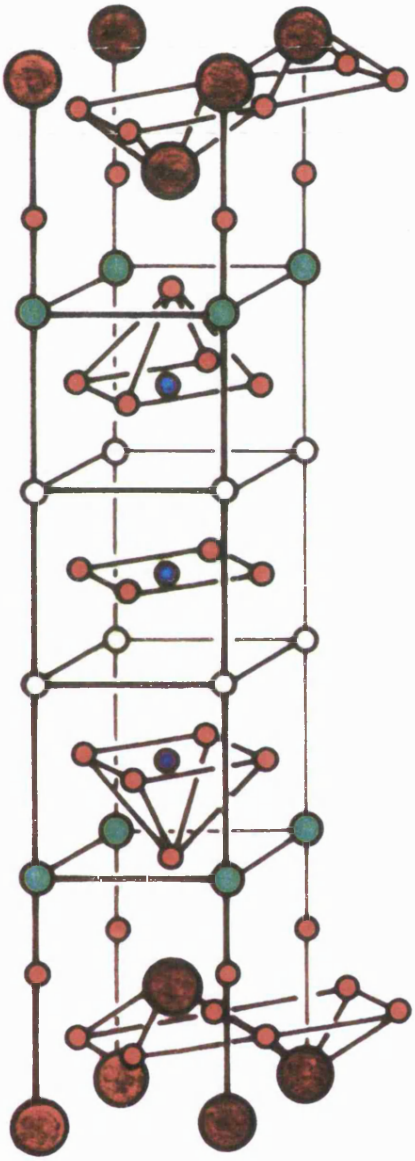

Figure 5.6
The crystal structure of $Bi_2Sr_2Ca_2Cu_3O_{10+y}$. The colours are as follows: red = O, open circle = Ca, blue = Cu, green = Sr, brown = Bi. Pb substitution occurs on Bi sites.

to a large (about 3Å) interlayer spacing [Bordet et al (1988)]. Crystallites of these compounds cleave easily between these layers.

Lead substitution has been extensively studied [Yanagisawa et al (1988), Murayama et al (1988) and Mazaki et al (1988)] in $Bi_{1-x}Pb_xCaSrCu_2O_5$ (Bi1112) and also in $Bi_{2-x}Pb_xCa_2Sr_2Cu_3O_{14}$ (Bi2223). The positive features of lead substitution are: (1) the effective copper valence is increased with doping, (2) lead and bismuth belong to the same group in the periodic table family and form the layer structure and (3) lead lowers the melting point of the host compound which is found to be advantageous for promoting the high T_c phase [Nobumasa et al (1988)]. Partial replacement of lead for bismuth in Bi1112 (x=0.3) compound increases the volume fraction of the high T_c phase which gets enhanced by increasing the annealing time, although the X-ray diffraction pattern show the system to remain multiphase [Yanagisawa et al (1988)]. The Bi2223 compound is also found to respond in a nearly identical fashion to lead substitution; for x=0.25 T_c is 105K [Murayama et al (1988)]. Similarly, the addition of lead in Bi2223 is also found to favour the formation of high T_c phase [Mizuno et al (1988)]. The crystal structure of the lead doped Bi2212 and Bi2223 are similar to that of the undoped compounds.

CHAPTER SIX

ELASTIC PROPERTIES OF THE ELECTRON SUPERCONDUCTOR $Nd_{1.85}Ce_{0.15}CuO_{4-y}$ AND ITS PARENT COMPOUND Nd_2CuO_{4-y}

6.1 INTRODUCTION

Measurements of the ultrasonic wave velocities as a function of hydrostatic pressure and temperature on the $Nd_{1.85}Ce_{0.15}CuO_{4-y}$ compound have been carried out. As the work proceeded, it became clear that an understanding of the properties of $Nd_{1.85}Ce_{0.15}CuO_{4-y}$ requires knowledge of the elastic properties of the host material Nd_2CuO_{4-y}, and this has formed an integral part of the study.

The samples studied here were prepared as described in chapter 4. X-ray diffraction techniques were employed to ascertain if the superconducting samples had the required composition as reported by other groups and also to make sure that they were single phase material. From those results the lattice parameters had been calculated. Subsequently the thermal expansion tensor components were obtained using a least square fit to the temperature dependence of the lattice parameters. The results of these studies are discussed in section 6.2.

To ensure that the $Nd_{1.85}Ce_{0.15}CuO_{4-y}$ samples were superconducting, resistivity measurements were made down to liquid helium temperature. The data obtained for the superconductor and its parent compound Nd_2CuO_4 are discussed in section 6.3.

To find out if the $Nd_{1.85}Ce_{0.15}CuO_{4-y}$ samples were n-type materials, the thermoelectric power was measured as a function of temperature. The results are presented in section 6.4.

The temperature and pressure dependences of ultrasonic longitudinal and shear wave velocities and the elastic constants in $Nd_{1.85}Ce_{0.15}CuO_{4-y}$ and Nd_2CuO_{4-y} samples were measured in order to detect any anomalies in the elastic behaviour of these materials. The results are fully analysed in section 6.5. The effects of porosity on the elastic properties are also discussed in that section.

6.2 THE X-RAY DIFFRACTION MEASUREMENTS

The main aim of these measurements was to ensure that the materials under investigation had the desired composition. The $Nd_{2-x}Ce_xCuO_{4-y}$ solid solutions have the tetragonal Nd_2CuO_{4-y} (*T'*) structure, comprising CuO_2 sheets with no apical oxygen. The X-ray diffraction measurements showed that the $Nd_{1.85}Ce_{0.15}CuO_{4-y}$ specimens consisted of a single phase with this Nd_2CuO_4 type structure. The lattice parameters of the superconductor measured at 292K are in excellent agreement with those obtained by other groups as shown in table 6.1.

The lattice parameters for the parent compound Nd_2CuO_{4-y} were calculated at 292K and the comparison in table 6.2 with those reported by other workers shows that the results were in good agreement.

That $Nd_{1.85}Ce_{0.15}CuO_{4-y}$ has a smaller c-axis lattice parameter than Nd_2CuO_{4-y} while the a-axis parameters are almost identical (figure 6.1), is consistent with the fact that Ce ions in $Nd_{1.85}Ce_{0.15}CuO_{4-y}$ being in the intermediate valence state (Prof. Saunders private communication). In the T' structure the a-axis parameter is determined by the rigid nature of the CuO_2 planes. Replacement of Nd^{3+} (ionic radius 1.08Å) by Ce^{3+} (ionic radius 1.14Å) should not lead to any marked change in the c-axis parameter. However, the

Table 6.1. Comparison between the lattice parameters for $Nd_{1.85}Ce_{0.15}CuO_{4-y}$ obtained in this work with the data reported by other groups.

Reference	a (Å)	c (Å)
This work	3.943±0.002	12.085±0.005
López-Morales et al (1989)	3.960	12.110
Paulus et al (1990)	3.942	12.060
Peng et al (1990)	3.951	12.100
Tokura et al (1989)	3.950	12.070

Table 6.2. Comparison between the lattice parameters for the parent compound Nd_2CuO_{4-y} obtained in this work with the data reported by other groups.

Reference	a (Å)	c (Å)
This work	3.945±0.001	12.154±0.003
Allan et al (1989)	3.945	12.171
Müller-Buschbaum and Wollschlager (1975)	3.945	12.171

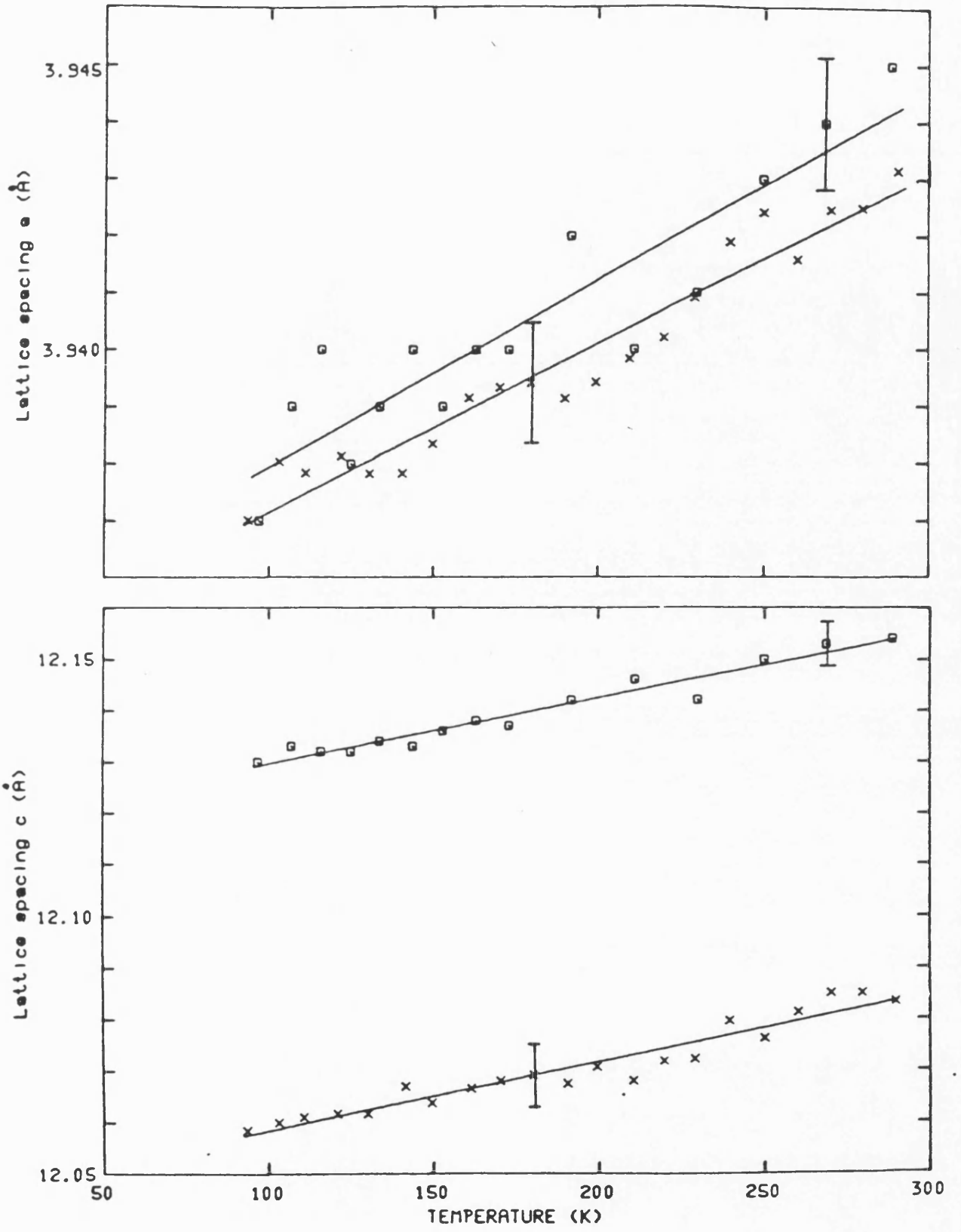

Figure 6.1
The temperature dependences of the lattice parameters of $Nd_{1.85}Ce_{0.15}CuO_{4-y}$ (sample 2) (crosses) and Nd_2CuO_{4-y} (squares).

intermediate valence Ce ion is substantially smaller than Ce^{3+} (by about 10% for $Ce^{3.5+}$), and its substitution for Nd^{3+} should only cause a reduction in the c-axis parameter as found [Fanggao et al (1990a)].

The temperature dependences of the lattice parameters of both the superconductor and the host material measured on cooling down to 92K are shown in figure 6.1 [Fanggao et al (1990a)]; similar results were obtained on warming. To obtain the thermal expansion tensor components, the results in figure 6.1 have been fitted to a straight line by a least mean square procedure; for $Nd_{1.85}Ce_{0.15}CuO_{4-y}$ α_{11} is equal to $(8.1\pm0.3)\times10^{-6}K^{-1}$ and α_{33} to $(1.5\pm0.1)\times10^{-5}K^{-1}$ and for Nd_2CuO_{4-y} α_{11} is equal to $(8.4\pm0.9)\times10^{-6}K^{-1}$ and α_{33} to $(10.5\pm0.6)\times10^{-6}K^{-1}$. The observed larger value of α_{33} than α_{11} in superconducting $Nd_{1.85}Ce_{0.15}CuO_{4-y}$ (whereas α_{33} is almost equal to α_{11} for Nd_2CuO_{4-y}) would be attributed for a temperature dependent Ce intermediate valence in the doped compound $Nd_{1.85}Ce_{0.15}CuO_{4-y}$. In layer-like crystals, binding between the successive layers tends to be weaker than that due to interlayer forces. Vibrational modes are more easily excited in the softer direction, so that the thermal expansion and linear compressibility are greater in this direction. The difference

between the two tensor components is not as great as might be expected for a truly layer-like compound (Prof. Saunders, private communication).

6.3 THE ELECTRICAL RESISTANCE MEASUREMENTS

One of the most important experiments to be done when working in the field of superconductivity is to measure the electrical resistance of the sample under investigation to check whether it is indeed a superconductor. The temperature dependences of the electrical resistance of the $Nd_{1.85}Ce_{0.15}CuO_{4-y}$ samples are shown in figure 6.2. The data for the sample as it was initially prepared are labelled sample 1 and those for the resintered sample are labelled sample 2. The electrical properties of the material were changed during the resintering process (which is clear in figure 6.2), the resintered sample (sample 2) having a higher normal state resistance (R_{292K} = 0.0252 Ω) and a broader superconducting transition than sample 1 (with R_{292K} = 0.0185 Ω). Initially, the superconducting onset temperature was about 23.5K and zero resistance was achieved at 19K. After resintering, the onset temperature had reduced slightly to around 23.3K and the material reached zero resistance at 17K. The normal state resistance for each sample increased with decreasing temperature, this increase developing more rapidly for the resintered material (8% for sample 2 and 4.2% for sample 1 in the temperature range 293-24K).

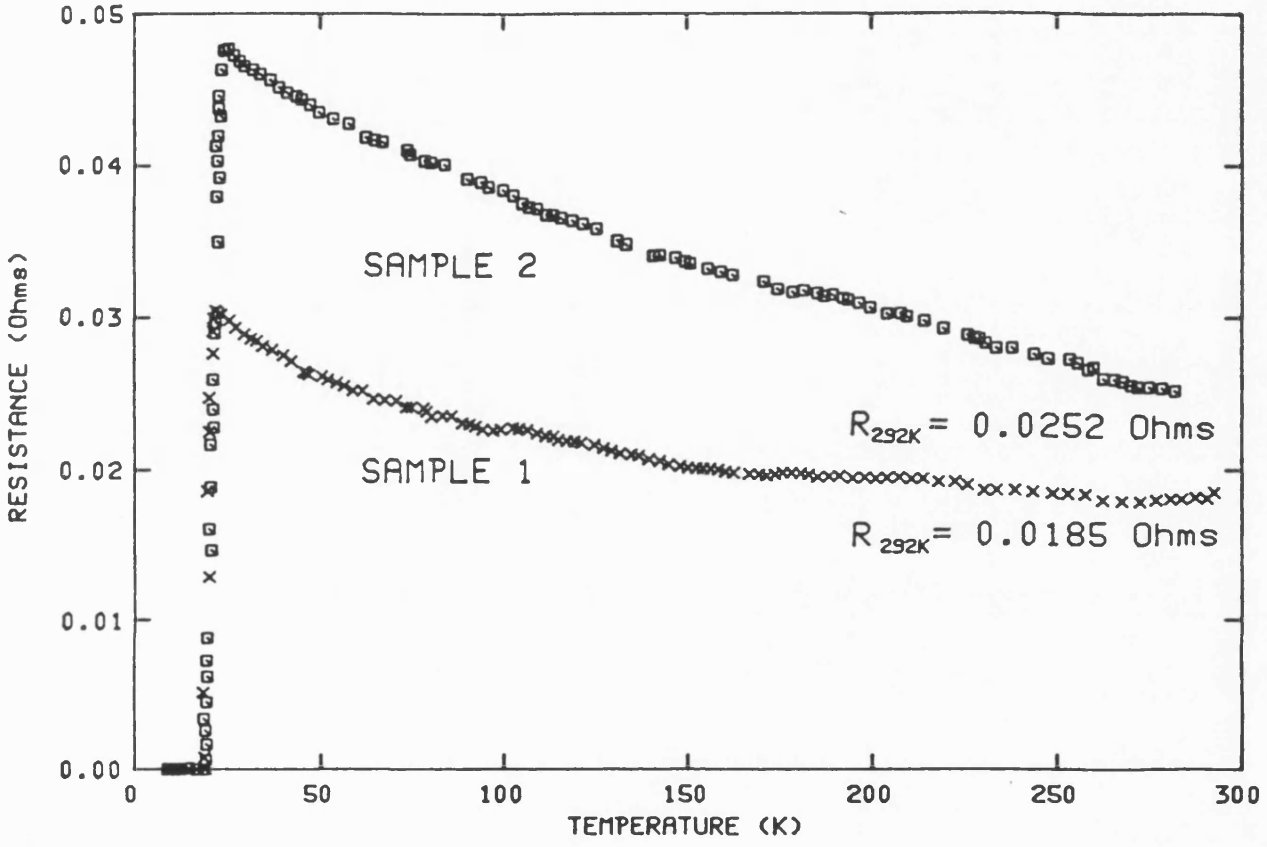

Figure 6.2
The temperature dependence of the electrical resistance of the $Nd_{1.85}Ce_{0.15}CuO_{4-y}$, after initial processing (sample 1) and after further grinding, pressing and re-firing (sample 2).

Peng et al (1990) measured the resistivity of a $Nd_{1.85}Ce_{0.15}CuO_{4-y}$ sample. They obtained a normal state room temperature resistivity of 0.028 $\Omega.cm$ and an increase in the resistivity (by about 18% in the temperature region 293-28K) as the temperature decreased followed by a sharp drop towards zero resistivity starting at 28K associated with the superconducting state and reaching zero resistivity at 15K. López-Morales et al (1989) found a similar behaviour in their $Nd_{1.85}Ce_{0.15}CuO_{4-y}$ sample with a normal state room temperature resistivity of 0.01 $\Omega.cm$. They found an increase in the resistivity by about 10% as the temperature decreased from room temperature to 24K. This increase was followed by a sharp decrease and a zero resistivity achieved at 16K. In contrast Tokura et al (1989) found that the resistivity for their $Nd_{1.85}Ce_{0.15}CuO_{4-y}$ sample was constant and show no change in the temperature range 300-24K, but they also found a sharp decrease in resistivity at 24K with zero resistivity achieved at 19K. They obtained a room temperature resistivity of 0.015 $\Omega.cm$. The results shown in figure 6.2 indicate that the $Nd_{1.85}Ce_{0.15}CuO_{4-y}$ compound sample made here shows temperature dependence of the electrical resistance similar to the temperature dependence of resistivity found by these other workers.

The electrical resistance measurements of the parent (or host) compound Nd_2CuO_{4-y} sample are shown in figure 6.3 [Fanggao et al (1990a)]. The results show that this parent sample was not a superconductor and had a room temperature resistance of 0.8 Ω. López-Morales et al (1989) measured the resistivity as a function of temperature in a Nd_2CuO_{4-y} sample. They obtained a room temperature resistivity of 10 Ω.cm. The electrical resistance above about 90K of the Nd_2CuO_{4-y} sample (figure 6.3) is similar to that obtained by López-Morales et al (1989). A new feature of the present work is that the electrical resistance measurements have been made below 90K and down to 25K. The data obtained (figure 6.3) show two peaks at 41K and 74K which might be related to the two magnetic transitions found from neutron and X-ray diffraction studies as broad peaks at about 30 and 75K [Skanthakumar et al (1989)].

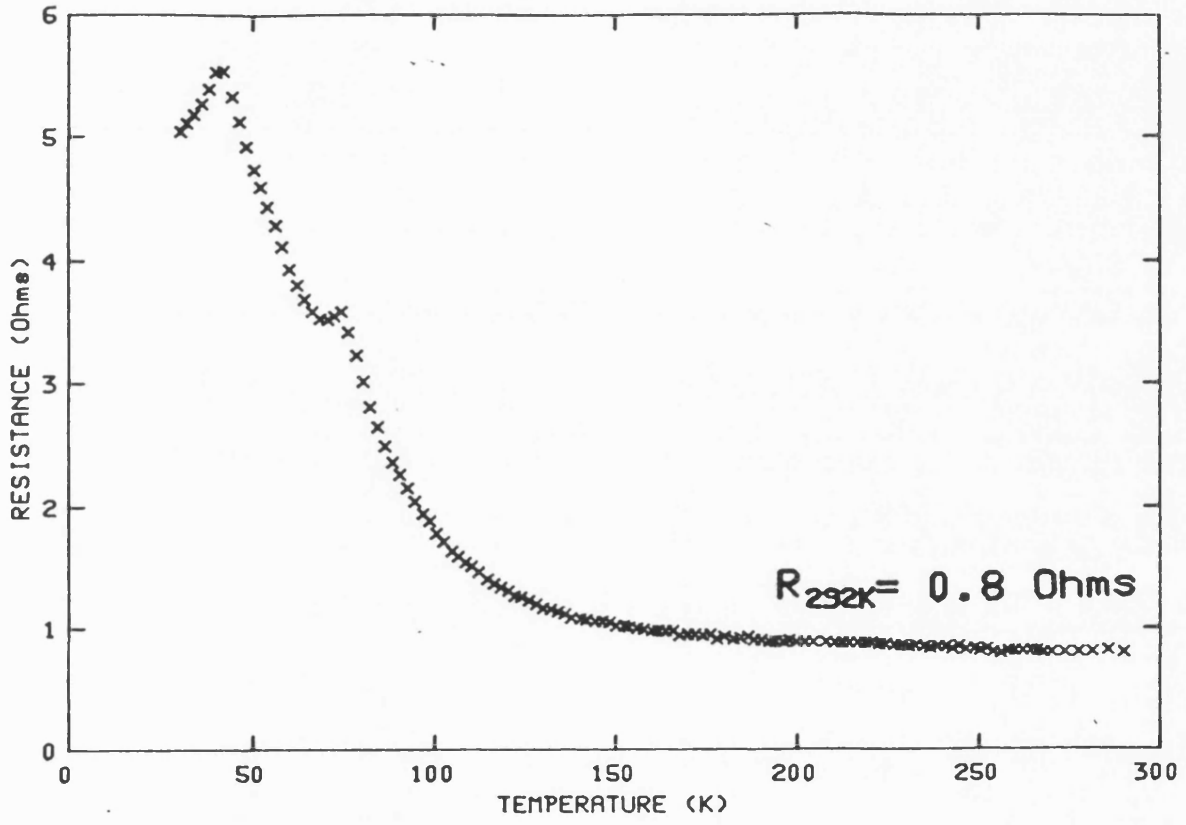

Figure 6.3
The electrical resistance of ceramic specimen of Nd_2CuO_{4-y} as a function of temperature.

6.4 THE THERMOELECTRIC POWER MEASUREMENTS

Thermoelectric power (*TEP*) measurements were made [Freestone (1990)] down to liquid helium temperature to ascertain whether the samples of $Nd_{1.85}Ce_{0.15}CuO_{4-y}$ were indeed n-type materials. The data shows that the absolute thermopower remains negative over the whole range of temperature above T_c (figure 6.4); it goes to zero in the superconducting state. The thermopower in the samples studied in this work is almost independent of temperature between 30K and 200K. A negative thermopower is evidence rather than conclusive proof that the superconductivity in the material is due to electrons. However, a note of caution must be made regarding the concept of holes and electrons, especially as shown by the Hall effect and thermoelectric power. In $YBa_2Cu_3O_{7-x}$ and $Bi_2Sr_2CaCu_2O_{8+x}$ the thermopower is negative, or electron-like, parallel to the copper oxide planes but positive, or hole-like, perpendicular to them [Yu et al (1988)]. Therefore, these measurements can be misleading and at best indicate the type of majority normal state carriers and not necessarily whether these, or minority carriers of opposite sign, pair to give superconductivity. In historical retrospective, it is interesting to note that the sign of the Seebeck effect for all undoped lanthanide 2-1-4 compounds, except La itself, is negative [Ganguly and Rao

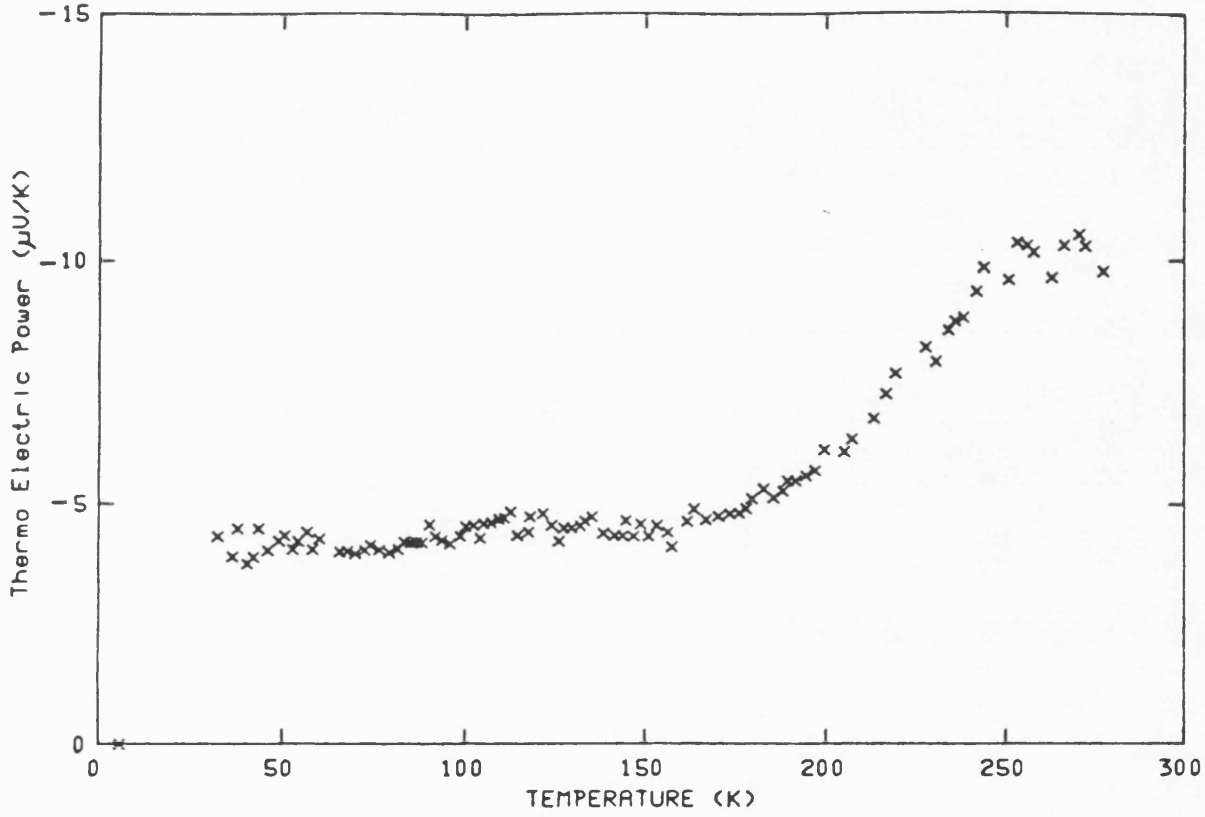

Figure 6.4
The temperature dependence of the absolute thermoelectric power of $Nd_{1.85}Ce_{0.15}CuO_{4-y}$ (sample 2).

(1973), Shaplygin et al (1979)]. A small, negative thermopower is observed in the $Nd_{1.85}Ce_{0.15}CuO_{4-y}$ compound sample studied here (S_{292K} = $-9.7\mu V/K$) compared with the data on $La_{2-x}Sr_xCuO_{4-y}$ which shows a large, positive thermopower (S_{292K} = $+84.8\mu V/K$ for $La_{1.9}Ba_{0.1}CuO_4$ and S_{292K} = $+52.5\mu V/K$ for $La_{1.9}Sr_{0.1}CuO_4$) [Cooper et al (1987)]. A negative thermopower in $Nd_{2-x}Ce_xCuO_{4-y}$ solid solutions has been observed by Takagi et al (1989) and López-Morales et al (1989) although, surprisingly, Lim et al (1989) found a small, positive thermopower (S_{292K} = $+0.4\mu V/K$) for their material which they suggested might indicate the presence of more than one type of charge carrier. The observation that the thermopower of $Nd_{1.85}Ce_{0.15}CuO_{4-y}$ does not follow a linear temperature dependence but becomes essentially independent of temperature below about 180K is consistent with an increasing electron density as the temperature decreases due to rising 4+ contribution to the Ce ion intermediate valence.

6.5 THE ULTRASONIC VELOCITY MEASUREMENTS

6.5.1 THE TEMPERATURE DEPENDENCES OF ULTRASONIC WAVE VELOCITIES

The measured 5MHz longitudinal and shear ultrasonic wave velocities of $Nd_{1.85}Ce_{0.15}CuO_{4-y}$ and Nd_2CuO_{4-y}, using Nonaq as a bonding material, increase continuously with decreasing temperature (figures 6.5 and 6.6). There is no reduction in the velocity as the temperature is reduced of the type found in $La_{2-x}Sr_xCuO_4$, which has been attributed to mode softening [Bishop et al (1987a), Horie et al (1987b) and Lüthi et al (1987)] and associated with the orthorhombic-tetragonal phase transition. However, the temperature dependence of the longitudinal wave velocity of $Nd_{1.85}Ce_{0.15}CuO_{4-y}$ shows a change of gradient near 220K. This is also observed, but is much less marked, in the shear wave velocity (figure 6.6). The data presented in figures 6.5 and 6.6 agree with those reported for a $Nd_{1.85}Ce_{0.15}CuO_{4-y}$ single crystal by Saint-Paul et al (1990a) who found a change in gradient near 200K but no anomaly in the sound velocity near T_c.

The parent Nd_2CuO_{4-y} sample does not show a remarkable change of slope in either the longitudinal or the shear ultrasonic wave velocity around 220K (figures 6.5 and 6.6). However, it does show quite marked hysteresis between warming and cooling in the temperature range 200-290K. Although such

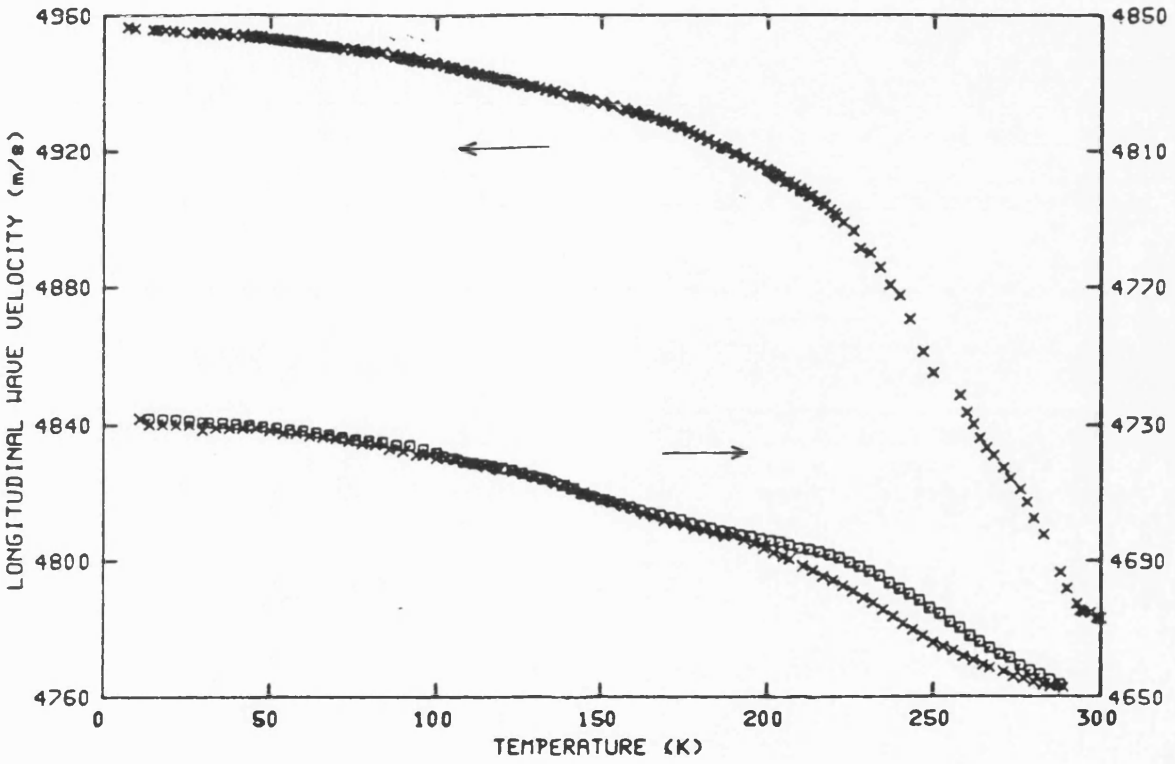

Figure 6.5
The temperature dependences of the ultrasonic longitudinal waves velocities for $Nd_{1.85}Ce_{0.15}CuO_{4-y}$ (the left hand co-ordinates) and Nd_2CuO_{4-y} (the right hand co-ordinates) samples. Hysteresis occurs between warming (squares) and cooling (crosses) for the Nd_2CuO_{4-y} sample. No hysteresis effect was found for $Nd_{1.85}Ce_{0.15}CuO_{4-y}$ sample.

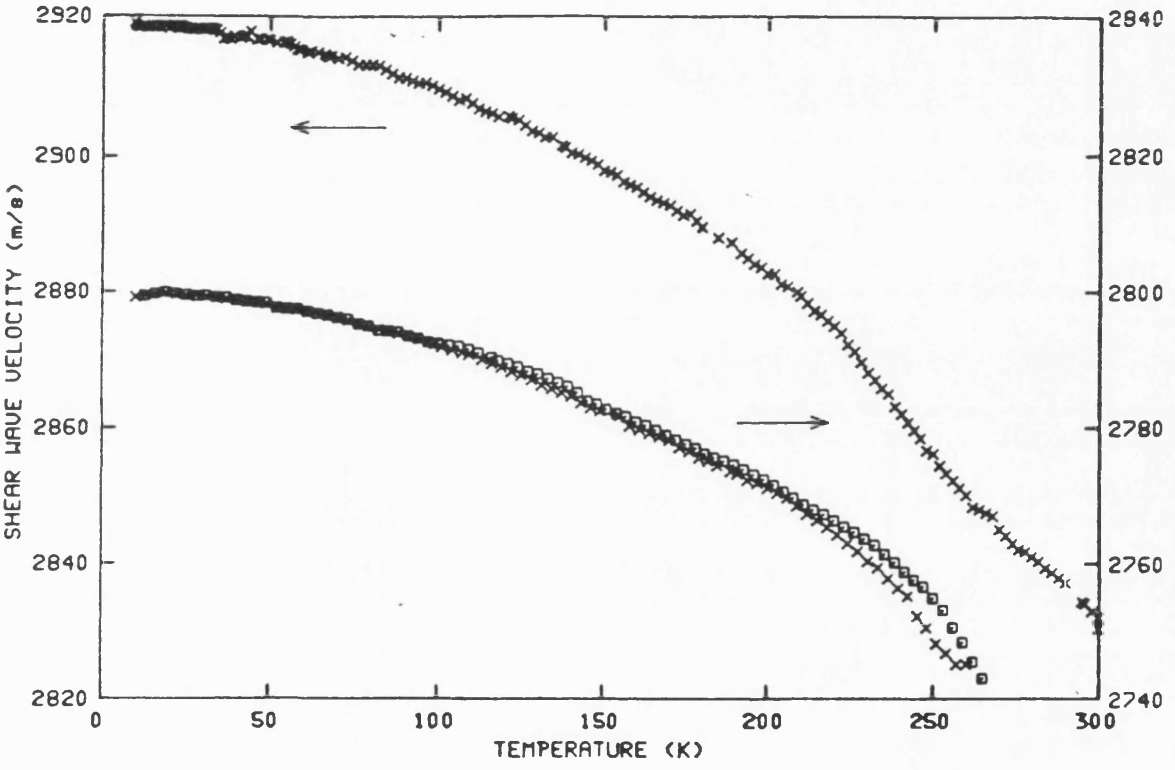

Figure 6.6
The temperature dependences of the ultrasonic shear waves velocities for $Nd_{1.85}Ce_{0.15}CuO_{4-y}$ (the left hand co-ordinates) and Nd_2CuO_{4-y} (the right hand co-ordinates) samples. As observed for the longitudinal velocity (figure 6.5) hysteresis occurs between warming (squares) and cooling (crosses) for the Nd_2CuO_{4-y} sample, but not in the $Nd_{1.85}Ce_{0.15}CuO_{4-y}$ sample.

behaviour is often associated with a structural transition, the X-ray diffraction and *DSC* studies indicate that this is not so for Nd_2CuO_{4-y}.

The unusual temperature dependence of the longitudinal wave velocity for $Nd_{1.85}Ce_{0.15}CuO_{4-y}$ (figure 6.5) may result from an intermediate valence effect. On cooling, a number of cerium compounds undergo a valence change from the Ce^{3+} ($4f_1$) state towards the Ce^{4+} ($4f_0$) state [Varma (1976), Robinson (1979) and Jayaraman (1979)]; however, the alteration in the number of $4f$ electrons per ion is smaller than expected for a transition from one integral valence state to another: the resultant phase has an intermediate valence. In addition to the present findings, there is mounting evidence that the Ce ions in $Nd_{2-x}Ce_xCuO_{4-y}$ solid solutions are in an intermediate valence configuration. Application of pressure at temperatures above T_c decreases the electrical resistivity by a rate of $R^{-1}dR/dP$ of -0.089 GPa^{-1} [Murayama et al (1989)]; this is consistent with an increasing valence with pressure and hence decreasing mean ion size of cerium.

Hall effect data for $Nd_{1.88}Ce_{0.12}CuO_{4-y}$ single crystals show that the electron density n_H falls with temperature down to about 150K where it levels out [Hidaka and Suzuki (1989)]. The levelling out below 150K is consistent with an inducement of the intermediate valence material towards the smaller

ion 4+ state: there is an increase of the electron density as the temperature falls and the increasing Ce^{4+} component supplies more electrons to the Fermi sea. The temperature dependences of the longitudinal wave velocity (figure 6.5), C_l^n (figure 6.7a) and the bulk B^n modulus (figure 6.8) for $Nd_{1.85}Ce_{0.15}CuO_{4-y}$ can be understood on the basis of this change of the degree of intermediate valence due to an increase in 4+ component as the temperature decreases [Fanggao et al (1990a)]. The change of gradient observed in the temperature dependence of the longitudinal wave velocity is consistent with this picture of an increasing coupling of the volume strain associated with the wave to that of the Ce ions whose net valence increases as the temperature is reduced below about 200K. Such enhanced coupling would cause the anomalous temperature dependence of the longitudinal wave velocity but not that of the volume independent shear modes. One can say that the intermediate valence of the cerium ion plays an important role in the electrical and elastic properties of this superconducting material (Prof. Saunders, private communication).

An interesting feature was found in the temperature dependence of the ultrasonic wave velocities in the $Nd_{1.85}Ce_{0.15}CuO_{4-y}$ sample after pressure cycling. The temperature dependence of the longitudinal wave velocity (figure 6.9a)

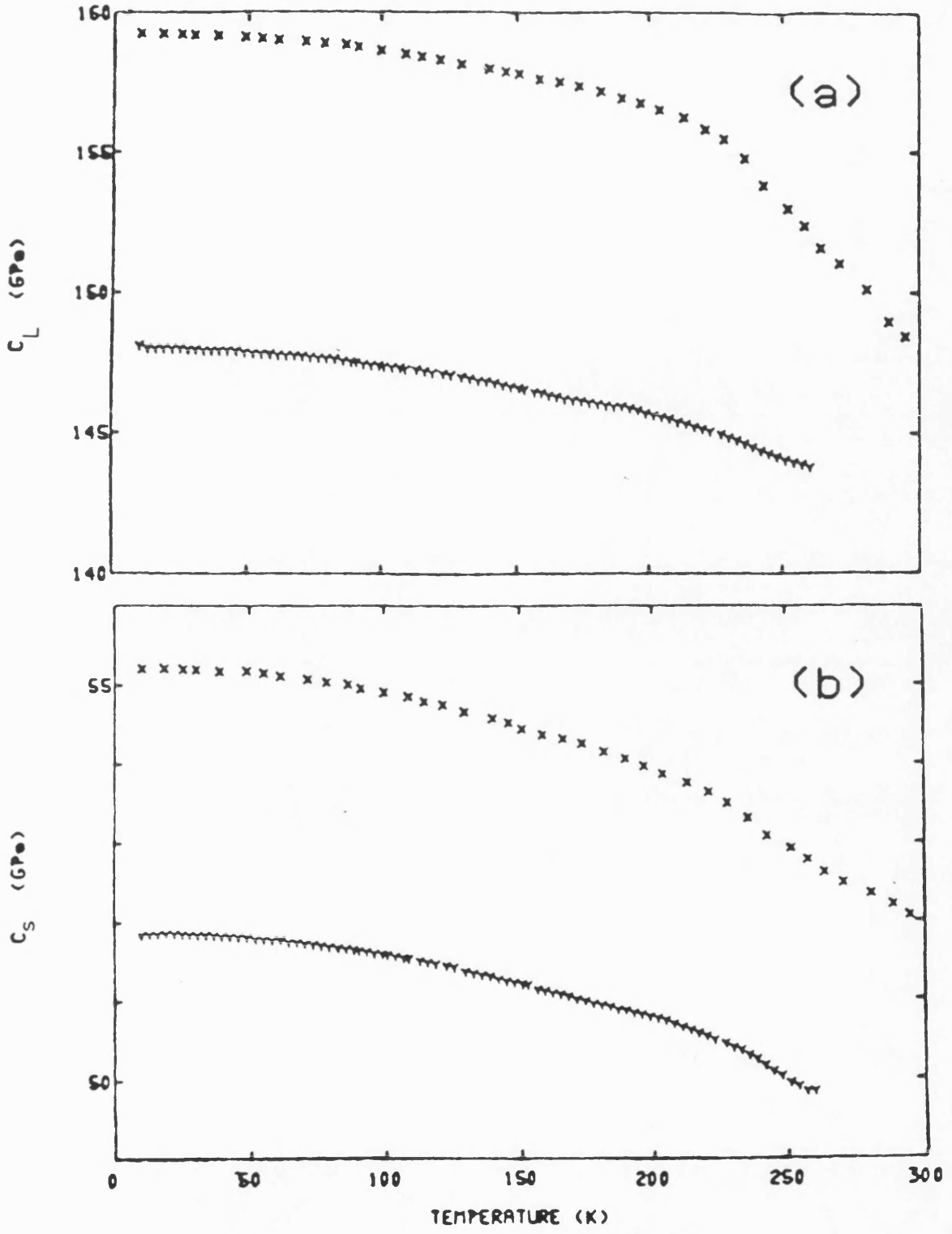

Figure 6.7
The temperature dependences of (a) the longitudinal modulus C_L and (b) the shear modulus C_S for $Nd_{1.85}Ce_{0.15}CuO_{4-y}$ (upper curves or crosses) and Nd_2CuO_{4-y} (lower curves or the Y symbols) samples.

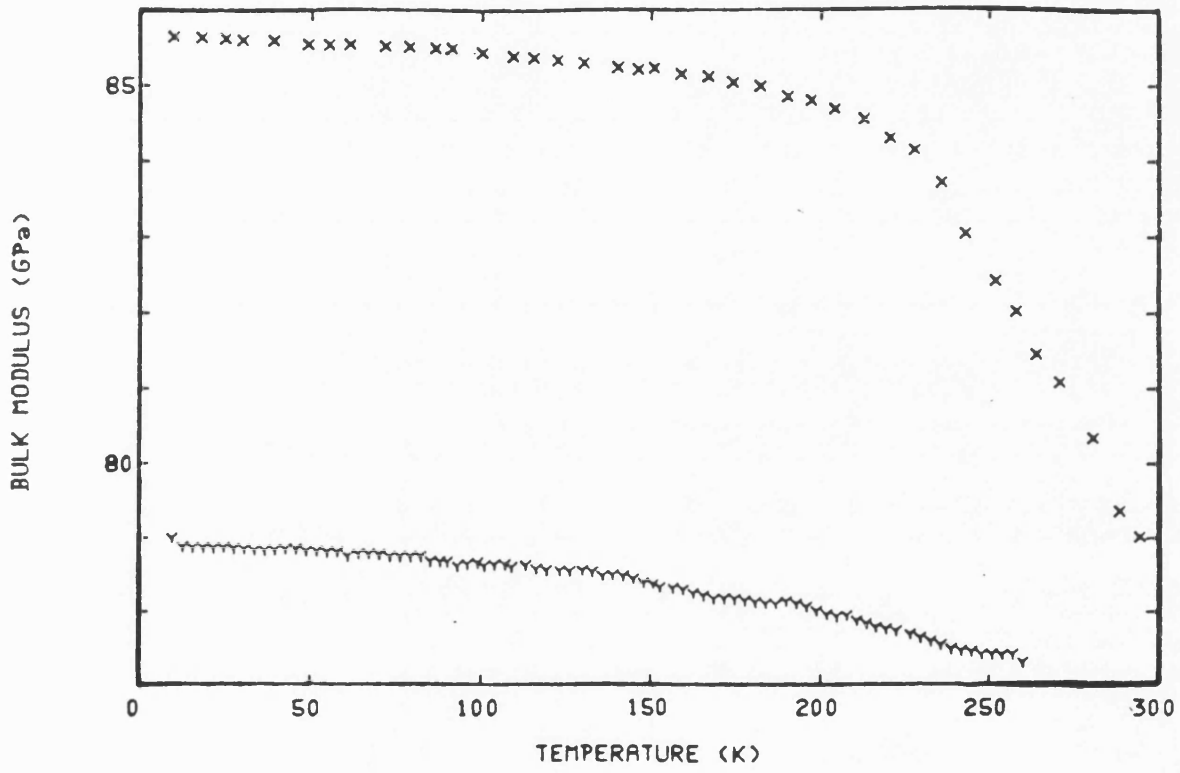

Figure 6.8
The temperature dependence of the bulk modulus for $Nd_{1.85}Ce_{0.15}CuO_{4-y}$ (upper curve) and Nd_2CuO_{4-y} (lower curve) samples.

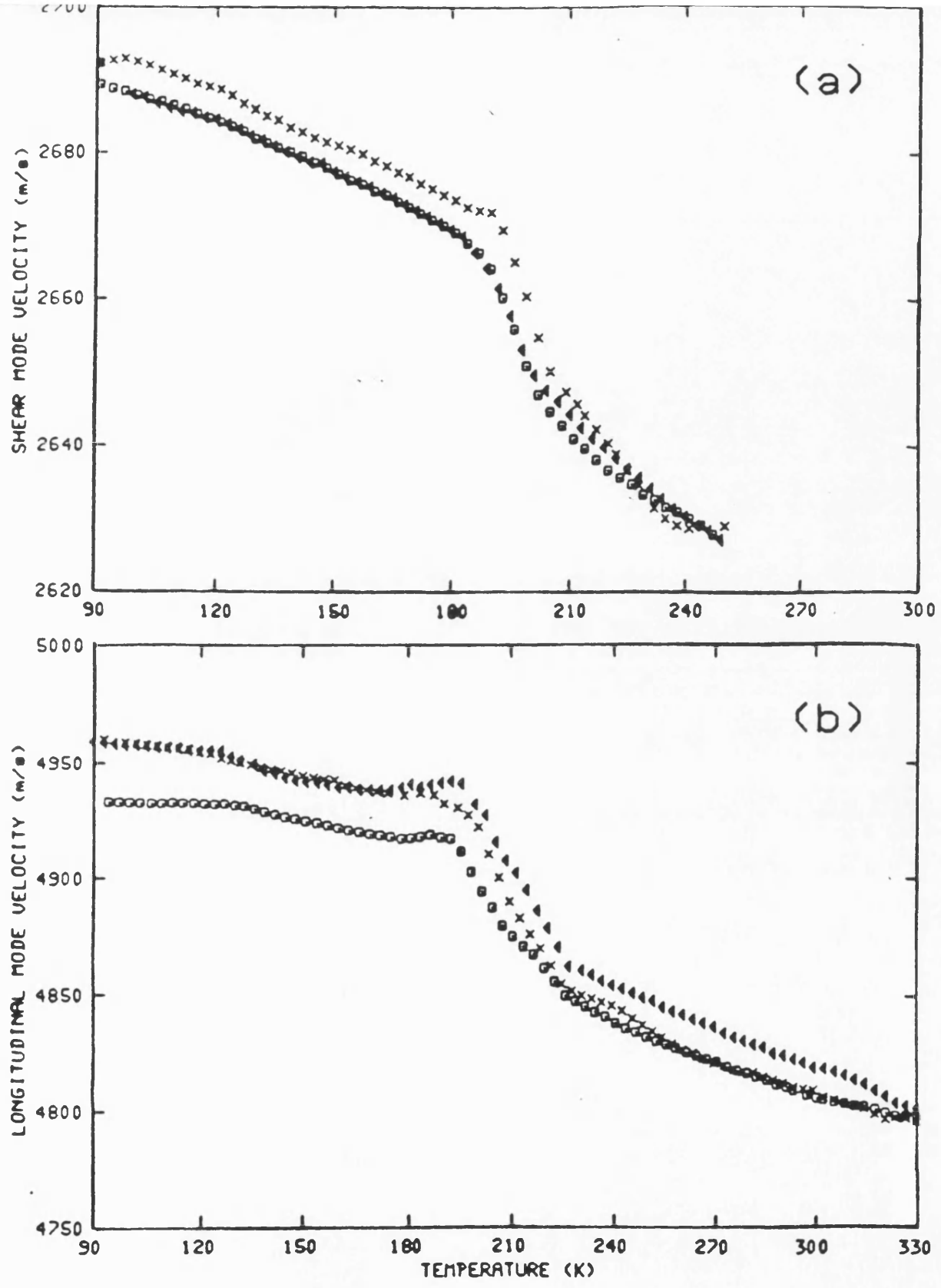

Figure 6.9

The temperature dependences of the velocities of (a) shear and (b) longitudinal ultrasonic waves for a $Nd_{1.85}Ce_{0.15}CuO_{4-y}$ sample at three different frequencies (5,10 and 15 MHz) (crosses, squares and triangles respectively). This data were taken after the sample was cycled under pressure and temperature.

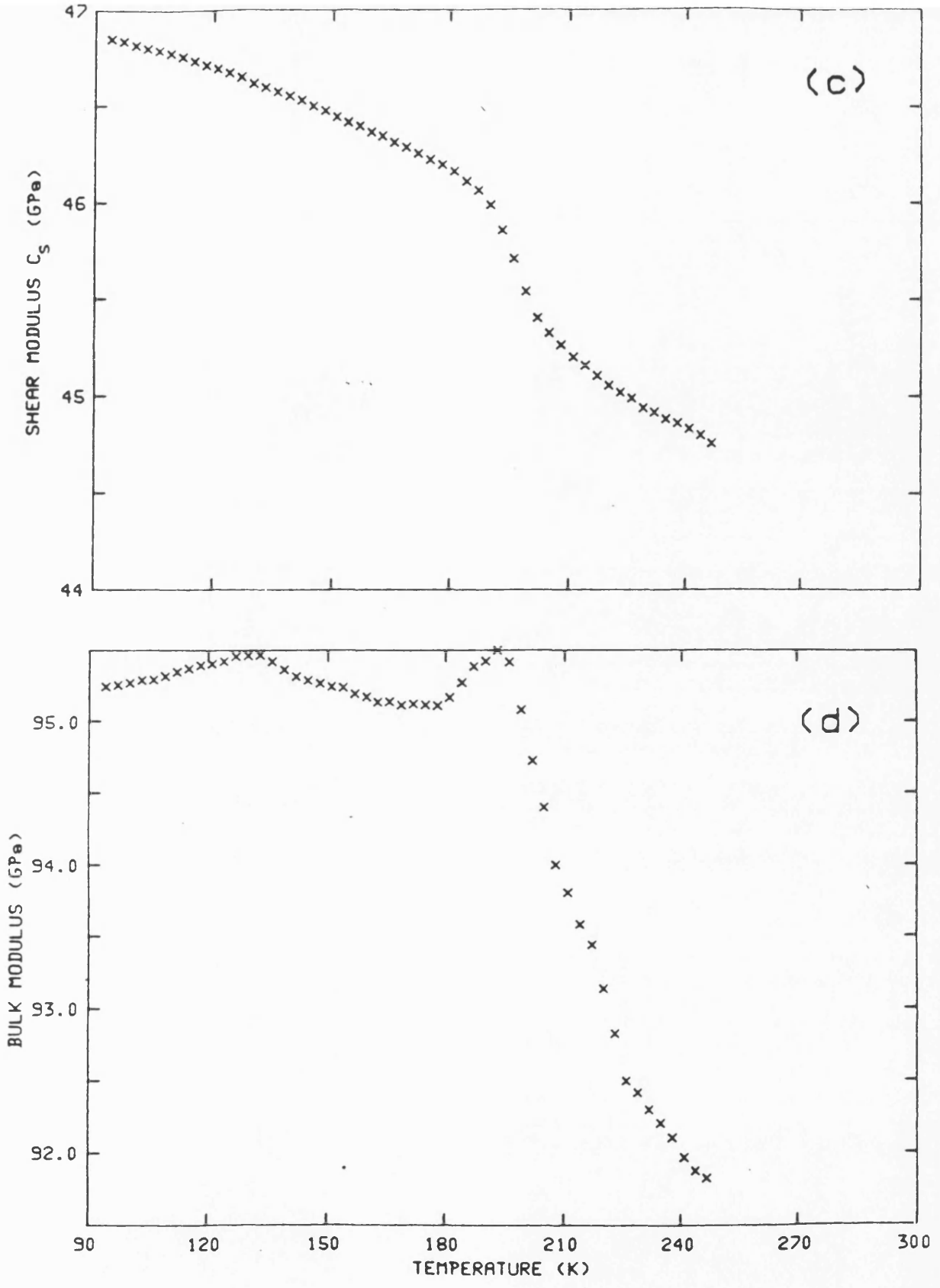

Figure 6.9
The temperature dependences of the (c) shear modulus C_S and (d) bulk modulus of the $Nd_{1.85}Ce_{0.15}CuO_{4-y}$ sample after it was cycled under pressure and temperature.

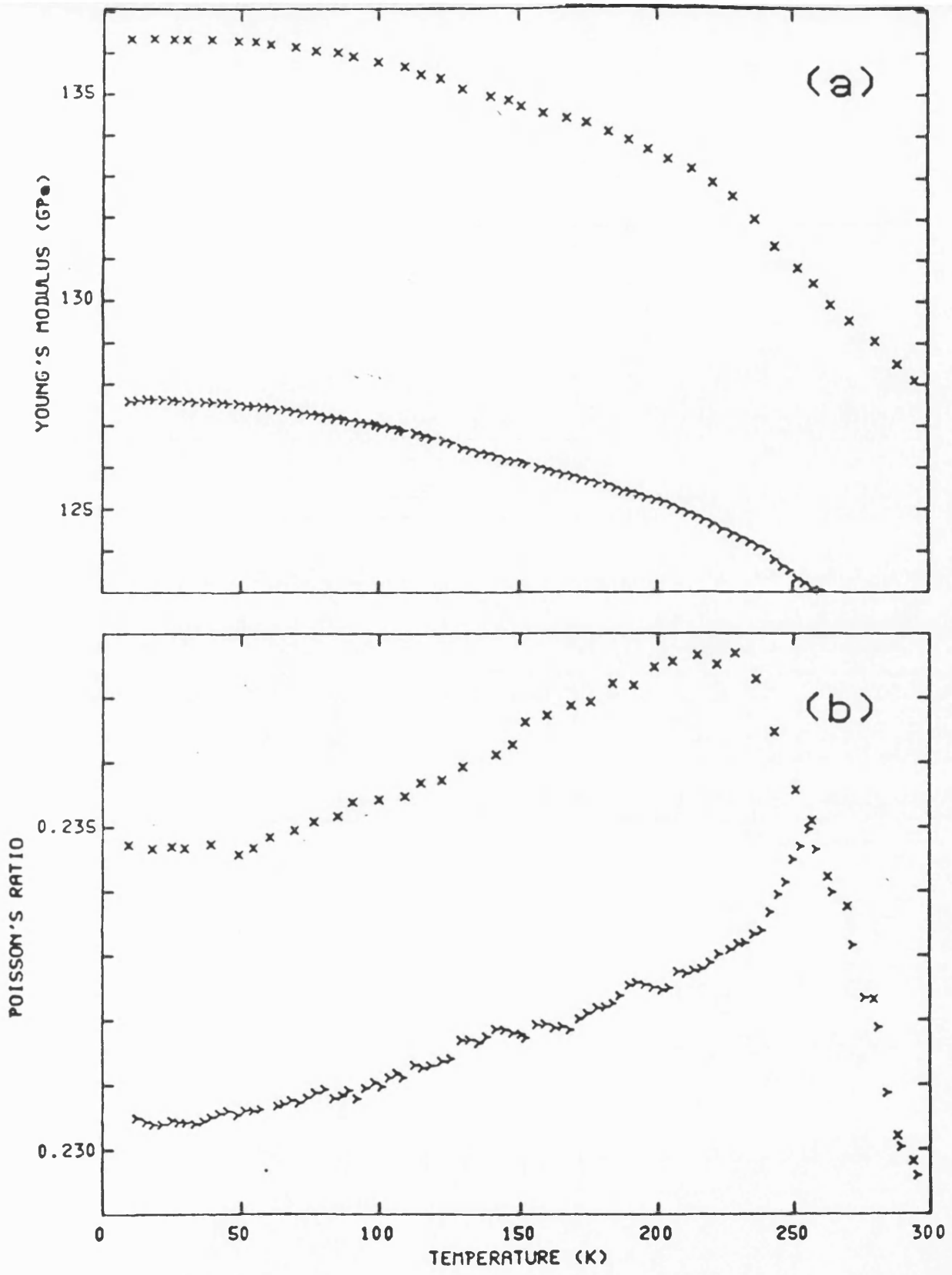

Figure 6.10
The temperature dependences of (a) the Young's modulus and (b) Poisson's ratio for $Nd_{1.85}Ce_{0.15}CuO_{4-y}$ (upper curves or crosses) and Nd_2CuO_{4-y} (lower curves or the Y symbols) samples.

shows a step-like behaviour (for three different frequencies) similar to that found in $YBa_2Cu_3O_{7-x}$ and $GdBa_2Cu_3O_{7-x}$ [Almond et al (1989)] with no hysteresis found between warming and cooling. The shear wave velocity shows the same behaviour (figure 6.9b). This behaviour, which was quite different from what was found earlier, can be attributed to the effect induced on the elastic properties of the material by the silicone oil (which is used as a pressure transmitting medium) forced into the pores under pressure.

6.5.2 THE PRESSURE DEPENDENCES OF ULTRASONIC WAVE VELOCITIES

The effect of hydrostatic pressure on the velocities of longitudinal and shear 5MHz ultrasonic waves propagated in a $Nd_{1.85}Ce_{0.15}CuO_{4-y}$ sample (using a 6mm quartz transducer and Resin as a bonding material) and its parent compound Nd_2CuO_{4-y} are shown in figures 6.11 and 6.12 respectively. The measured values of the ultrasonic velocities are given in table 6.3 together with the velocities values corrected for porosity (see section 4.12). In each case the measurements were reproducible and showed no hysteresis effects. The ultrasonic velocities increase linearly with pressure, much more steeply for the longitudinal than for the shear mode. The linear dependence of ultrasonic wave velocities on pressure found for $Nd_{1.85}Ce_{0.15}CuO_{4-y}$ and its parent compound Nd_2CuO_{4-y} contrasts markedly with the non-linear behaviour observed in superconducting $YBa_2Cu_3O_{7-x}$ and $GdBa_2Cu_3O_{7-x}$ (see chapters 8 and 9 respectively), indicating that the higher order vibrational anharmonicity of the long wavelength phonons is much less in the Nd-based compounds.

6.5.3 THE ELASTIC CONSTANTS AND THEIR TEMPERATURE AND PRESSURE DEPENDENCES

From the measurements of the ultrasonic wave velocities, the two independent mean elastic constants C_L^n and C_S^n for an isotropic medium can be determined. These elastic constants

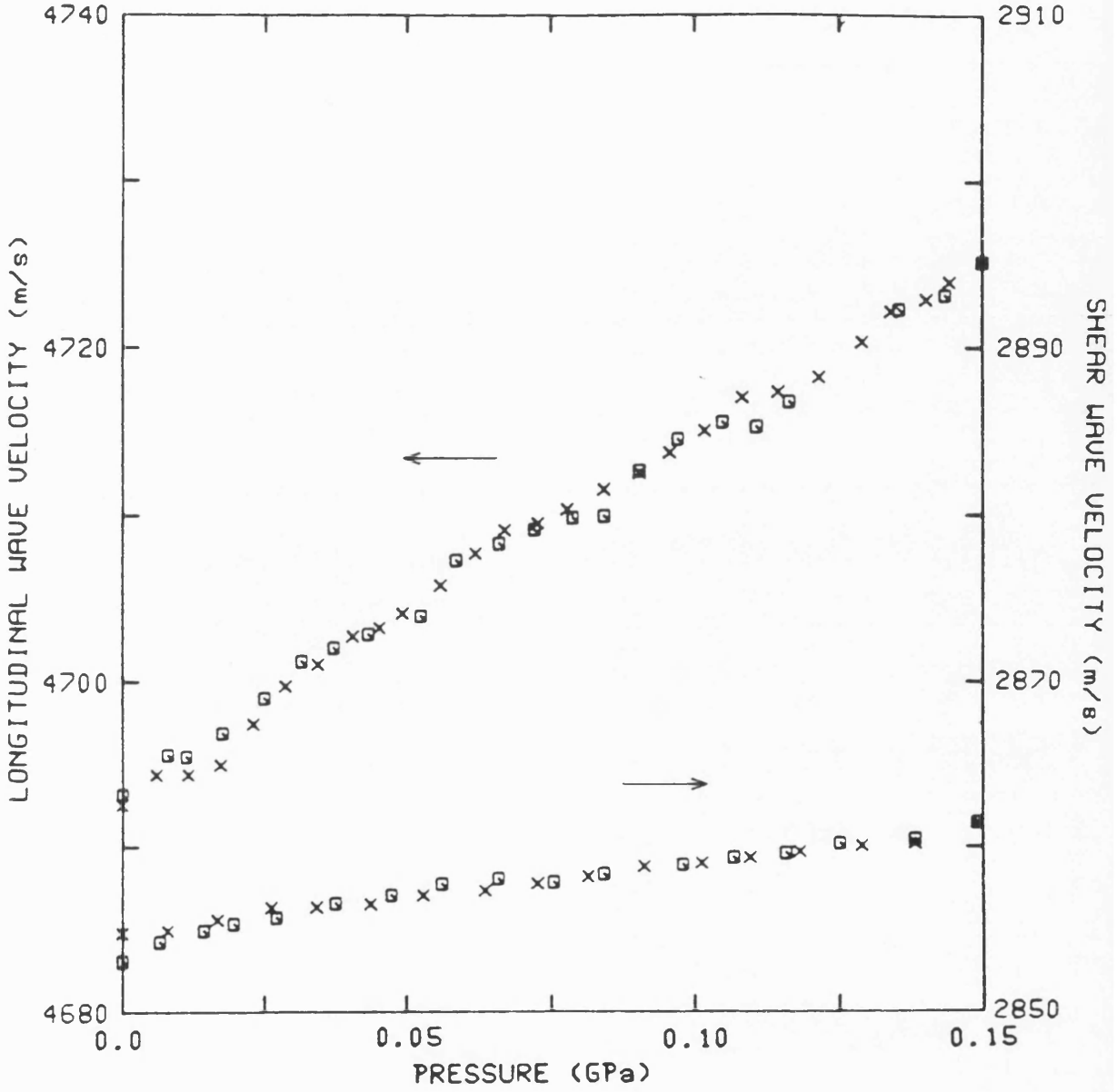

Figure 6.11
The hydrostatic pressure dependences of velocities of longitudinal (upper curve) and shear (lower curve) ultrasonic waves velocities propagated in $Nd_{1.85}Ce_{0.15}CuO_{4-y}$ at 295K. The crosses correspond to velocity measurements made with increasing pressure and the squares to data obtained as the pressure was decreased.

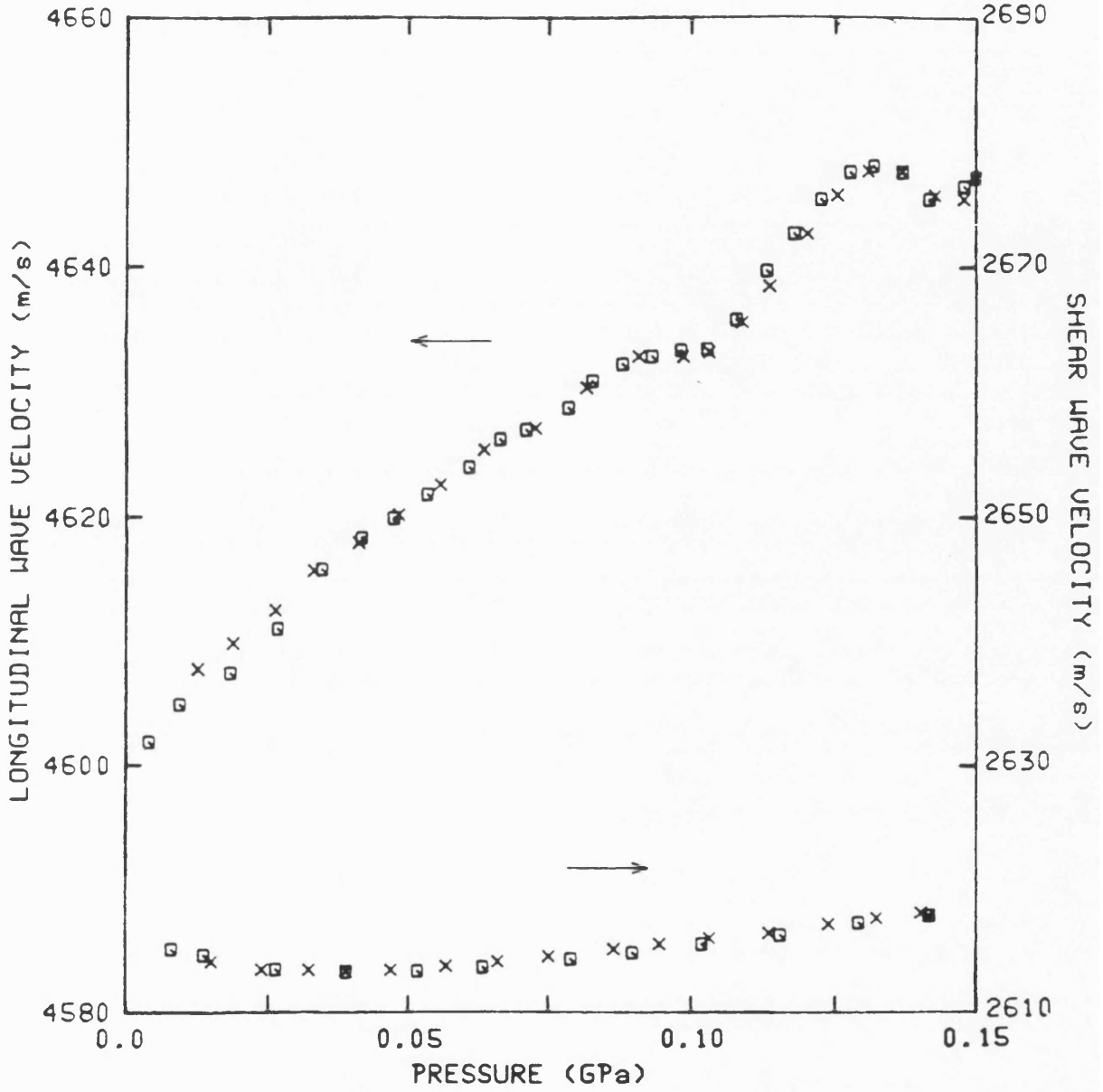

Figure 6.12
The hydrostatic pressure dependences of velocities of longitudinal (upper curve) and shear (lower curve) ultrasonic waves velocities propagated in Nd_2CuO_{4-y} at 295K. The crosses correspond to velocity measurements made with increasing pressure and the squares to data obtained as the pressure was decreased.

Table 6.3. Ultrasonic, elastic and physical properties at room temperature for the $Nd_{1.85}Ce_{0.15}CuO_{4-y}$ high temperature superconductor and its parent compound Nd_2CuO_{4-y}.

Property	$Nd_{1.85}Ce_{0.15}CuO_{4-y}$		Nd_2CuO_{4-y}	
	Porous	Non-porous matrix	Porous	Non-porous matrix
Density Kgm^{-3}	6481	7330	6425	7336
Porosity	0.12	-	0.13	-
Ultrasonic Velocities ms^{-1}				
Longitudinal V_L	4694	5010	4602	5069
Shear V_S	2854	3045	2609	2824
Bulk modulus B (GPa)	72	93	77	110
Young's modulus E (GPa)	128	164	111	150
Poisson's ratio	0.207	0.207	0.263	0.275
C_L (GPa)	143	184	136	189
C_S (GPa)	53	68	44	59
Acoustic Debye temperature (Θ_D^{el}) (K)	379	422	347	394
$(\partial B/\partial P)_{P=0}$	10.4	15.6	17.8	29.1
$(\partial C_L/\partial P)_{P=0}$	12.9	18.3	23	35.7
$(\partial C_S/\partial P)_{P=0}$	1.7	1.9	3.9	4.0
Superconducting transition temperature T_C (K)	21	-	-	-

at 295K together with the bulk B^n and Young's moduli, Poisson's ratio and the acoustic Debye temperature (Θ_D^{el}) for $Nd_{1.85}Ce_{0.15}CuO_{4-y}$ and its parent compound Nd_2CuO_{4-y} are given in table 6.3.

The temperature dependences of C_L^n and C_S^n for the $Nd_{1.85}Ce_{0.15}CuO_{4-y}$ and the Nd_2CuO_{4-y} compounds are shown in figure 6.7 and the bulk B^n modulus as a function of temperature for each compounds is shown in figure 6.8. The temperature dependences of the Young's modulus and Poisson's ratio for both the superconductor and the parent material are shown in figure 6.10. In $Nd_{1.85}Ce_{0.15}CuO_{4-y}$ for each property there is a clear change in slope around 220K which is not apparent in the parent material; furthermore the elastic constants of $Nd_{1.85}Ce_{0.15}CuO_{4-y}$ vary much more strongly with temperature than do those of Nd_2CuO_{4-y}. This marked contrast between the two compounds suggests that the elastic behaviour of $Nd_{1.85}Ce_{0.15}CuO_{4-y}$ is influenced by the presence of the cerium ions.

The ultrasonic wave velocities were measured in a $Nd_{1.85}Ce_{0.15}CuO_{4-y}$ sample after being cycled under pressure and temperature. The temperature dependences of C_S^n and the bulk modulus B^n in that sample are shown in figure 6.9c,d and it can be seen that the behaviour is different from that found

before the pressure cycling (figures 6.7b and 6.8). This difference can be attributed to the effects of the silicone oil (which was used as a pressure transmitting medium) injected into the pores on the elastic properties of that compound.

The as-measured hydrostatic pressure dependences of longitudinal C_L^n , shear C_S^n and the bulk B^n moduli for the superconductor $Nd_{1.85}Ce_{0.15}CuO_{4-y}$ are shown in part (a) of figures 6.13, 6.14 and 6.15 respectively and for the parent compound Nd_2CuO_{4-y} sample are shown in part (a) of figures 6.16, 6.17 and 6.18 respectively. These results have been corrected for the effect of porosity using the technique described in section 4.12. The pressure dependences of C_L^m , shear C_S^m and the bulk B^m moduli in the non-porous matrix (corrected for porosity) for $Nd_{1.85}Ce_{0.15}CuO_{4-y}$ and Nd_2CuO_{4-y} obtained by inserting the experimental data into equations (4.4) and (4.5) are shown in part (b) of figures 6.13-6.18. The hydrostatic pressure derivatives $(\partial C_L/\partial P)_{P-0}$, $(\partial C_S/\partial P)_{P-0}$ and $(\partial B/\partial P)_{P-0}$ determined at room temperature in the limit as pressure tends towards zero are given in table 6.3. Comparison between the elastic moduli measured for the porous medium with those determined for the non-porous matrix shows that

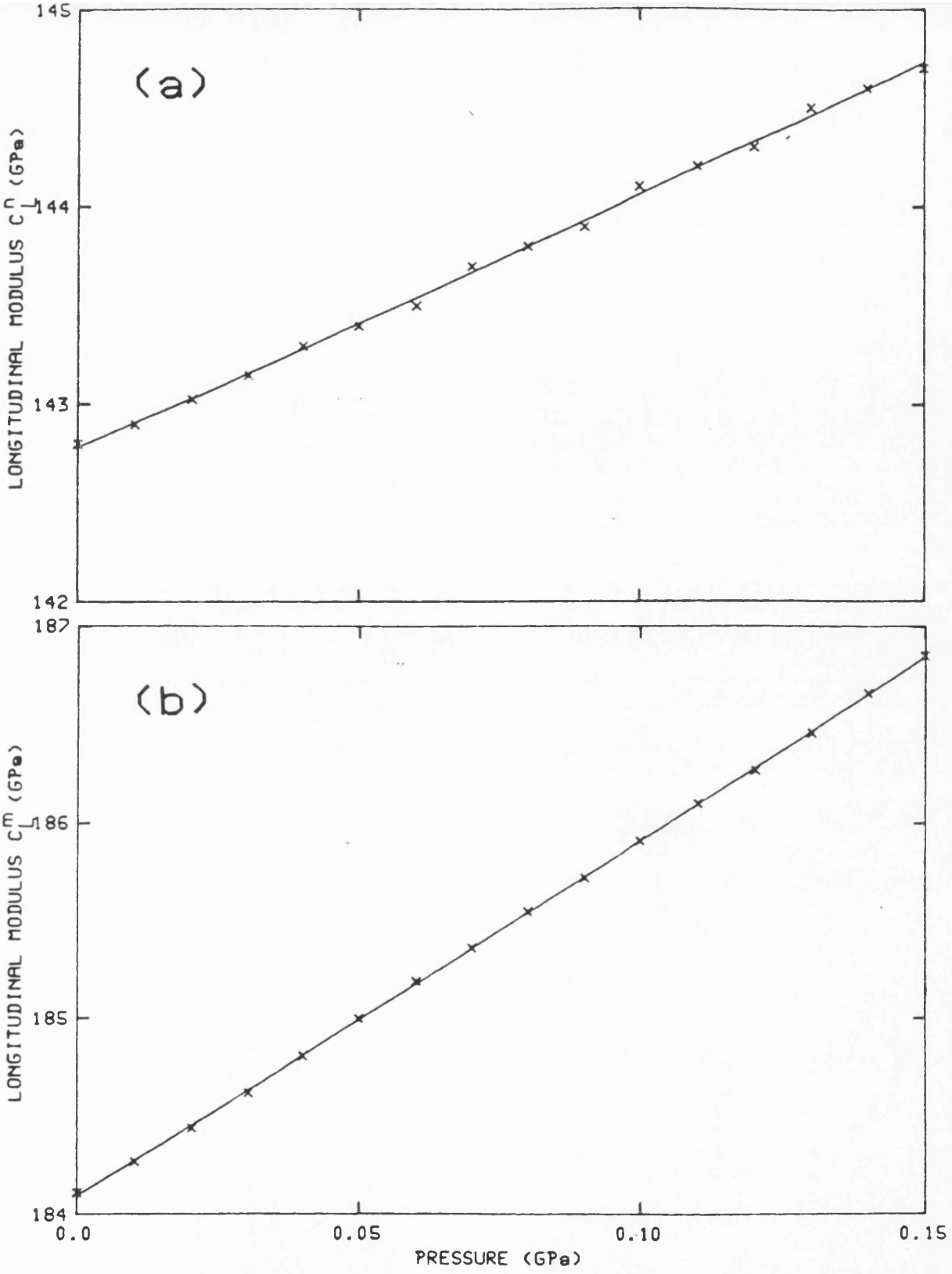

Figure 6.13
The hydrostatic pressure dependences of the longitudinal modulus (a) C_L^n (porous material) and (b) C_L^m (non-porous matrix) of $Nd_{1.85}Ce_{0.15}CuO_{4-y}$ at 295K calculated from the experimental data and using equations 4.4 and 4.5. The solid lines are least square fits to the data.

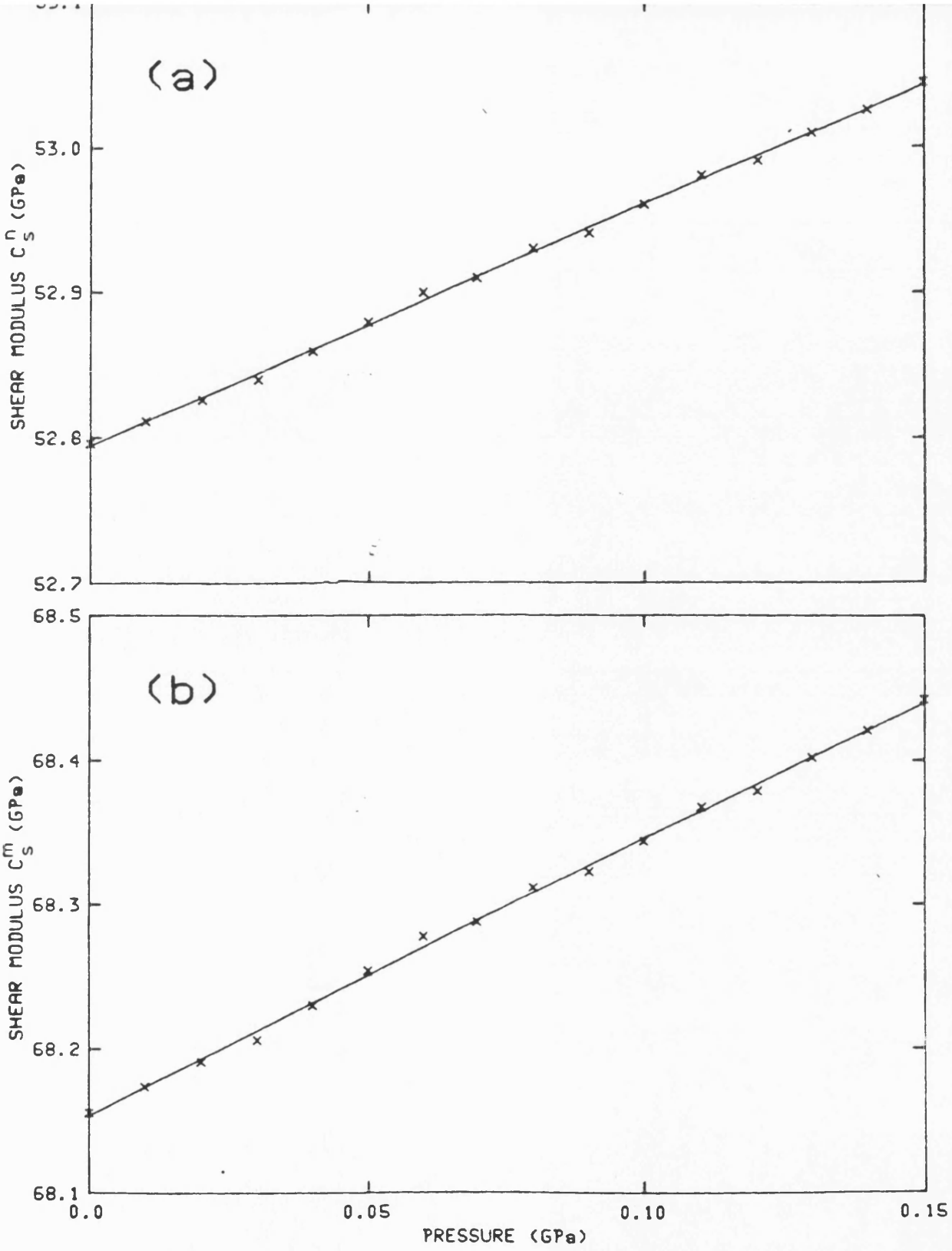

Figure 6.14
The hydrostatic pressure dependences of the shear modulus (a) C_S^n (porous material) and (b) C_S^m (non-porous matrix) of $Nd_{1.85}Ce_{0.15}CuO_{4-y}$ at 295K calculated from the experimental data and using equations 4.4 and 4.5. The solid lines are least square fits to the data.

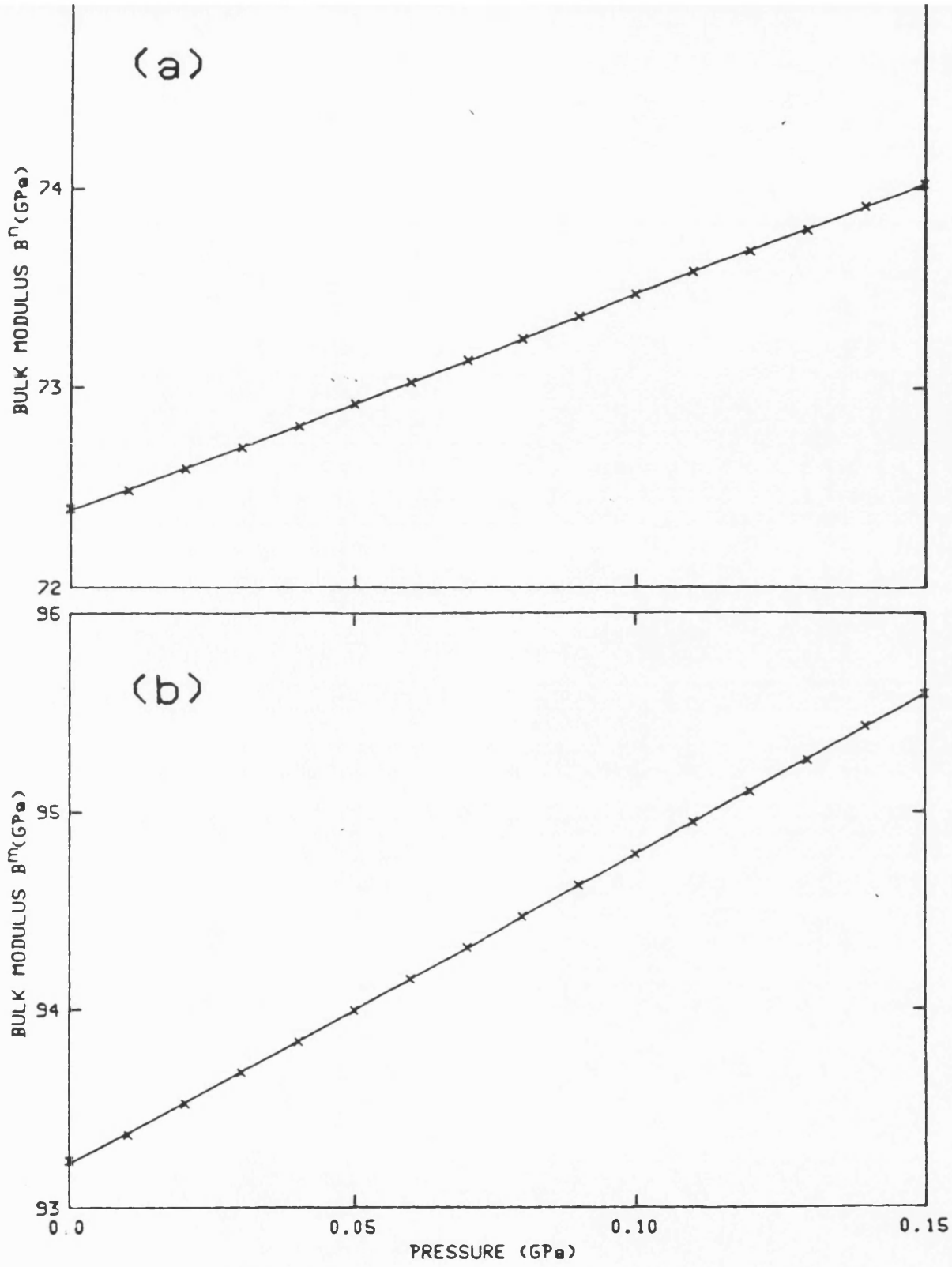

Figure 6.15
The hydrostatic pressure dependences of the bulk modulus (a) B^n (porous material) and (b) B^m (non-porous matrix) of $Nd_{1.85}Ce_{0.15}CuO_{4-y}$ at 295K calculated from the experimental data and using equations 4.4 and 4.5. The solid lines are least square fits to the data.

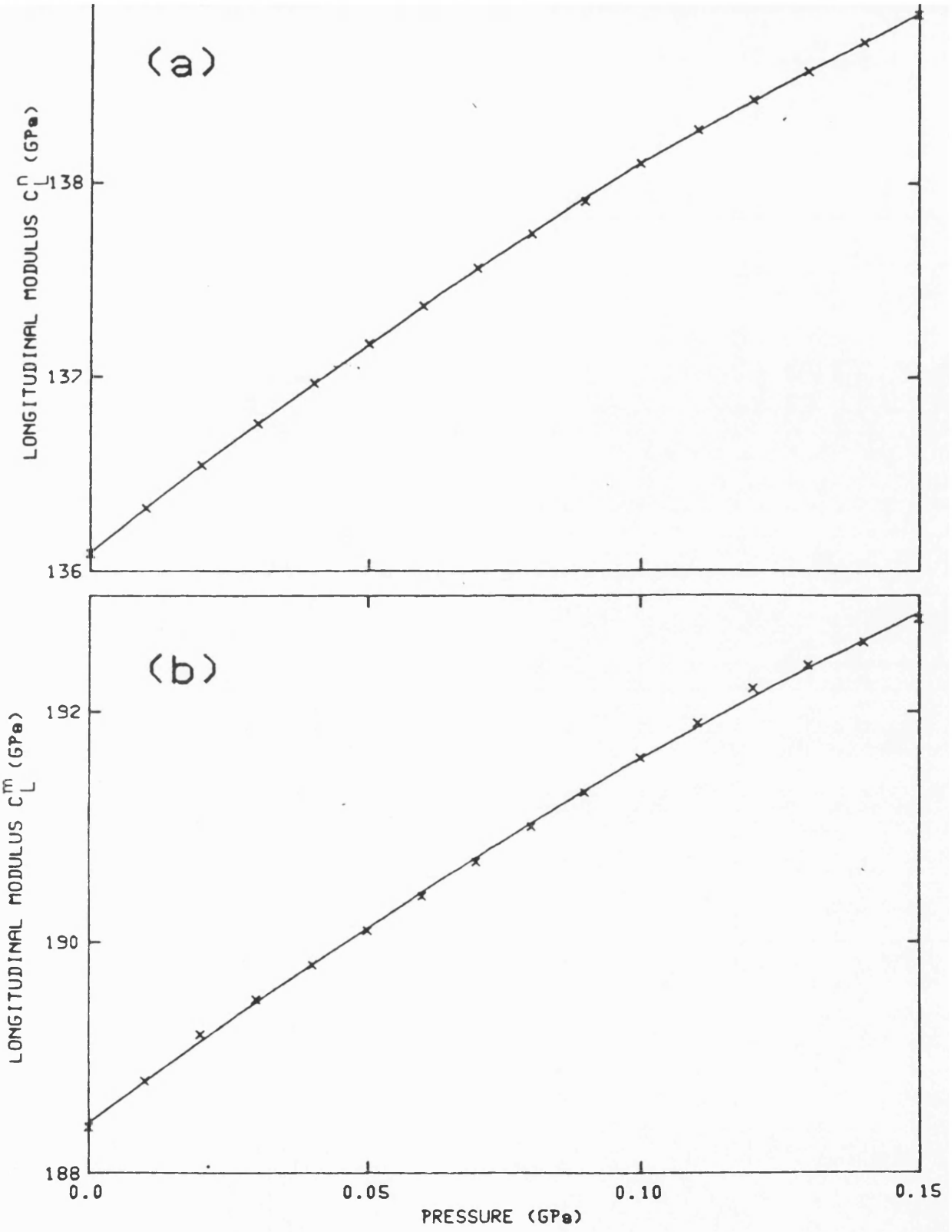

Figure 6.16
The hydrostatic pressure dependences of the longitudinal modulus (a) C_L^n (porous material) and (b) C_L^m (non-porous matrix) of Nd_2CuO_{4-y} at 295K calculated from the experimental data and using equations 4.4 and 4.5. The solid lines are least square fits to the data.

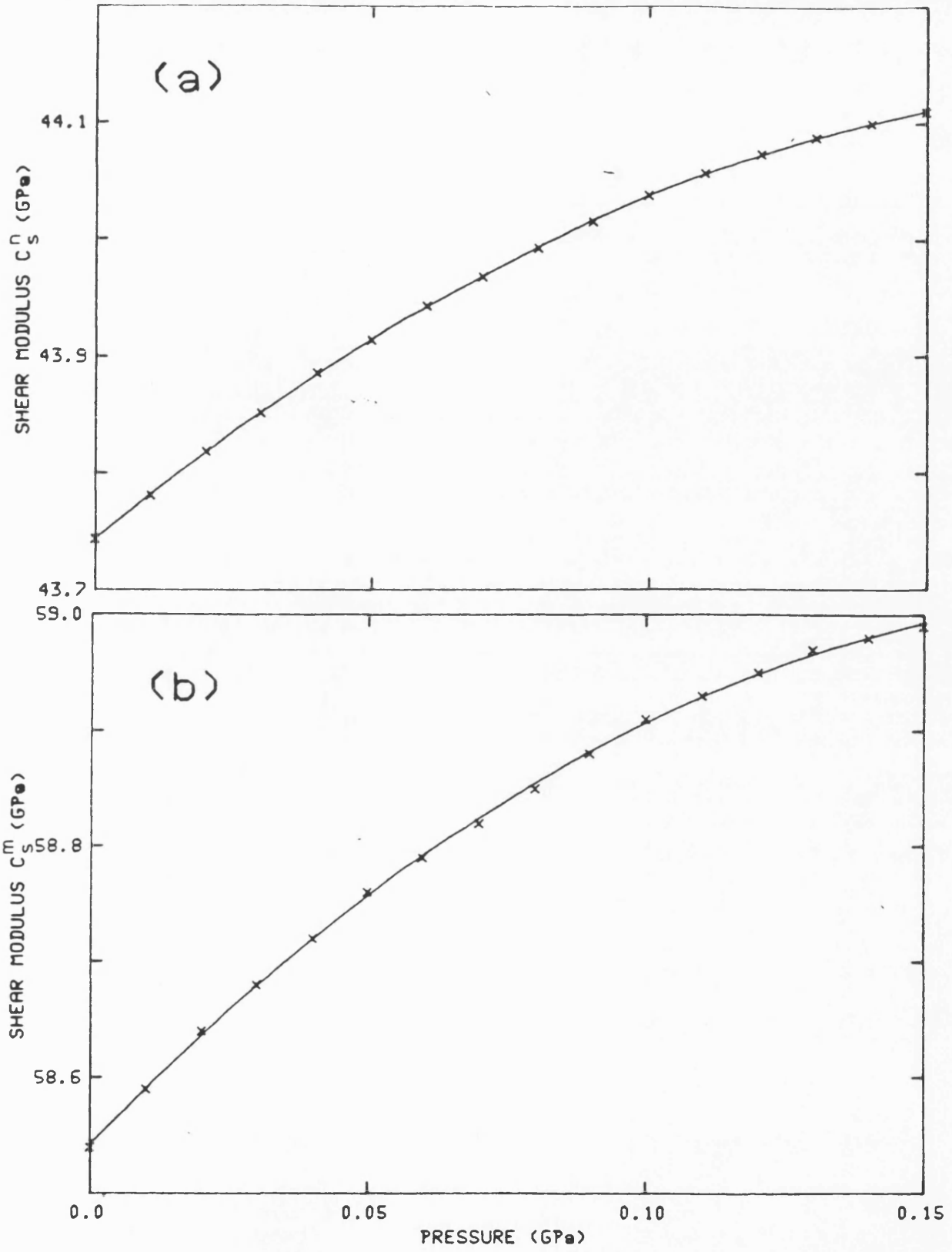

Figure 6.17
The hydrostatic pressure dependences of the shear modulus (a) C_S^n (porous material) and (b) C_S^m (non-porous matrix) of Nd_2CuO_{4-y} at 295K calculated from the experimental data and using equations 4.4 and 4.5. The solid lines are least square fits to the data.

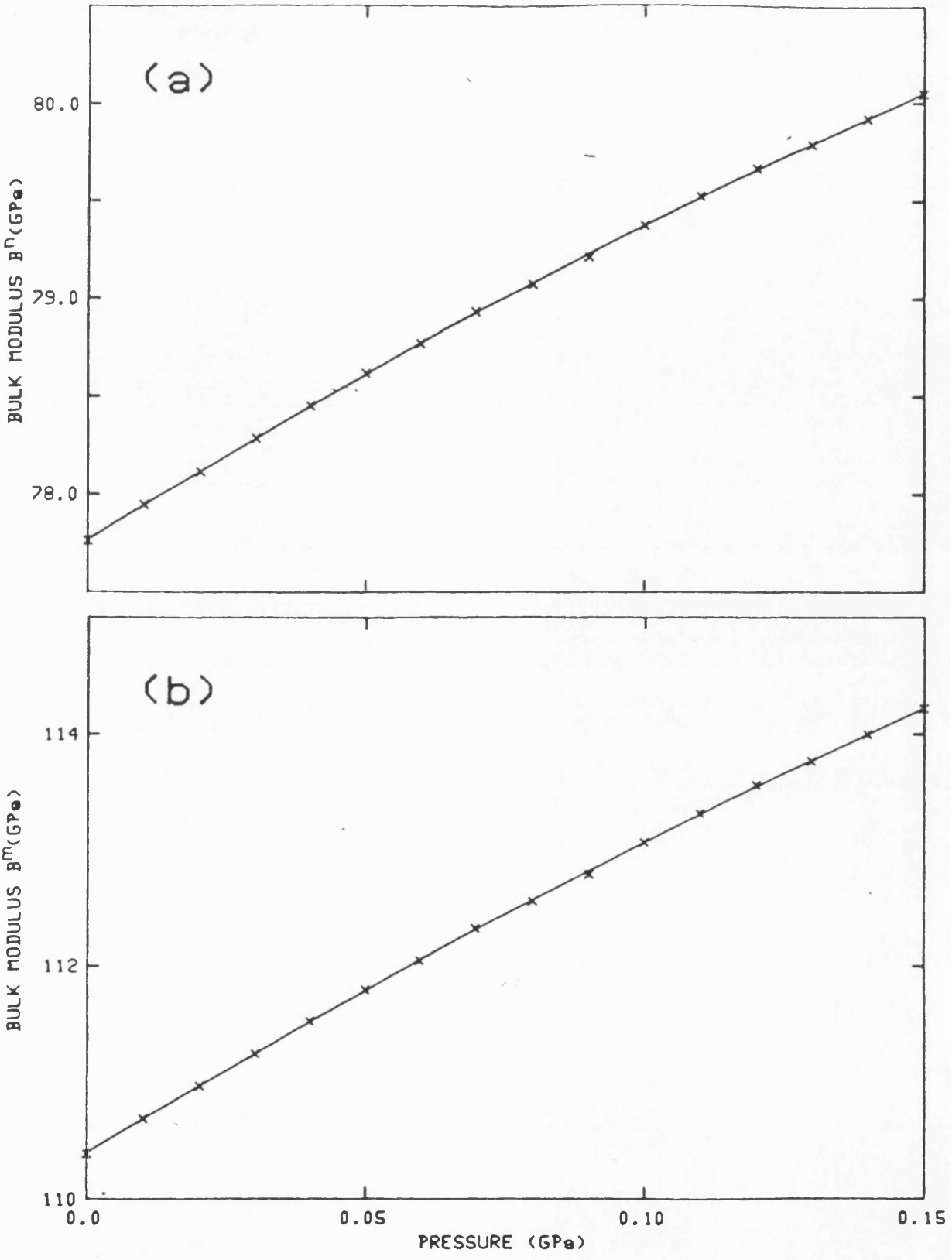

Figure 6.18
The hydrostatic pressure dependences of the bulk modulus (a) B^n (porous material) and (b) B^m (non-porous matrix) of Nd_2CuO_{4-y} at 295K calculated from the experimental data and using equations 4.4 and 4.5. The solid lines are least square fits to the data.

the effect of porosity is to reduce the elastic stiffness moduli (including the bulk modulus) and their pressure derivatives.

The values for the elastic constants in table 6.3 were calculated using the measured ultrasonic wave velocities at atmospheric pressure and room temperature using Dow Resin as a bonding material. These values differ from those calculated at the same conditions using Nonaq as a bonding material (figures 6.7, 6.8 and 6.10). These differences are attributed to the different bonding materials used in different experiments.

The effects of porosity on the results obtained for the $Nd_{1.85}Ce_{0.15}CuO_{4-y}$ and its parent Nd_2CuO_{4-y} compound will be fully discussed and compared with the results obtained for the other high T_c superconducting compounds in a separate chapter (chapter 11) at the end of this work after all the results for the other compounds have been presented.

CHAPTER SEVEN

ELASTIC PROPERTIES OF THE HIGH T_C SUPERCONDUCTOR $La_{1.8}Sr_{0.2}CuO_{4-y}$ AND ITS PARENT COMPOUND La_2CuO_{4-y}

7.1 INTRODUCTION

The ultrasonic wave velocities were measured as a function of hydrostatic pressure and temperature to investigate the elastic behaviour of the high T_c superconducting compound $La_{1.8}Sr_{0.2}CuO_{4-y}$ together with that of its parent La_2CuO_{4-y} material.

After preparing the samples as described in chapter 4, the purity of the samples was checked using the X-ray powder diffractometry technique, which were found to be single phase in each case within the resolution of this type of experiment.

To ensure that $La_{1.8}Sr_{0.2}CuO_{4-y}$ samples were superconducting, the temperature dependence of the electrical resistance was measured. The results with the data for the parent material (La_2CuO_{4-y}) are discussed in section 7.2.

In order to determine the elastic behaviour for the $La_{1.8}Sr_{0.2}CuO_{4-y}$ compound and the parent compound La_2CuO_{4-y}, the ultrasonic longitudinal and shear wave velocities and consequently the elastic constants were measured as a

function of hydrostatic pressure and temperature. The effects of porosity on the results have been considered. This will be discussed in section 7.3.

7.2 THE ELECTRICAL RESISTANCE MEASUREMENTS

To verify that the $La_{1.8}Sr_{0.2}CuO_{4-y}$ sample used in this work was superconducting, *dc* electrical resistance measurements were carried out from room temperature down to liquid helium boiling temperature. The results are shown in figure 7.1. From that figure it can be seen that the material displayed an approximately linear decrease in resistance (metallic behaviour) from room temperature down to the onset temperature which was about 35K where the rapid decrease in resistivity occurs. Zero resistance was achieved at 29.7K (within instrumental noise).

Cava et al (1987a) measured the resistivity of two $La_{1.8}Sr_{0.2}CuO_{4-y}$ samples with different annealing conditions. They found that the resistivity decreases as the temperature decreases for the sample annealed in oxygen [similar to the behaviour of the electrical resistance found for the present sample (figure 7.1)] with a sharp drop at around 36K, while the resistivity increases as the temperature decreases for the air annealed sample with a sharp drop towards zero resistivity at around 34K. They obtained a room temperature resistivity of 2200 $\mu\Omega.cm$ and 5500 $\mu\Omega.cm$ for the air annealed and the oxygen annealed samples respectively. Gopalakrishnan et al (1987b) measured the resistivity as a function of temperature for a number of $La_{1.8}Sr_{0.2}CuO_{4-y}$ samples with

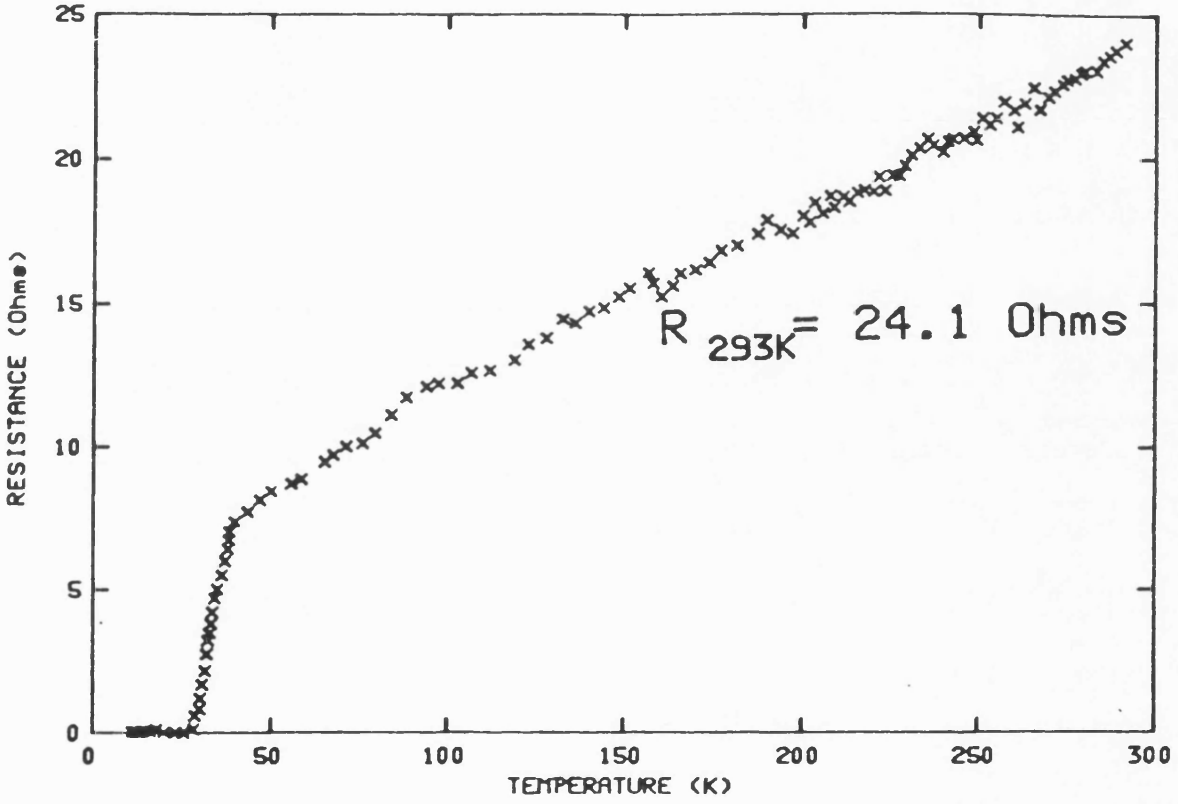

Figure 7.1
The temperature dependence of the electrical resistance of a $La_{1.8}Sr_{0.2}CuO_{4-y}$ ceramic sample.

different annealing temperatures. They found that the sample annealed at 1130°C had the highest T_c (34K) of all of their samples. They also found that the resistivity decreases as the temperature decreases with a sharp drop towards zero resistivity at about 37K. Decroux et al (1987) measured the electrical resistivity of a $La_{1.85}Sr_{0.15}CuO_4$ sample and reported that the resistivity decreases as the temperature decreases from room temperature with a sharp drop towards zero resistivity at around 41K. They obtained a room temperature resistivity for their sample of about 5 $m\Omega.cm$. Meanwhile Oh-Ishi et al (1988) measured the resistivity of the $La_{2-X}Sr_XCuO_{4-y}$ compound with different Sr (X) concentrations. They found that the normal state resistivity decreases as X increases, and they also found that T_c first increases with X and then decreases with increasing X through a maximum at X=0.15. They suggested that the decrease in the normal state resistivity as X increases is consistent with the increase in the carrier concentration and they concluded that a highly metallic behaviour is unfavourable for superconductivity in this compound. Sudhakar et al (1991) measured the resistivity as a function of temperature in $La_{1.8}Sr_{0.2}CuO_{4-y}$. They found similar behaviour to that found

by others [Cava et al (1987a), Gopalakrishnan et al (1987b) and Decroux et al (1987)]; they obtained a room temperature resistivity of $2m\Omega.cm$.

The electrical resistance of the parent La_2CuO_{4-y} compound was measured as a function of temperature down to 4.2K (figure 7.2). The room temperature resistance was determined as 0.305Ω . It can be seen that the sample was not a superconductor; the resistance decreased slowly from room temperature to around 100K, followed by a steep rise at lower temperatures. This behaviour is characteristic of a doped semiconductor. For example, Mott and Davis (1979) found that by doping germanium with n- or p-type donors and acceptors respectively, the room temperature resistivity increases as the donor or acceptor concentration decreases. The behaviour of the resistivity as a function of temperature for doped semiconductors is the same as the behaviour of the temperature dependence of electrical resistance obtained for the La_2CuO_{4-y} sample (figure 7.2) investigated here which follows the relation [Mott and Davis (1979)]:

$$\rho = \rho_o \exp(E/kT) \qquad (7.1)$$

Here ρ is the resistivity at any temperature, ρ_o is the resistivity at the absolute zero, E is a constant, k is Boltzmann's constant and T is the temperature in Kelvin.

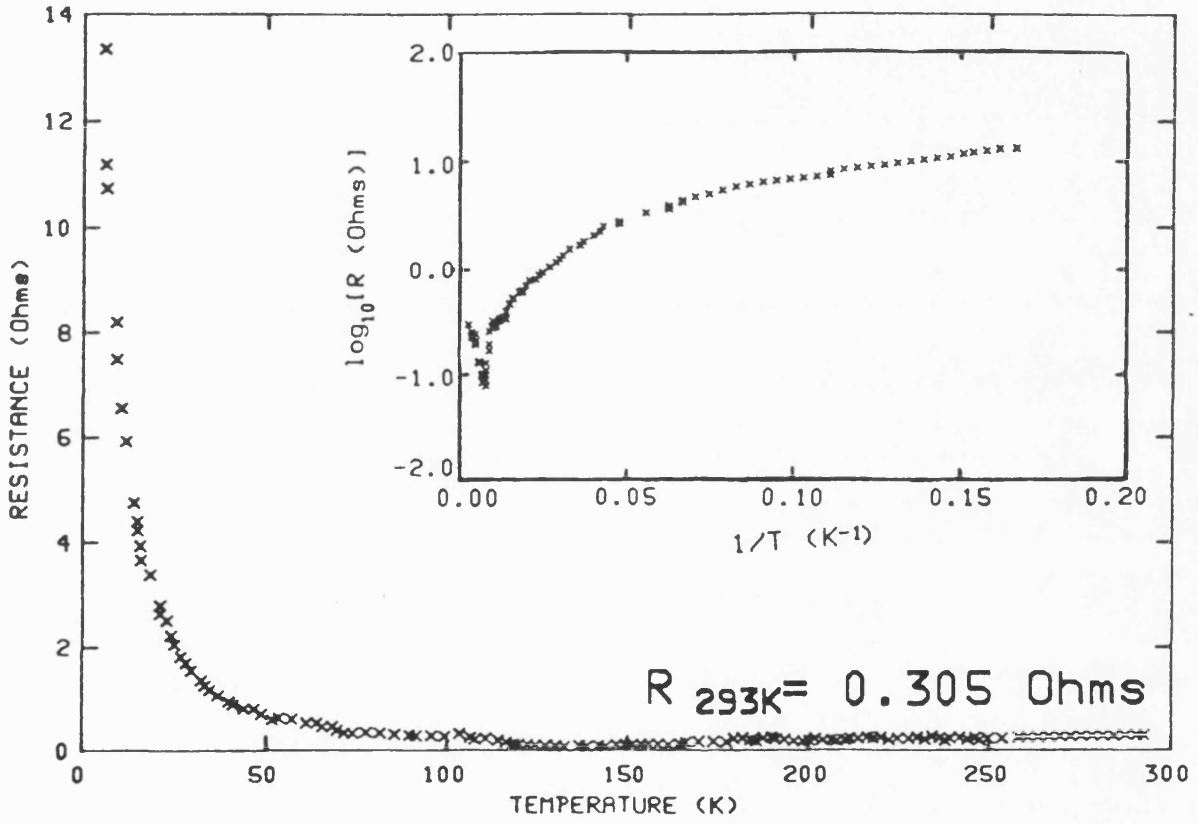

Figure 7.2
The electrical resistance of a ceramic specimen of La_2CuO_{4-y} as a function of temperature. The insert is the logarithmic value of the electrical resistance as a function of the inverse of temperature and it has been plotted to compare the results with the semiconducting behaviour.

Hence, to compare the results obtained here with semiconductor behaviour, the logarithmic values of the resistance ($\log_{10}(R)$) were plotted as a function of the inverse of the measured temperature. The results shown in the insert in figure 7.2 indicate that La_2CuO_4 does not behave as an ordinary semiconductor. The same procedure was carried out for a La_2CuO_4 sample by Jorgenson et al (1987) where they found similar behaviour to that observed here. They obtained a room temperature resistance for their sample of 1.5Ω .

Johnston et al (1987) measured the resistivity as a function of temperature of three different La_2CuO_{4-y} samples with different oxygen stoichiometry (different y). They found a strong upturn in the resistivity at around 100K and they concluded that this upturn is suggestive of an insulating ground state. Kaneko et al (1987) measured the electrical resistance in a La_2CuO_{4-y} sample as a function of temperature. They found that the resistance was almost constant through the temperature range 220-160K and then starts to increase exponentially below 130K. They obtained a room temperature resistance of 0.6Ω. The behaviour of the resistance as a function of temperature obtained by these groups is almost the same as that found for the La_2CuO_{4-y} sample investigated here (figure 7.2). Cooper et al (1987) measured the electrical resistance in two La_2CuO_{4-y} samples prepared by two different

processes. They found that for the sample prepared by the amorphous citrate process a trace of superconductivity could be observed with an onset temperature of 90K and T_c of around 30K, but for the sample prepared by the normal solid state reaction a trace of superconductivity was observed with zero resistivity obtained at a temperature as low as 5K. A similar trace of superconductivity was also found by Grant et al (1987) for a La_2CuO_4 sample at 16K when they measured the temperature dependence of the electrical resistivity. They obtained a room temperature resistivity for their sample of 0.5$\Omega.cm$.

7.3 THE ULTRASONIC MEASUREMENTS

7.3.1 THE TEMPERATURE DEPENDENCES OF ULTRASONIC WAVE VELOCITIES

To examine the elastic behaviour of the $La_{1.8}Sr_{0.2}CuO_{4-y}$ and its parent La_2CuO_{4-y} compound, 5MHz ultrasonic wave velocities were measured as a function of temperature down to liquid helium boiling temperature using quartz transducers and Nonaq as a bonding material. The results are shown in figures 7.3 and 7.4 respectively.

From the ultrasonic velocity data obtained for $La_{1.8}Sr_{0.2}CuO_{4-y}$, it is clear that there is a substantial softening in this material structure below about 170K. This elastic softening was also reported by several groups. Horie et al (1987b, 1990) found a decrease in the sound velocity by about 10% when they cooled their $La_{1.86}Sr_{0.14}CuO_{4-y}$ sample below 240K. Bourne et al (1987) measured the sound velocity in the $La_{2-x}Sr_xCuO_{4-y}$ compound with different Sr concentrations (different X). They found that elastic softening occurs when X=0.15 but it was absent when X=0.30. Bishop et al (1987) found a large decrease in sound velocity measured in a $La_{1.85}Sr_{0.15}CuO_{4-y}$ sample as the temperature decreased below 250K with a minimum at T_c (37K for their sample). Esquinazi et al (1987) observed an elastic softening as the temperature decreased with a minimum at 20K in their $La_{1.8}Sr_{0.2}CuO_4$ sample.

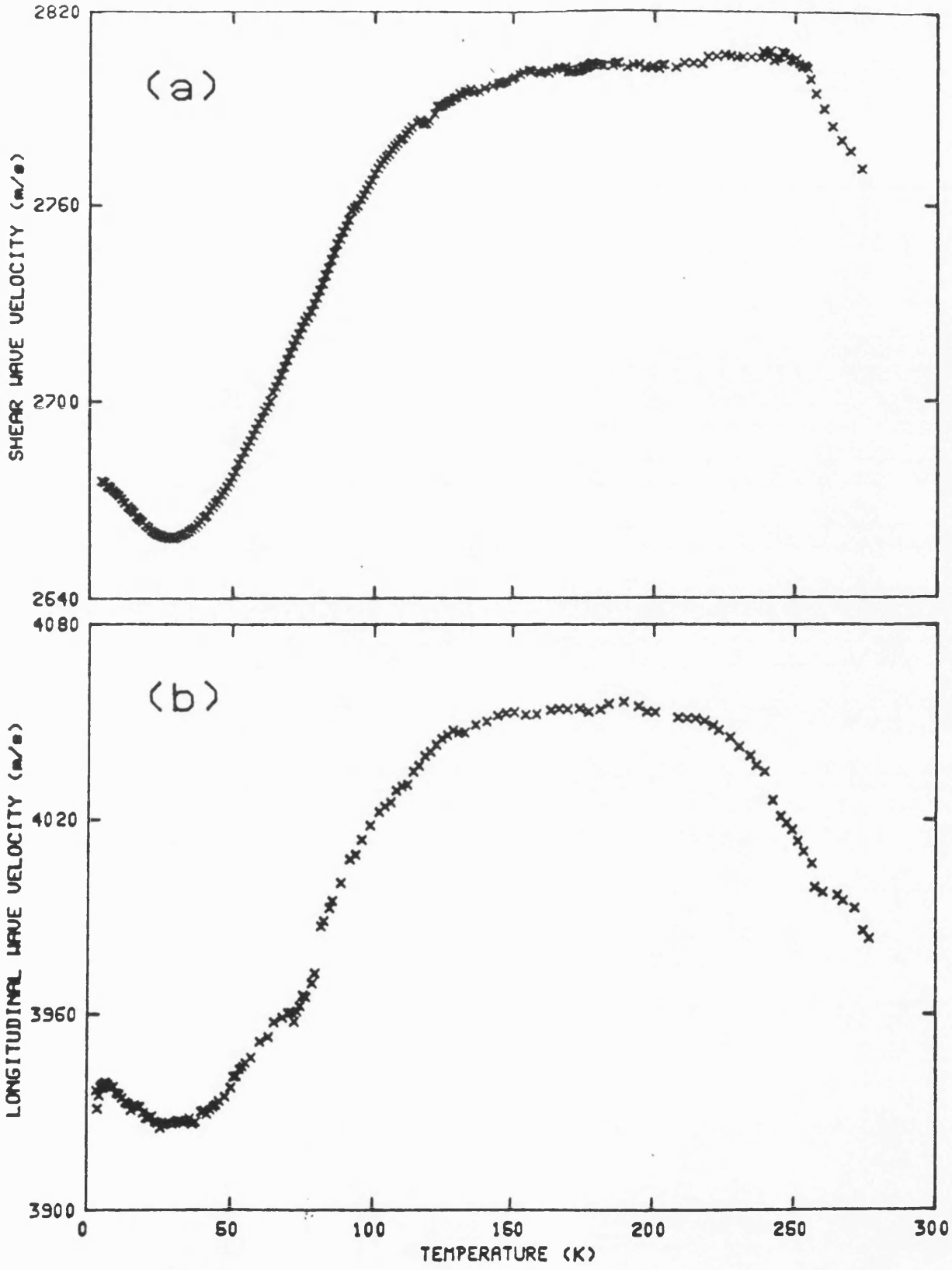

Figure 7.3
The temperature dependences of the ultrasonic (a) shear and (b) longitudinal waves velocities for a $La_{1.8}Sr_{0.2}CuO_{4-y}$ sample. No hysteresis was found between warming and cooling.

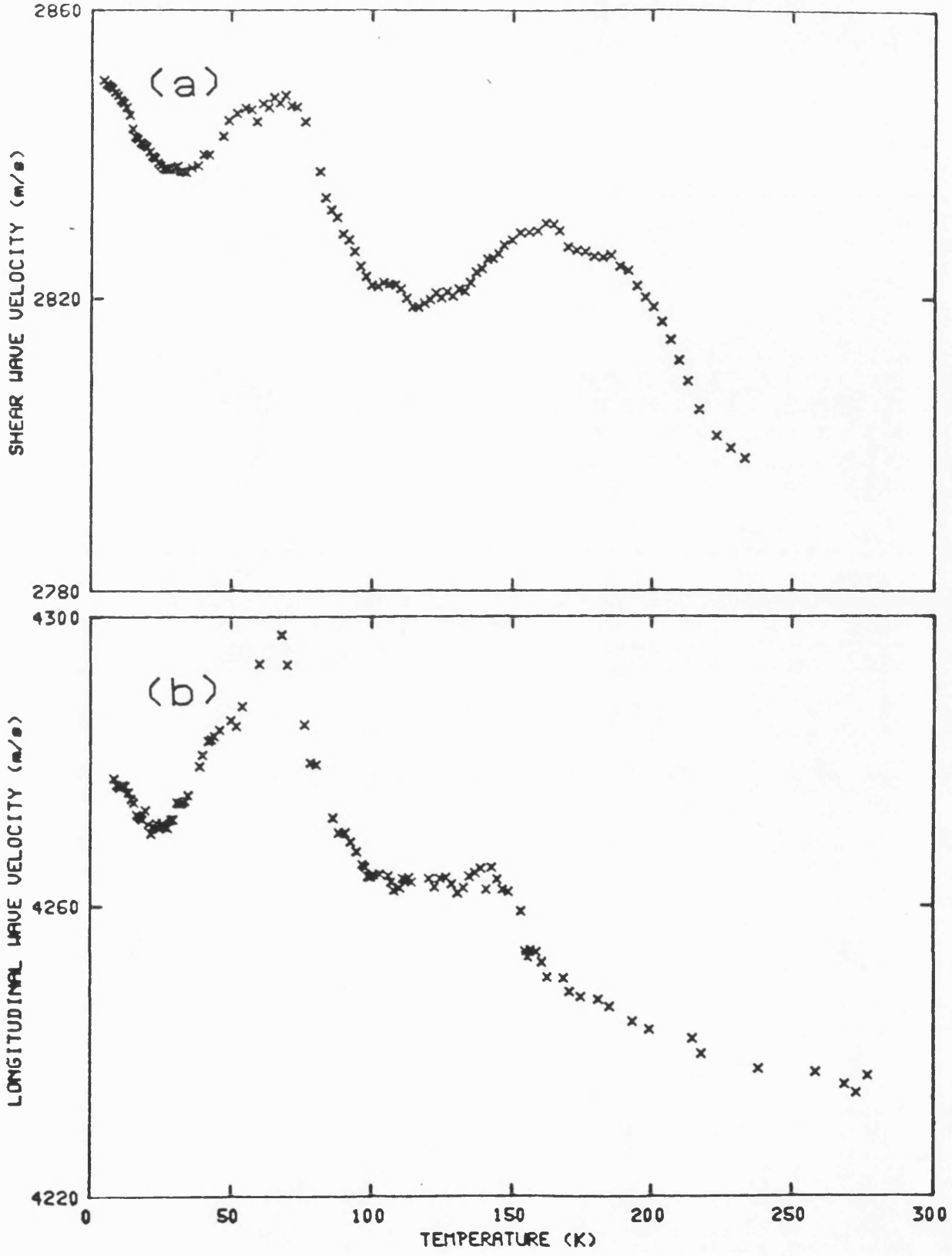

Figure 7.4
The temperature dependences of the ultrasonic (a) shear and (b) longitudinal waves velocities for a La_2CuO_{4-y} sample. As in figure 7.3, no hysteresis was found between warming and cooling.

Finally, Lüthi et al (1987) found a clear softening in both mode velocities measured in $La_{1.85}Sr_{0.15}CuO_{4-y}$ as the temperature decreased.

The ultrasonic wave velocities measured for the $La_{1.8}Sr_{0.2}CuO_{4-y}$ sample under investigation are compared in table 7.1 with those obtained by other groups for the same compound but with different Sr composition.

The first conclusion that can be drawn from the temperature dependence of the ultrasonic wave velocities data in $La_{1.8}Sr_{0.2}CuO_{4-y}$ is that one or more of the elastic constants become soft at the zone centre. The physical origins of the striking ultrasonic effects found solely in the hole-doped La_2CuO_{4-y} superconductors have emerged from a clarification of the structural phase transformation in $La_{2-x}Ba_xCuO_4$ [Axe et al (1989)]. It is reported that in addition to the already known [Paul et al (1987)] higher-temperature orthorhombic-tetragonal phase transformation, a further transformation to a second phase occurs at lower temperatures. An examination of the reported phase diagram shows that the substantial softening below room temperature measured in $La_{1.85}Ba_{0.15}CuO_4$ by Fossheim et al (1987) is associated with the higher-temperature orthorhombic-tetragonal transformation, whilst modulus hardening occurs at lower temperatures where the low-temperature tetragonal phase develops. At a

Table 7.1. Comparison between the ultrasonic wave velocities measured in this work with those obtained by other groups for the $La_{2-X}Sr_XCuO_{4-y}$ compound.

References	X (Sr concentration)	Ultrasonic wave velocities		Temperature (K)
		Longitudinal (m/s)	Shear (m/s)	
This Work	0.2	3960	2759	293
Bishop et al 1987	0.15	5000	-	293
Esquinazi et al 1987	0.2	5600	-	293
Horie et al 1990	0.14	5120	-	293
Kim et al 1988b	0.15	4166	2676	220
Lüthi et al 1987	0.15	4170	2680	293
Slaski et al 1990	0.12 (single crystal)	5720	-	293

composition with X=0.2, the two phase transition temperatures, and T_c, coincide with each other, eliminating the intermediate orthorhombic state. If one assumes that the phase diagram for strontium and barium doped La_2CuO_{4-y} are similar, this explains the minimum in the sound velocity data at T_c .

Several mechanisms have been suggested to describe the elastic softening which occurs in the $La_{2-X}M_XCuO_{4-y}$ system (where M = Ba or Sr). The main approach to solve the problem was the similarity in the elastic softening observed in this material and the $A15$ compounds. Despite all of these efforts, the origin of the high-superconducting transition temperatures in the new ceramic superconductors remains uncertain. The standard approaches for estimating the strength of the electron-phonon interaction do not lead to coupling strengths which are large enough to produce the higher T_c and it is believed [Cava (1990)] that this mechanism is almost certainly not responsible.

The ultrasonic wave velocities were also measured in the La2CuO4-y sample. A comparison is carried out in table 7.2 between the ultrasonic wave velocities obtained for the sample investigated in this work with those reported by other groups. The temperature dependences of the ultrasonic wave velocities for La_2CuO_{4-y} (figure 7.4) do not show the

Table 7.2. Comparison between the ultrasonic wave velocities obtained in this work with those obtained by other workers for the La_2CuO_{4-y} compound.

References	Ultrasonic wave velocities		Temperature (K)
	Longitudinal (m/s)	Shear (m/s)	
This Work	4233	2788	293
Lüthi et al 1987	5040	2840	293
Kim et al 1988b	5039	2841	220

same softening of the doped compound sample, confirming that the softening is a feature of the doped structure. However, inspection of the low temperature data in figure 7.4 reveals that a minimum in the ultrasound velocity also occurs in La_2CuO_{4-y} in a temperature region similar to that present in the data for $La_{1.8}Sr_{0.2}CuO_{4-y}$. This casts some doubts on reports [for example Bishop et al (1987)] that the minimum in the ultrasound velocity near T_c in $La_{2-x}Sr_xCuO_{4-y}$ is a consequence of superconductivity. Lang et al (1987 and 1989) found a thermal expansion anomaly near 36K in a La_2CuO_{4-y} compound sample and attributed it to a structural phase transition. Meanwhile, Lüthi et al (1987) found very small changes (about 2%) in both mode velocities as a function of temperature in their La_2CuO_{4-y} sample in the temperature range 0-300 K with a minimum at around 20K.

7.3.2 THE TEMPERATURE DEPENDENCE OF THE ELASTIC CONSTANTS

By measuring the ultrasonic wave velocities in the $La_{1.8}Sr_{0.2}CuO_{4-y}$ and the La_2CuO_{4-y} samples, the elastic constants can be obtained. Values for the longitudinal C_l^n , shear C_s^n , bulk B^n and Young's moduli as well as poisson's ratio obtained at 295K for both the superconducting and the parent compounds are given in table 7.3. The temperature dependences of the longitudinal, shear and Young's moduli are shown in figures 7.5, 7.6 and 7.7 respectively. In each of these properties, a minimum in the data at T_c exists for the superconducting compound. For the parent compound the behaviour of the elastic constants as a function of temperature was similar to the temperature dependences of the ultrasonic wave velocities. Figure 7.8 shows the temperature dependence of the bulk modulus in both the superconducting and the parent compounds. The bulk modulus for the superconductor shows a minimum at 75K which is associated with the elastic softening (figure 7.8b), while the bulk modulus in the parent compound shows a minimum at about 160K (figure 7.8a) which is the same temperature where the ultrasonic shear wave velocity shows a maximum (figure 7.4a).

The temperature dependences of Poisson's ratio for both the superconducting and the parent compound materials are shown in figure 7.9. A maximum in the data was found for

Table 7.3. The ultrasonic wave velocities and the elastic constants at room temperature for the polycrystalline ceramic $La_{1.8}Sr_{0.2}CuO_{4-y}$ high temperature superconductor and its parent compound La_2CuO_{4-y}. The results obtained using Nonaq as a bonding material.

Property	$La_{1.8}Sr_{0.2}CuO_{4-y}$	La_2CuO_{4-y}
Density Kgm^{-3}	6000	6495
Ultrasonic wave velocities ms^{-1} Longitudinal V_L	3960	4233
Shear V_S	2759	2788
Bulk modulus B (GPa)	33.2	49.1
Young's modulus E (GPa)	94	113
Poisson's ratio	0.028	0.116
C_L (GPa)	94	116
C_S (GPa)	45.7	51

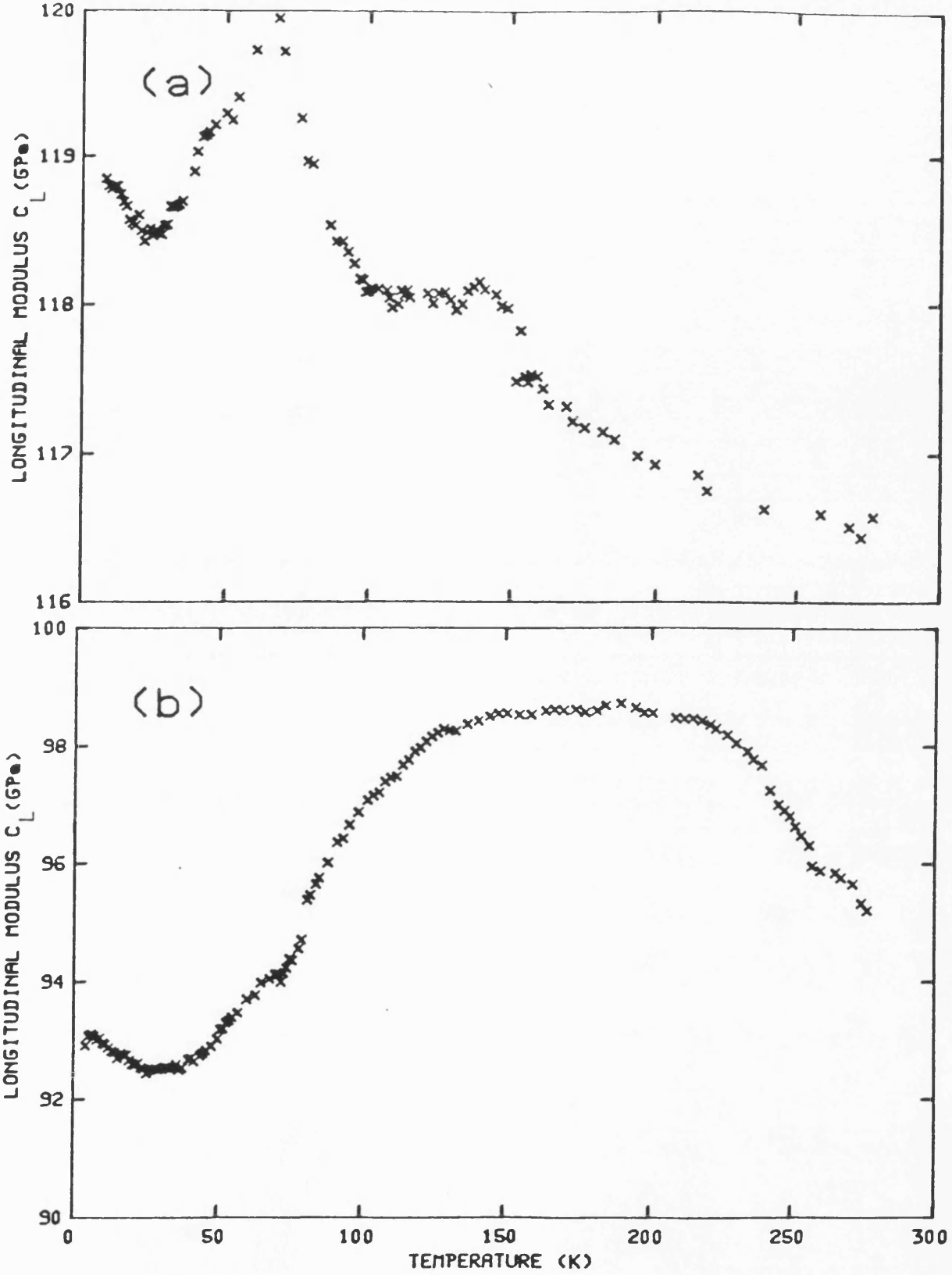

Figure 7.5
The temperature dependences of the longitudinal modulus C_L for (a) La_2CuO_{4-y} and (b) $La_{1.8}Sr_{0.2}CuO_{4-y}$ samples.

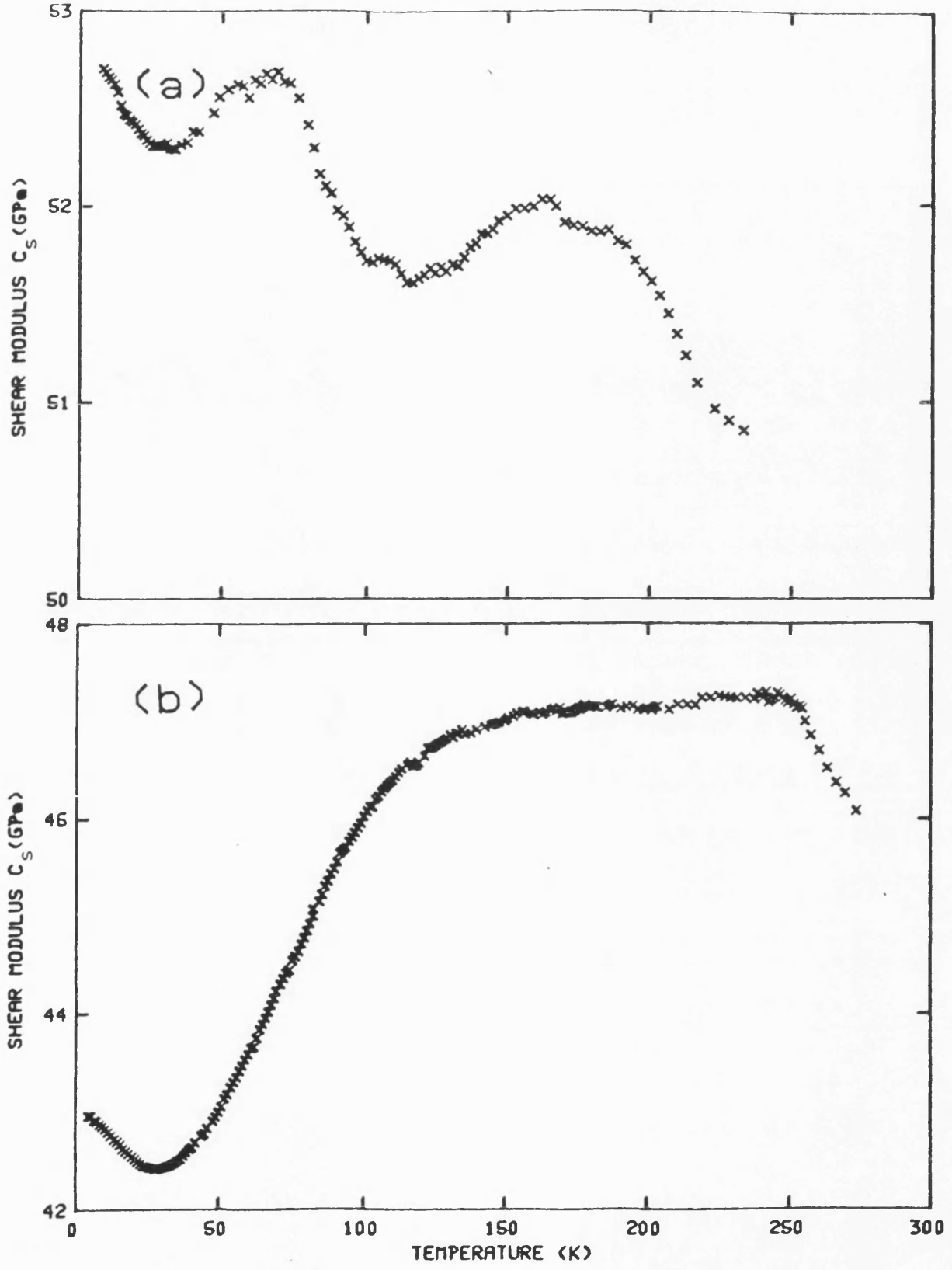

Figure 7.6
The temperature dependences of the shear modulus C_S for (a) La_2CuO_{4-y} and (b) $La_{1.8}Sr_{0.2}CuO_{4-y}$ samples.

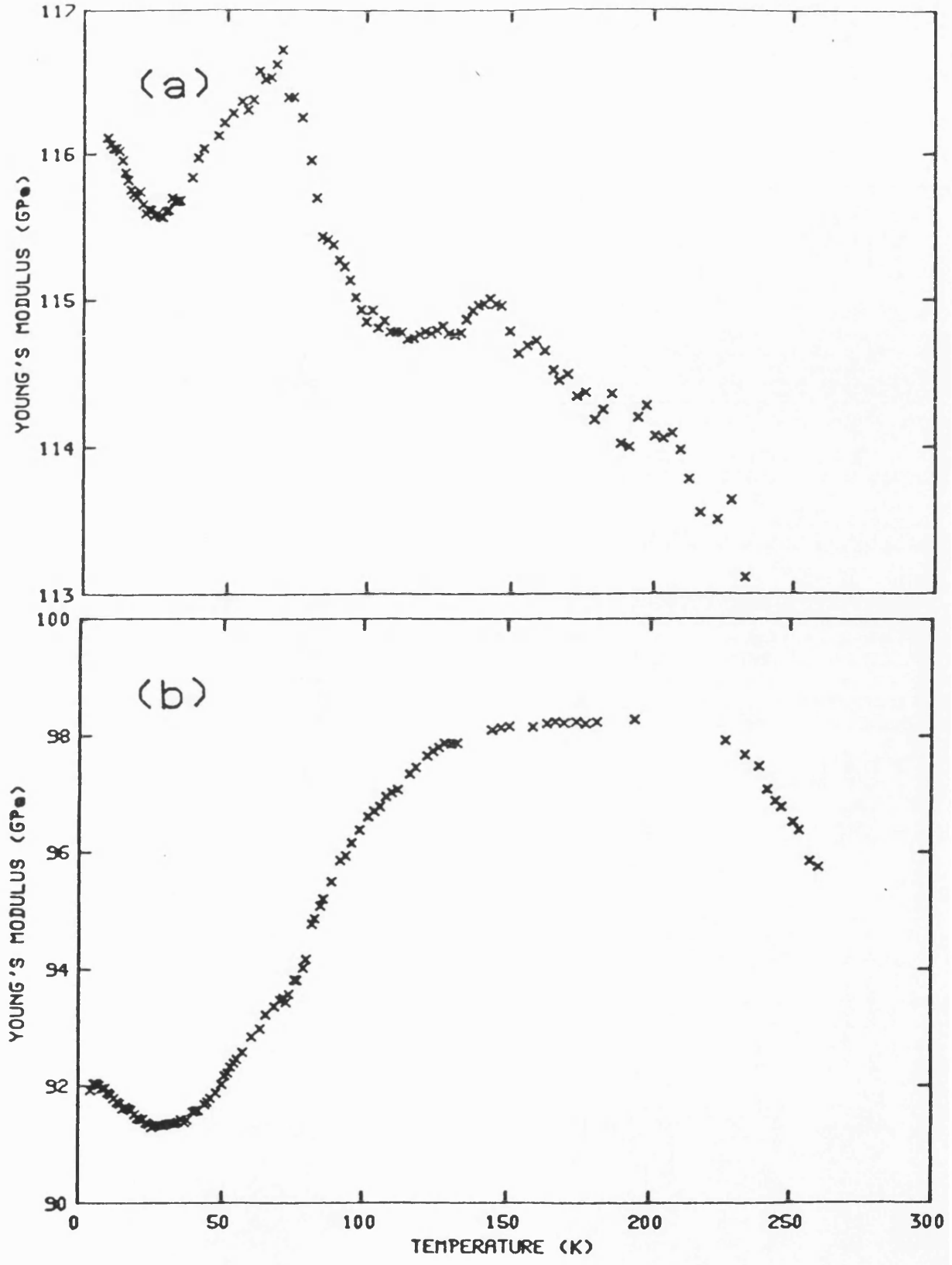

Figure 7.7
The temperature dependences of the Young's modulus for (a) La_2CuO_{4-y} and (b) $La_{1.8}Sr_{0.2}CuO_{4-y}$ samples.

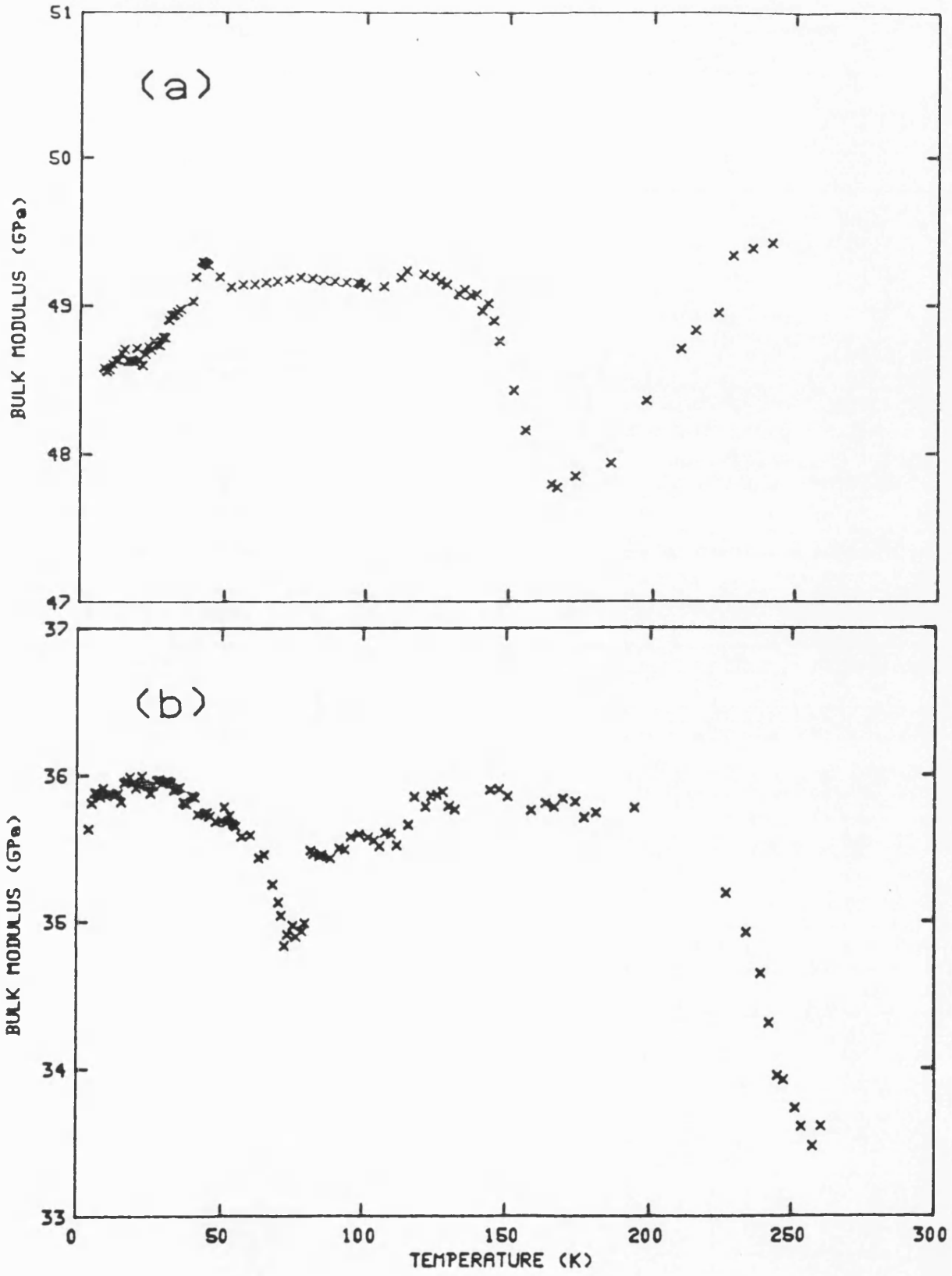

Figure 7.8
The temperature dependences of the bulk modulus for (a) La_2CuO_{4-y} and (b) $La_{1.8}Sr_{0.2}CuO_{4-y}$ samples.

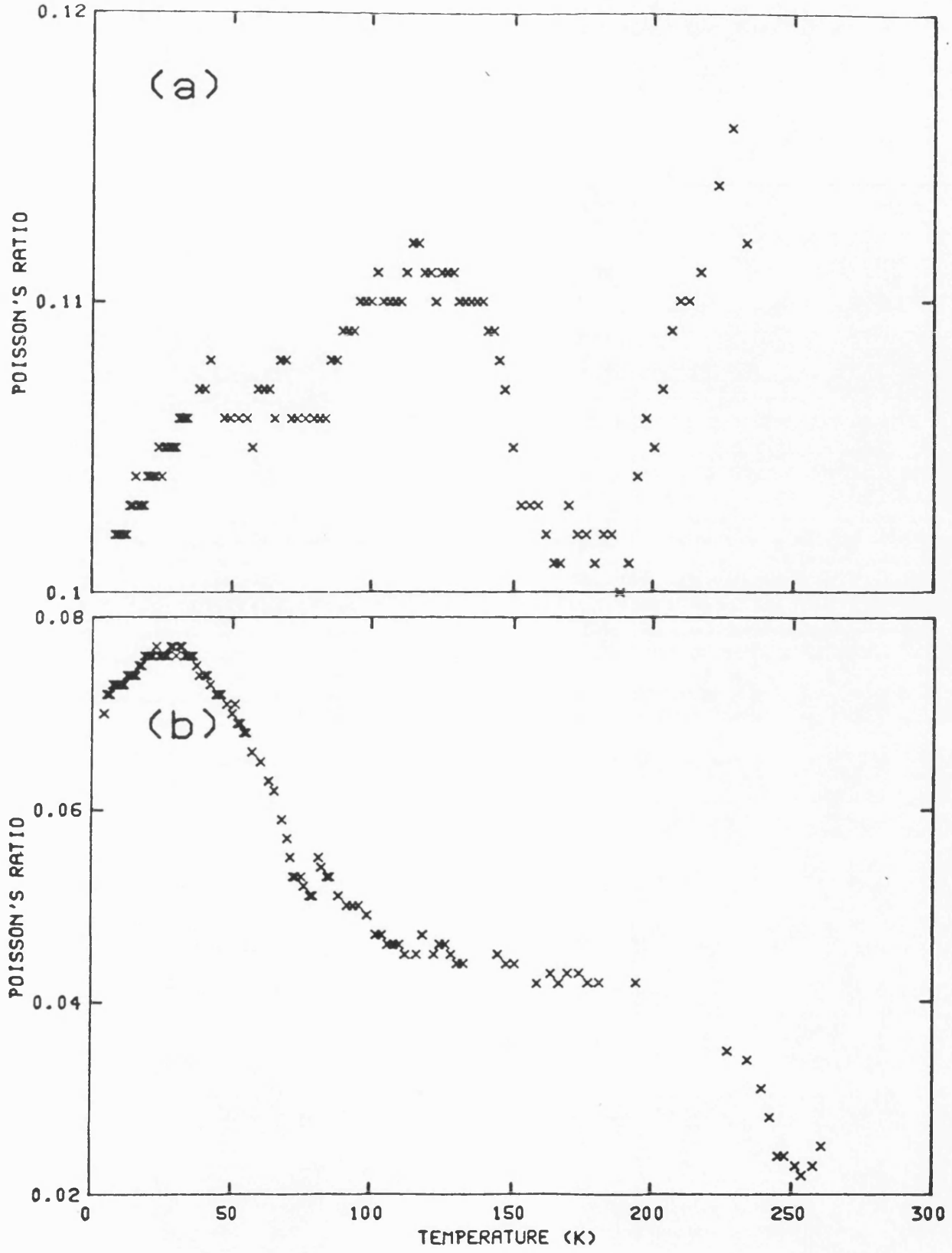

Figure 7.9
The temperature dependences of the Poisson's ratio for (a) La_2CuO_{4-y} and (b) $La_{1.8}Sr_{0.2}CuO_{4-y}$ samples.

the superconducting sample at T_c . While for the parent compound the data are opposite to the temperature dependence of the ultrasonic wave velocities i.e a maximum was found in Poisson's ratio as a function of temperature at the same temperature as a minimum was found in the temperature dependences of the ultrasonic wave velocities and vice versa.

A large drop in the elastic moduli below 180K was found in a $La_{1.85}Sr_{0.15}CuO_4$ compound by Xiang et al (1988). They obtained a shear modulus at room temperature of 16GPa and a Young's modulus of 45GPa. Bourne et al (1987) found that at about 200K the Young's modulus in their $La_{1.85}Sr_{0.15}CuO_4$ sample shows an anomalous turnover and decreases with decreasing temperature until about 100K where it saturates abruptly. Kim et al (1988b) measured the elastic properties in $La_{1.85}Sr_{0.15}CuO_4$ and La_2CuO_4 compounds at 220K. They obtained a bulk modulus and a Poisson's ratio of 55GPa and 0.148 respectively for the superconducting compound and 103GPa and 0.266 for the parent compound.

7.3.3 THE PRESSURE DEPENDENCES OF ULTRASONIC WAVE VELOCITIES

The effects of hydrostatic pressure on the velocities of longitudinal and shear 5MHz ultrasonic waves propagated in $La_{1.8}Sr_{0.2}CuO_{4-y}$ and its parent compound La_2CuO_{4-y}, using Resin as a bonding material, are shown in figures 7.10 and 7.11 respectively. In each case the measurements were reproducible and showed no hysteresis effects; the ultrasonic velocities increase linearly with pressure, much more steeply for the longitudinal than for the shear mode. Although a large softening effect dominates the temperature dependence of ultrasonic wave velocities in $La_{1.8}Sr_{0.2}CuO_{4-y}$ (figure 7.3), the effect of pressure is to cause elastic stiffening. The linear dependence of ultrasonic wave velocities on pressure found for $La_{1.8}Sr_{0.2}CuO_{4-y}$ and its parent compound are similar to that found in the $Nd_{1.85}Ce_{0.15}CuO_{4-y}$ and its parent compound (chapter 6) but contrasts with the non-linear behaviour observed in $YBa_2Cu_3O_{7-x}$ and $GdBa_2Cu_3O_{7-x}$ (chapters 8 and 9 respectively), indicating that the vibrational anharmonicity of the long wavelength phonons is much less in the doped and undoped La_2CuO_{4-y} compounds.

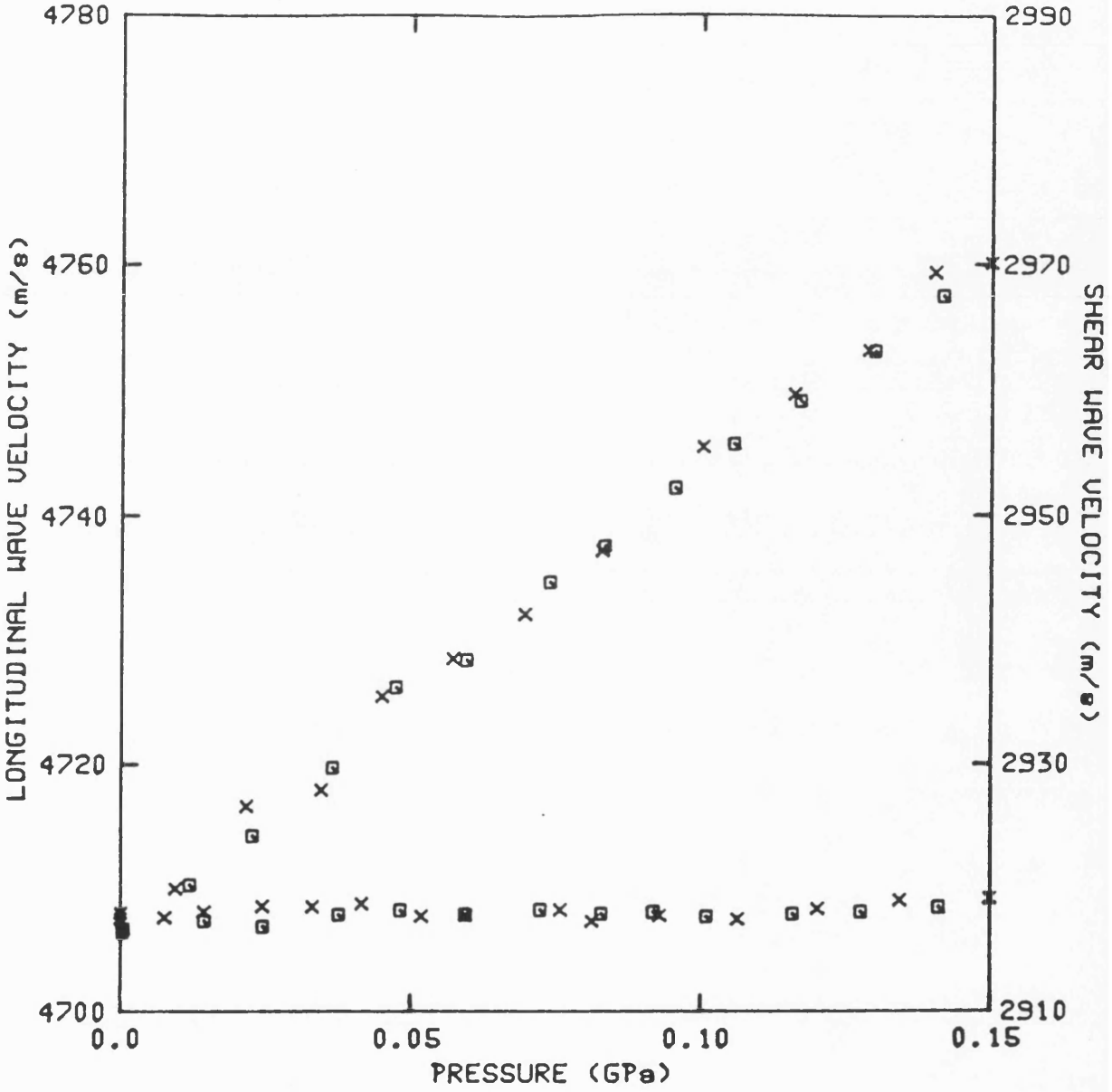

Figure 7.10
The hydrostatic pressure dependences of velocities of longitudinal (upper curve) and shear (lower curve) ultrasonic waves velocities propagated in $La_{1.8}Sr_{0.2}CuO_{4-y}$ at 295K. The crosses correspond to velocity measurements made with increasing pressure and the squares to data obtained as the pressure was decreased.

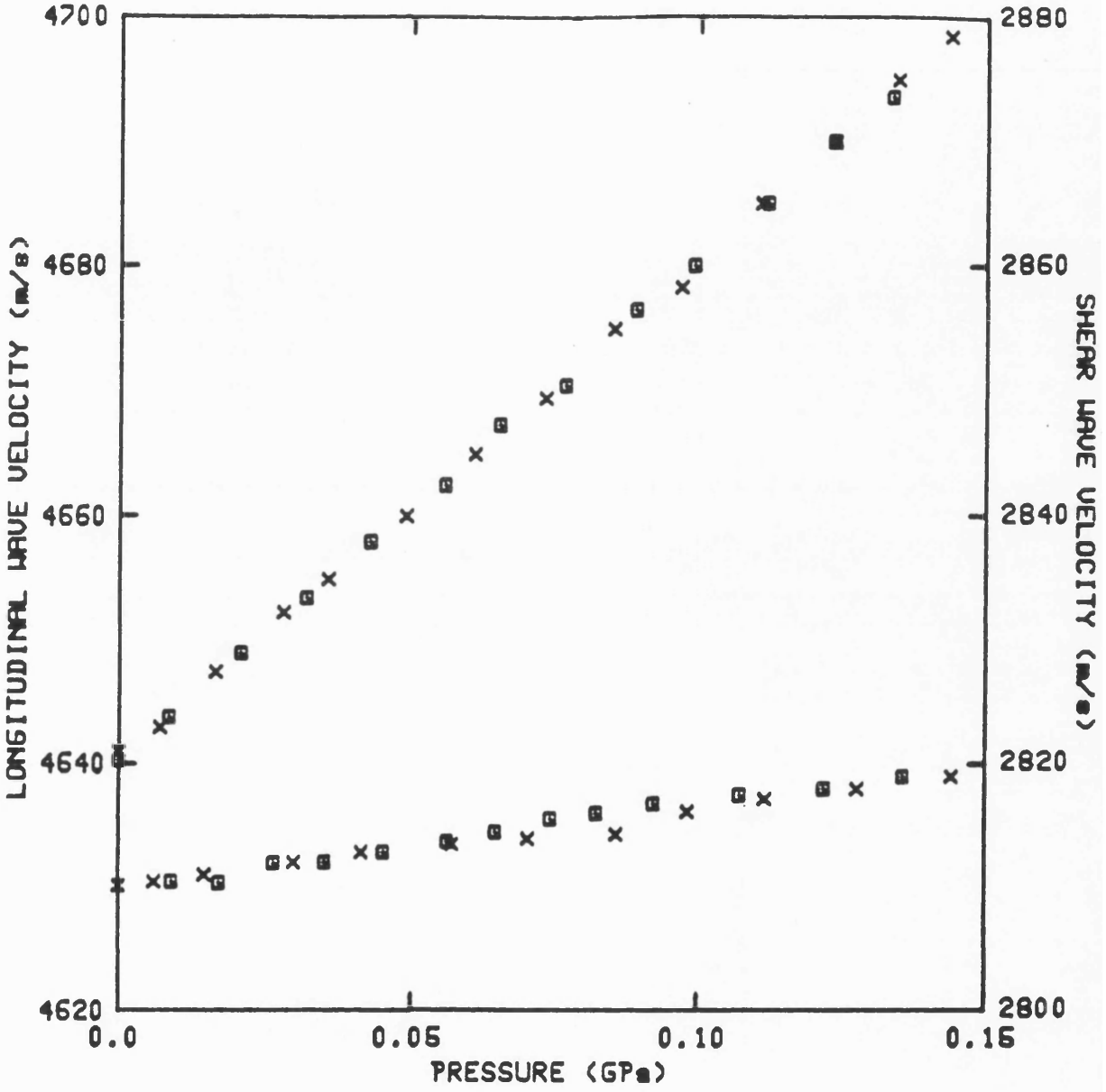

Figure 7.11
The hydrostatic pressure dependences of velocities of longitudinal (upper curve) and shear (lower curve) ultrasonic waves velocities propagated in La_2CuO_{4-y} at 295K. The crosses correspond to velocity measurements made with increasing pressure and the squares to data obtained as the pressure was decreased.

7.3.4 THE PRESSURE DEPENDENCES OF THE ELASTIC CONSTANTS

The elastic constants and their pressure derivatives have been obtained at room temperature from the measurements of the ultrasonic wave velocities as a function of pressure. The as-measured pressure dependences of C_L^n , shear C_S^n and the bulk B^n moduli for $La_{1.8}Sr_{0.2}CuO_{4-y}$ and La_2CuO_{4-y} compounds are shown in part (a) of figures 7.12 to 7.14 and part (a) of figures 7.15 to 7.17 respectively. The values of the elastic constants at room temperature are listed in table 7.4. The difference between the values of the elastic constants measured using Nonaq as a bonding material from those obtained by using Resin, can be seen by comparing the values in tables 7.3 and 7.4. Differences can be attributed to the use of two different bonding materials and also to the long time between the temperature experiment and the pressure experiment when the sample had to be left in a desiccator. The hydrostatic pressure derivatives $(\partial C_L/\partial P)_{P=0}$,$(\partial C_S/\partial P)_{P=0}$ and $(\partial B/\partial P)_{P=0}$ for both $La_{1.8}Sr_{0.2}CuO_{4-y}$ and La_2CuO_{4-y} compounds are also given in table 7.4.

Using the technique described in section 4.12, corrections for the effects of porosity on the elastic properties have been made: by inserting the experimental results into equations (4.4) and (4.5), the elastic properties for the non-porous matrix have been calculated. The values of C_L^m ,

Table 7.4. Elastic and physical properties at room temperature for the $La_{1.8}Sr_{0.2}CuO_{4-y}$ high temperature superconductor and its parent compound La_2CuO_{4-y} obtained from the ultrasonic wave velocities using Resin as a bonding material.

Property	$La_{1.8}Sr_{0.2}CuO_{4-y}$		La_2CuO_{4-y}	
	Porous	Non-porous matrix	Porous	Non-porous matrix
Density Kgm^{-3}	6000	7122	6495	7105
Porosity	0.16	-	0.09	-
Ultrasonic wave Velocities ms^{-1}				
Longitudinal V_L	4706	5206	4641	4906
Shear V_S	2917	3245	2810	2978
Bulk modulus B (GPa)	65	93	72	87
Young's modulus E (GPa)	121	177	124	152
Poisson's ratio	0.188	0.182	0.211	0.210
C_L (GPa)	133	193	140	171
C_S (GPa)	51	75	51	63
Acoustic Debye temperature (Θ_D^{el}) (K)	383	452	377	410
$(\partial B/\partial P)_{P=0}$	21	36	19.7	28.7
$(\partial C_L/\partial P)_{P=0}$	22.4	36.6	23.2	31.7
$(\partial C_S/\partial P)_{P=0}$	1.3	0.9	2.6	2.7
Superconducting transition temperature T_C (K)	32	-	-	-

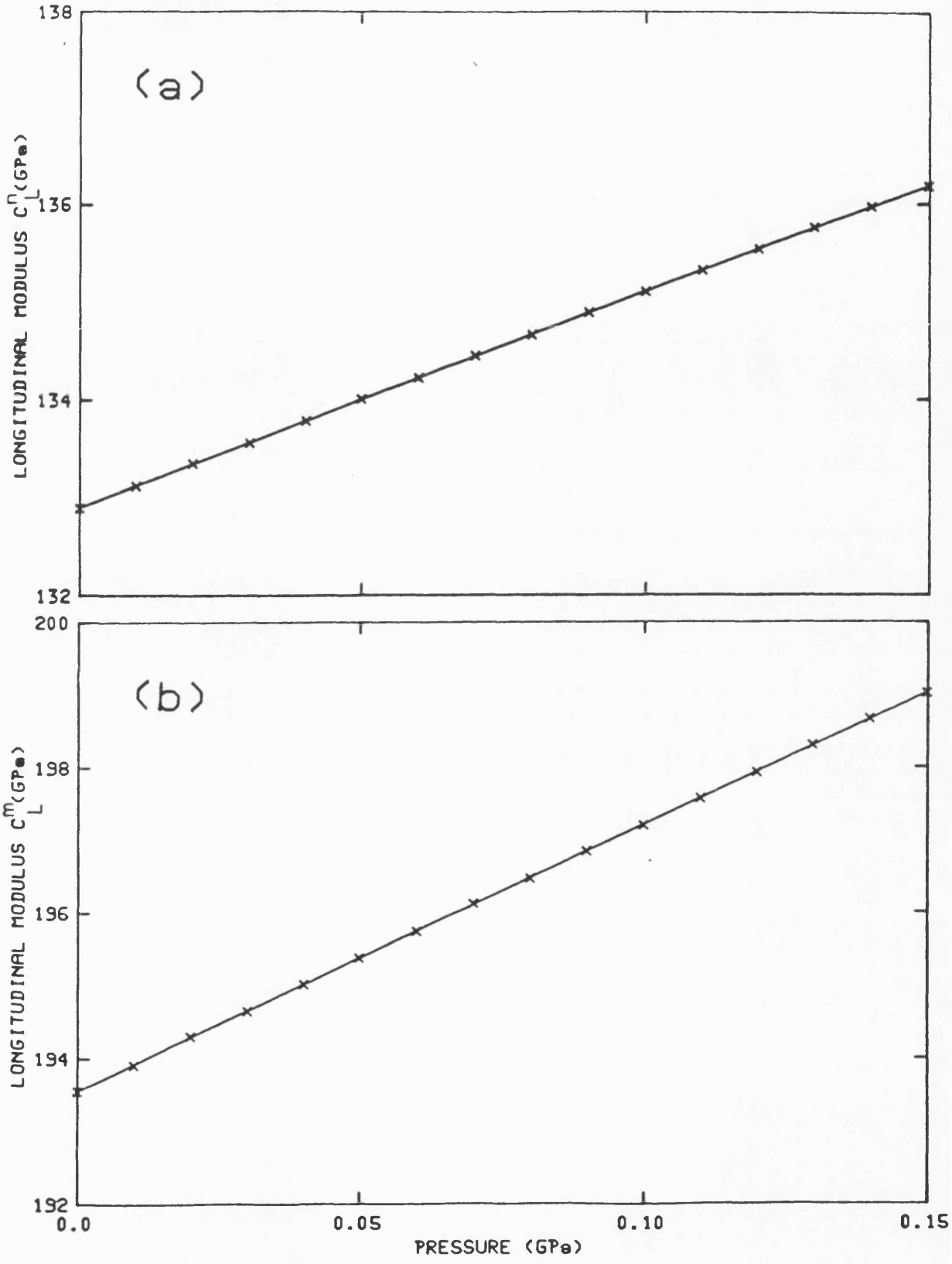

Figure 7.12
The hydrostatic pressure dependences of the longitudinal modulus (a) C_L^n (porous material) and (b) C_L^m (non-porous matrix) of $La_{1.8}Sr_{0.2}CuO_{4-y}$ at 295K calculated from the experimental data and using equations 4.4 and 4.5. The solid lines are least square fits to the data.

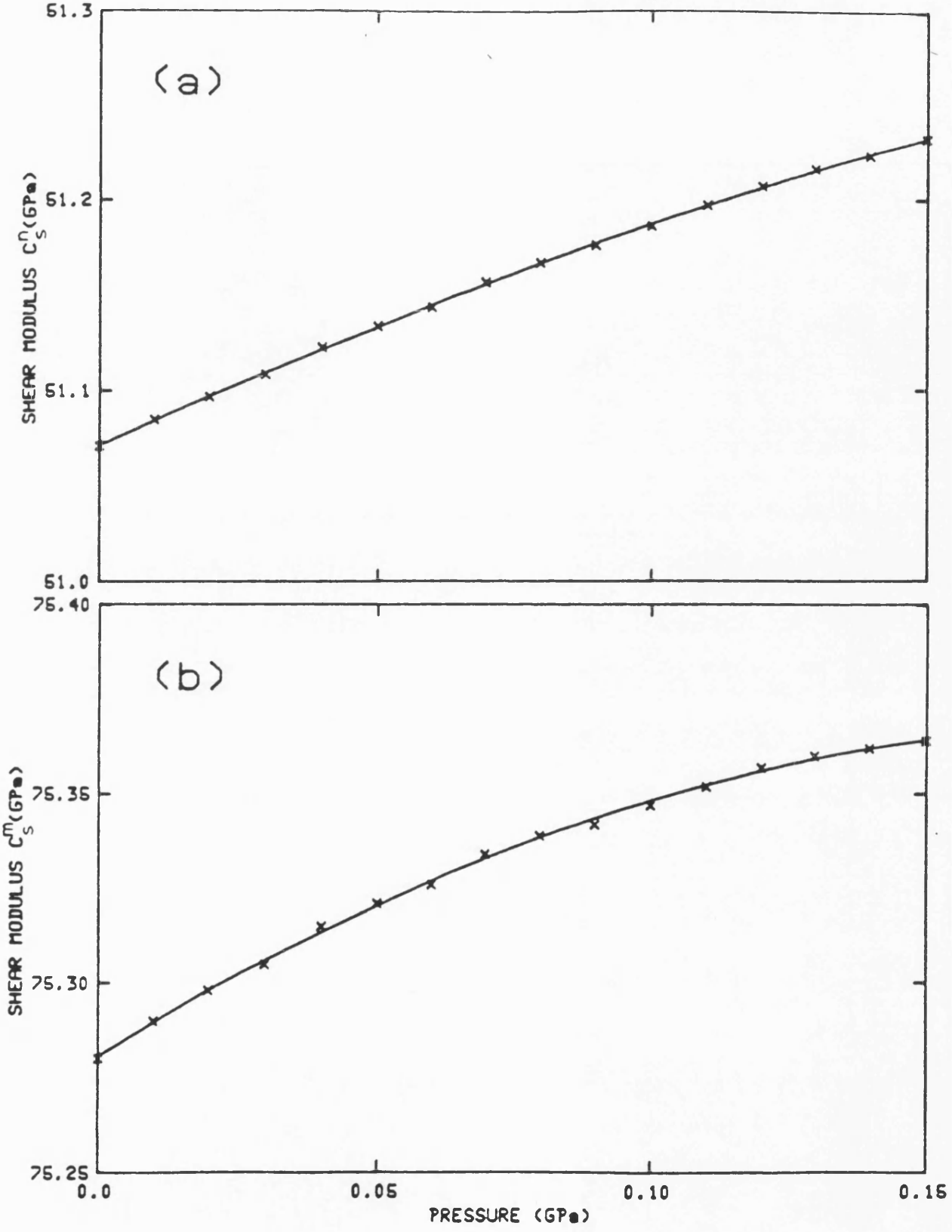

Figure 7.13
The hydrostatic pressure dependences of the shear modulus (a) C_S^n (porous material) and (b) C_S^m (non-porous matrix) of $La_{1.8}Sr_{0.2}CuO_{4-y}$ at 295K calculated from the experimental data and using equations 4.4 and 4.5. The solid lines are least square fits to the data.

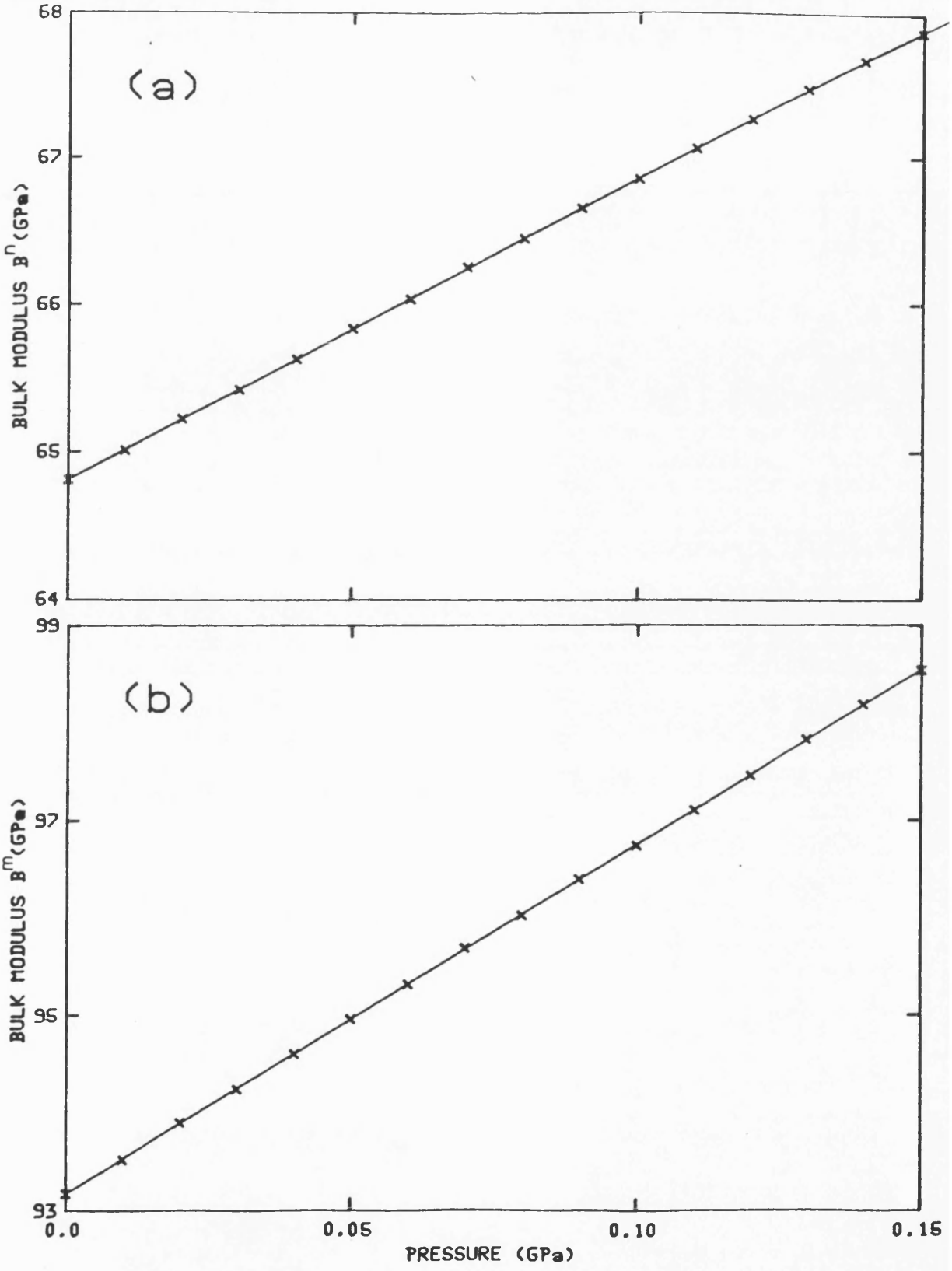

Figure 7.14
The hydrostatic pressure dependences of the bulk modulus (a) B^n (porous material) and (b) B^m (non-porous matrix) of $Nd_{1.85}Ce_{0.15}CuO_{4-y}$ at 295K calculated from the experimental data and using equations 4.4 and 4.5. The solid lines are least square fits to the data.

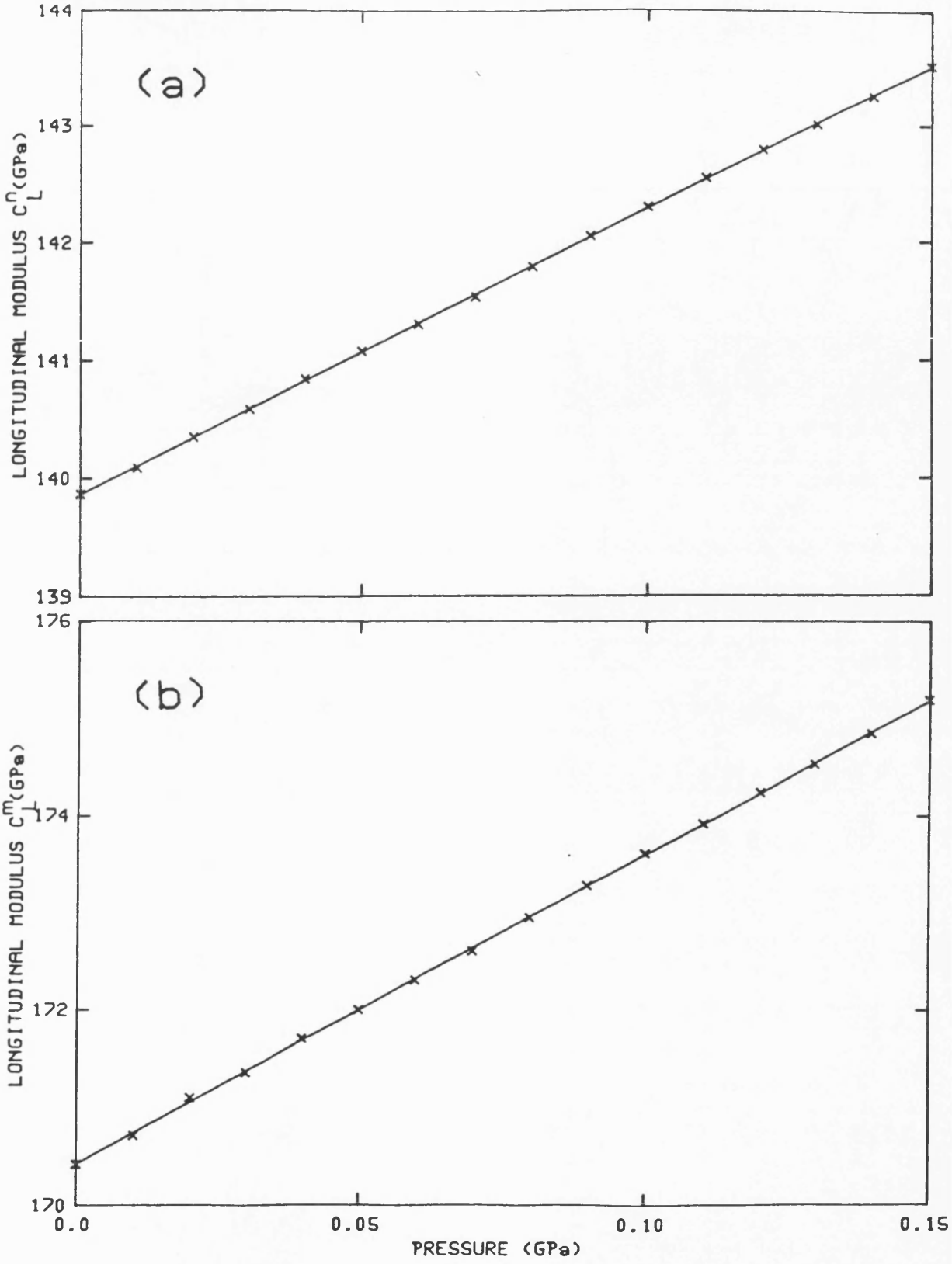

Figure 7.15
The hydrostatic pressure dependences of the longitudinal modulus (a) C_l^n (porous material) and (b) C_l^m (non-porous matrix) of La_2CuO_{4-y} at 295K calculated from the experimental data and using equations 4.4 and 4.5. The solid lines are least square fits to the data.

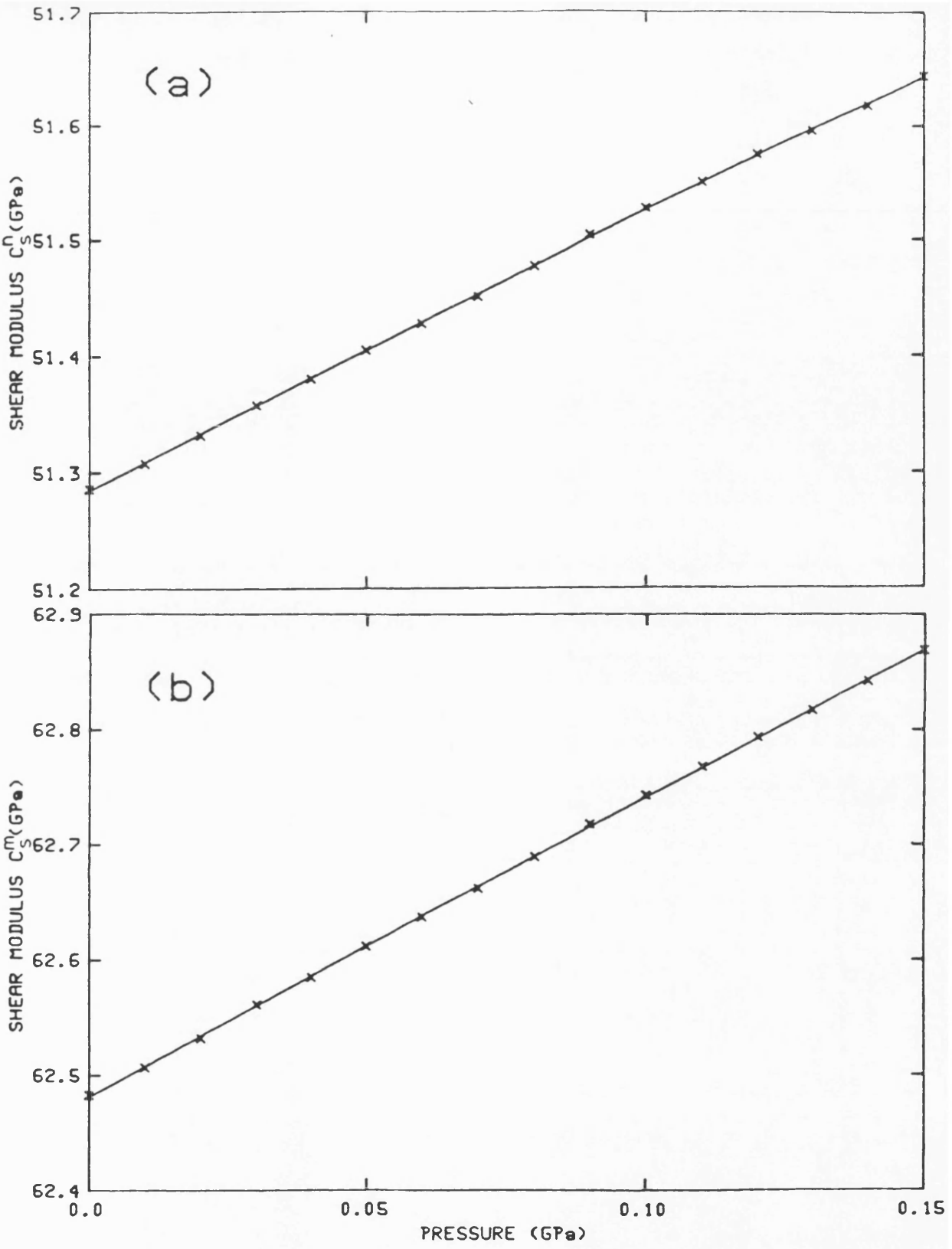

Figure 7.16
The hydrostatic pressure dependences of the shear modulus (a) C_S^n (porous material) and (b) C_S^m (non-porous matrix) of La_2CuO_{4-y} at 295K calculated from the experimental data and using equations 4.4 and 4.5. The solid lines are least square fits to the data.

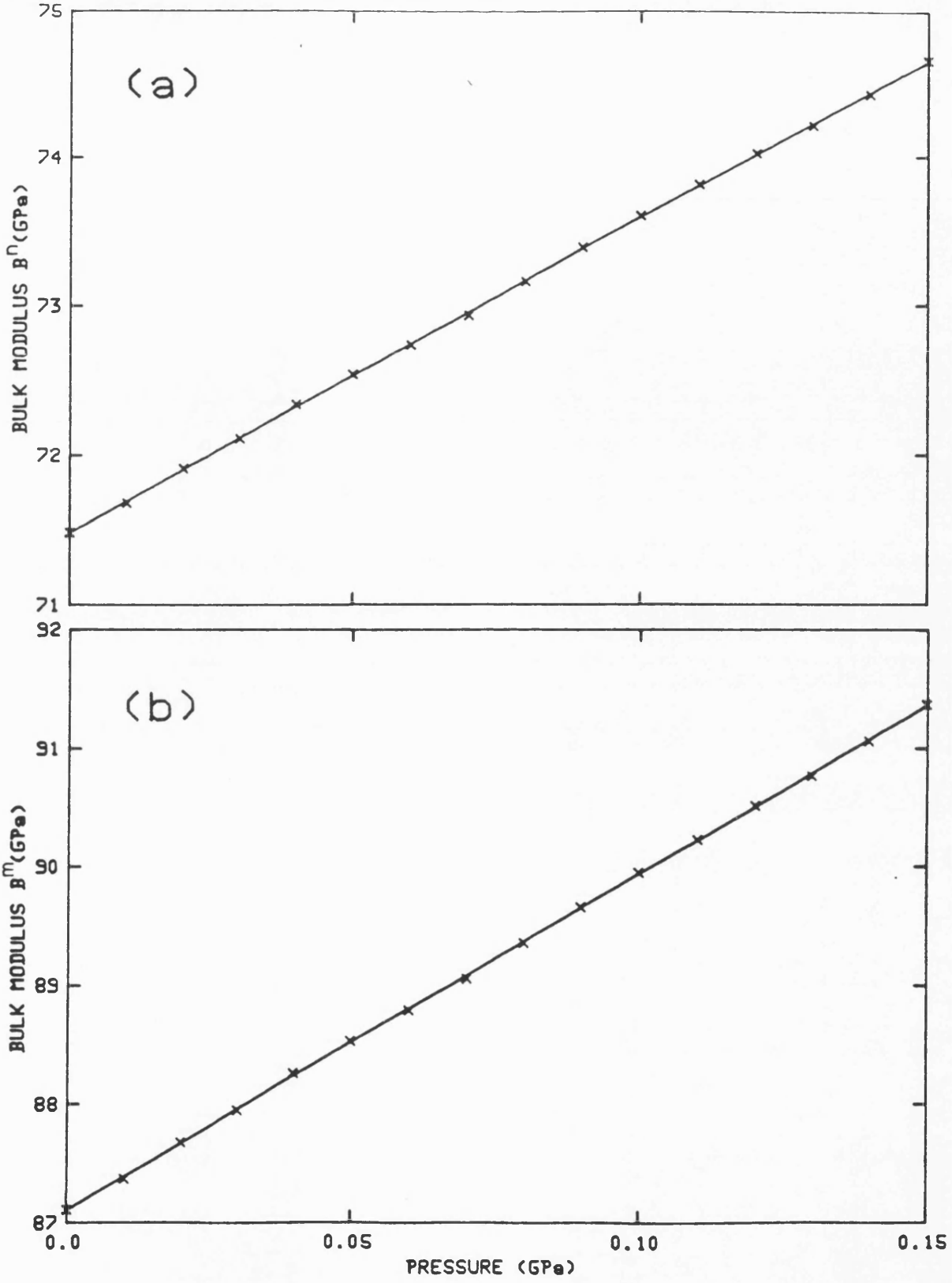

Figure 7.17
The hydrostatic pressure dependences of the bulk modulus (a) B^n (porous material) and (b) B^m (non-porous matrix) of La_2CuO_{4-y} at 295K calculated from the experimental data and using equations 4.4 and 4.5. The solid lines are least square fits to the data.

shear C_S^m and the bulk B^m moduli taking porosity into account are listed in table 7.4 together with those for Young's modulus and Poisson's ratio. The pressure dependences of C_L^m, shear C_S^m and the bulk B^m moduli of the non-porous matrix for $La_{1.8}Sr_{0.2}CuO_{4-y}$ and La_2CuO_{4-y}, obtained by using equations (4.4) and (4.5), are shown in part (b) of figures 7.12-7.17. The hydrostatic pressure derivatives $(\partial C_L/\partial P)_{P-0}$, $(\partial C_S/\partial P)_{P-0}$ and $(\partial B/\partial P)_{P-0}$ determined at room temperature in the limit as pressure tends to zero are given in table 7.4. It can be seen from that table and figures 7.12-7.17 that the effects of porosity are to reduce the elastic moduli and their pressure derivatives. It can also be seen that $(\partial C_S/\partial P)_{P-0}$ is much smaller than $(\partial C_L/\partial P)_{P-0}$. The effects of porosity found here are similar to those found for $Nd_{1.85}Ce_{0.15}CuO_{4-y}$ and its parent compound Nd_2CuO_{4-y} (chapter 6). If the large values of $(\partial B/\partial P)_{P-0}$ and $(\partial C_L/\partial P)_{P-0}$ were solely a consequence of porosity, then $(\partial C_S/\partial P)_{P-0}$ would also be expected to be influenced by porosity and be quite large, which is not the case for any of these materials.

Ledbetter et al (1989a) reported the ultrasonic wave velocities, elastic constants and the Debye temperatures (Θ_D^{el}) of the "void-free state" of both La_2CuO_{4-y} and $La_{1.85}Sr_{0.15}CuO_{4-y}$. Although they have used a different method than the one used here to correct for the effects of porosity,

their results are in reasonable agreement with the present results given in table 7.4. The lattice parameters under pressure were determined at room temperature for a $La_{1.8}Sr_{0.2}CuO_{4-y}$ sample up to 70GPa by Takahashi et al (1987a,b) and also by Terada et al (1987) on $La_{1.4}Sr_{0.6}CuO_{4-y}$ sample. The effects of pressure on the lattice parameters were measured by Dietrich et al (1987a,b) at 150K, 60K and 15K up to a maximum of 15GPa on a $La_{1.8}Sr_{0.2}CuO_{4-y}$ sample. They obtained a bulk modulus averaged over the pressure range 0 to 8GPa of 107GPa at 300K and 150GPa at 15K. They concluded from their measurements that the sample was compressed isotropically although the ratio c/a changes discontinuously when the orthorhombic to tetragonal line is crossed on the phase diagram.

An important test of our method of correcting for the influence of porosity based on the results of wave scattering theory is to compare the corrected ultrasonic wave velocities for the non-porous matrix with single crystal data. All nine elastic constants of an untwinned single crystal of La_2CuO_{4-y} have been measured using a resonant ultrasound technique [Migliori et al (1990)]. The average longitudinal wave velocity derived from this single crystal data is 5050ms^{-1}

and that for shear modes is 3260ms^{-1}, in good agreement with the values (V_L =4906ms^{-1} and V_S =2978ms^{-1}) obtained here for the non-porous matrix of polycrystalline La_2CuO_{4-y}.

The values of the bulk modulus B^m obtained for both $La_{1.8}Sr_{0.2}CuO_{4-y}$ and La_2CuO_{4-y} compounds using the correction technique described in section 4.12, are compared in table 7.5 with those obtained by other groups using different techniques. The bulk modulus at atmospheric pressure B_o of monocrystalline La_2CuO_4 measured as 113GPa [Migliori et al (1990)] is similar to the values determined ultrasonically for the non-porous matrix of ceramic material as 122GPa [Ledbetter et al (1989a)] and that given here in table 7.5, but is much smaller than the isothermal bulk modulus $B^T(P)$ (182GPa and 176GPa) obtained from lattice constant data determined at very high pressure using the diamond cell technique [Fietz et al (1989) and Akhtar et al (1988) respectively]. The substantial differences between B_o and $B^T(P)$ seem to be arising from the contribution to the bulk modulus at high pressure of the large pressure derivative $(\partial B/\partial P)_{P=0}$. This point will be discussed later when the results obtained for the $La_{1.8}Sr_{0.2}CuO_{4-y}$ and its parent La_2CuO_{4-y} compounds will be compared in chapter 11 with those obtained for the other high temperature superconducting compounds.

Table 7.5. Comparison between the values of bulk modulus obtained for the non-pouros matrices of $La_{1.8}Sr_{0.2}CuO_{4-y}$ and La_2CuO_{4-y} compounds using the technique described in section 4.12 and those obtained by other groups using different techniques.

References	Bulk modulus (GPa)		Methods
	$La_{1.8}Sr_{0.2}CuO_{4-y}$	La_2CuO_{4-y}	
This work	93	87	correction for porosity using the technique in section 4.12
Akhtar et al (1988)	-	176	lattice parameters under high pressure using the diamond cell technique and energy dispersive diffraction
Allan and Mackrodt (1988)	-	156 (orthorhombic) 232 (tetragonal)	theoretical technique to calculate the elastic constants
Fietz et al (1989)	-	182	lattice parameters under high pressure using the diamond cell technique and X-ray diffraction
Ledbetter et al (1989)	137.4	122	using a technique for correction for the effects of porosity on the ultrasonic wave velocities
Migliori et al (1990)	-	113	by measuring the ultrasonic wave velocities in a single crystal using ultrasound resonant technique
Pei et al (1990)	147	-	lattice parameters under high pressure using the diamond cell technique and neutron powder diffraction

CHAPTER EIGHT

ULTRASONIC STUDIES OF SUPERCONDUCTING $YBa_2Cu_3O_{7-x}$ COMPOUNDS OF DIFFERENT GRAIN SIZE

8.1 INTRODUCTION

Ultrasonic wave velocities in $YBa_2Cu_3O_{7-x}$ compound have been measured as a function of hydrostatic pressure and temperature. Similar measurements have been reported by different groups [see for example Srinivasan (1988a), Dominec (1989) and Mase (1989)]. They have revealed considerable sample to sample variations and in some cases extensive thermal hysteresis in the temperature dependences of ultrasonic wave velocities in this ceramic of highly variable microstructural properties including density, pores, grain size and oxygen content. Differences between the various findings about the temperature dependence of the sound velocity are most striking. This is not too surprising because of the porous and defect nature of the material. Taking into account that in typical 123 ceramics the porosity varies between 4% and 30% and applying the formalism of Sayers (1981), it follows that the elastic moduli depend on the amount and the strength of the interconnecting regions between the sintered grains.

The $YBa_2Cu_3O_{7-x}$ samples investigated were prepared as described in chapter 4. Debye-Scherrer X-ray powder photography was carried out on the fine grain sample (sample Y1) which gave lattice parameters a = 3.826±0.002 Å, b = 3.888±0.002 Å and c = 11.677±0.003 Å, and a theoretical density of 6338 kgm^{-3}. The correlation between oxygen content and c-axis lattice parameter [Cava et al (1987b)] suggests an oxygen composition of 6.85 per molecular unit (i.e., X in $YBa_2Cu_3O_{7-x}$ is equal to 0.15).

The temperature dependences of the ultrasonic wave velocities and the elastic constants for a fine grain sample with a grain size of ≈ 10μ (sample Y1) and a coarse grain sample with a grain size of ≈ 50μ (sample Y2) of $YBa_2Cu_3O_{7-x}$ are presented in sections 8.2 and 8.3 respectively. The hydrostatic pressure dependences of the ultrasonic wave velocities in the fine grain sample (Y1) with a porosity of 0.18 are discussed in section 8.4 and those for the coarse grain sample (Y2) with a porosity of 0.056 in section 8.5. The elastic constants as a function of pressure of the $YBa_2Cu_3O_{7-x}$ samples are explained in section 8.6. The compression of samples Y1 and Y2 are calculated and discussed in section 8.7. In section 8.8 the temperature dependences of the hydrostatic pressure derivative of C_L $[(\partial C_L/\partial P)_{P=0,T}]$ is

presented and discussed. Finally in section 8.9 the preparation of a halide flux grown large grained sample of $YBa_2Cu_3O_{7-x}$ together with its electrical resistance and ultrasonic studies are presented and discussed in comparison with the results from the ceramic material.

8.2 THE TEMPERATURE DEPENDENCES OF ULTRASONIC WAVE VELOCITIES

The velocities of ultrasonic waves propagated in a fine grain sample of $YBa_2Cu_3O_{7-x}$ compound (designated sample Y1, with density about 82% of the theoretical density) were measured as a function of temperature in the temperature region 90-300K. X- and Y-cut 5MHz quartz transducers, bonded to the sample by Nonaq stopcock grease, were used to generate longitudinal and shear ultrasonic waves respectively. The results obtained are shown in figure 8.1. It can be seen from that figure that at about 190K during the cooling process there is a step-like increase in both the longitudinal and shear wave velocities, while on warming a step-like decrease at about 230K occurs for both modes. Thus there is a marked thermal hysteresis for this effect of width ΔT which is almost the same for both mode velocities. The thermal hysteresis and the step-like behaviour contrast markedly with the elastic behaviour of $Nd_{2-x}Ce_xCuO_{4-y}$ and $La_{2-x}Sr_xCuO_{4-y}$ compounds (chapters 6 and 7 respectively) where elastic softening was found in the $La_{2-x}Sr_xCuO_{4-y}$ compound and no thermal hysteresis was found for both materials. The reproducibility of the results was examined by running a second thermal cycle. The results obtained in the second thermal cycle fell almost on those obtained during the first one, as shown in figure 8.1.

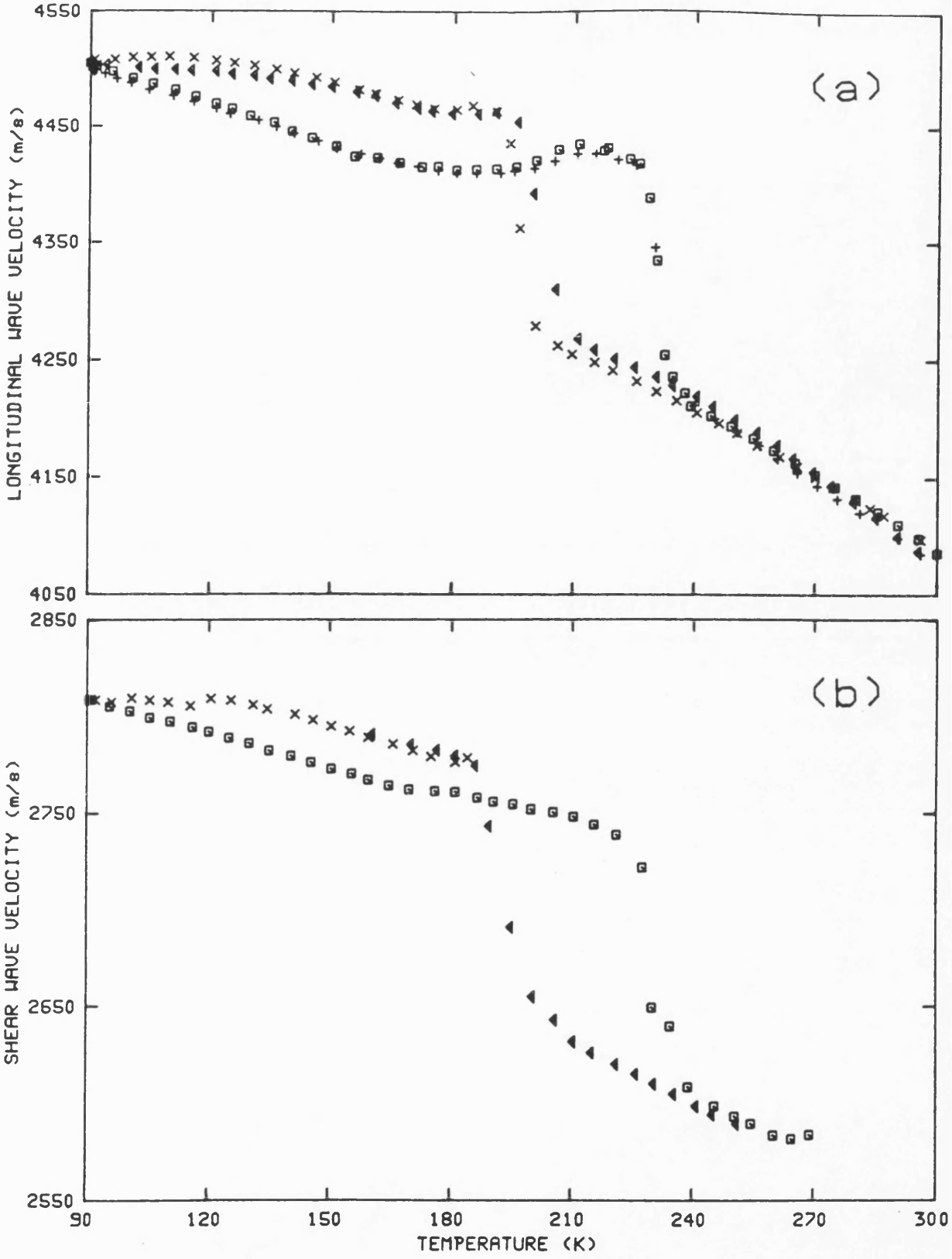

Figure 8.1

The temperature dependences of ultrasonic (a) longitudinal and (b) shear waves velocities for $YBa_2Cu_3O_{7-x}$ (sample Y1). The crosses (x) correspond to the data obtained during cooling and the squares to those obtained during warming. The triangles correspond to the data obtained during the second cooling cycle and the pluses (+) to those obtained in the second warming cycle.

The temperature dependences of ultrasonic wave velocities were measured in another sample of $YBa_2Cu_3O_{7-x}$ compound with coarse grains (sample Y2, with a density of 94.4% of the theoretical density). The results are shown in figure 8.2 [Almond et al (1987)]. For this sample there is a distinct dip in sound velocity at about 80K. Above this temperature there are significant differences between data obtained on cooling and those obtained on warming. In the lowest temperature region, below the transition temperature of the superconductor (92K), the ultrasonic wave velocities exhibit little elastic hysteresis. At much higher temperatures (170-180K) a markedly increasing velocity for both longitudinal and shear waves was consistently observed during cooling. By comparing figures 8.1 and 8.2 it can be seen that in both samples the ultrasonic wave velocities increase with decreasing temperature and that both samples exhibit a large thermal hysteresis but in different temperature regions. The ultrasonic wave velocities at room temperature measured in the present work are compared in table 8.1 with those obtained by other groups.

Some groups observed an anomalous behaviour in the ultrasonic wave velocities in the temperature range 200-240K in $YBa_2Cu_3O_{7-x}$ compound [Yusheng et al (1987), Ramachandran et al (1988) and Toulouse et al (1988)]. Many groups found

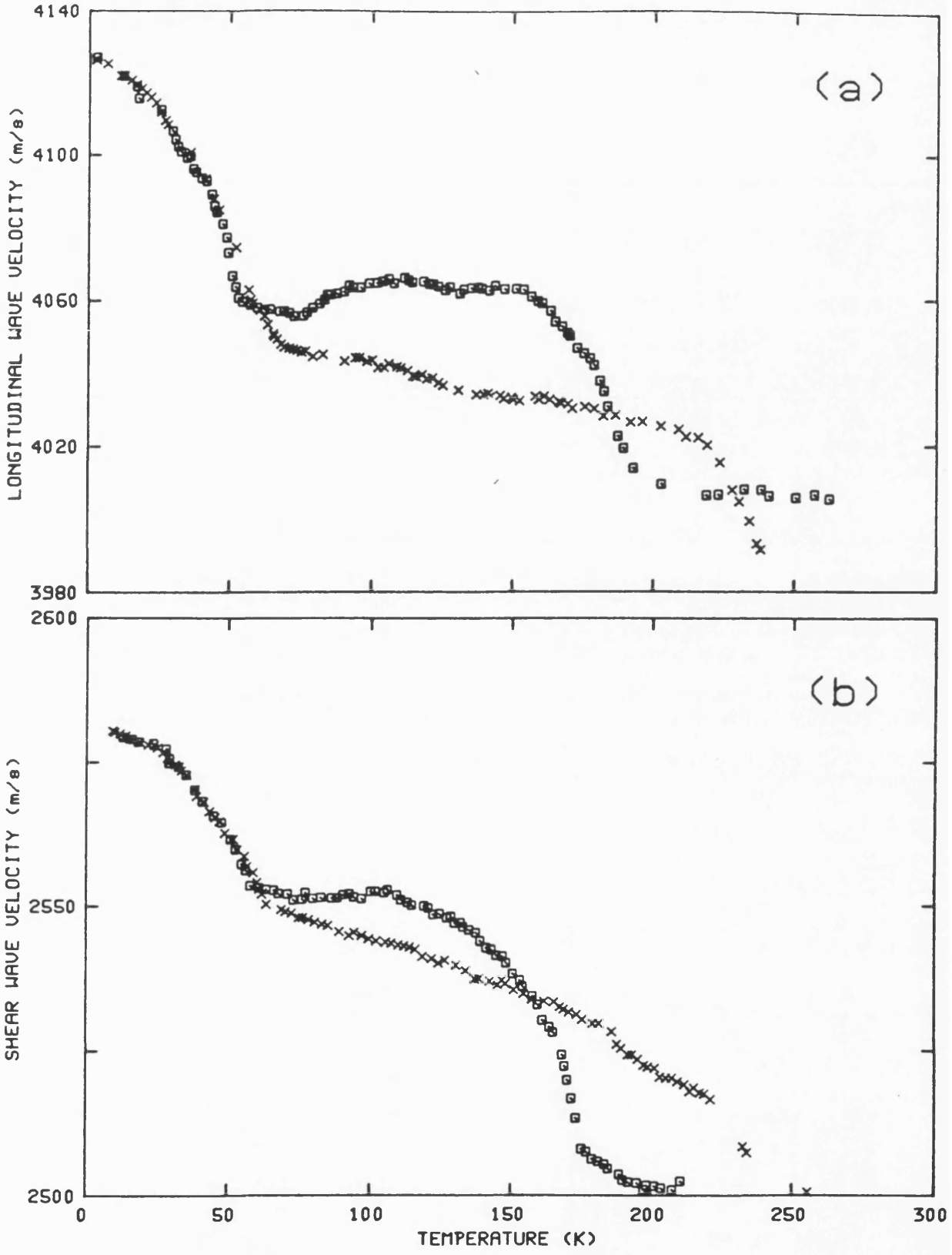

Figure 8.2
The temperature dependences of ultrasonic (a) longitudinal and (b) shear waves velocities for $YBa_2Cu_3O_{7-x}$ (sample Y2). The crosses (x) correspond to the data obtained during cooling and the squares to those obtained during warming. The data taken from Almond et al (1987).

Table 8.1. Comparison between the ultrasonic wave velocities for the $YBa_2Cu_3O_{7-X}$ compound obtained in this work with some of those obtained by other groups. The theoretical density is 6338 Kg/m^3 taken from the measurements of the lattice parameters.

References	(%) of the theoretical density	Ultrasonic wave velocities		Temperature (K)
		Longitudinal (m/s)	Shear (m/s)	
This Work Y1 Y2	 82 94.4	 4099 4000	 2559 2475	 293 293
Choi et al 1989 A B C D	 84 76 71 70	 4143 4048 3680 3060	- 	 80 80 80 80
Golding et al 1987	-	3800	2800	293
Kim et al 1990 (Single Crystal)	-	5617	2191	220
Laegreid et al 1988	-	3920	-	293
Lang et al 1988	-	4130	2540	220
Lemmens et al 1988	78 92	3480 4980	2010 2910	250 250
Mathias et al 1987	70	-	1700	293
Ramachandran et al 1988	85	4700	-	293
Saint-Paul and Henry 1989b (Single Crystal)	-	6000	3600	293
Sun et al 1988	70	3140	-	293
Suzuki et al 1988 (Ortho.) (Tetra.)	- 83 88	 4500 4900	- 	 293 293
Toulouse et al 1988	-	3930	2228	293
Wolf et al 1988	-	3520	2170	220

a thermal hysteresis in the temperature dependences of ultrasonic wave velocities in the $YBa_2Cu_3O_{7-x}$ compound [Almond et al (1987), Xiaorong et al (1987), Yusheng et al (1987), Laegreid et al (1988b), Ledbetter and Kim (1988), Muller et al (1988), Ramachandran et al (1988), Choi et al (1989), Ivanov and Tsymbal (1990), Kim et al (1990) and Wang et al (1990)]. In most of forementioned papers it is found that the ultrasonic wave velocities in the $YBa_2Cu_3O_{7-x}$ compound increase as the temperature is decreased with a sharper increase in the superconducting state below T_c [Almond et al (1987), Bishop et al (1987b), Migliori et al (1987), Xiaorong et al (1987), Bhattacharya et al (1988), Durán et al (1988), Jericho et al (1988), Sun et al (1988) and Saint-Paul et al (1989a)]. Lemmens et al (1988) measured the sound velocities in two $YBa_2Cu_3O_{7-x}$ samples with different grain size. They found that for the coarse grained sample there is a thermal hysteresis and a decrease in the ultrasonic velocities above 60K on warming while these anomalies were absent in the fine grained sample. Suzuki et al (1988) measured the ultrasonic wave velocities in two samples of $YBa_2Cu_3O_{7-x}$: one in the orthorhombic structure with $x = 0.1$ and the second one in the tetragonal structure with $x = 0.8$. They found that in both samples the ultrasonic wave velocities increase as the temperature is decreased with an additional

increase below T_c in the orthorhombic sample but not into the tetragonal sample. Ledbetter and Kim (1988) found that both mode velocities show thermal hysteresis in their $YBa_2Cu_3O_{7-x}$ sample. They suggested that a hysteretic phase change occurs between 160 and 70K during cooling and between 170 and 260K during warming. Ramachandran et al (1988) measured the ultrasonic wave velocities in two samples of $YBa_2Cu_3O_{7-x}$ with different densities. They found that in both samples the velocities increase as the temperature is decreased with a drop at 250K during the cooling cycle and a large increase below T_c , but they observed a thermal hysteresis in the low density sample but not in the high density sample.

Anomalies in the temperature region 200-240K have also been observed in the measurements of other physical properties as a function of temperature. Francois et al (1988) observed an anomaly in the lattice parameters near 90K and 240K when they measured them as a function of temperature in a $YBa_2Cu_3O_7$ sample. Cheng et al (1988) have measured the lattice parameters as a function of temperature in $YBa_2Cu_3O_x$ samples with different oxygen content. They found a step-like increase in the lattice parameter b at around 210K in all the samples they have investigated. Srinivasan et al (1988b) used a powder diffractometer to determine the lattice

parameters for a $YBa_2Cu_3O_{7-x}$ sample in the temperature range 300-80K. They observed a sharp drop in c parameter around 240K. Xu et al (1988) measured the ultrasonic attenuation in a single-phase $YBa_2Cu_3O_7$ sample as a function of temperature. They observed an attenuation peak in their measurements at 252K. Cannelli et al (1988) found a maximum around 240K in their measurements of internal friction as a function of temperature in a $YBa_2Cu_3O_{7-x}$ sample. They observed that the maximum only appeared when the sample was cooled but was suppressed and only a trace of it appeared on warming. Yening et al (1987) also found a peak in their internal friction measurements as a function of temperature around 240K in their $YBa_2Cu_3O_{9-x}$ sample. Meanwhile, Kusz and Murawski (1988) found an internal friction peak at 212K in their measurements as a function of temperature in a $YBa_2Cu_3O_7$ sample. Finally, Laegreid and Fossheim (1988) found a peak in their specific heat measurements as a function of temperature at around 217K in their $YBa_2Cu_3O_{7-x}$ sample. They suggested that the observed behaviour is caused by an intrinsic structural instability related to the oxygen vacancies.

The anomalies found around 240K were attributed by all these workers to a possible structural phase transition and the thermal hysteresis to internal pressures generated in

the individual crystallites during structural phase transitions. These transitions produce anisotropic expansions which are constrained, producing internal pressures, in polycrystalline samples. The reversibility of the elastic properties below T_c appear to indicate a transformation to an elastically isotropic structure. However, it is also possible that the thermal expansion is small enough at low temperatures to preclude the development of hysteresis driven by the internal strain effect [Almond et al (1987)].

As a matter of fact there are many papers published in the literature about the physical properties as a function of temperature of the $YBa_2Cu_3O_{7-x}$ compound which make it the most studied compound from all of the new high temperature superconducting compounds and the results mentioned above are just the most major papers in the literature.

8.3 THE TEMPERATURE DEPENDENCES OF THE ELASTIC MODULI

The elastic constants of $YBa_2Cu_3O_{7-x}$ samples were calculated using the measured ultrasonic wave velocities and the experimental density in the isotropic approximation. The temperature dependences of longitudinal C_L^n and shear C_S^n moduli for samples Y1 and Y2 are shown in figures 8.3 and 8.4 respectively. From those figures it can be seen that both moduli increase as the temperature is decreased with a thermal hysteresis effect in both samples. The temperature dependences of the bulk modulus B^n for both samples are shown in figure 8.5. The anomaly around 240K and the thermal hysteresis are clearly pronounced. The temperature dependences of Young's modulus and Poisson's ratio are shown in figures 8.6 and 8.7 respectively. Again the anomaly in the results and the thermal hysteresis can be seen in these properties. The triangles in part a of figures 8.4 to 8.7 correspond to the data obtained in the second cooling cycle. The experimental values for the elastic constants of samples Y1 and Y2 measured at room temperature are given in table 8.2.

The temperature dependences of the elastic constants have been measured and reported by many groups. Hoen et al (1988) found a sharp increase in Young's modulus as the temperature decreased below T_c in their $YBa_2Cu_3O_7$ sample.

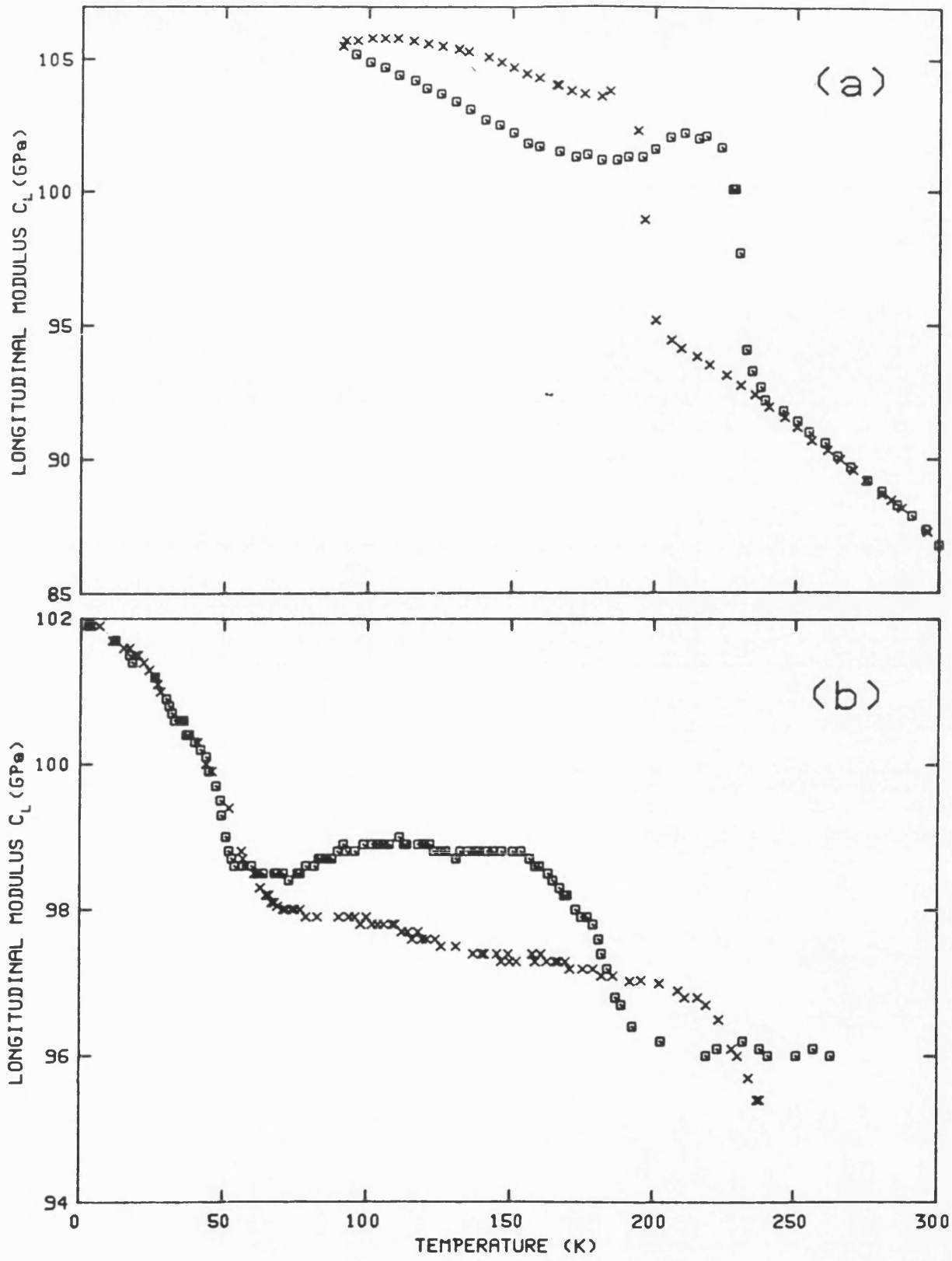

Figure 8.3
The temperature dependences of the longitudinal modulus C_L for (a) $YBa_2Cu_3O_{7-x}$ (sample Y1) and (b) $YBa_2Cu_3O_{7-x}$ (sample Y2). The crosses (x) correspond to the data obtained during cooling and the squares to those obtained during warming.

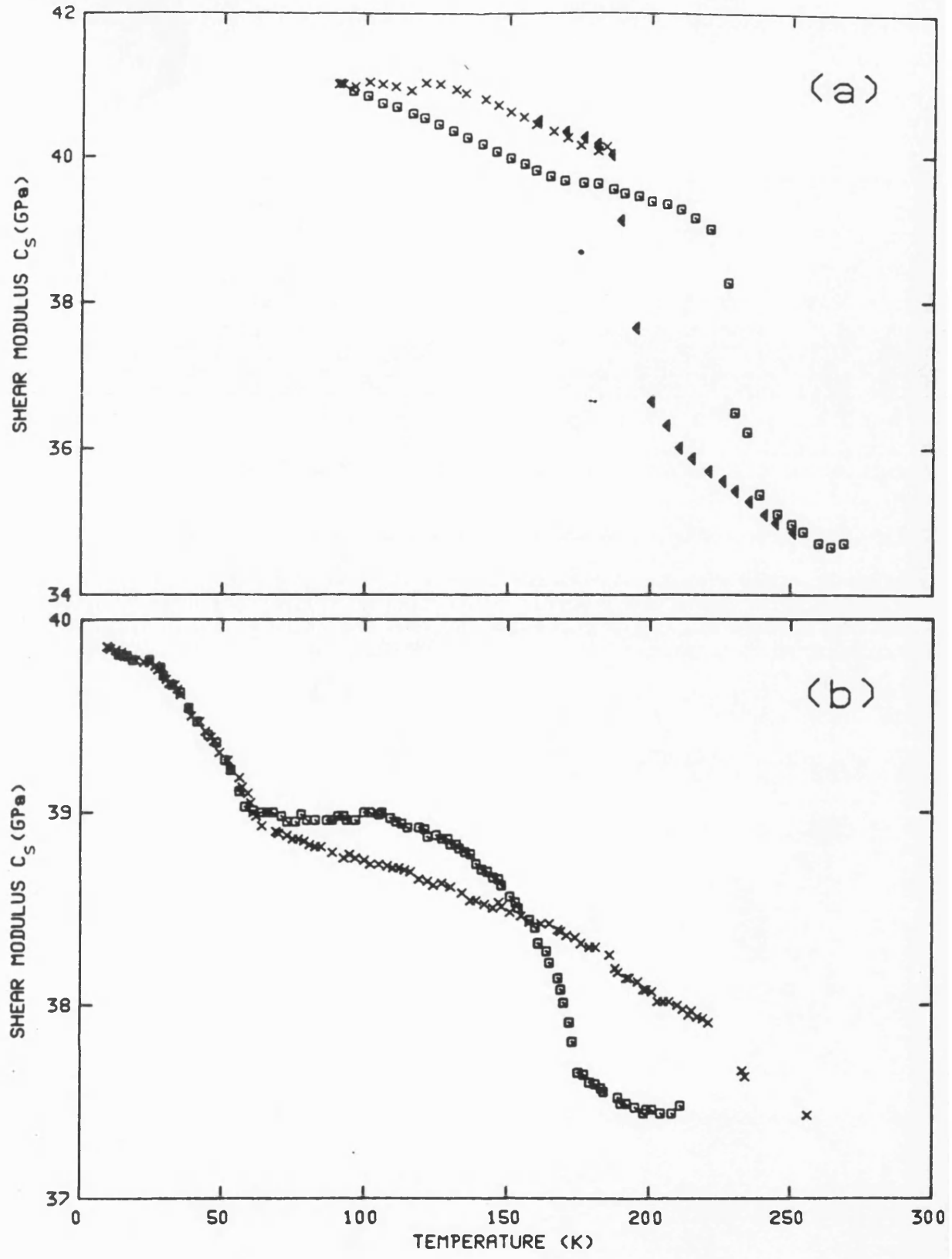

Figure 8.4
The temperature dependences of the shear modulus C_S for (a) $YBa_2Cu_3O_{7-x}$ (sample Y1) and (b) $YBa_2Cu_3O_{7-x}$ (sample Y2). The crosses (x) correspond to the data obtained during cooling and the squares to those obtained during warming.

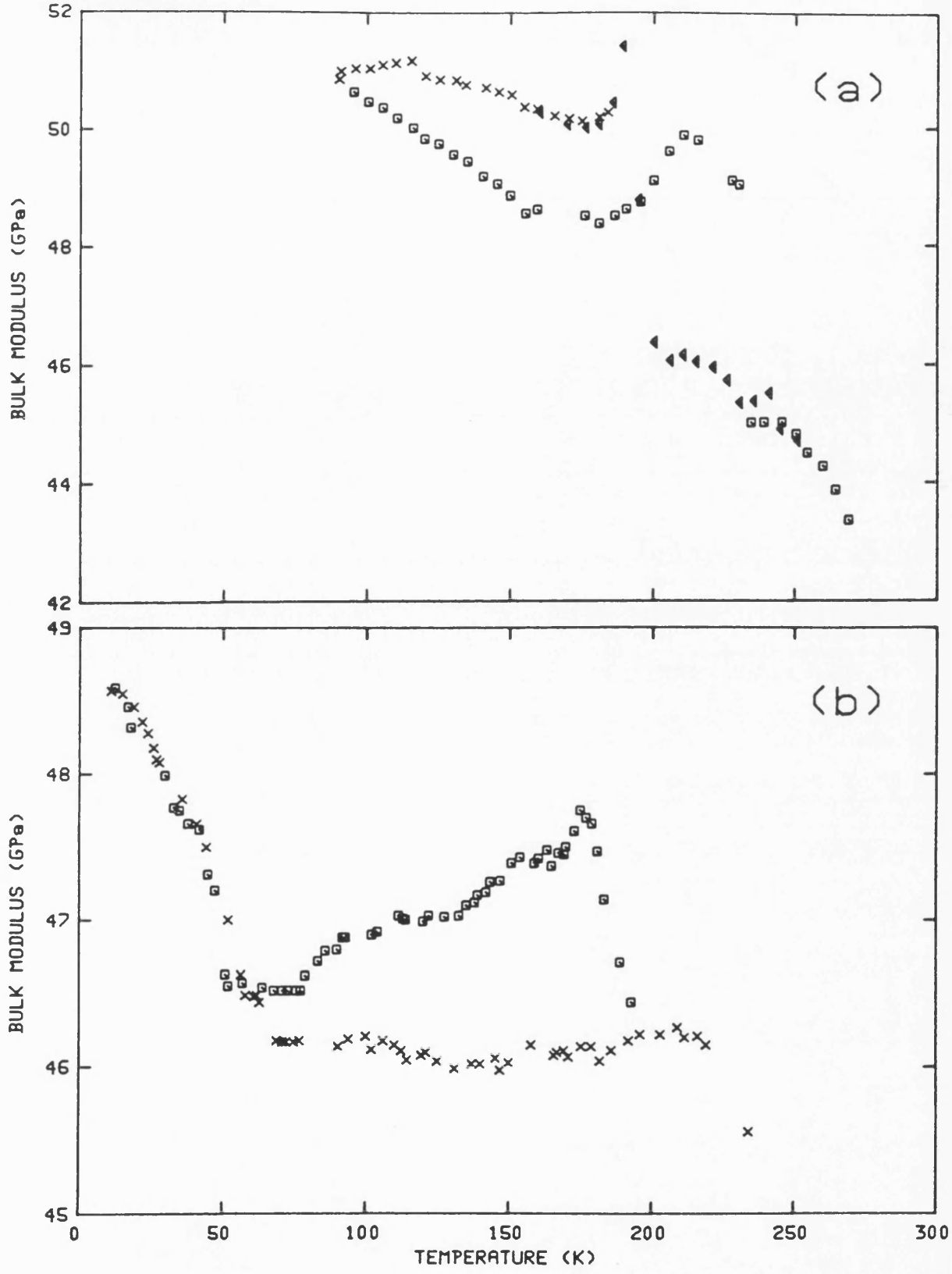

Figure 8.5
The temperature dependences of the bulk modulus for (a) $YBa_2Cu_3O_{7-x}$ (sample Y1) and (b) $YBa_2Cu_3O_{7-x}$ (sample Y2). The crosses (x) correspond to the data obtained during cooling and the squares to those obtained during warming.

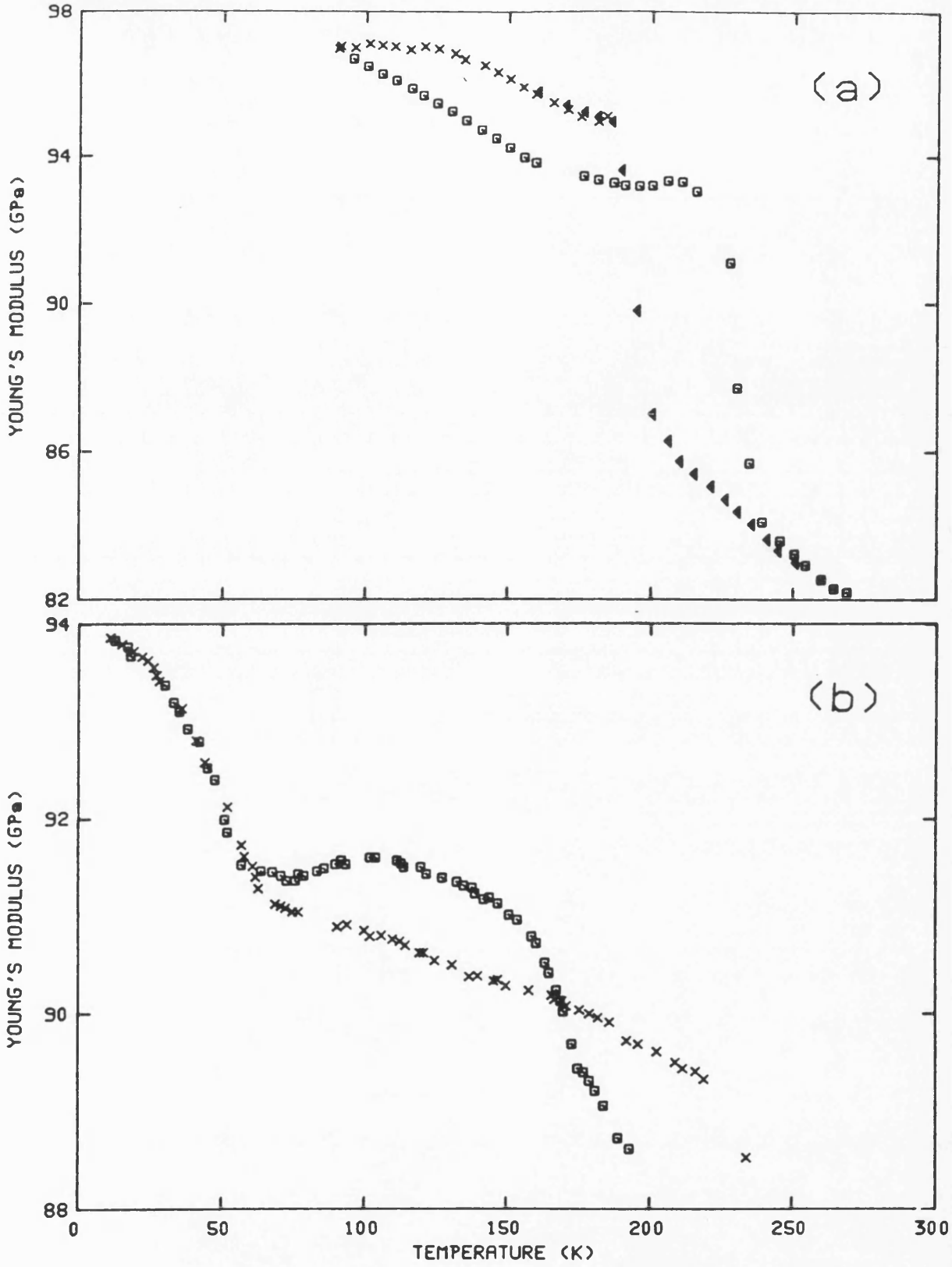

Figure 8.6
The temperature dependences of Young's modulus for (a) $YBa_2Cu_3O_{7-x}$ (sample Y1) and (b) $YBa_2Cu_3O_{7-x}$ (sample Y2). The crosses (x) correspond to the data obtained during cooling and the squares to those obtained during warming.

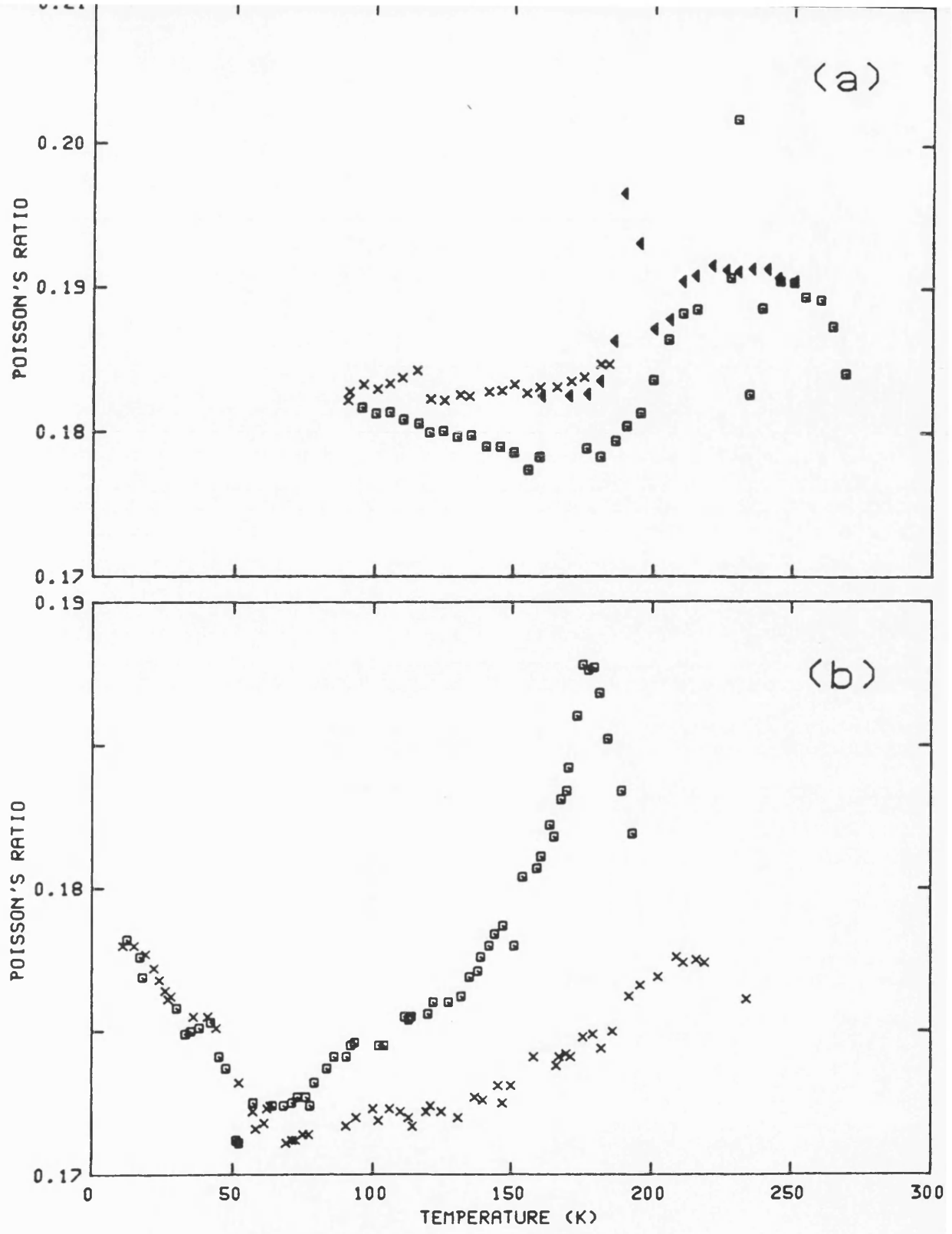

Figure 8.7
The temperature dependences of Poisson's ratio for (a) $YBa_2Cu_3O_{7-x}$ (sample Y1) and (b) $YBa_2Cu_3O_{7-x}$ (sample Y2). The crosses (x) corresponds to the data obtained during cooling and the squares to those obtained during warming.

Table 8.2. The ultrasonic wave velocities and the elastic constants at room temperature for the polycrystalline ceramic $YBa_2Cu_3O_{7-X}$ high temperature superconductor obtained using Nonaq as a bonding material.

	Sample Y1	Sample Y2
Density Kgm^{-3}	5199	5985
Ultrasonic wave velocities ms^{-1}		
Longitudinal V_L	4099	4000
Shear V_S	2559	2475
C_L (GPa)	87.3	95.8
C_S (GPa)	34	36.7
Bulk modulus B (GPa)	42	46.9
Young's modulus E (GPa)	80	87
Poisson's ratio	0.181	0.190

Ledbetter and Kim (1988) measured the temperature dependences of the elastic constants C_s , bulk modulus and Poisson's ratio in a $YBa_2Cu_3O_{7-x}$ sample. They observed a thermal hysteresis between cooling and warming with a sharp increase in these moduli as the temperature was lowered below T_c . Shi et al (1989) measured Young's modulus as a function of temperature in a single crystal of $YBa_2Cu_3O_{7-x}$. They found a softening at T_c with a sharp increase below that temperature. They obtained Young's modulus at room temperature of 220GPa for their crystal. Kim et al (1990) found a thermal hysteresis in the temperature dependences of the elastic constants of a single crystal of $YBa_2Cu_3O_{7-x}$. This means that the hysteretic behaviour is probably not due to porous and defect nature of pollycrystalline ceramic $YBa_2Cu_3O_{7-x}$ samples. Ramakrishnan and Krishnamurthy (1991) calculated the elastic constants for $YBa_2Cu_3O_{7-x}$ compound employing the method of long waves and unscreened rigid ion model. They found that their results are in good agreement with those reported by others. Finally, Ivanov and Tsymbal (1990) attempted to explain the temperature dependence of the elastic constants in granular $YBa_2Cu_3O_{7-x}$ in terms of elastic domains. Using a value of 69 for $(\partial C_L/\partial P)_{P-0}$ obtained in the present programme (see table 8.5) they estimated a decrease in sound velocity $(\Delta V/V)$ of $2x10^{-2}$ due to the change of the domain strains.

The elastic constants for $YBa_2Cu_3O_{7-x}$ compound have been reported by many groups. [Kusz and Murawski (1988), Lang et al (1988), Lemmens et al (1988), Wolf et al (1988), Horie and Mase (1989), Saint-Paul and Henry (1989b) and Ivanov and Tsymbal (1990)]. The results obtained here for the fine grained sample (Y1) and for the coarse grained sample (Y2) are compared with those obtained by others in table 8.3.

Table 8.3. Comparison between the elastic constants for $YBa_2Cu_3O_{7-X}$ samples Y1 and Y2, calculated from the measured ultrasonic wave velocities at room temperature, with those obtained by other groups.

Reference	C_L (GPa)	C_S (GPa)	Bulk modulus (GPa)	Young's modulus (GPa)	Poisson's ratio
This work Y1 Y2	 87.3 95.8	 34 36.7	 42 46.9	 80 87	 0.181 0.190
Horie and Mase (1989)	-	-	102	-	-
Ivanov and Tsymbal (1990)	54.2	20	-	50.4	0.26
Kusz and Murawski (1988)	-	-	-	52* 68#	-
Lang et al (1988)	-	-	54	-	0.2
Lemmens et al (1988) 78% dense 92% dense	-	-	 33.6 79.2	-	 0.25 0.24
Saint-Paul and Henry (1989b) (single crystal)	230	82	-	-	-
Shi et al (1989)	-	-	-	220	-
Wolf et al (1988)	-	-	38.8	-	0.19

* superconducting sample.
# semiconducting sample.

8.4 THE PRESSURE DEPENDENCES OF THE ULTRASONIC WAVE VELOCITIES

Ultrasonic longitudinal and shear waves velocities were measured as a function of pressure in $YBa_2Cu_3O_{7-x}$ (sample Y1) using 5MHz X- and Y-cut quartz transducers respectively and Dow Resin as a bonding material. The results are shown in figure 8.8. The non-linear behaviour of the results clearly seen in these data contrasts markedly with the linear behaviour found for $Nd_{2-x}Ce_xCuO_{4-y}$ and $La_{2-x}Sr_xCuO_{4-y}$ compounds (see figures 6.11 and 7.10 respectively). The pressure dependence of the shear wave velocity is smaller than that of the longitudinal wave. The effects of the silicone oil, which was used as pressure transmitting medium, on the elastic behaviour of the material were considered. Sample Y1 has a measured density of 5199 Kgm^{-3}, that is about 82% of the theoretical density (6338 Kgm^{-3}). It weighed 3.4720gm at the beginning of the experimental programme; after undergoing three pressure cycles up to 0.15 GPa, it weighed 3.5734gm. Hence it had taken up 2.92% by weight of oil. The density of the silicone oil is 0.97Kgm^{-3}. The pore volume in the sample was 0.1068 cm^3; the volume filled by the oil was 0.1045 cm^3. Hence 98% of the pore volume had become filled with silicone oil after the three pressure cycles. The pores must be interconnected. An extensive experimental programme

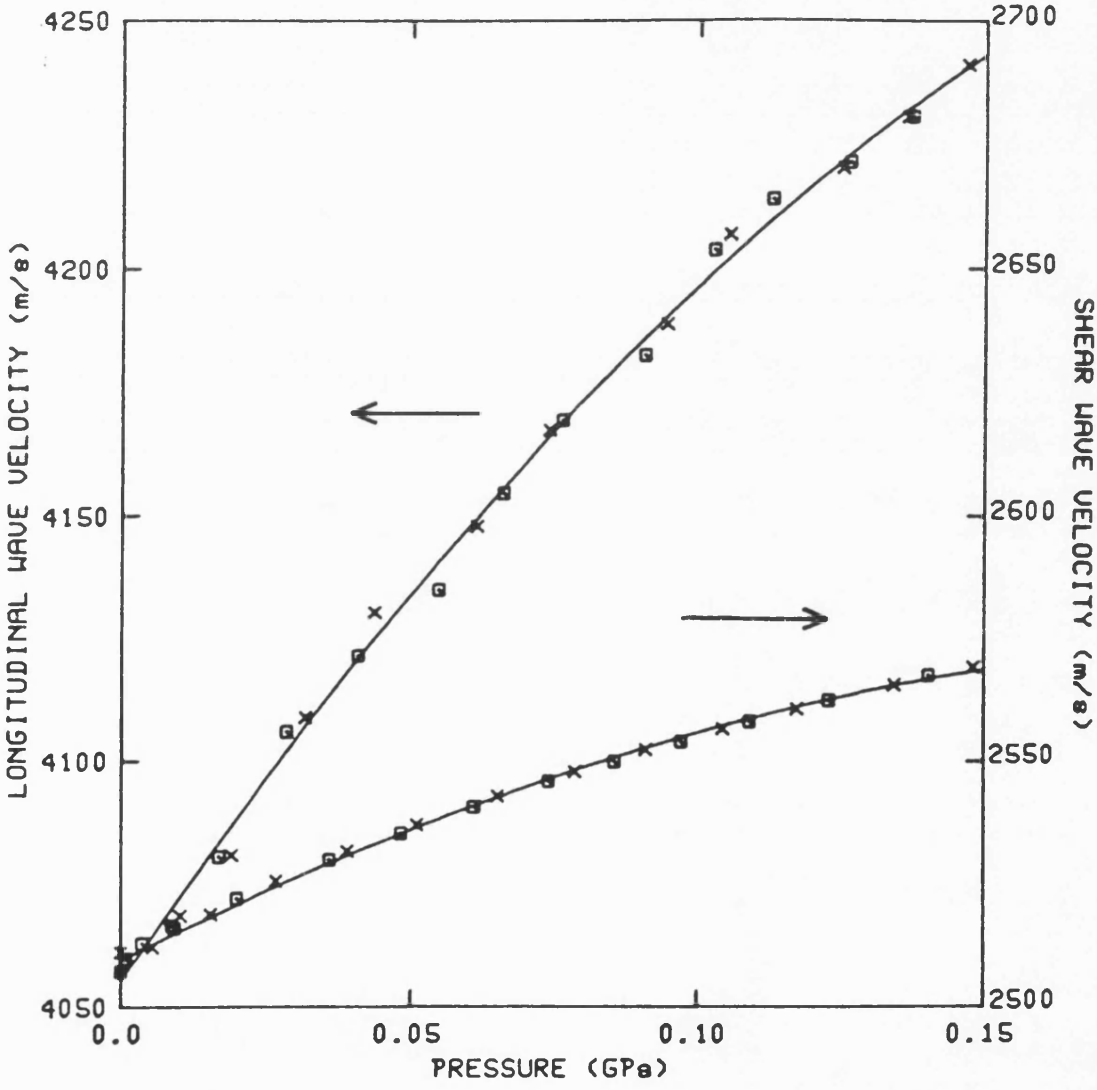

Figure 8.8
The hydrostatic pressure dependences of velocities of longitudinal (upper curve) and shear (lower curve) ultrasonic waves velocities propagated in $YBa_2Cu_3O_{7-X}$ (sample Y1) at 295K. The crosses correspond to velocity measurements made with increasing pressure and the squares to data obtained as the pressure was decreased.

has been undertaken to ascertain the extent to which this oil uptake alters the ultrasonic wave velocities and its behaviour under pressure; typical sets of data obtained are given in table 8.4. It has been found that for sample Y1 the change in velocity caused by pressure cycling under oil is substantially less than 1% and that in $\alpha = ((dV/dP)_{P=0})$ is only a few percent. In spite of the oil uptake, the results are remarkably reproducible and show that the effect of oil inclusion in the pores on the elastic constants themselves is small. To examine this further, after a number of experiments had been completed on the effects of cycling under pressure up to 0.15 GPa on the ultrasonic wave velocities, sample Y1 was re-annealed in an oxygen atmosphere at 400°C for 24hours. On re-weighing after this annealing process, it was found that the sample had reverted to its original weight before oil immersion: the oil had been driven out. This annealed sample is designated sample Y1A. The pressure dependences of the ultrasonic wave velocities in sample Y1A are shown in figure 8.9. Again the non-linearity in the results are clear in that figure. It can be seen also that the elastic behaviour under pressure was not much altered by this extensive pressure cycling and annealing process. However, the velocities of both longitudinal and shear waves became rather smaller after the sample had

Table 8.4. To establish the effect of repeated cycling under pressure in silicon oil on the ultrasonic wave velocities in a polycrystalline ceramic $YBa_2Cu_3O_{7-X}$ high temperature superconducting sample. The data for velocity $V(P)$ at pressure P have been fitted by an equation of the form

$$V(P) = V_o + aP + bP^2$$

where V_o is the ultrasonic velocity at atmospheric pressure and a is $(dV/dP)_{P=0}$. Results have been corrected for transducer effects. Before cycle one the sample had not been exposed to oil, so V_o (cycle one) corresponds to the velocity of longitudinal wave in the oil-free sample at atmospheric pressure.

Cycle number	Ultrasonic mode	Ultrasonic wave velocity V_o (ms^{-1})	a ($ms^{-1}Pa^{-1}$)	b ($ms^{-1}Pa^{-2}$)
Sample Y1				
1	Longitudinal	4055	174	-32
2	Longitudinal	4070	178	-40
3	Longitudinal	4076	171	-36
4	Shear	2504	54	-11
5	Shear	2509	60	-13
Sample Y1A (sample Y1 after annealing in oxygen for 24hours at 400°C				
1	Longitudinal	3993	180	-49
2	Lonigtudinal	4002	165	-41
3	Shear	2366	32	-7
4	Shear	2364	32	-7

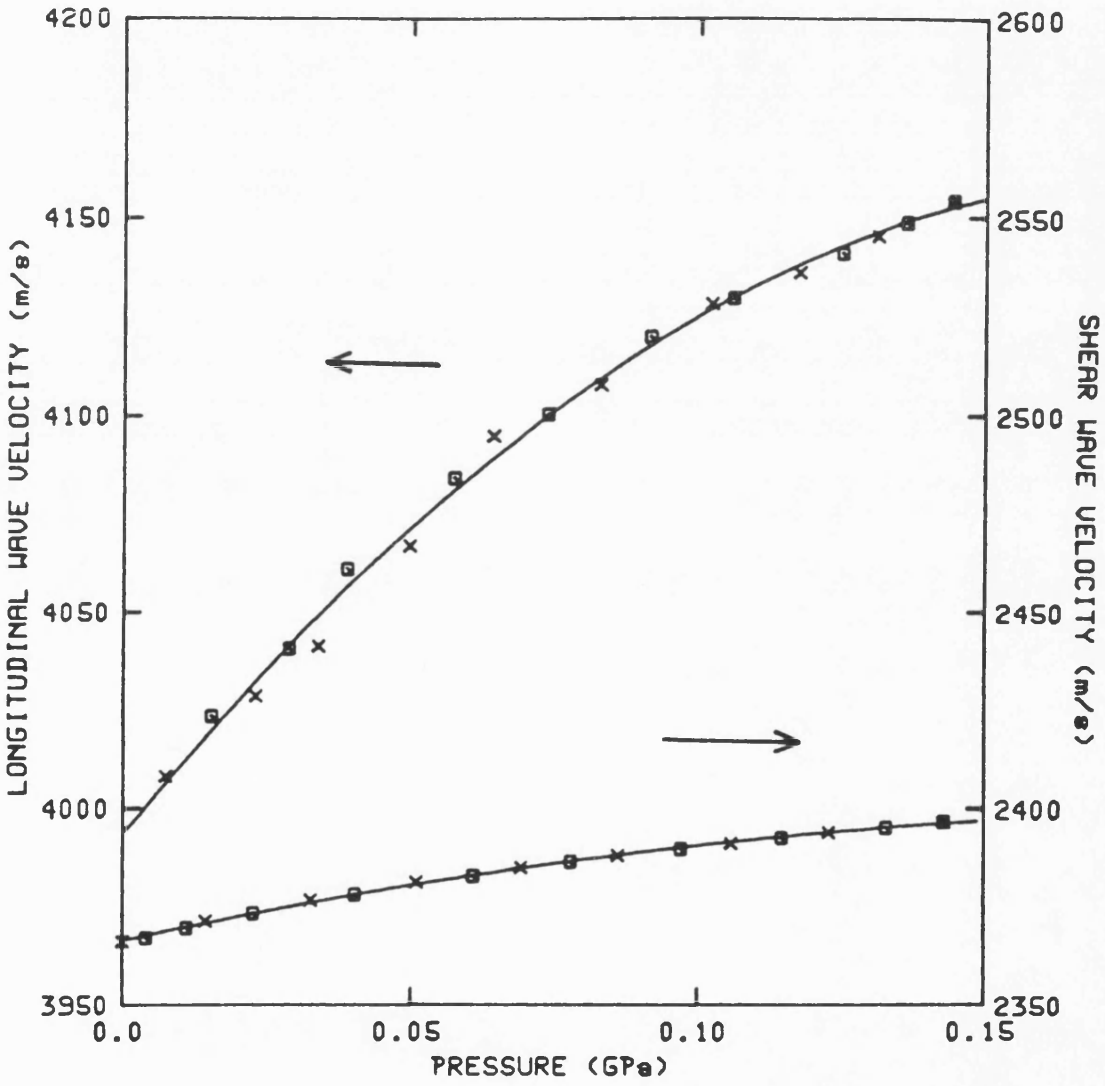

Figure 8.9
The hydrostatic pressure dependences of velocities of longitudinal (upper curve) and shear (lower curve) ultrasonic waves velocities propagated in $YBa_2Cu_3O_{7-x}$ (sample Y1A) at 295K. The crosses correspond to velocity measurements made with increasing pressure and the squares to data obtained as the pressure was decreased.

undergone this process than they had been in the sample at the very onset of the experimental programme before oil immersion (by comparing the results for samples Y1 and Y1A in table 8.4). These experiments show that the effects of oil injected into the pores on the ultrasonic wave velocities themselves are not large.

The next step is to examine further the effects of cycling under pressure on the ultrasonic wave velocity dependence upon pressure. The change in longitudinal wave velocity in sample Y1 during the first pressure cycle is shown in figure 8.8; the results obtained on reducing the pressure fall almost upon those obtained when the pressure was increased (at lower pressures the velocities obtained on decreasing pressure were a little faster). The longitudinal velocities obtained in the second pressure cycle were identical (within experimental error) to those from the first cycle, again indicating that the effects of uptake of the oil were small. The shear wave velocity followed the same pattern under pressure, falling on the same curve when the pressure was reduced as that obtained as the pressure was increased. Since oil was introduced by application of pressure but was not extruded as the pressure was reduced, the agreement between the velocity data obtained as the pressure was

increased and decreased indicates that the effect of forcing oil into the pores does not produce substantial affects on the value of the sound velocity under pressure.

By comparing figures 8.8 and 8.9 it can be seen that for sample Y1A the non-linearity is more pronounced than that of sample Y1 and the shear wave velocity changes less in sample Y1A than in sample Y1 as the pressure changes. Jiang and Breazeale (1990) estimated the ultrasonic non-linearity parameter (β) in $YBa_2Cu_3O_{7-x}$ sample with experimental density of 76% of the theoretical density (6338 kgm^{-3}) as 14.3. They used the results obtained here for samples Y1, Y1A and Y2 (table 8.4) and estimated the nonlinearity parameter for our samples to be in the range of 20 to 40. They suggested that the differences between the results are due to the different samples densities.

8.5 HYSTERESIS ARISING FROM PRESSURE CYCLING

Hysteresis effects may occur on pressure cycling. Like thermal hysteresis, they are sample dependent. They are absent from the pressure dependences of the ultrasonic wave velocities in samples Y1 and Y1A (figure 8.8 and 8.9) while being large in the more dense, course grained sample Y2. The pressure dependences of the ultrasonic wave velocities in sample Y2 are shown in figure 8.10. This material shows pronounced hysteresis effects with pressure in both its longitudinal and shear wave velocities (figure 8.10). After each pressure cycle the velocity was found to have increased slightly (1% for the longitudinal mode and 0.2% for the shear mode) in this sample. There is a direct correspondence between thermal and pressure hysteresis. Although hysteresis does occur in sample Y1 at low temperatures, the ultrasonic wave velocities on the cooling and warming cycle measured above 240K fall on the same curve (figure 8.1): there is no thermal hysteresis in the room temperature region. The ultrasonic wave velocities versus pressure results obtained at room temperature in samples Y1 and Y1A with increasing and reducing pressure do not show any hysteresis (figures 8.8 and 8.9). This is also true for $Nd_{2-x}Ce_xCuO_{4-y}$ and $La_{2-x}Sr_xCuO_{4-y}$ compounds (chapters 6 and 7 respectively). However, the much denser and coarse grain specimen Y2 shows

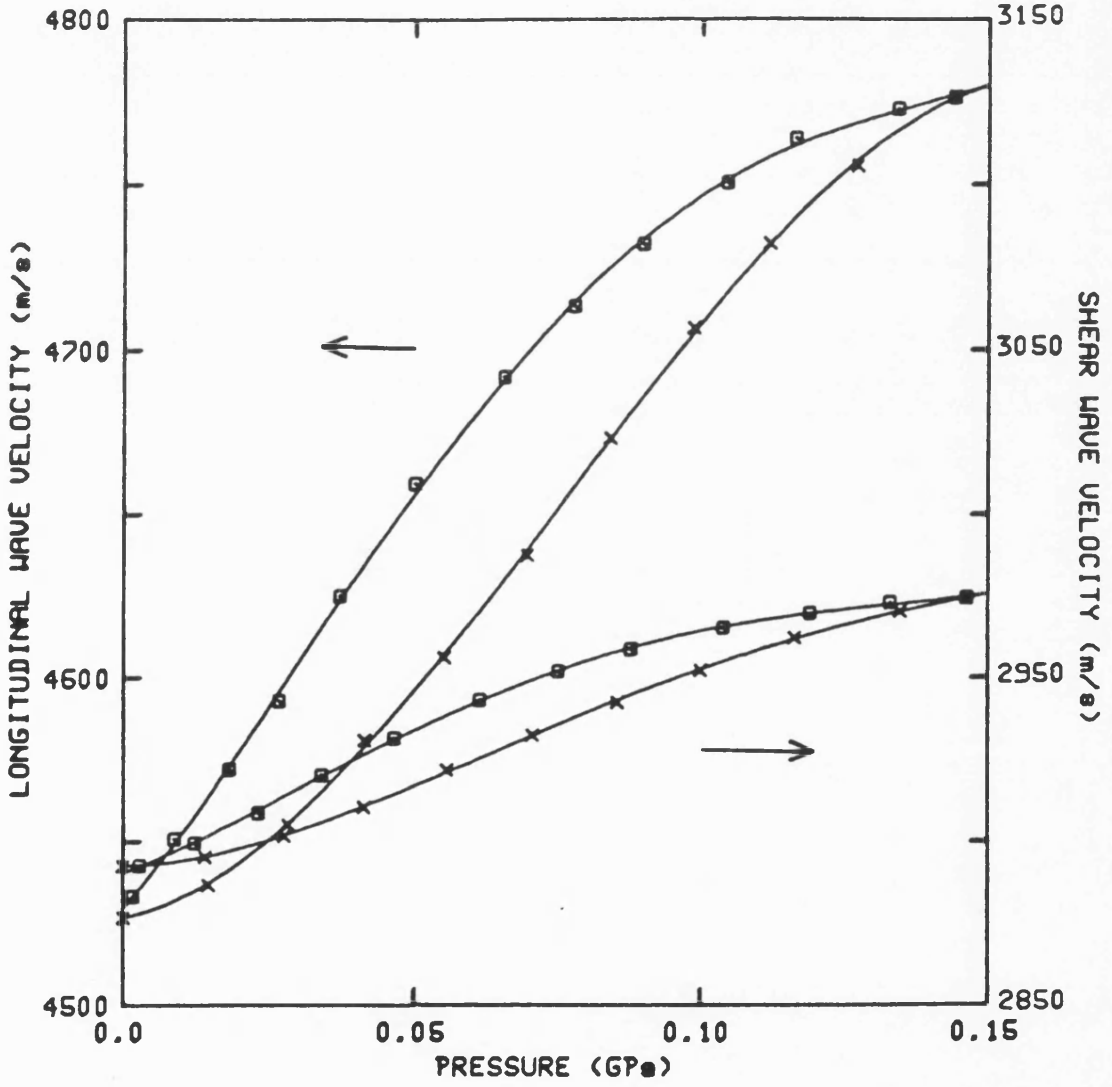

Figure 8.10
The hydrostatic pressure dependences of velocities of longitudinal (upper curve) and shear (lower curve) ultrasonic waves velocities propagated in $YBa_2Cu_3O_{7-X}$ (sample Y2) at 295K. The crosses correspond to velocity measurements made with increasing pressure and the squares to data obtained as the pressure was decreased.

pronounced hysteresis both as a function of temperature (figure 8.2) and pressure (figure 8.10). It seems that the appearance of hysteresis during pressure cycling has the same origin as that which occurs during temperature cycling. The ultrasonic wave velocities obtained at room temperature by using Resin as a bonding material in sample Y2 are given in table 8.5.

Table 8.5. The ultrasonic wave velocities, the elastic constants and their hydrostatic pressure derivatives at room temperature for the polycrystalline ceramic $YBa_2Cu_3O_{7-X}$ high temperature superconductor using Dow Resin as a bonding material. The hydrostatic pressure derivatives for the non-porous matrix are the slopes of the straight lines fitted through the points in the linear part of the data (as the pressure tends toward zero). The numbers in brackets are the hydrostatic pressure derivatives obtained by taking the slopes of the curves fitted through all the points.

Property	Sample Y1		Sample Y1A		Sample Y2	
	Porous	Non Porous	Porous	Non Porous	Porous	Non Porous
Density Kgm^{-3}	5199	6338	5199	6338	5985	6338
Porosity	0.18	-	0.18	-	0.056	-
Ultrasonic wave velocities ms^{-1}						
Longitudinal V_L	4053	4564	3993	4529	4527	4658
Shear V_S	2504	2837	2366	2665	2892	2986
C_L (GPa)	85.4	132	83	130	123	137.5
C_S (GPa)	32.6	51	29	45	50	56.5
Bulk modulus B (GPa)	42	64	44	70	56	62
Young's modulus E (GPa)	77.7	121	71.6	111	115.6	130
Poisson's ratio	0.191	0.185	0.229	0.235	0.155	0.151
Acoustic Debye temperature (Θ_D^{el}) (K)	324	392	307	370	391	411
$(\partial B/\partial P)_{P=0}$	50	111 (119.5)	58	114 (133)	108	118 (148)
$(\partial C_L/\partial P)_{P=0}$	69	136 (152)	68	125 (145)	145	162 (205)
$(\partial C_S/\partial P)_{P=0}$	14	19 (24)	8.7	8.2 (9)	28	33 (42.5)
Superconducting transition temperature T_C (K)	90	-	90	-	92	-

8.6 THE PRESSURE DEPENDENCES OF THE ELASTIC MODULI

The elastic moduli of the $YBa_2Cu_3O_{7-x}$ samples investigated in this work were calculated using the ultrasonic wave velocities measured as a function of pressure. The pressure dependences of longitudinal C_L^n , shear C_S^n and the bulk B^n moduli in sample Y1 are shown in part (a) of figures 8.11, 8.12 and 8.13 respectively and those for sample Y1A are shown in part (a) of figures 8.14, 8.15 and 8.16 respectively. The changes produced in the longitudinal modulus C_L^n and the bulk modulus B^n by the application of pressure are almost the same in both Y1 and Y1A samples, while the variation of the shear modulus C_S^n with pressure is smaller in sample Y1A than that in sample Y1. The non-linear behaviour of the elastic constants as a function of pressure are also a main feature in those figures. The pressure dependences of longitudinal C_L^n , shear C_S^n and the bulk B^n moduli in sample Y2 are shown in part (a) of figures 8.17, 8.18 and 8.19 respectively. Elastic hysteresis due to pressure is clear in the results presented in these figures.

Correction for the effects of porosity was carried out by inserting the experimental results into equations 4.4 and 4.5. The corrected values for longitudinal C_L^m , shear C_S^m and the bulk B^m moduli as a function of pressure for sample Y1 are plotted in part (b) of figures 8.11, 8.12 and

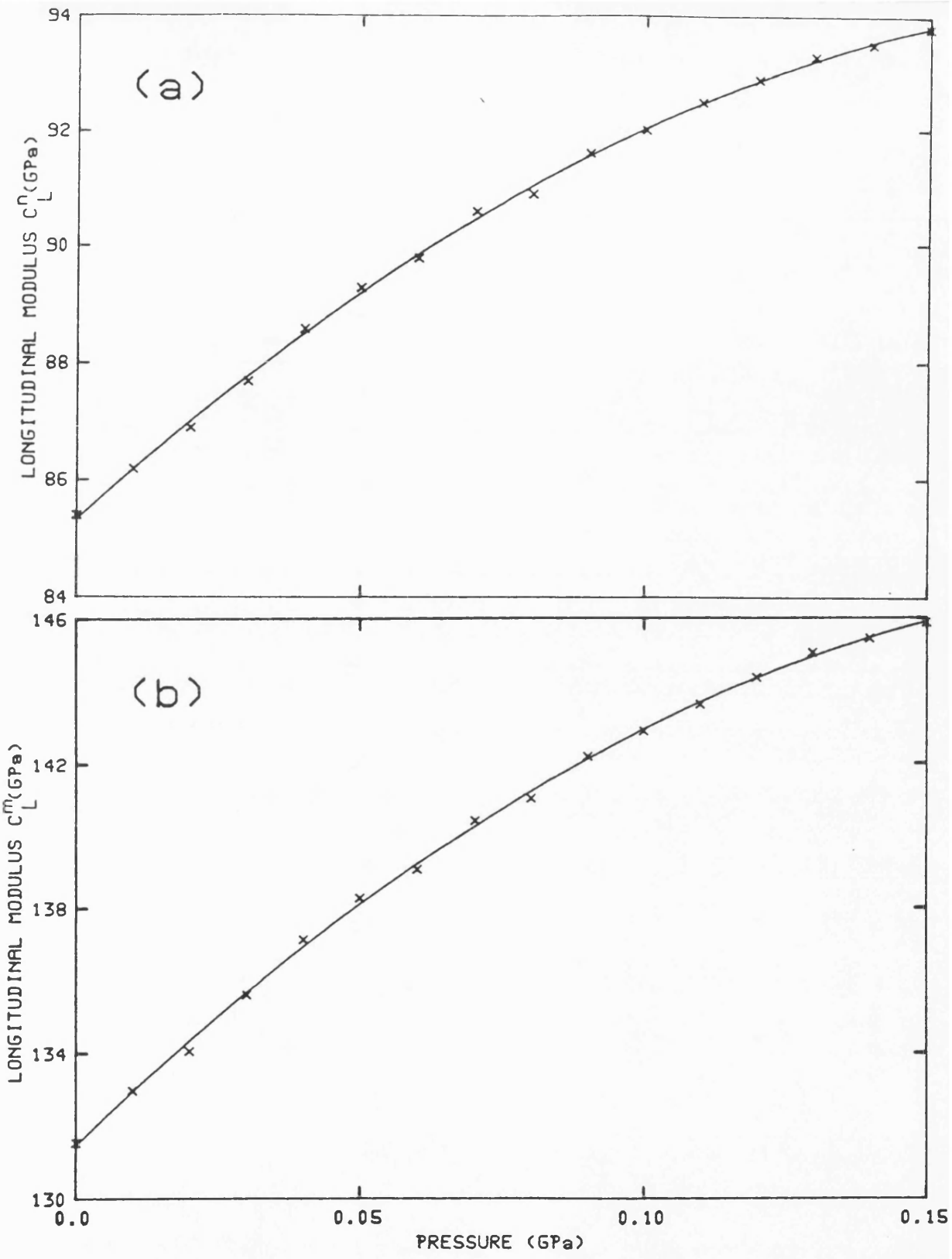

Figure 8.11
The hydrostatic pressure dependences of the longitudinal modulus (a) C_L^n (porous material) and (b) C_L^m (non-porous matrix) of $YBa_2Cu_3O_{7-x}$ (sample Y1) at 295K calculated from the experimental data and using equations 4.4 and 4.5. The solid lines are least square fits to the data.

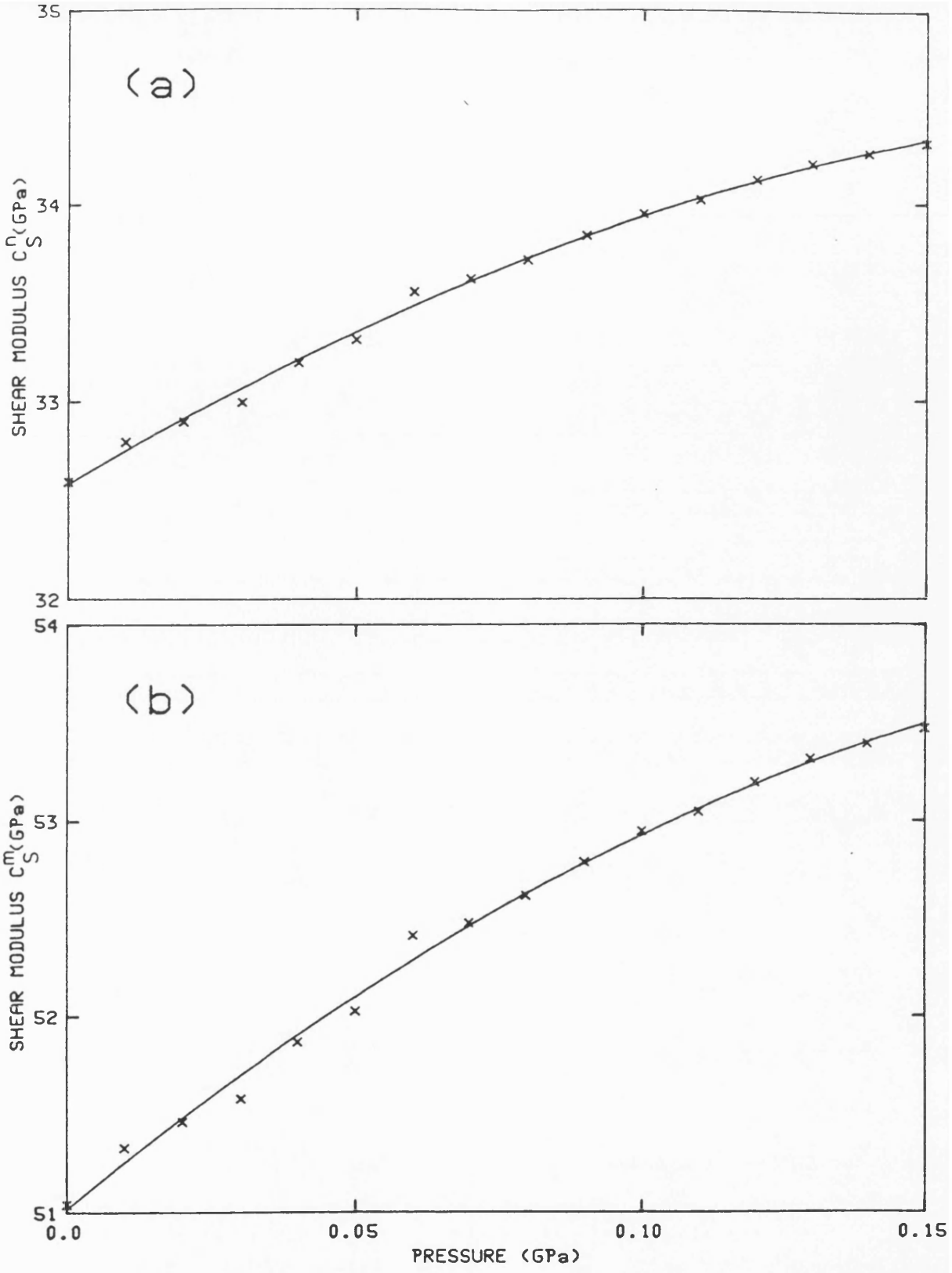

Figure 8.12
The hydrostatic pressure dependences of the shear modulus (a) C_S^n (porous material) and (b) C_S^m (non-porous matrix) of $YBa_2Cu_3O_{7-x}$ (sample Y1) at 295K calculated from the experimental data and using equations 4.4 and 4.5. The solid lines are least square fits to the data.

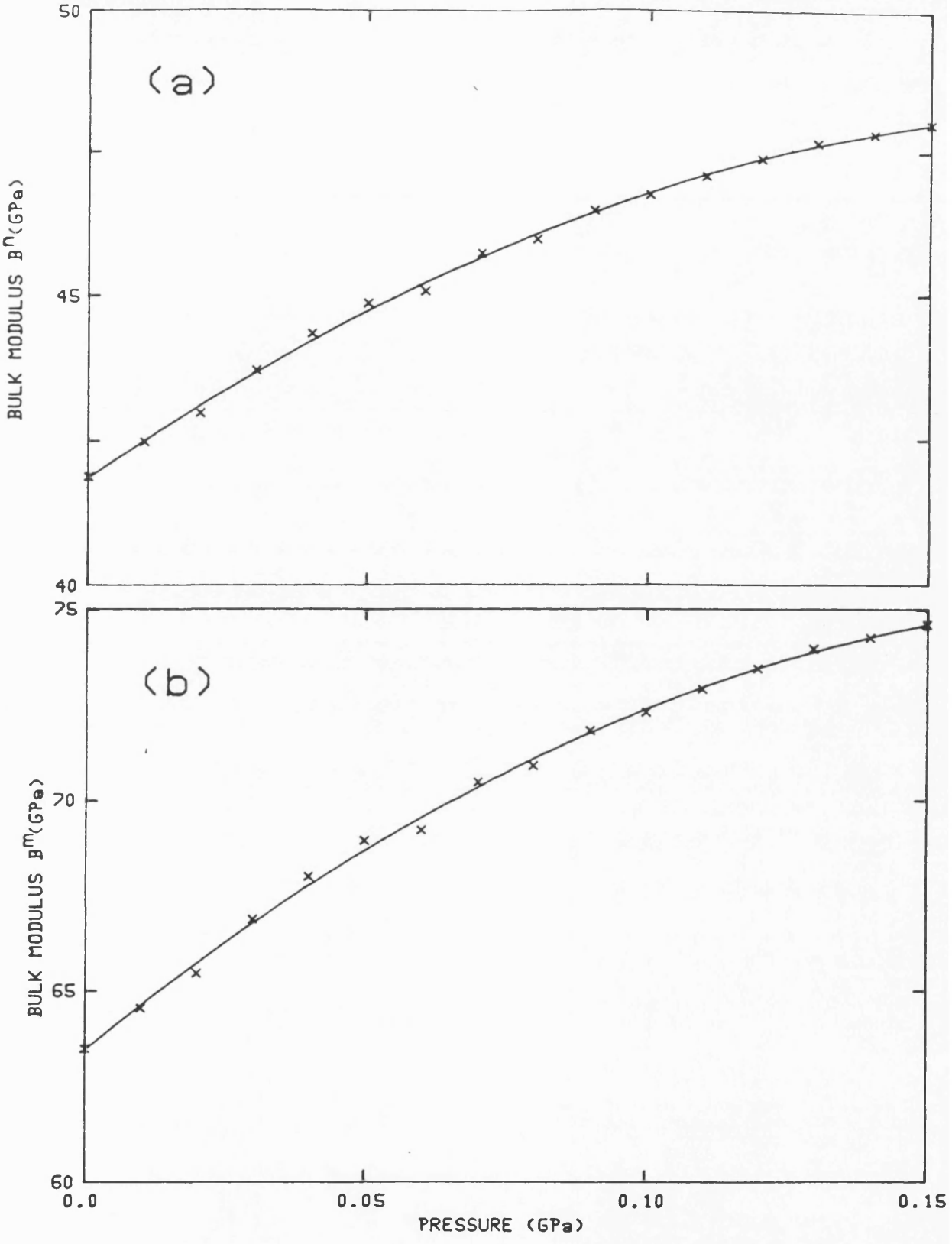

Figure 8.13
The hydrostatic pressure dependences of the bulk modulus (a) B^n (porous material) and (b) B^m (non-porous matrix) of $YBa_2Cu_3O_{7-x}$ (sample Y1) at 295K calculated from the experimental data and using equations 4.4 and 4.5. The solid lines are least square fits to the data.

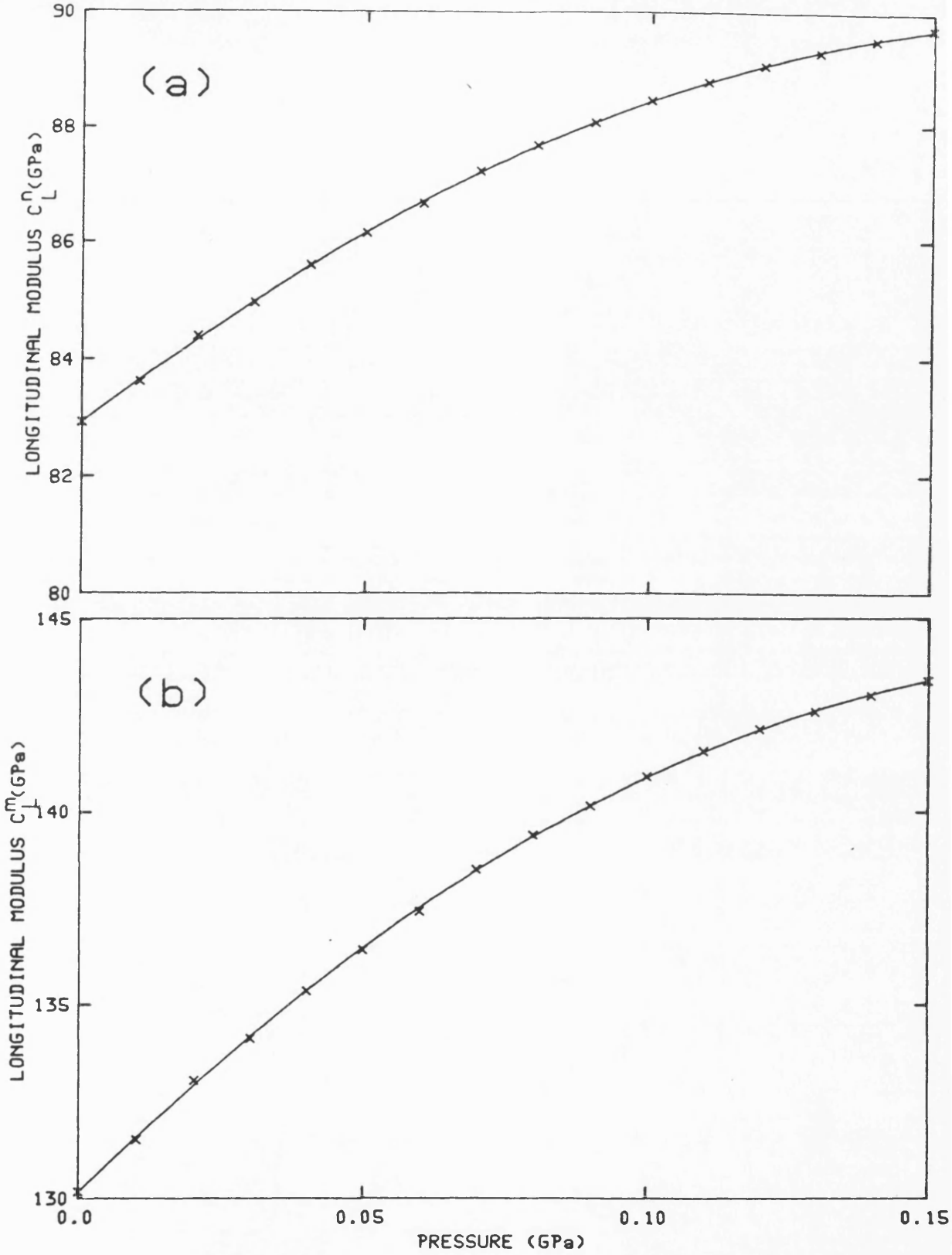

Figure 8.14
The hydrostatic pressure dependences of the longitudinal modulus (a) C_L^n (porous material) and (b) C_L^m (non-porous matrix) of $YBa_2Cu_3O_{7-x}$ (sample Y1A) at 295K calculated from the experimental data and using equations 4.4 and 4.5. The solid lines are least square fits to the data.

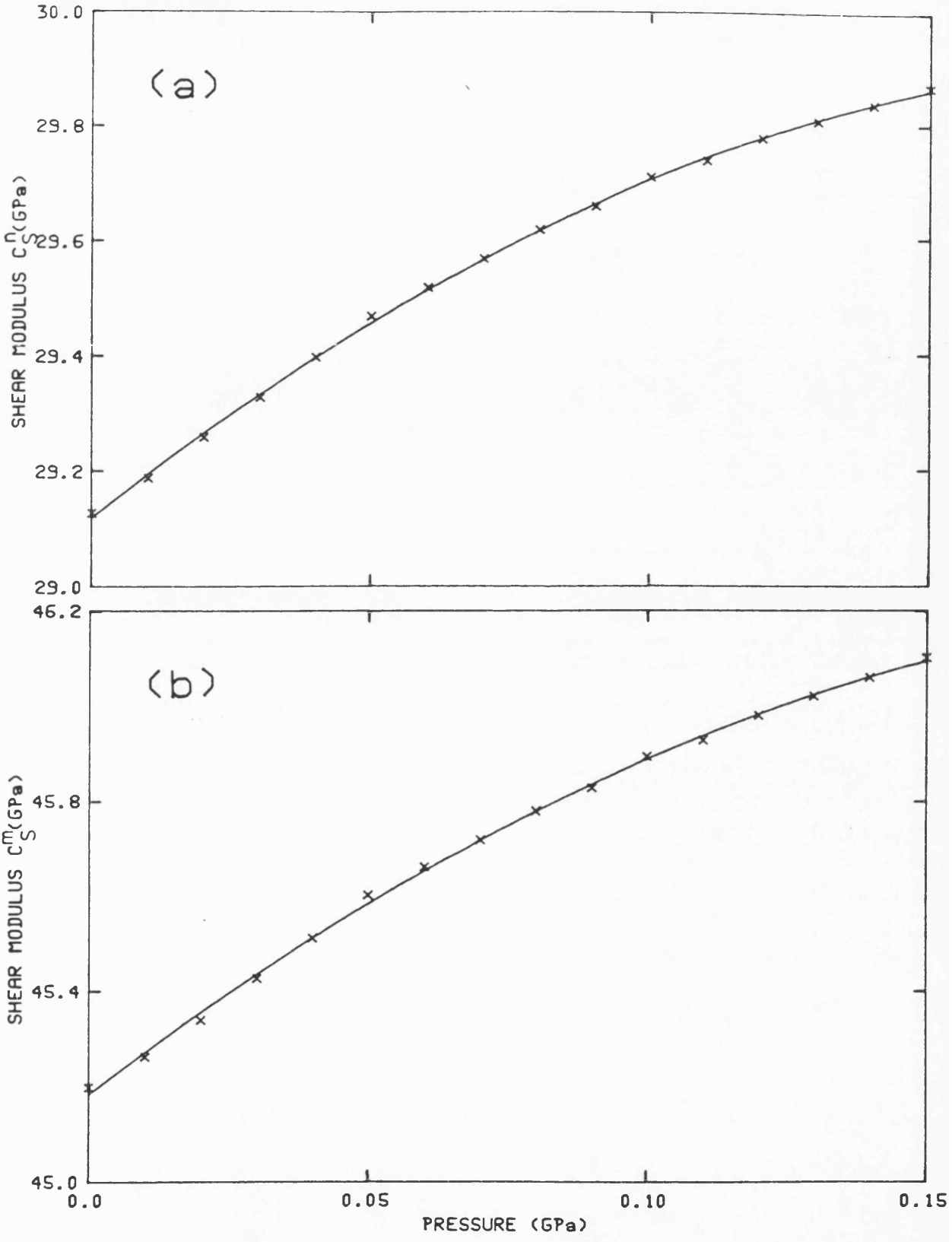

Figure 8.15
The hydrostatic pressure dependences of the shear modulus (a) C_S^n (porous material) and (b) C_S^m (non-porous matrix) of $YBa_2Cu_3O_{7-x}$ (sample Y1A) at 295K calculated from the experimental data and using equations 4.4 and 4.5. The solid lines are least square fits to the data.

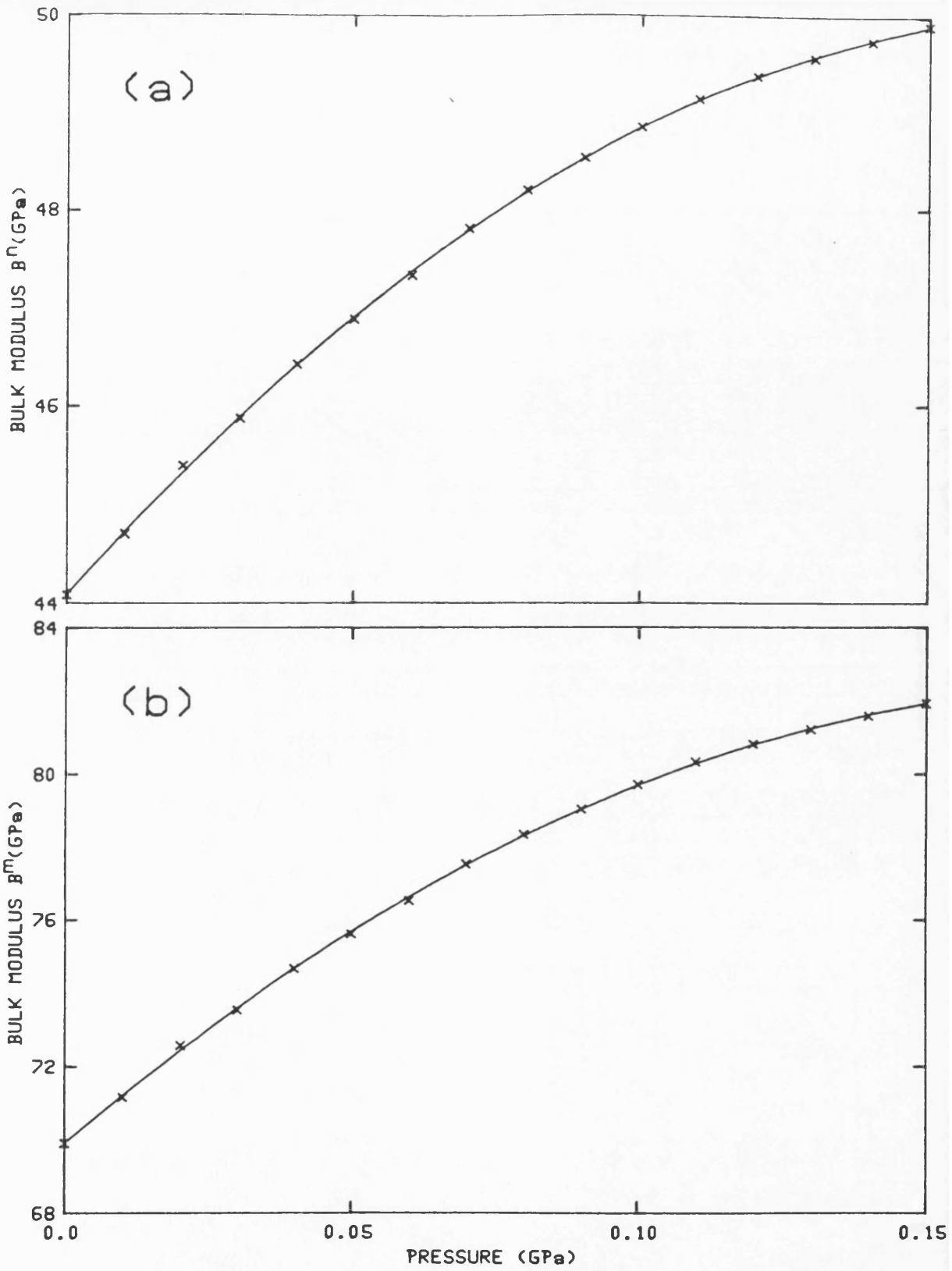

Figure 8.16
The hydrostatic pressure dependences of the bulk modulus (a) B^n (porous material) and (b) B^m (non-porous matrix) of $YBa_2Cu_3O_{7-x}$ (sample Y1A) at 295K calculated from the experimental data and using equations 4.4 and 4.5. The solid lines are least square fits to the data.

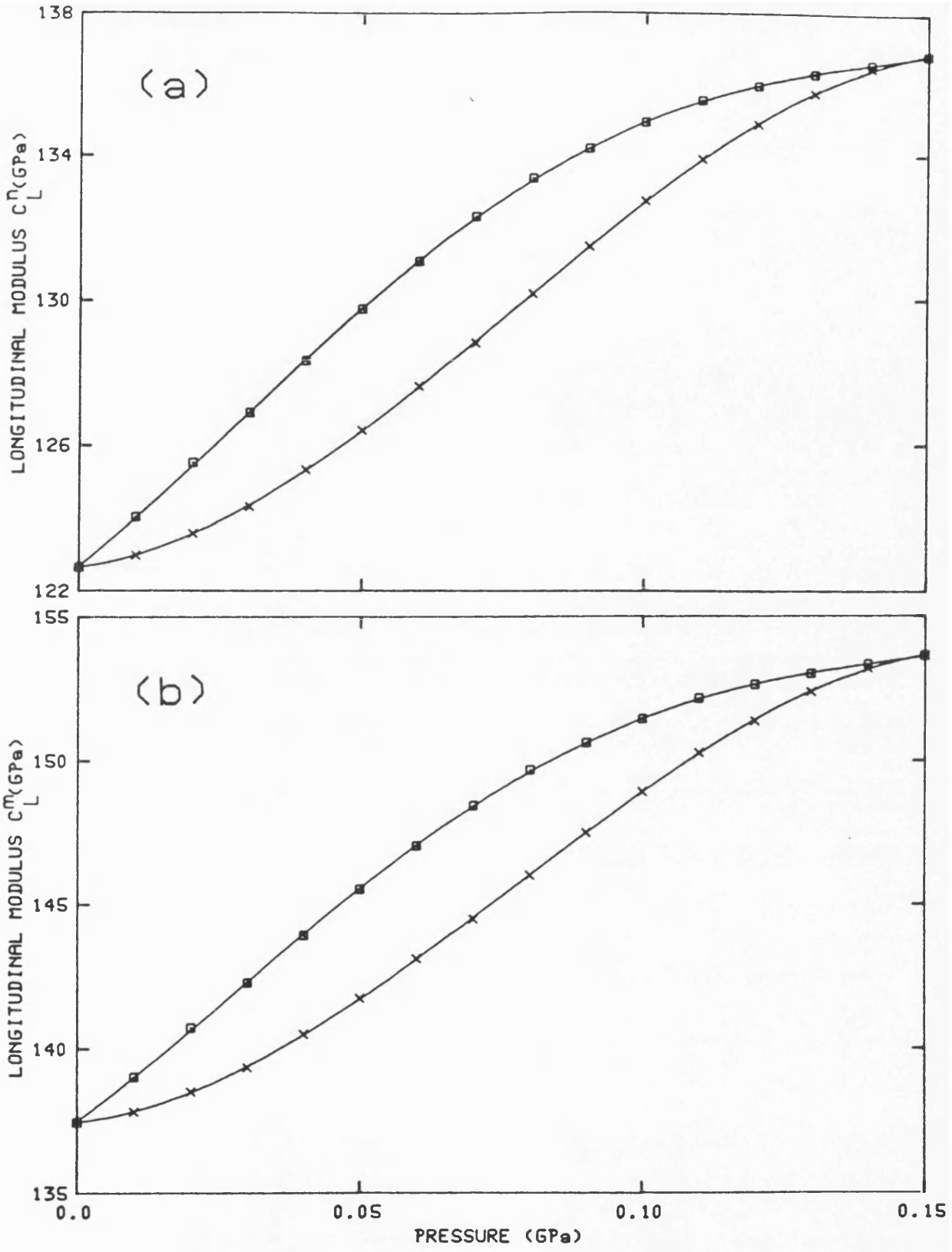

Figure 8.17
The hydrostatic pressure dependences of the longitudinal modulus (a) C_L^n (porous material) and (b) C_L^m (non-porous matrix) of $YBa_2Cu_3O_{7-x}$ (sample Y2) at 295K calculated from the experimental data and using equations 4.4 and 4.5. The solid lines are least square fits to the data.

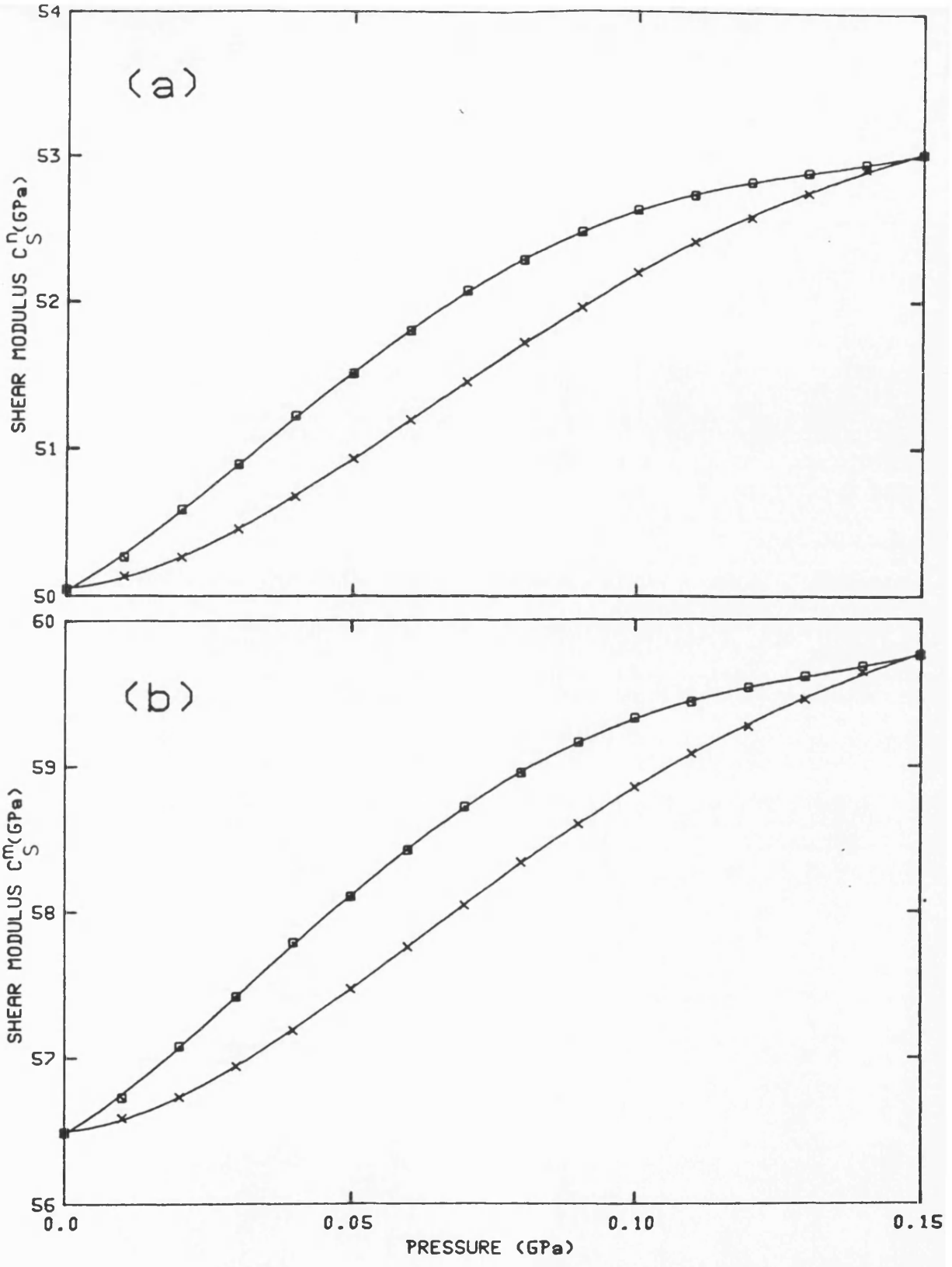

Figure 8.18
The hydrostatic pressure dependences of the shear modulus (a) C_S^n (porous material) and (b) C_S^m (non-porous matrix) of $YBa_2Cu_3O_{7-x}$ (sample Y2) at 295K calculated from the experimental data and using equations 4.4 and 4.5. The solid lines are least square fits to the data.

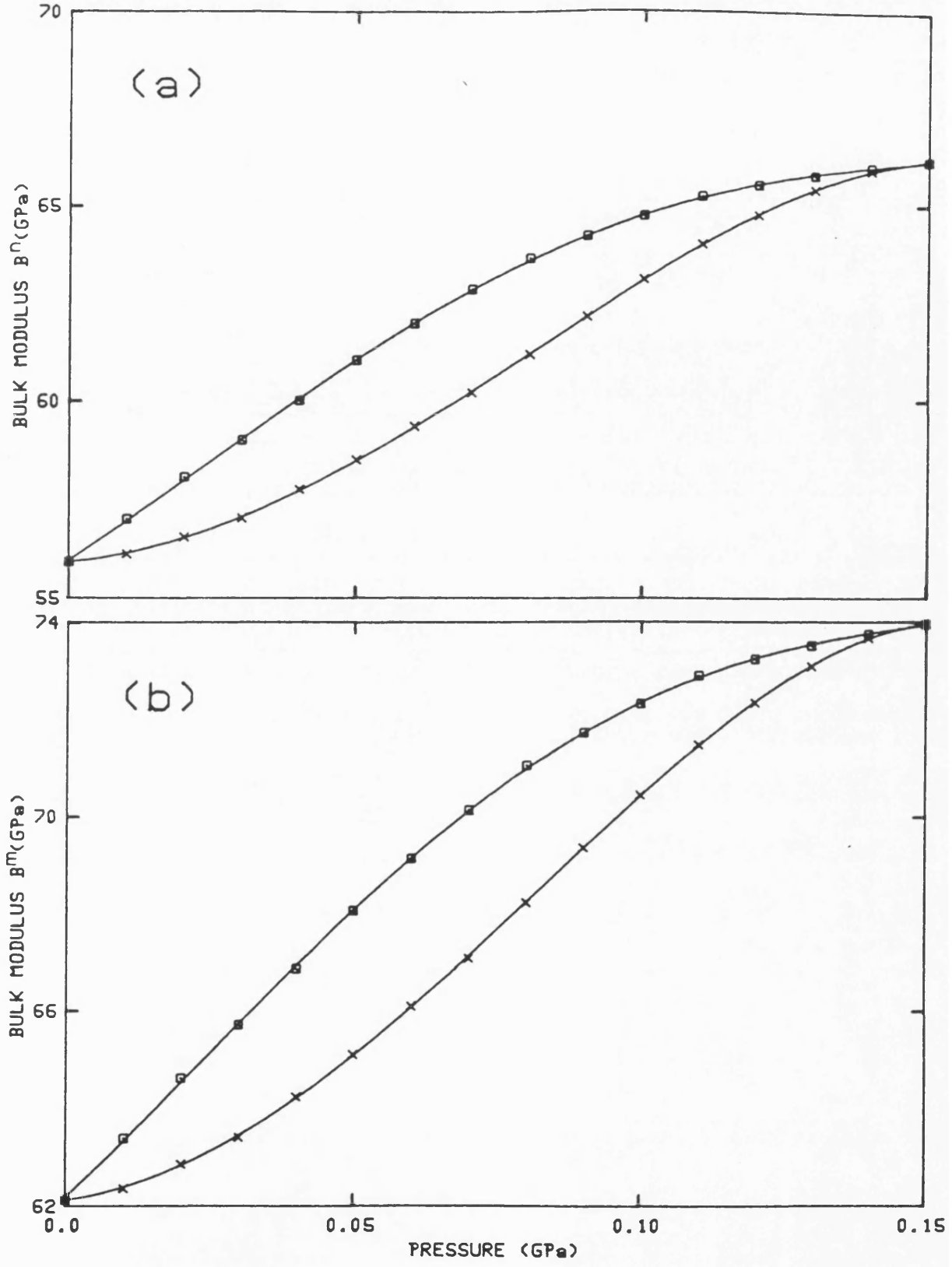

Figure 8.19
The hydrostatic pressure dependences of the bulk modulus (a) B^n (porous material) and (b) B^m (non-porous matrix) of $YBa_2Cu_3O_{7-x}$ (sample Y2) at 295K calculated from the experimental data and using equations 4.4 and 4.5. The solid lines are least square fits to the data.

8.13 respectively and those for sample Y1A are plotted in part (b) of figures 8.14, 8.15 and 8.16 respectively and finally those for sample Y2 are plotted in part (b) of figures 8.17, 8.18 and 8.19 respectively. The hydrostatic pressure derivatives $(\partial C_L/\partial P)_{P=0}$, $(\partial C_S/\partial P)_{P=0}$ and $\partial B/\partial P_{P=0}$ in the limit as the pressure tends towards zero together with the elastic constants for the porous and the non-porous matrix (the corrected values) for samples Y1, Y1A and Y2 are given in table 8.5. The effect of porosity is to reduce the elastic constants as well as their hydrostatic pressure derivatives; this is made clear by comparing the results presented in table 8.5. Also it is clear from the results presented in that table that the sample with highest density has the largest values of the elastic constants. The hydrostatic pressure derivatives of the elastic constants are very large compared even with those of $Nd_{1.85}Ce_{0.15}CuO_{4-y}$ (chapter 6) and for $La_{1.8}Sr_{0.2}CuO_{4-y}$ (chapter 7) which suggests that the large values of the pressure derivatives in $YBa_2Cu_3O_{7-x}$ are of an intrinsic origin rather than being a characteristic of all the new high temperature superconducting compounds.

High pressure studies of lattice parameters of $YBa_2Cu_3O_{7-x}$ have been carried out and reported by several different groups. Jaya et al (1988) employed high pressure X-ray diffraction studies on a $YBa_2Cu_3O_7$ sample up to 11GPa at room

temperature. They found an orthorhombic to tetragonal phase transition above 7GPa and reported a bulk modulus value of 90GPa. Block et al (1987) measured the lattice parameters as a function of pressure using a diamond anvil pressure cell and an X-ray diffraction method. They determined the isothermal bulk modulus as 196GPa and Young's modulus as 235GPa by assuming Poisson's ratio of 0.3. Akhtar et al (1990) performed high pressure studies up to 11GPa to investigate the nature of the structural phases of $YBa_2Cu_3O_7$ using an energy dispersive diffraction technique. They also found a reversible orthorhombic to tetragonal phase transition between 7 and 8GPa. They obtained a bulk modulus for their sample of 128GPa. Olsen et al (1988) studied the crystal structure of the superconducting compound $YBa_2Cu_3O_{7-x}$ at room temperature at pressures up to 60GPa by synchrotron X-ray powder diffraction in a diamond anvil cell using the energy dispersive method. They found a phase transition from an orthorhombic to a tetragonal structure at around 20GPa and that this transition was without a volume change and showed no hysteresis. They calculated the bulk modulus and its pressure derivative to be 157GPa and 2.9 respectively. Chaplot (1990) calculated the bulk modulus and its pressure derivative theoretically for $YBa_2Cu_3O_{7-x}$ compound with $x = 0$ and 1. He obtained a bulk modulus of 109GPa and 92GPa for

x = 0 and 1 respectively and a pressure derivative of the bulk modulus of 4.1 and 5 respectively. Salomons et al (1987) determined the bulk isothermal compressibility from direct measurement of the pressure-volume relation on compacted samples of $YBa_2Cu_3O_{7-x}$ by means of a simple powder model which takes into account the porosity of the sample. They obtained a bulk modulus of 56.3GPa from their calculation. Baetzold (1990) described the orthorhombic structure of $YBa_2Cu_3O_{7-x}$ in terms of the shell model; he obtained a rather smaller value for the pressure derivative of the bulk modulus than that obtained in the present work. Favrot et al (1991) found that the twinned structure of orthorhombic $YBa_2Cu_3O_{7-x}$ superconductor crystal can be de-twinned experimentally by applying an external mechanical stress. They calculated the stress component (σ_n) normal to the twin wall, which will provoke a de-twinning, to be 130 to 400MPa by using $C_{66} \approx C_S$ = 60GPa obtained in the present work (taking C_S as 60GPa from table 8.5). Recently, Wijngaarden and Griessen (1989) published a very useful review of the high pressure studies which have been carried out on the high temperature superconducting compounds. There is clearly a problem here: what is the true bulk modulus of $YBa_2Cu_3O_{7-x}$? this will be discussed in chapter 11 in relation also to the other cuprates studied here.

8.7 THE COMPRESSION OF $YBa_2Cu_3O_{7-x}$

Knowledge of the compression $V(P)/V_o$ (the ratio of the volume $V(P)$ at a pressure P to that V_o at atmospheric pressure) is useful both as a technological parameter of a material and in theoretical studies of the physical properties under pressure. The dependence of the ultrasonic wave velocity upon pressure can only be measured up to limited pressure, and it is usual practice to determine the compression at higher pressures by using an extrapolation procedure based on an equation-of-state. In the present instance that of Murnaghan (1944) written in the form

$$\ln\left\{\frac{V_o}{V(P)}\right\} = \frac{1}{B'^T_o}\ln\left\{B'^T_o\left(\frac{P}{B^T_o}\right)+1\right\} \qquad (8.1)$$

has been used to obtain the compression at room temperature. Ultrasonic experiments determine adiabatic elastic constants. So the isothermal bulk modulus B^T_o has been determined using

$$B^T_o = B^S_o(1+\alpha\gamma T)^{-1} \qquad (8.2)$$

where γ (assumed = 0.75) is the thermal Grüneisen parameter (γ^{th}), α is the volume thermal expansion [=34.1 x $10^{-6}K^{-1}$ from Lang et al (1988)] and the adiabatic bulk modulus B^S_o is 42GPa (table 8.5). The hydrostatic pressure derivative

$B'^{T}_{o}(=(\partial B^{T}_{o}/\partial P)_{P=0,T})$ **of the isothermal bulk modulus for Y1 has been obtained as 50 using [Overton (1962) and Anderson (1966)]**

$$B'^{T}_{o} = B'^{S}_{o} + T\alpha\gamma\left(\frac{B^{T}_{o}}{B^{S}_{o}}\right)\left\{1 - \frac{2}{\alpha B^{T}_{o}}\left(\frac{\partial B^{T}_{o}}{\partial T}\right)_{P} - 2B'^{S}_{o}\right\} \tag{8.3}$$

$$+\left\{T\alpha\gamma\left(\frac{B^{T}_{o}}{B^{S}_{o}}\right)\right\}^{2}\left\{B'^{S}_{o} - 1 - \frac{1}{\alpha^{2}}\left(\frac{\partial \alpha}{\partial T}\right)_{P}\right\}$$

Here $(\partial B^{T}_{o}/\partial T)$ **(= -0.044GPaK^{-1}) has been calculated from**

$$\left(\frac{\partial B^{T}_{o}}{\partial T}\right)_{P} = \frac{\partial B^{S}_{o}/\partial T}{(1+T\alpha\gamma)} \tag{8.4}$$

$$-\frac{B^{S}_{o}T\alpha\gamma}{T(1+T\alpha\gamma)^{2}}\left\{1 + \frac{(\partial\alpha/\partial T)_{P}}{\alpha/T}\right\}$$

using data determined experimentally. The compression of $YBa_2Cu_3O_{7-x}$ calculated using the Murnaghan equation of state (8.1) is plotted in figure 8.20.

Crystal structure determinations under pressure have been carried out on $YBa_2Cu_3O_{7-x}$ by Fietz et al (1987). The volume decrease induced by pressure obtained from their X-ray measurements on powdered $YBa_2Cu_3O_{7-x}$ is also plotted in

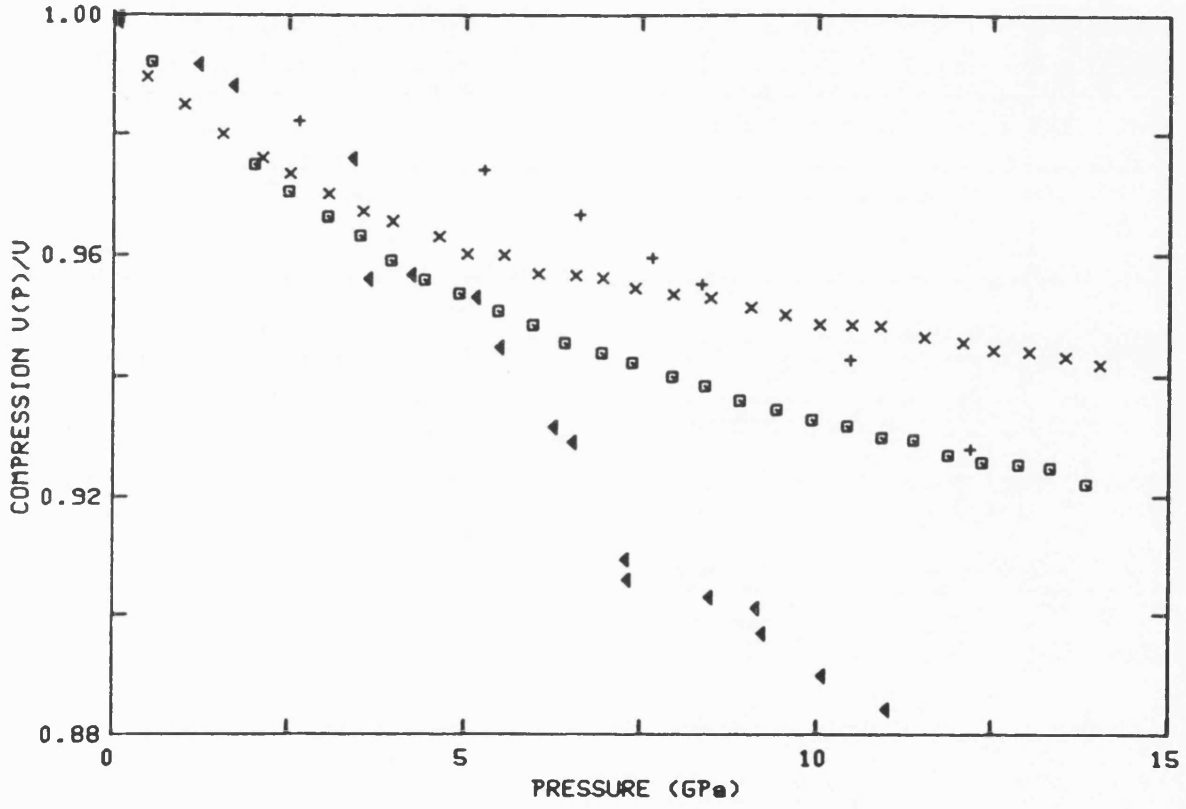

Figure 8.20
The compression of $YBa_2Cu_3O_{7-x}$. The crosses (x) (sample Y1) and squares (sample Y2) correspond to compression calculated from ultrasonic measurements of B_o and $(\partial B/\partial P)_{P=0}$ using the Murnaghan equation of state (equation 8.1). The other points correspond to compression determined from X-ray measurements under pressure: triangles [Jaya et al (1988)], pluses (+) [Fietz et al (1987)].

figure 8.20. They obtained a bulk modulus of 180GPa for their sample. The nearly linear dependence of volume decrease with pressure up to 10 GPa is unusual, and the increasing slope above this pressure which can be seen in their compression data is strikingly anomalous and they suggested that this is possibly due to a phase transformation. At pressures below about 8GPa the compression determined from the ultrasonic data is substantially greater than that measured by the X-ray technique; porosity may contribute to the enhanced compression determined ultrasonically.

8.8 THE TEMPERATURE DEPENDENCE OF $(\partial C_L/\partial P)_{P=0,T}$

To extend the experimental information about the pressure derivative $(\partial C_L/\partial P)_{P=0,T}$, a set of measurements for the denser sample Y2 has been made to establish its variation with temperature. The pressure dependences of the ultrasonic longitudinal wave velocities in sample Y2 at -15, 70, 110 and 120°C are shown in figure 8.21 (a, b, c and d respectively).

In materials in which there is no incipient lattice instability in the form of acoustic phonon mode softening, the temperature dependences of the hydrostatic pressure derivatives of elastic constants is usually small, typically of the order of a few percent change in $(\partial C_{IJ}/\partial P)_{P=0}$ over a temperature range of 100 degrees. However, for $YBa_2Cu_3O_{7-x}$ $(\partial C_L/\partial P)_{P=0,T}$ shows a very large change with temperature (figure 8.22). The influence of porosity on the measured effect of pressure on ultrasound velocity is not expected to show a strong temperature dependence. Hence the most straightforward explanation of such a result would be that there is a substantial change in the interatomic repulsion forces with temperature leading to the variation of $(\partial C_L/\partial P)_{P=0,T}$. The large magnitude of $(\partial C_L/\partial P)_{P=0,T}$ implies that the anharmonicity of the zone centre acoustic phonons is substantial in $YBa_2Cu_3O_{7-x}$ and the increase of $(\partial C_L/\partial P)_{P=0,T}$ with temperature

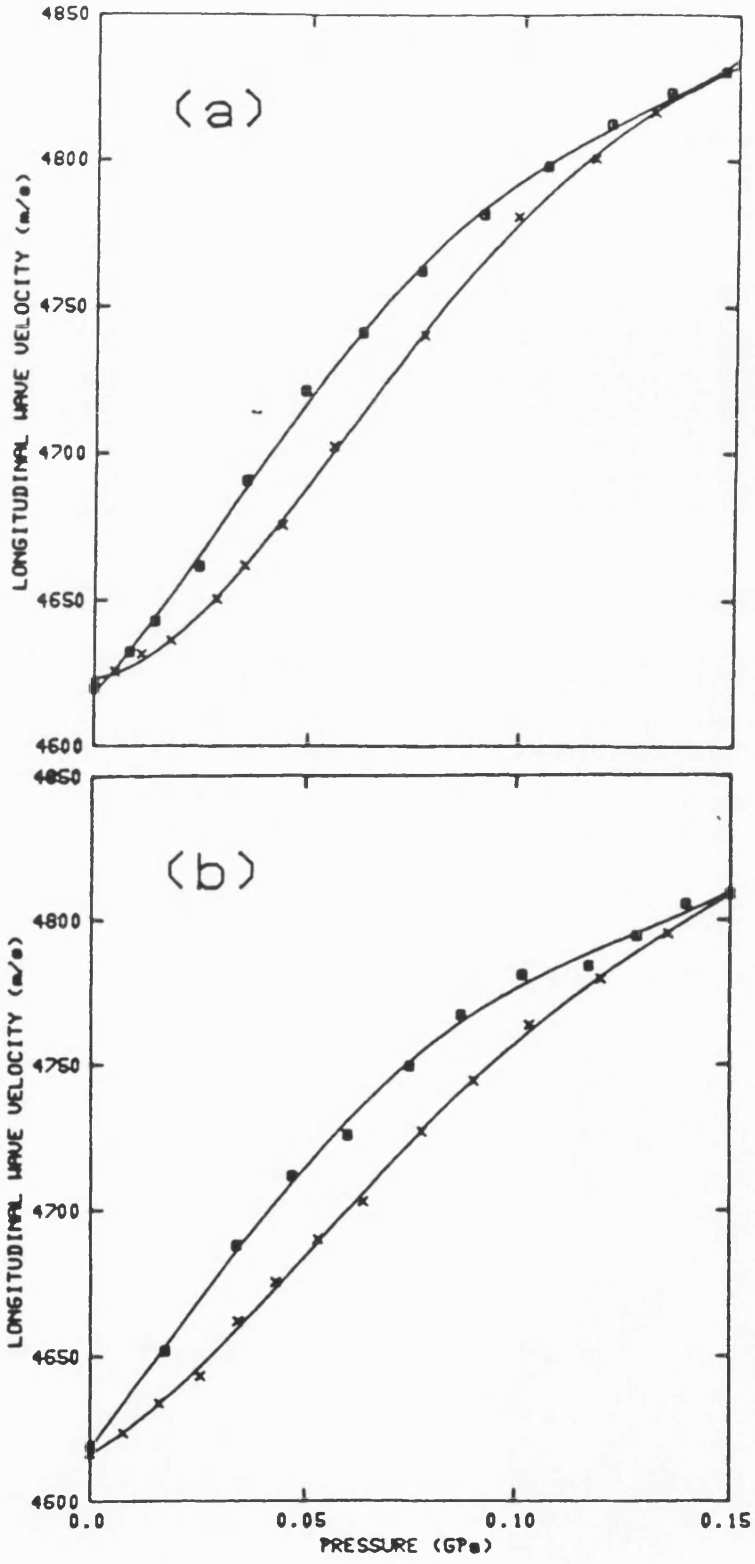

Figure 8.21
The hydrostatic pressure dependences of velocities of longitudinal ultrasonic wave velocity propagated in $YBa_2Cu_3O_{7-x}$ (sample Y2) at (a) -15°C and (b) 70°C . The crosses correspond to velocity measurements made with increasing pressure and the squares to data obtained as the pressure was decreased.

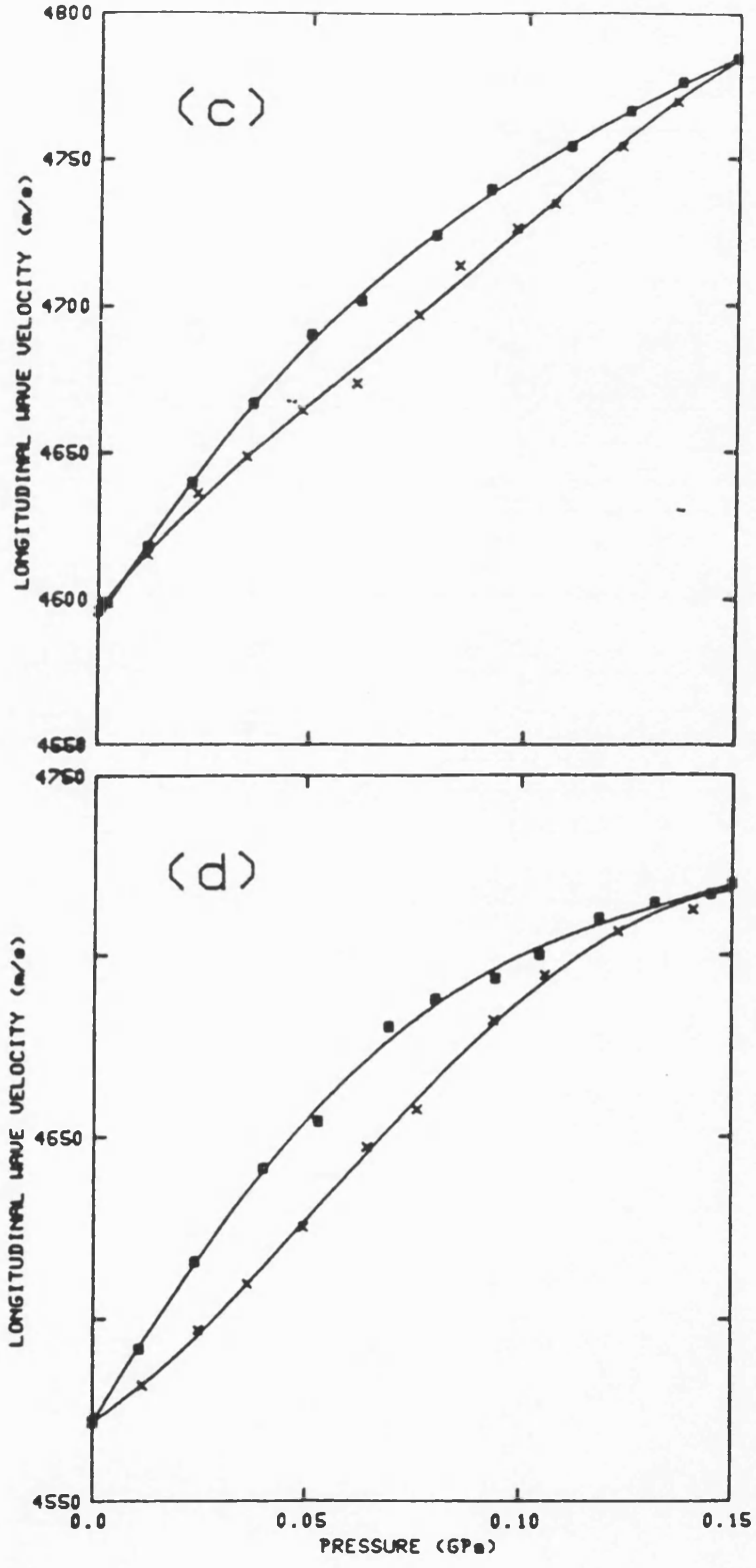

Figure 8.21
The hydrostatic pressure dependences of velocities of longitudinal ultrasonic wave velocity propagated in $YBa_2Cu_3O_{7-x}$ (sample Y2) at (c) 110°C and (d) 120°C . The crosses correspond to velocity measurements made with increasing pressure and the squares to data obtained as the pressure was decreased.

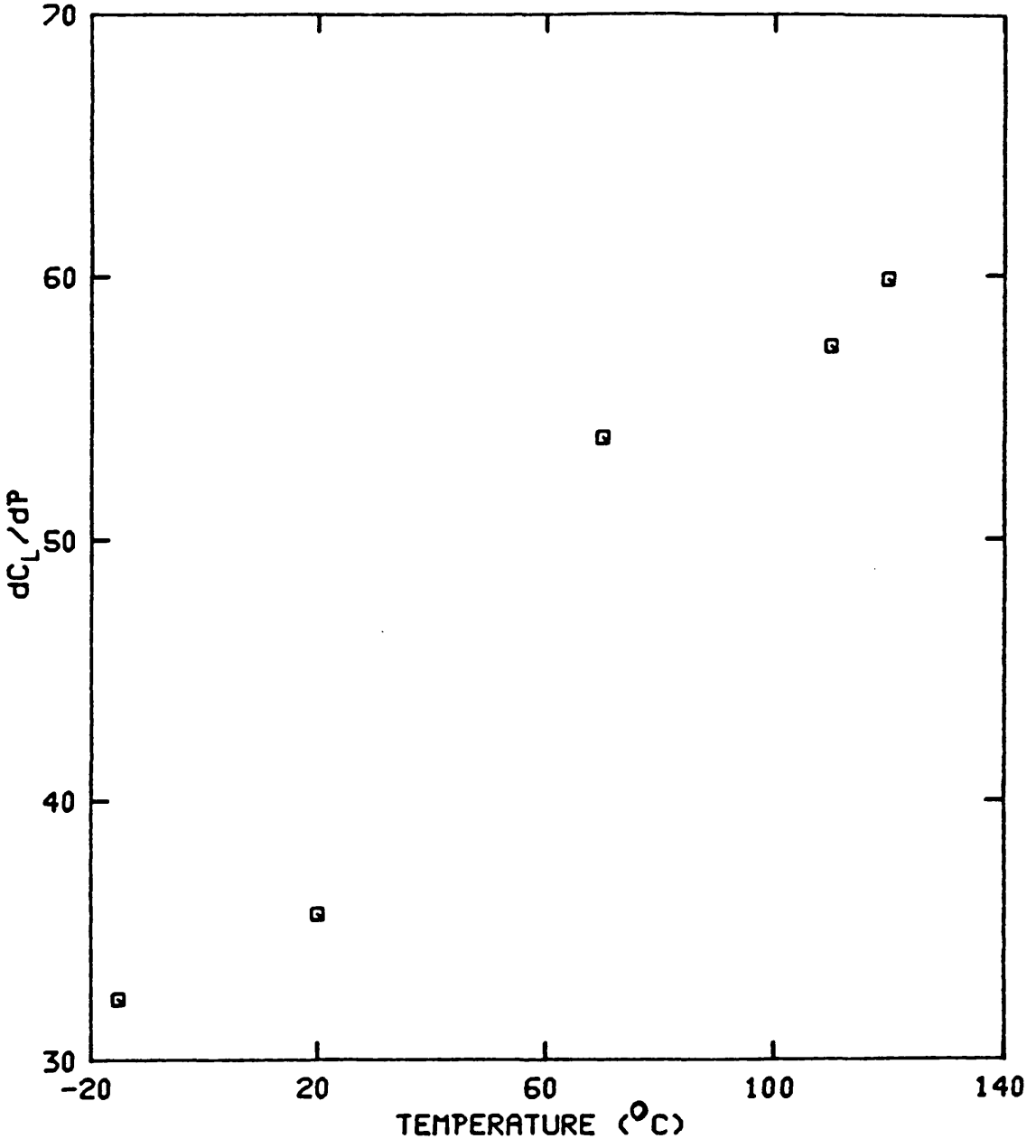

Figure 8.22
The temperature dependence of the hydrostatic pressure derivative $(\partial C_L/\partial P)_{P=0}$ of $YBa_2Cu_3O_{7-x}$ (sample Y2).

suggests that this anharmonicity is enhanced as the temperature raised and is associated with combined effects of pressure and temperature on the fluctuating valence of the copper ions.

8.9 THE PREPARATION AND PROPERTIES OF A LARGE GRAIN SAMPLE OF $YBa_2Cu_3O_{7-x}$

8.9.1 SAMPLE PREPARATION

Another sample studied here was a halide-flux-grown very large grain size $YBa_2Cu_3O_{7-x}$. The halide flux growth technique employed was that described by Taylor et al (1990), developed for the growth of large $YBa_2Cu_3O_{7-x}$ "single crystals". A quantity of $YBa_2Cu_3O_{7-x}$ powder (4 parts) was mixed with a flux consisting of a 1:1 eutectic mixture of NaCl and KCl (1 part) in an alumina crucible. This charge was heated in a tube furnace under flowing oxygen at a rate of 25°*C* per hour up to 1020°*C* and held at that temperature for 10 hours. Then it was slowly cooled down to room temperature at a rate of less than 1°*C* per hour. This produced a large boule of dense (5720 Kgm^{-3}) polycrystalline material, with grain size ranging between 1 and 3mm.

8.9.2 ELECTRICAL RESISTANCE STUDIES

Several samples with dimensions of about 20x3x3mm were cut from the boule for resistance characterization. A conventional *DC* four-lead technique was employed and the measurements were performed on the samples in vacuum with temperatures controlled in the range 10-300K by a closed cycle helium refrigerator. Typical cooling/warming rates were about 0.4 $Kmin^{-1}$. The majority of the samples studied

exhibited unexceptional transitions to zero resistance in the temperature range 83-87K. However, one of the samples (designated A), during the cooling and subsequent warming, displayed hysteresis and resistance jumps shown in figure 8.23a [Almond et al (1990)]. On repeating the measurements a significantly different characteristic (figure 8.23b) showing a distinct knee at 164K was produced. Thermal cycling, 300K to 10K to 300K, was repeated a further eleven times, after which the very clear resistive transition at 164K without hysteresis (figure 8.23c) was found.

This resistive transition found at 164K is not thought to be superconductive in origin for two reasons. Firstly, there is no evidence of an accompanying Meisssner effect in the susceptibility data [Almond et al (1990)]. Secondly, whilst a sharp resistance drop was found at 164K, zero resistance did not occur until temperatures below the accepted $YBa_2Cu_3O_{7-x}$ transition temperature were reached. It is instructive to compare the resistance temperature characteristics of the anomalous sample with one typical of the other samples, cut from the same boule, which showed no anomalies at high temperatures (figure 8.24). The room temperature normal state resistance of the anomalous sample

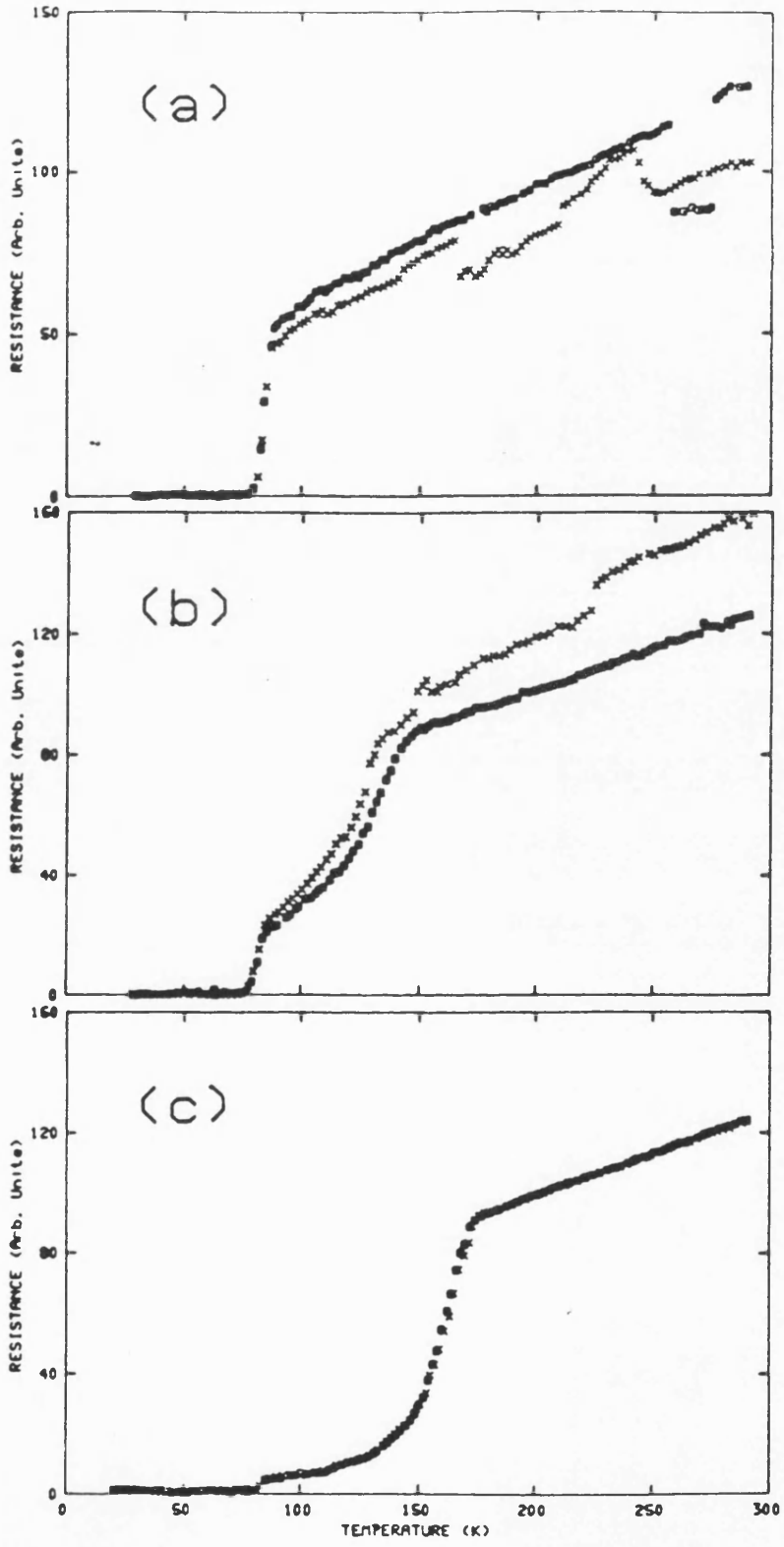

Figure 8.23
The temperature dependence of the electrical resistance of a halide-flux grown sample A of $YBa_2Cu_3O_{7-x}$: (a) first thermal cycle between 10K and room temperature, (b) second cycle and (c) 13th cycle [Almond et al (1990)].

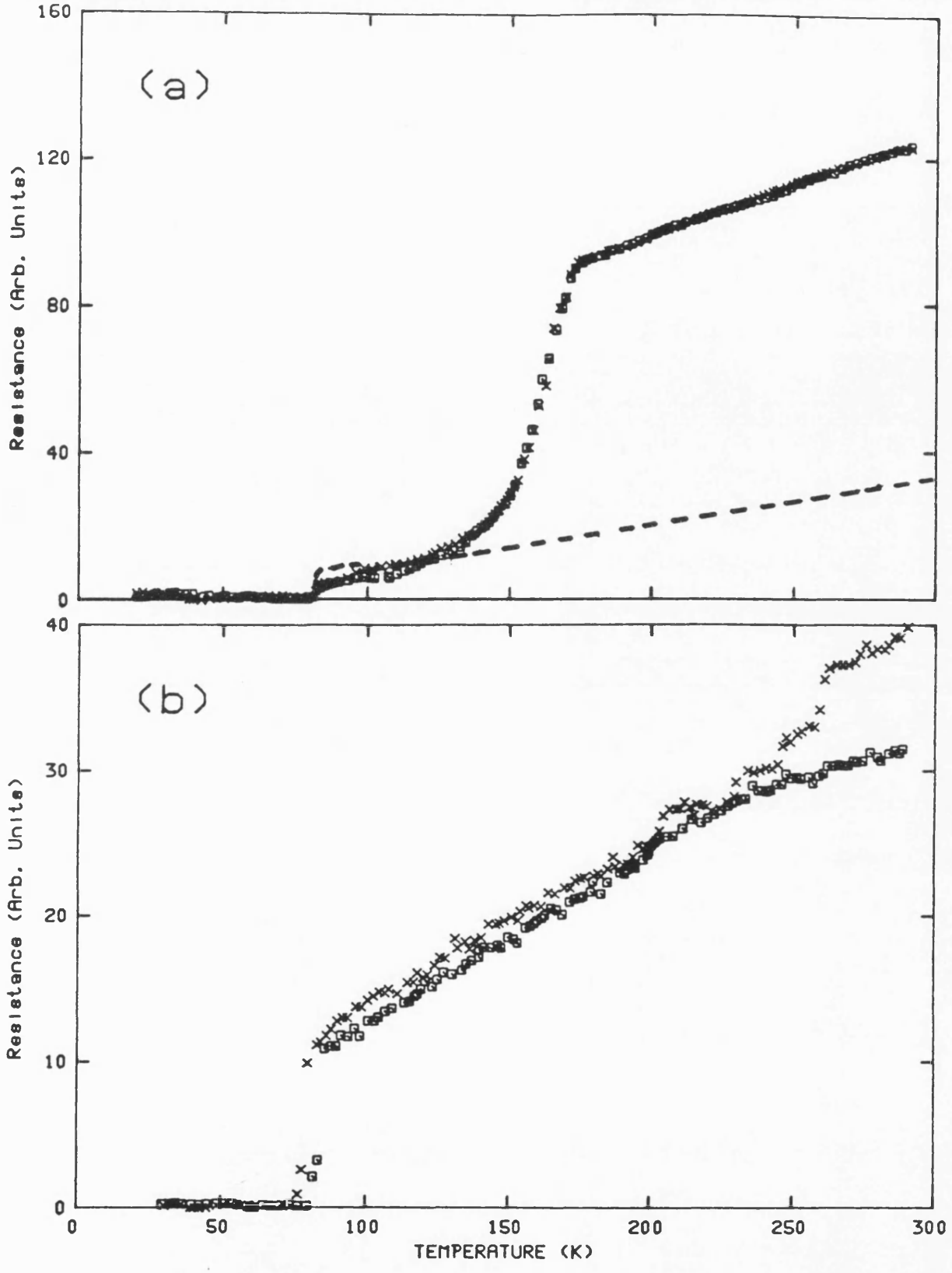

Figure 8.24
The temperature dependence of the electrical resistance of a halid-flux grown (a) the anomalous sample A [figure 23(c)] and (b) a sample B from the same boule that did not exhibit a sharp resistance drop at 164K. Both samples were measured using the same current and the broken line in (a) is the sample B replotted for comparison.

A (figure 8.24a) is clearly much higher than that of sample B (figure 8.24b). It seems to be roughly this difference in normal state resistance that vanishes below 164K.

8.9.3 THE TEMPERATURE AND PRESSURE DEPENDENCES OF THE ULTRASONIC LONGITUDINAL WAVE VELOCITY

The temperature dependences of the ultrasonic longitudinal wave velocity in the large grained, halide flux grown $YBa_2Cu_3O_{7-x}$ specimen were measured, using a 5MHz *PZT* transducer, in the temperature range 10-300K in a closed cycle helium refrigerator. The results obtained are shown in figure 8.25. From this figure it can be seen that the longitudinal wave velocity increases as the temperature is reduced from room temperature down to about 140K where it decreases as the temperature is decreased, then it starts increasing sharply as the temperature is decreased below T_c . Below 140K the data obtained on cooling fall almost on the data obtained on warming. However, there is a marked hysteresis between the data obtained on cooling and those obtained on warming in the temperature range 140-300K. This behaviour contrasts with that found for samples Y1 and Y2 (figures 8.1 and 8.2) indicating the effects of the microstructure and the grain size on the elastic properties of the $YBa_2Cu_3O_{7-x}$ compound.

The ultrasonic longitudinal wave velocity in the large grained $YBa_2Cu_3O_{7-x}$ specimen were measured at room temperature as a function of pressure using 5MHz *PZT* transducer with Dow Resin as the bonding agent. The results obtained are

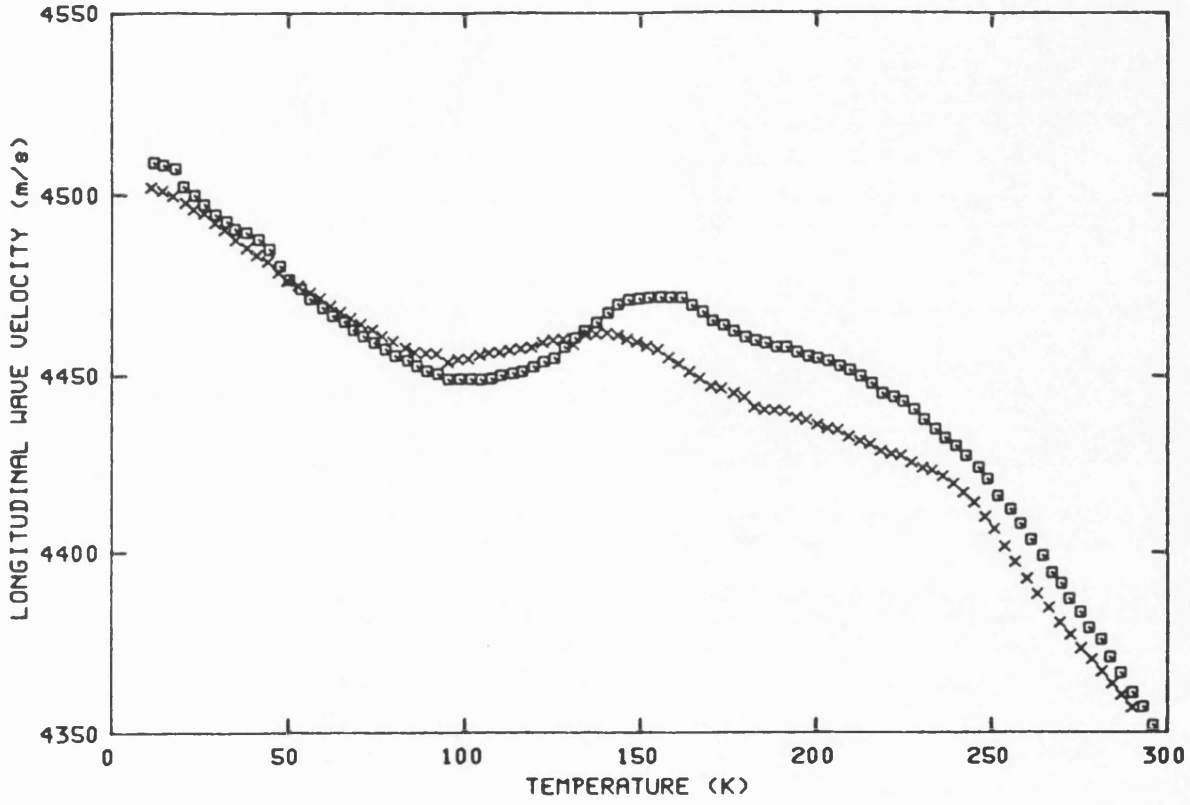

Figure 8.25
The temperature dependences of ultrasonic longitudinal wave velocity for the halide-flux grown $YBa_2Cu_3O_{7-x}$ sample. The crosses (x) corresponds to the data obtained during cooling and the squares to those obtained during warming.

shown in figure 8.26a. The longitudinal wave velocity value and therefore the elastic stiffness C_L , are in the same range of values as those measured for the fine and coarse grained ceramic materials (samples Y1 and Y2) (Table 8.6). Hence the bulk modulus of this very large grained $YBa_2Cu_3O_{7-x}$ must be similar to that of the ceramic material. Also shown in table 8.6 is the average longitudinal wave velocity calculated [Fanggao et al (1991a)] from data [Kim et al (1990)] for single crystal $YBa_2Cu_3O_{7-x}$. Kim et al (1990) found a large anisotropy in the velocities of the longitudinal modes: V_{11} = (5617±17)ms^{-1}, V_{33} = (3096±7)ms^{-1}. The average longitudinal velocity of 4460ms^{-1} has been obtained assuming an ellipsoidal velocity surface with major and minor axes of V_{11} and V_{33}. That this value is also similar to those values obtained for fine and coarse grain materials shows that the ultrasonic technique gives the right value for the mean longitudinal velocity in these $YBa_2Cu_3O_{7-x}$ ceramics.

The hydrostatic pressure dependence of the longitudinal modulus C_L^n of the large grained, halide flux grown, $YBa_2Cu_3O_{7-x}$ specimen is shown in Figure 8.26b. The straight line is the least-mean-square fit to the experimental data. The value of $(\partial C_L/\partial P)_{P=0}$ obtained from these data (table 8.6) can be seen

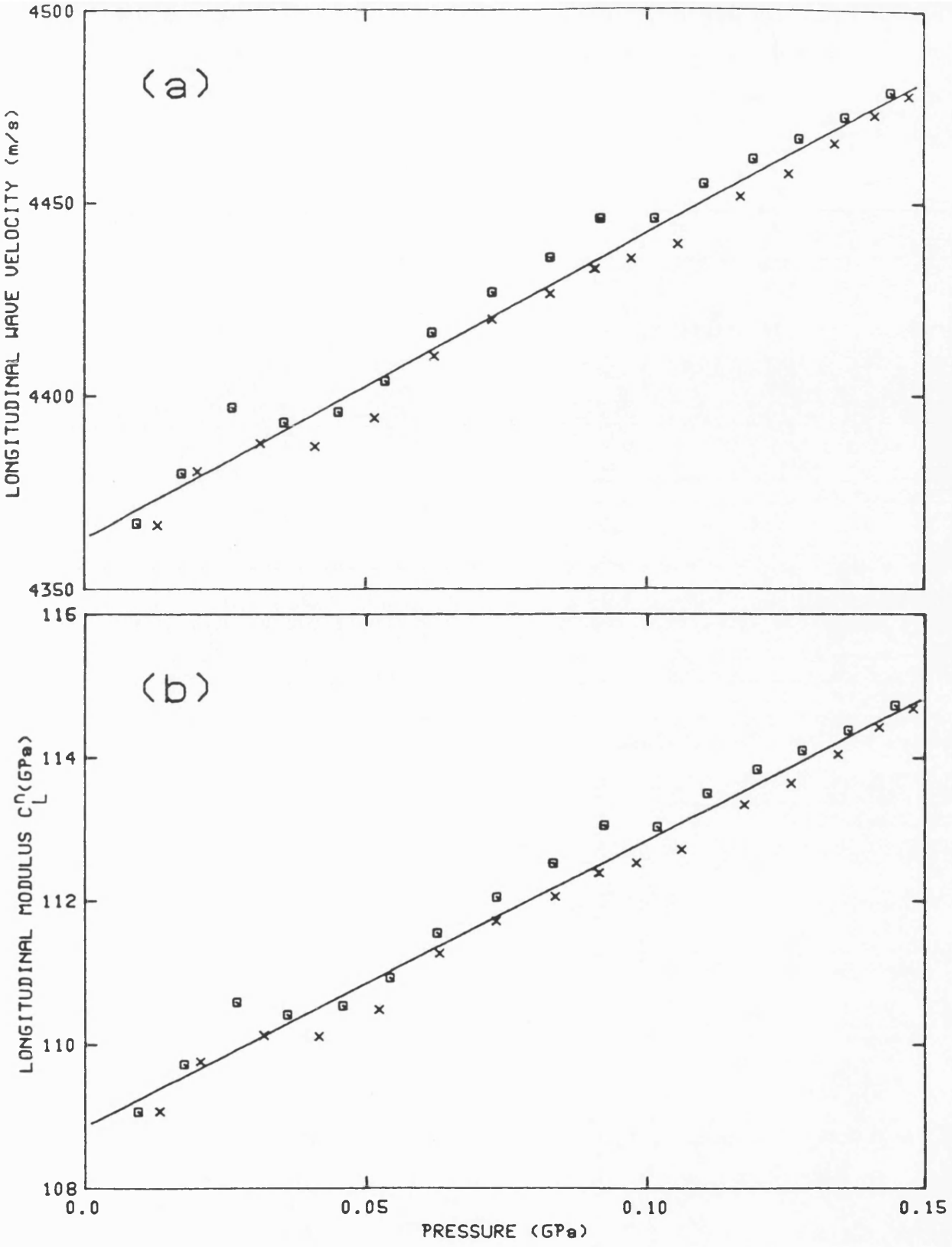

Figure 8.26
The hydrostatic pressure dependences of (a) longitudinal wave velocity and (b) longitudinal modulus C_L^n for the halide-flux grown $YBa_2Cu_3O_{7-x}$ sample. The crosses (x) corresponds to the data obtained with increasing pressure and the squares to those obtained as the pressure was decreased.

Table 8.6. Comparison between the longitudinal-mode properties of single-crystal, very large-grained halide-flux-grown material and ceramic samples of $YBa_2Cu_3O_{7-x}$. The value of $(\partial C_L/\partial P)_{P=0}$ for the coarse-grained ceramic (sample Y2) was determined with increasing pressure. Data are not corrected for porosity.

Property	Single crystal (Kim et al 1990)	Large grained (halide flux grown)	Ceramic (coarse grained)	Ceramic (fine grained)
Density (kg/m^3)		5720	5985	5199
Mean grain size	3x3x5 mm^3	1-3 mm	50μ	10μ
Longitudinal wave velocity (m/s)	4460	4354	4537	4067
C_L (GPa)	-	108	123	86
$(\partial C_L/\partial P)_{P=0}$	-	40	37	69

to have the large magnitude found for the more usual ceramic form of $YBa_2Cu_3O_{7-x}$. This implies that $(\partial B/\partial P)_{P=0}$ must also be substantial for this very large grained material.

Many attempts were made to propagate an ultrasonic shear waves through the large grained $YBa_2Cu_3O_{7-x}$ sample but unfortunately all of those trials ended in failure.

A separate chapter (chapter 11) will contain a full discussion and comparison between the results obtained for the $YBa_2Cu_3O_{7-x}$ compound in all the forms presented here with those results obtained for the other high temperature superconducting compounds.

CHAPTER NINE

ELASTIC PROPERTIES OF ORTHORHOMBIC AND TETRAGONAL $GdBa_2Cu_3O_{7-x}$

9.1 INTRODUCTION

A comparative study of the elastic properties as a function of hydrostatic pressure and temperature of a low density, small grain size sample of $GdBa_2Cu_3O_{7-x}$ in a well annealed orthorhombic state and also in the non-superconducting tetragonal state, is presented in this chapter. The orthorhombic phase of $GdBa_2Cu_3O_{7-x}$ is extensively twinned with (110) twin boundaries formed when the material undergoes the transition from the high-temperature (>600° C) tetragonal phase to the orthorhombic phase [Hewat et al (1987), van Tendezoo et al (1987)]. The tetragonal phase is not twinned. Hence the comparison between the elastic properties of the two phases provides an experimental test of the possibility that the small bulk modulus and its large hydrostatic pressure derivative $(\partial B/\partial P)_{P=0}$, found for the 123 compounds, might be due in part at least to strain-induced movement of twin boundaries.

The orthorhombic sample was prepared as described in chapter 4. The density of this sample was 5549 kgm^{-3}, indicating its mean porosity to be 0.22 (assuming an X-ray density of 7138 kgm^{-3}). Subsequent to the completion of the

study of the sample in its orthorhombic state, it was heated in vacuum at 700°*C* for 24 hours to reduce its oxygen content and quenched down to convert it to the non-superconducting tetragonal state. This structural transformation to the tetragonal phase involves two changes: (i) lowering the oxygen content, (ii) an increase in unit cell volume [Tarascon et al (1987)]. After both of these effects have been taken into account the density of the tetragonal phase still corresponds to a porosity of 0.22. Micrographic investigation showed that the orthorhombic form was heavily twinned but the tetragonal form not at all.

Results on the X-ray powder diffraction studies made on the orthorhombic $GdBa_2Cu_3O_{7-x}$ sample are presented in section 9.2. Electrical resistance data obtained for both orthorhombic and tetragonal $GdBa_2Cu_3O_{7-x}$ samples are discussed in section 9.3. The temperature dependences of the ultrasonic longitudinal and shear wave velocities and attenuation measured for the $GdBa_2Cu_3O_{7-x}$ sample in both orthorhombic and tetragonal forms are presented and discussed in section 9.4 together with temperature dependences of the elastic moduli. The hydrostatic pressure effects on the ultrasonic wave velocities are discussed in section 9.5. Finally, the pressure dependences of the elastic constants are presented in section 9.6.

9.2 X-RAY DIFFRACTION STUDIES

$GdBa_2Cu_3O_{7-x}$ powder from the same batch as that used to make the ultrasonic samples was analysed by X-ray diffractometry at temperatures down to 92K. Extensive measurements were made between 200 and 250K to seek evidence of any lattice parameter changes that might be consistent with a phase transition in this temperature range. The lattice parameters of the material in the orthorhombic state measured between 92 and 293K are shown in figure 9.1 [Almond et al (1989)]. The lattice parameters at 293K are a = 3.925±0.002Å, b = 3.863±0.002Å and c = 11.755±0.002Å. These values are in good agreement with those obtained by others (see table 9.1).

The lattice parameters temperature dependences have been fitted [Almond et al (1989)] by a least-mean-square procedure which leads to the thermal expansion tensor components (table 9.2). The mean linear thermal expansion coefficient is in good agreement with that ($\alpha = 1.2 \times 10^{-5} K^{-1}$) at 270K measured dilatometrically by Kadowaki et al (1988). The lack of an-isotropy shown by these thermal expansion tensor components gives useful insight into the relative strengths of the interatomic binding forces in different directions in these materials. The similarity between α_{11}, α_{22} and α_{33} (table 9.2) indicates that the an-isotropy of the interatomic

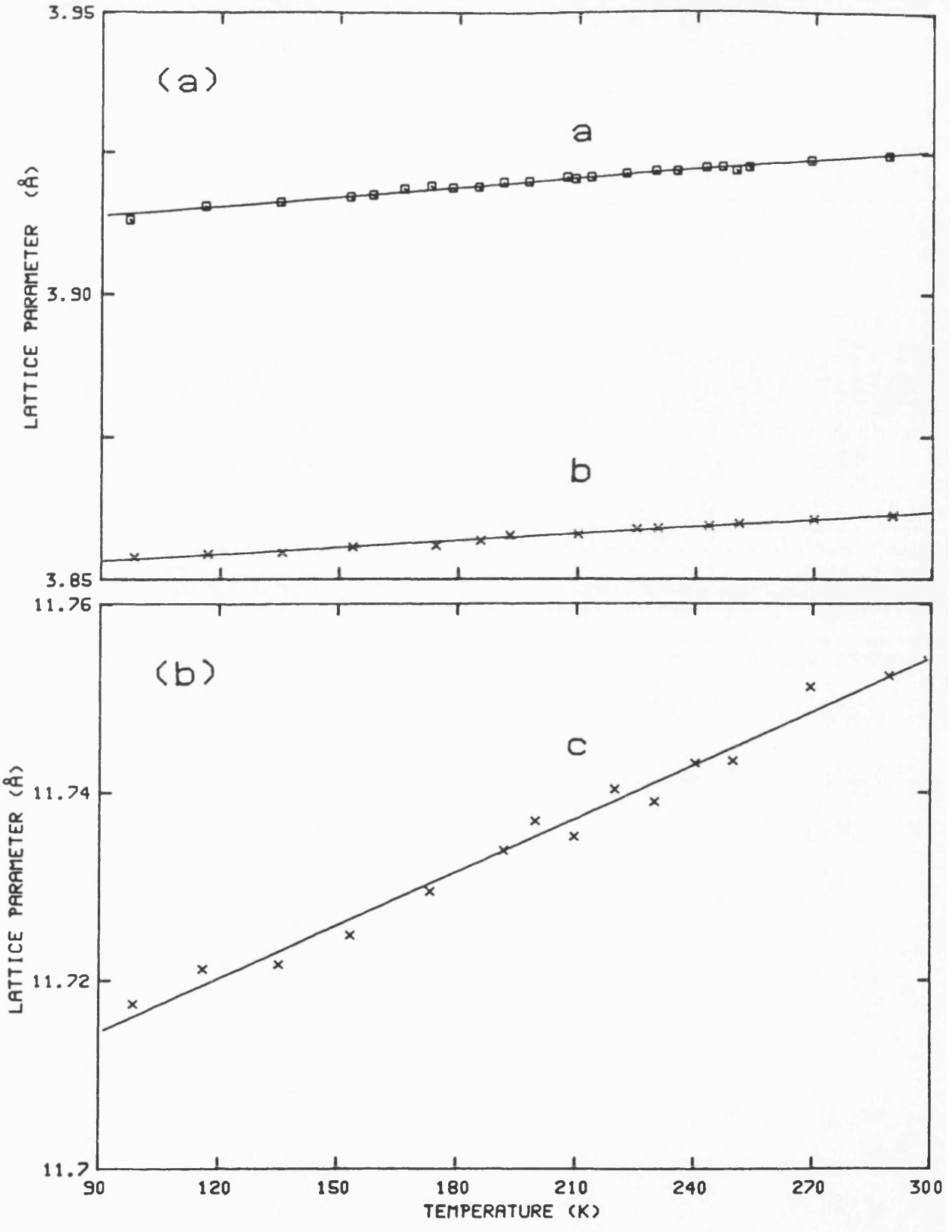

Figure 9.1
The temperature dependences of lattice parameters (a) *a*, *b* and (b) *c* for an orthorhombic (superconducting) $GdBa_2Cu_3O_{7-x}$ sample. The solid lines are the least square fits to the data taken from Almond et al (1989).

Table 9.1. Comparison between the lattice parameters for a $GdBa_2Cu_3O_{7-X}$ sample in the orthorhombic form obtained in this work with the data reported by other groups.

Reference	a (Å)	b (Å)	c (Å)
This work	3.925±0.002	3.863±0.002	11.755±0.002
Ecke et al (1988)	3.839	3.893	11.686
Hor et al (1987)	3.890	3.890	11.730
Liang et al (1987)	3.909	3.847	11.682
Saint-Paul (1989)	3.820	3.880	11.670
Xu et al (1987)	3.909	3.849	11.682

Table 9.2. The thermal expansion tensor components of orthorhombic $GdBa_2Cu_3O_{7-x}$.

α_{11}	$(1.22\pm0.03)\times10^{-5}K^{-1}$
α_{22}	$(1.12\pm0.03)\times10^{-5}K^{-1}$
α_{33}	$(1.64\pm0.03)\times10^{-5}K^{-1}$
Mean linear thermal expansion	$1.30\times10^{-5}K^{-1}$
Volume thermal expansion	$(3.98\pm0.09)\times10^{-5}K^{-1}$

binding forces may not be large. In layer-like crystals, binding between the successive layers tends to be weaker than that due to inter-layer forces; vibrational modes are more easily excited in the softer direction, so the thermal expansion and linear compressibility are greater in this direction [Pace et al (1970)]. With increasing temperature the lower-energy phonons in the more weakly bound direction are excited first, so α_{33} would be expected to be larger than α_{11} or α_{22} if $GdBa_2Cu_3O_{7-x}$ was a layer-like compound with weaker inter-layer bonding along the c-axis direction. However, the similarity between the three tensor components implies that inter-atomic binding forces are probably similar in magnitude both between and within the layers as was found for $Bi_2CaSr_2Cu_2O_8$ [Almond et al (1988)].

Del Moral et al (1988) measured the thermal expansion coefficient α in different samples with the chemical formula $RBa_2Cu_3O_{7-x}$ (where R = rare earth elements). They obtained a value of $13.4 \times 10^{-6} K^{-1}$ for the thermal expansion coefficient in their $GdBa_2Cu_3O_{7-x}$ sample and found no phase transition anomaly in α at T_c within their experimental accuracy. This result is in good agreement with that found here for the orthorhombic sample (table 9.2).

9.3 THE ELECTRICAL RESISTANCE MEASUREMENTS

The temperature dependences of the electrical resistance of the GdBa2Cu307-X compound, in its orthorhombic and tetragonal forms, were measured using a glass cryostat system and the four-probe method. The results are shown in figure 9.2 (Freestone 1990). The resistance data, for the sample in the orthorhombic structure, indicate that, in the normal region, the electrical behaviour is metallic. The resistance began to fall steeply at 93.5K; zero resistance (within instrumental noise) was achieved at 89.6K with the midpoint at 91.7K. In the tetragonal form the resistance increases as the temperature was decreased, in a manner similar to that of a semiconductor, but with a small decrease in resistance developing below 94K. The room temperature resistance for the sample with the orthorhombic structure was 3.1$m\Omega$ and that with the tetragonal structure was 50.2$m\Omega$. Similar behaviour for the temperature dependence of the electrical resistance for $GdBa_2Cu_3O_{7-x}$ sample in the orthorhombic form was found in the temperature dependence of the electrical resistivity by Heremans et al (1988). They obtained a room temperature electrical resistivity of $6x10^{-3}\Omega cm$ for their sample and T_c of 89.4K. Similar behaviour was found by Matsuda et al (1988) in the temperature

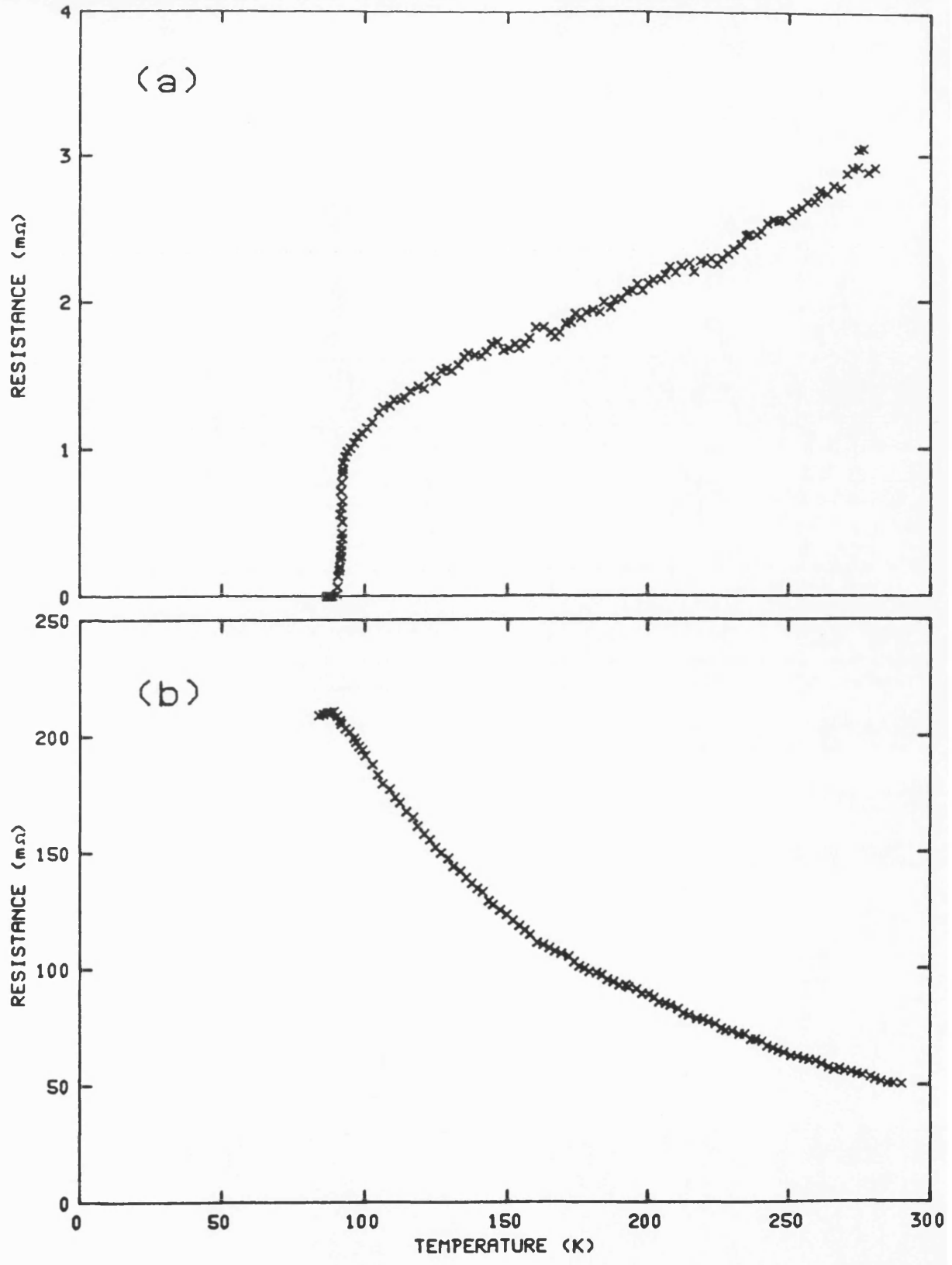

Figure 9.2
The temperature dependences of the electrical resistance for (a) orthorhombic (superconducting) and (b) tetragonal (non-superconducting) $GdBa_2Cu_3O_{7-x}$. Data taken from Freestone (1990).

dependence of the electrical resistivity in a $GdBa_2Cu_3O_{7-x}$ sample. They obtained a room temperature resistivity of 1.6$m\Omega cm$ and T_c of 90K for their sample.

9.4 THE TEMPERATURE DEPENDENCES OF ULTRASONIC WAVE VELOCITIES, ATTENUATION AND ELASTIC MODULI

Ultrasonic wave velocities and attenuation were measured as a function of temperature in the orthorhombic $GdBa_2Cu_3O_{7-x}$ sample in the temperature range 10-300K using the glass dewar system. 10 MHz X-cut and 5MHz Y-cut quartz transducers (X-cut for longitudinal, Y-cut for shear) were used to excite and detect the ultrasonic waves. Nonaq stopcock grease was used as a bonding agent between the sample and the transducer. After vacuum annealing the orthorhombic sample at 700°C for 24 hours to obtain the tetragonal form, the ultrasonic wave velocities and attenuation were measured as a function of temperature using 5,10 and 15MHz quartz transducers for the longitudinal mode and a 10MHz quartz transducer for the shear mode. The results obtained for the ultrasonic wave velocities for both the orthorhombic and the tetragonal forms are shown in figure 9.3 [Cankurtaran et al (1990a)]. The annealing process reduced the velocity in the sample, i.e. the ultrasonic wave velocities in the tetragonal sample are slower than those in the orthorhombic form. A striking feature of the velocity data for the sample in the orthorhombic structure is the abrupt change of the sound velocity on cooling at 200K and on warming at 240K; there is a large warming versus cooling hysteresis over the whole temperature

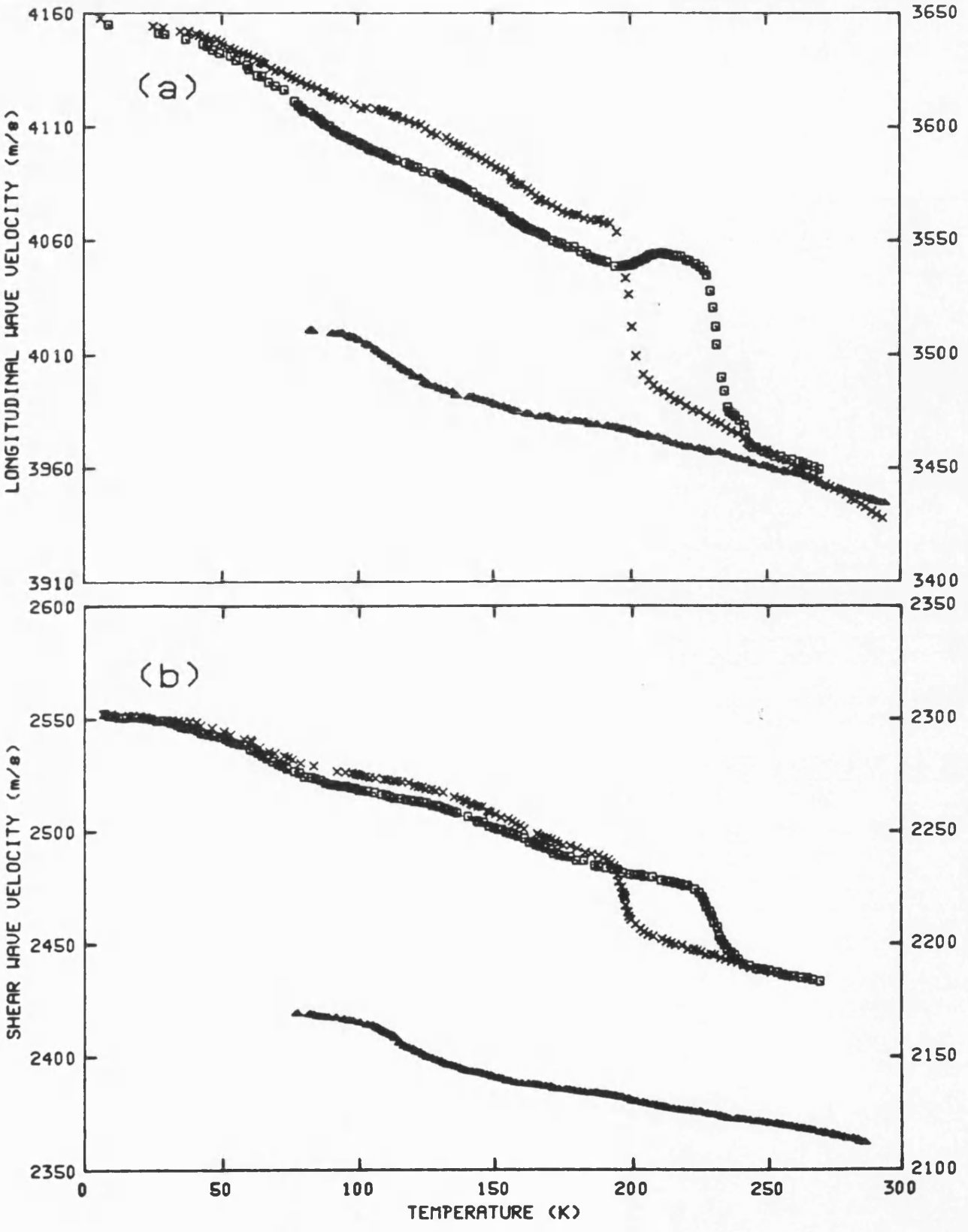

Figure 9.3

The temperature dependences of ultrasonic (a) longitudinal and (b) shear waves velocities for $GdBa_2Cu_3O_{7-x}$ compound in both orthorhombic (the left hand coordinates) and tetragonal (the right hand coordinates) forms. The crosses (x) correspond to the data obtained during cooling and the squares to those obtained during warming for the orthorhombic sample. The triangles correspond to the data obtained during cooling for the tetragonal sample. The data taken from Almond et al (1989).

range investigated. This dramatic change in ultrasound velocity was absent in the tetragonal form, as was the hysteresis; that is warming data fell on the cooling data within experimental error. The velocity data for the sample in its orthorhombic form (superconducting) shows an inflection giving the appearance of softening at a temperature corresponding to T_c . The data for the oxygen reduced (tetragonal) sample show a similar inflection but at a substantially higher temperature of around 120K.

The ultrasonic attenuation as a function of temperature in the orthorhombic and tetragonal forms is plotted in figures 9.4 and 9.5 respectively [Cankurtaran et al (1990a)]. Peaks in the attenuation data can be seen in both the orthorhombic and tetragonal phases. The longitudinal and shear waves attenuation peaks occur at the same temperature for a particular frequency and a particular form (orthorhombic or tetragonal) and the position of the attenuation peak is found in each case to rise in temperature as the measuring frequency is increased.

The dramatic feature in the ultrasonic wave velocity in the $GdBa_2Cu_3O_{7-x}$ sample investigated here is similar to that found in the fine grain $YBa_2Cu_3O_{7-x}$ (sample Y1) presented in chapter 8 (figure 8.1) where thermal hysteresis and change in the ultrasonic wave velocity in the temperature range

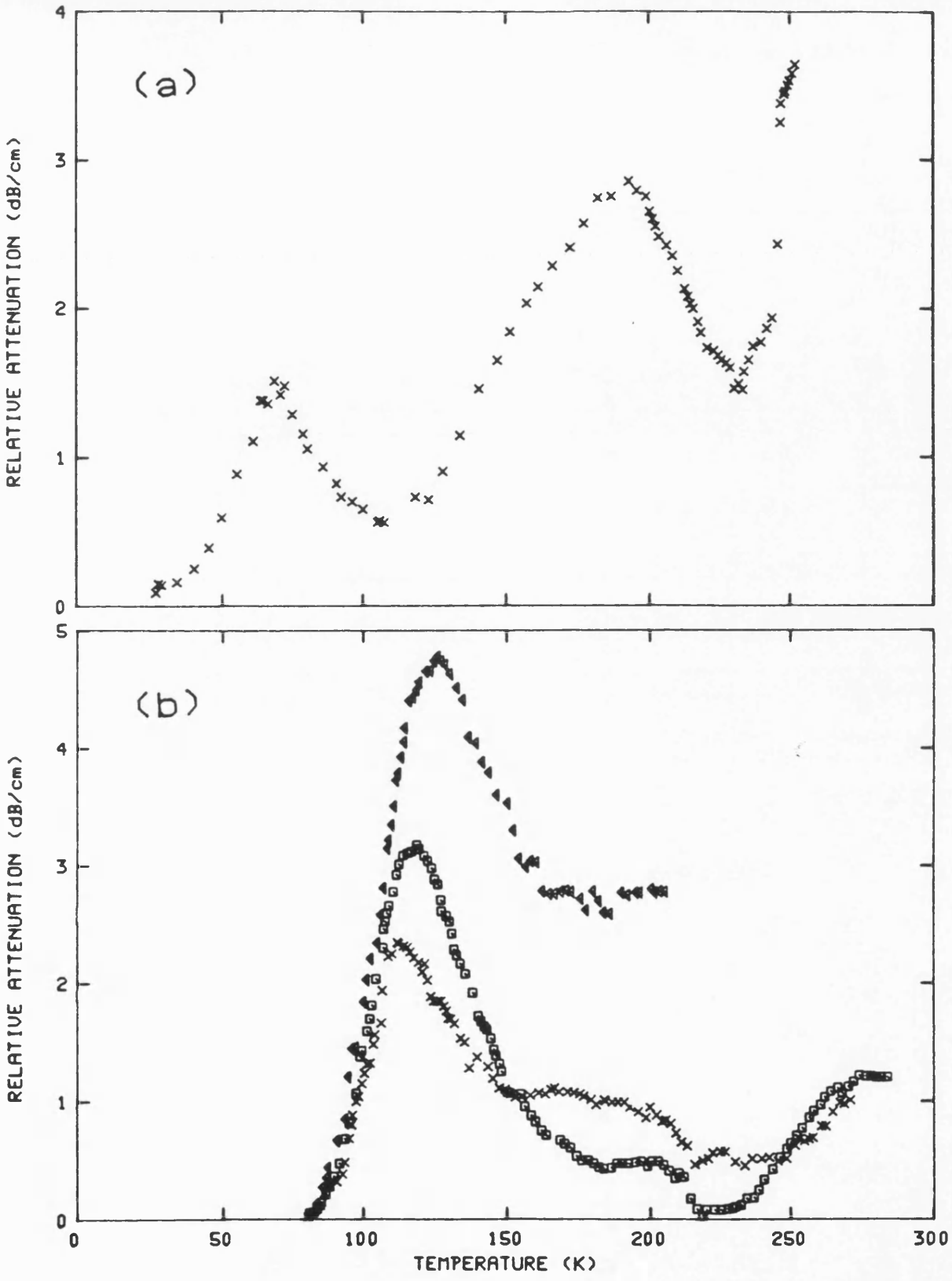

Figure 9.4
The temperature dependences of the longitudinal ultrasonic wave attenuation for (a) orthorhombic and (b) tetragonal $GdBa_2Cu_3O_{7-x}$ sample. The crosses (x) in (a) correspond to the data obtained using a carrier frequency of 10MHz while in (b) the crosses, squares and triangles correspond to the data obtained using carrier frequencies of 5, 10 and 15MHz respectively. The data taken from Almond et al (1989).

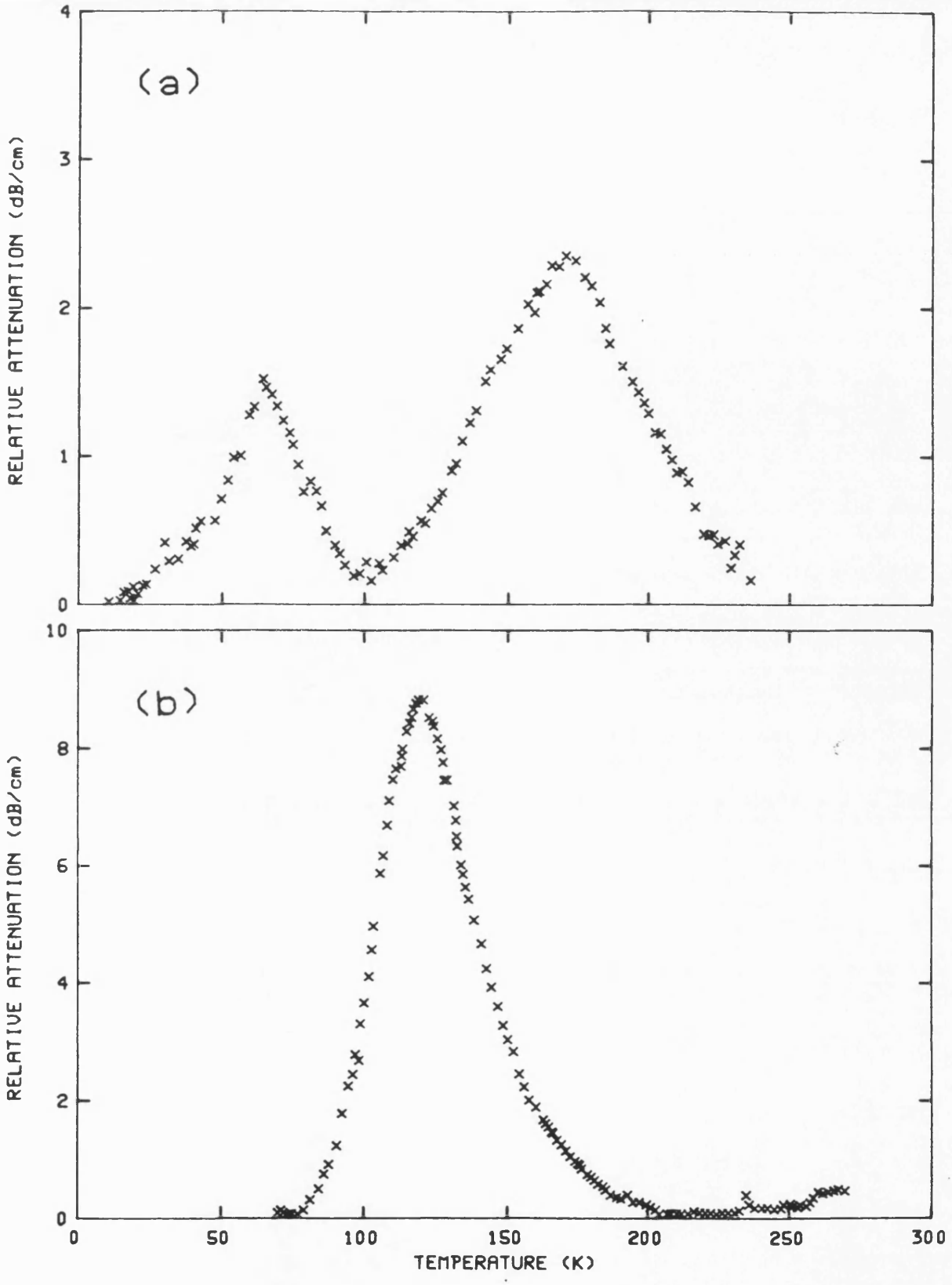

Figure 9.5
The temperature dependences of the shear ultrasonic wave attenuation for (a) orthorhombic and (b) tetragonal $GdBa_2Cu_3O_{7-x}$ sample. The crosses (x) in (a) correspond to the data obtained using a carrier frequency of 5MHz while in (b) the crosses correspond to the data obtained using a carrier frequency of 10MHz. The data taken from Almond et al (1989).

200-240K was found. That anomalous behaviour found in sample Y1 was attributed to a possible structural phase transition occurring in the temperature region 200-240K so this could also be responsible for the behaviour of the orthorhombic $GdBa_2Cu_3O_{7-x}$. A major structural difference between the orthorhombic and the tetragonal phases of $GdBa_2Cu_3O_{7-x}$ is that the orthorhombic structure is heavily twinned while the tetragonal is un-twinned. So the appearance of hysteresis and of the abrupt change at 200K and 240K in the ultrasonic wave velocities in the orthorhombic sample might be related to the twinned nature of that phase.

Brown et al (1988) measured the ultrasonic wave velocities in a $GdBa_2Cu_3O_7$ sample, which had an experimental density of 84% of the theoretical density, using the pulse-echo overlap technique. They obtained a longitudinal velocity of 4400 ms^{-1} and a shear velocity of 2600 ms^{-1} which are faster than the velocities obtained for the orthorhombic sample investigated here (longitudinal velocity = 3938 ms^{-1} and shear velocity = 2430 ms^{-1}). Meanwhile, Saint-Paul et al (1989) measured the shear velocity in single crystal $GdBa_2Cu_3O_{7-x}$. They obtained a value of 2000 ms^{-1} which is much slower compared with that found by Brown et al (1988) and for the samples investigated here (V_S = 2430ms^{-1} for the orthorhombic form and 2112ms^{-1} for the tetragonal form).

Elastic moduli have been calculated using the measured ultrasonic wave velocities as a function of temperature. The temperature dependences of longitudinal C_L^n , shear C_S^n , bulk B^n and Young's moduli for $GdBa_2Cu_3O_{7-x}$ sample in both orthorhombic and tetragonal forms are plotted in figures 9.6, 9.7, 9.8 and 9.9 respectively. The thermal hysteresis and the anomaly in the temperature range 200-240K are clear in these elastic moduli for the sample in the orthorhombic form while they are absent in the tetragonal form. These moduli together with the ultrasonic wave velocities obtained in the $GdBa_2Cu_3O_{7-x}$ sample in both orthorhombic and tetragonal forms are given in table 9.3.

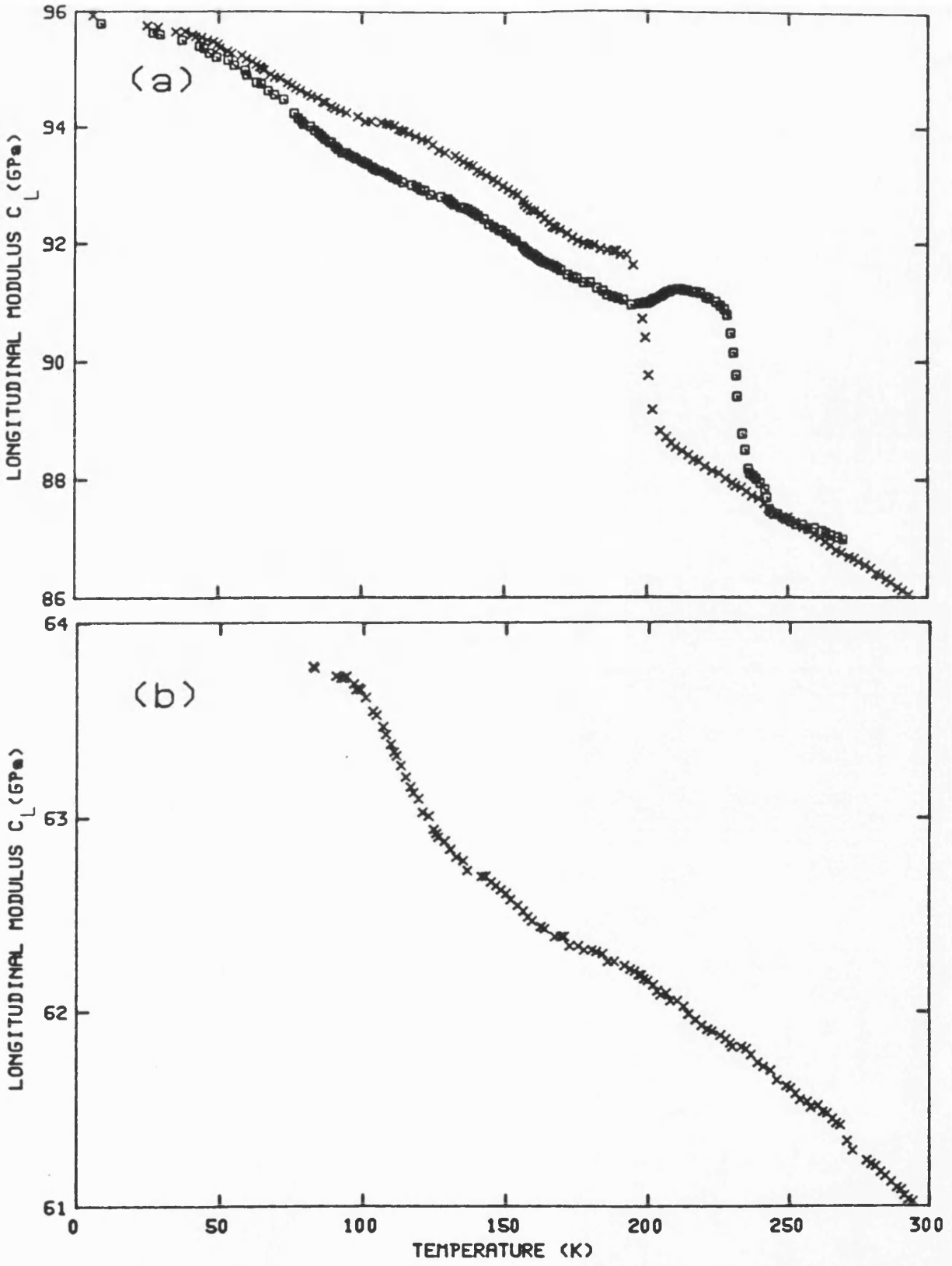

Figure 9.6
The temperature dependences of the longitudinal modulus C_L for (a) orthorhombic and (b) tetragonal $GdBa_2Cu_3O_{7-x}$ samples. The crosses (x) correspond to the data obtained during cooling and the squares to those obtained during warming.

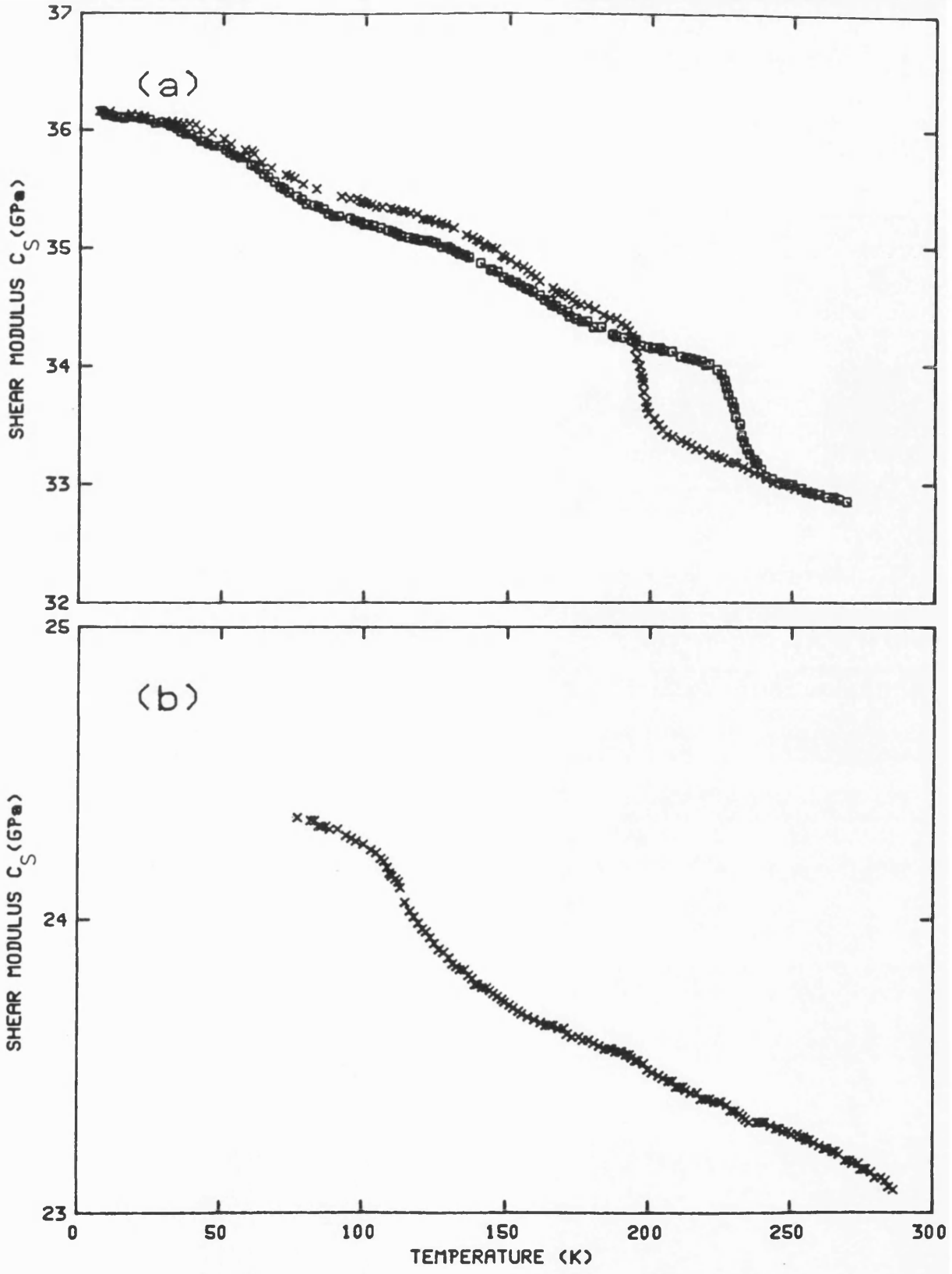

Figure 9.7
The temperature dependences of the shear modulus C_S for (a) orthorhombic and (b) tetragonal $GdBa_2Cu_3O_{7-x}$ samples. The crosses (x) correspond to the data obtained during cooling and the squares to those obtained during warming.

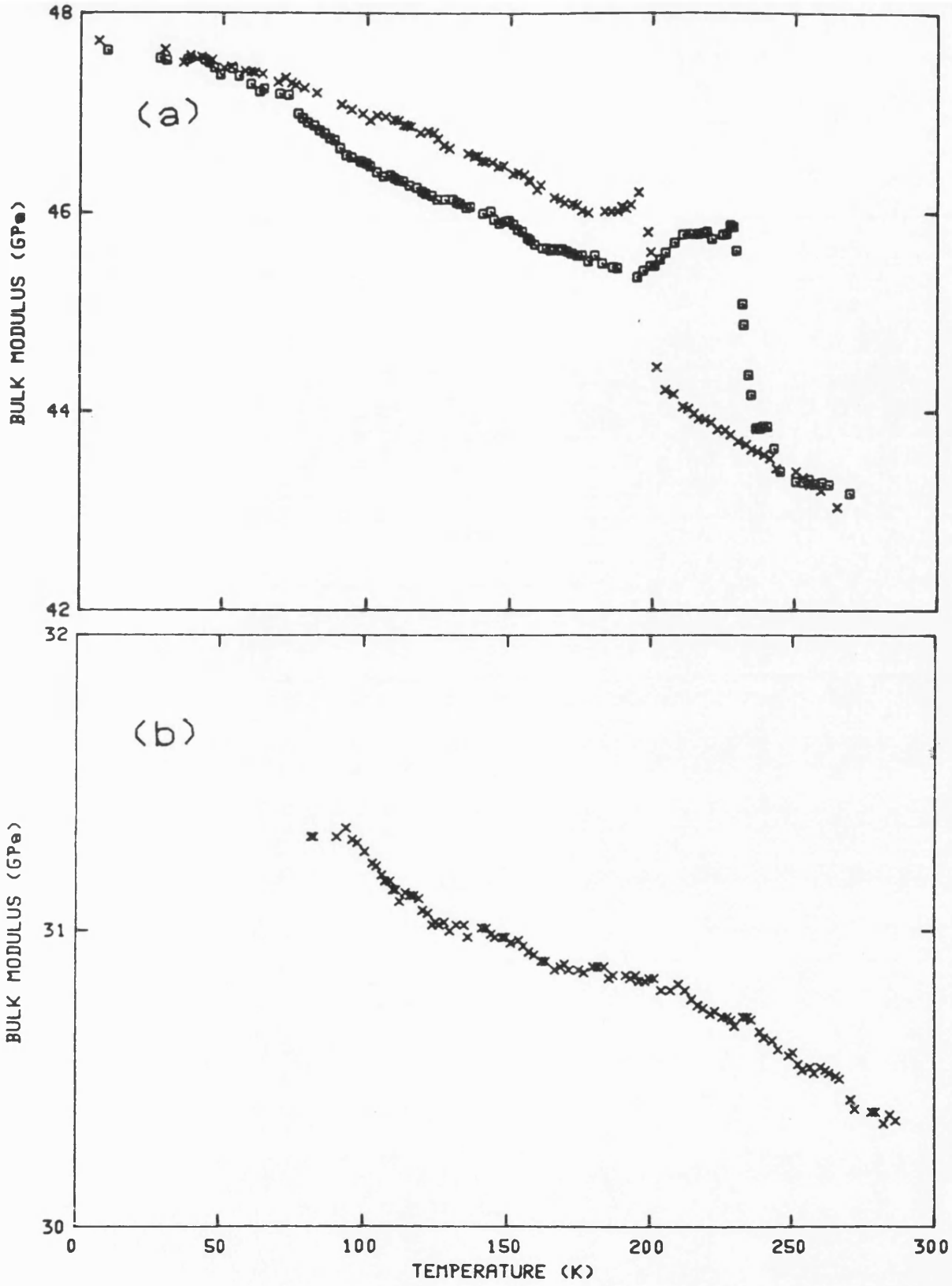

Figure 9.8
The temperature dependences of the bulk modulus for (a) orthorhombic and (b) tetragonal $GdBa_2Cu_3O_{7-x}$ samples. The crosses (x) correspond to the data obtained during cooling and the squares to those obtained during warming.

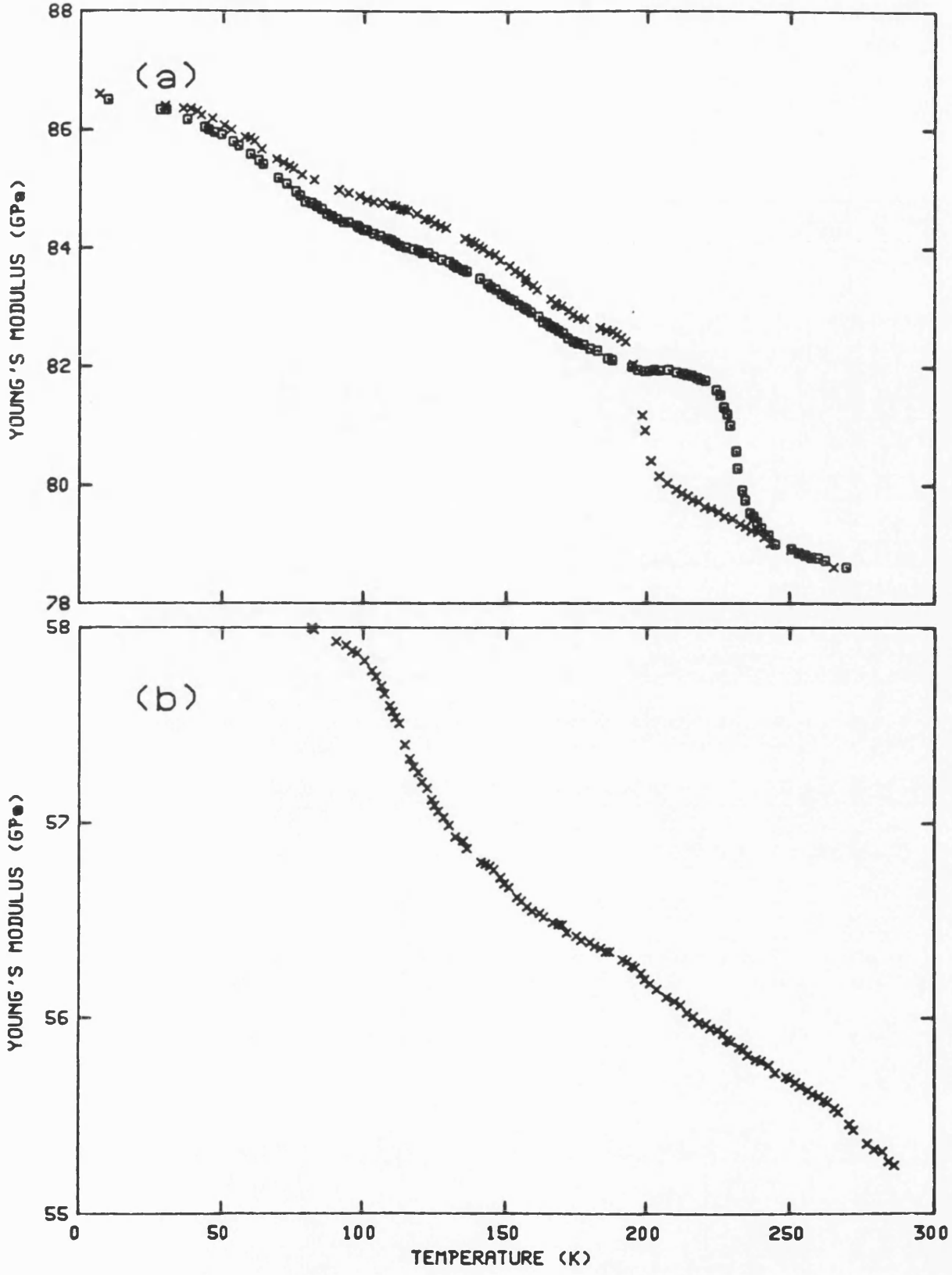

Figure 9.9
The temperature dependences of Young's modulus for (a) orthorhombic and (b) tetragonal $GdBa_2Cu_3O_{7-x}$ samples. The crosses (x) correspond to the data obtained during cooling and the squares to those obtained during warming.

Table 9.3. The ultrasonic wave velocities and the elastic constants at room temperature for the polycrystalline ceramic $GdBa_2Cu_3O_{7-X}$ in both orthorhombic (superconducting) and tetragonal (non-superconducting) forms obtained using Nonaq as a bonding material.

Property	Orthorhombic	Tetragonal
Density Kgm^{-3}	5549	5174
Ultrasonic wave velocities ms^{-1}		
Longitudinal V_L	3938	3434
Shear V_S	2428	2110
C_L (GPa)	86	61
C_S (GPa)	32.7	23
Bulk modulus (GPa)	42.4	30.3
Young's modulus (GPa)	78	55
Poisson's ratio	0.193	0.197
Superconducting transition temperature T_C (K)	89.6	-

9.5 THE PRESSURE DEPENDENCES OF ULTRASONIC WAVE VELOCITIES

The effects of hydrostatic pressure on longitudinal and shear ultrasonic wave velocities for orthorhombic and tetragonal $GdBa_2Cu_3O_{7-x}$ were measured using X- or Y-cut 5MHz quartz transducers and Dow Resin as a bonding material. The results obtained are shown in figure 9.10 for the orthorhombic sample and in figure 9.11 for the tetragonal sample [Cankurtaran et al (1989b), (1990b)]. The velocities for orthorhombic $GdBa_2Cu_3O_{7-x}$ show the unusual feature of a non-linear pressure dependence, although this non-linearity of ultrasonic wave velocities and elastic stiffnesses is not so pronounced as found for $YBa_2Cu_3O_{7-x}$ (figures 8.8 and 8.9). It is interesting to note that the pressure dependences of the ultrasonic wave velocities in the tetragonal form (figure 9.11) are almost linear: the vibrational anharmonicity of the long wavelength phonons is much less than that of the orthorhombic form. If porosity were to be the cause of the change in slopes with increasing pressure, then because the porosities are the same (0.22) in each form, the changes in gradient would be expected to be the same - but they are not. This porous $GdBa_2Cu_3O_{7-x}$ does not show hysteresis effects during pressure cycling. For $YBa_2Cu_3O_{7-x}$ hysteresis effects

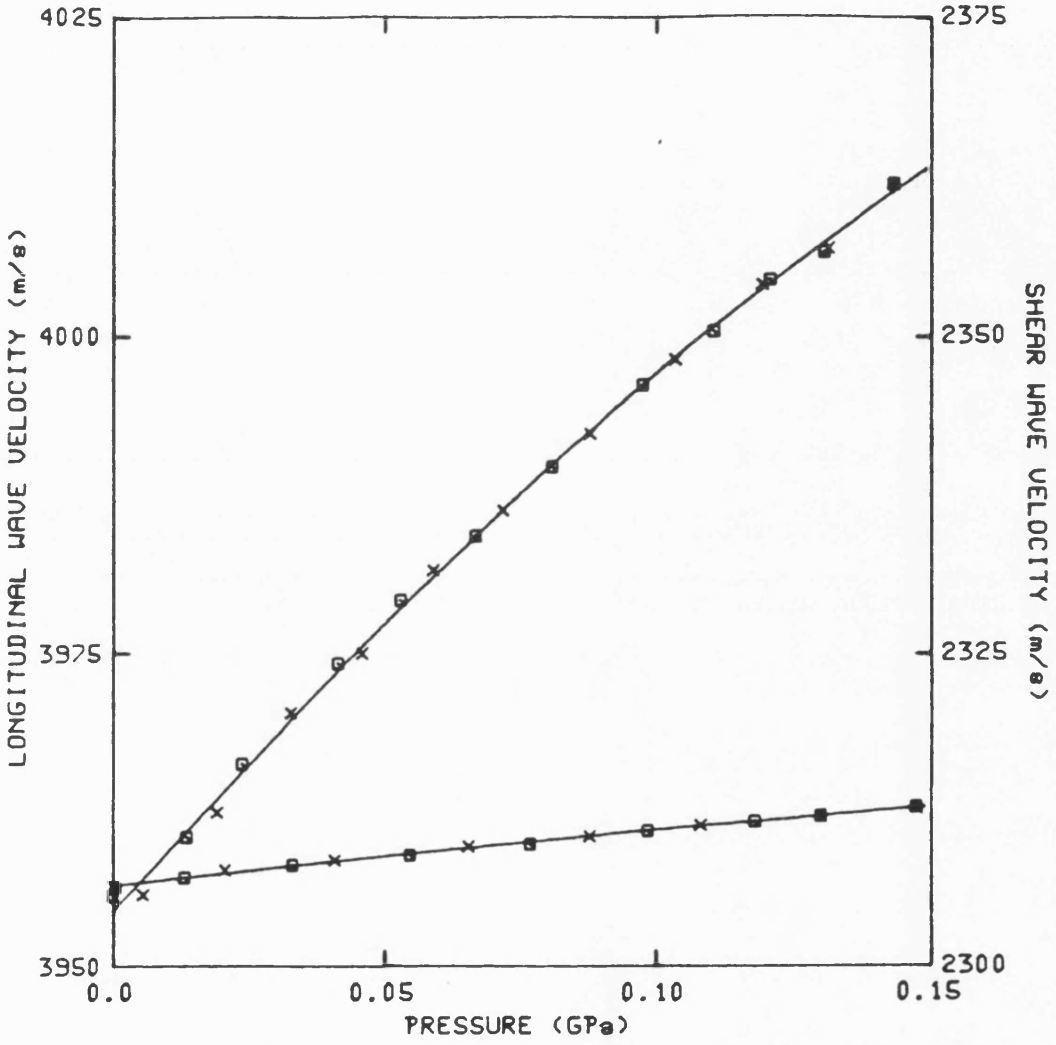

Figure 9.10
The hydrostatic pressure dependences of velocities of longitudinal (upper curve) and shear (lower curve) ultrasonic waves velocities propagated in orthorhombic $GdBa_2Cu_3O_{7-x}$ sample at 295K. The crosses correspond to velocity measurements made with increasing pressure and the squares to data obtained as the pressure was decreased.

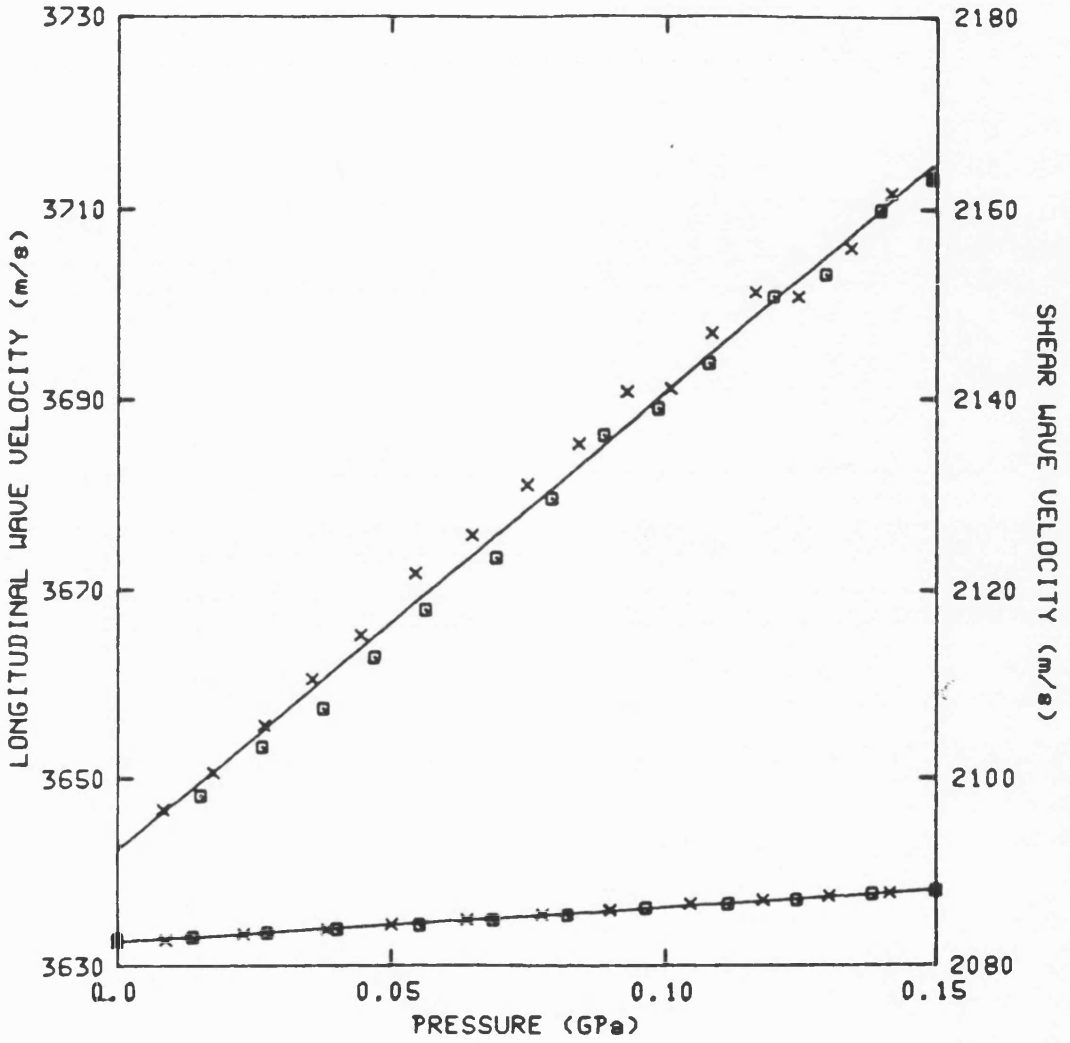

Figure 9.11
The hydrostatic pressure dependences of velocities of longitudinal (upper curve) and shear (lower curve) ultrasonic waves velocities propagated in tetragonal $GdBa_2Cu_3O_{7-x}$ sample at 295K. The crosses correspond to velocity measurements made with increasing pressure and the squares to data obtained as the pressure was decreased.

occur on pressure cycling for coarse grained dense samples but not in those of high porosity and small grain size (figure 8.10).

9.6 THE PRESSURE DEPENDENCES OF ELASTIC MODULI

Elastic moduli as a function of pressure for the $GdBa_2Cu_3O_{7-x}$ sample in both orthorhombic and tetragonal forms were calculated using the measured ultrasonic wave velocities and density. The pressure dependences of longitudinal C_L^n , shear C_S^n and bulk B^n moduli for the orthorhombic $GdBa_2Cu_3O_{7-x}$ sample are shown in part (a) of figures 9.12, 9.13 and 9.14 respectively and those for the tetragonal sample are plotted in part (a) of figures 9.15, 9.16 and 9.17 respectively [Cankurtaran et al (1989b), (1990a,b)]. Correction for the effects of porosity were made by inserting the experimental results into equations 4.4 and 4.5 to obtain the elastic moduli for the non-porous matrix. The pressure dependences of longitudinal C_L^m , shear C_S^m and bulk B^m moduli for the non-porous matrix of the orthorhombic $GdBa_2Cu_3O_{7-x}$ sample are plotted in part (b) of figures 9.12, 9.13 and 9.14 respectively and those for the tetragonal sample are shown in part (b) of figures 9.15, 9.16 and 9.17 respectively [Cankurtaran et al (1990a,b)]. The ultrasonic wave velocities, elastic constants and their pressure derivatives as the pressure tend towards zero are given in table 9.4.

The hydrostatic pressure derivatives $(\partial C_L/\partial P)_{P-0}$ and $(\partial B/\partial P)_{P-0}$ obtained directly from experimental data are very large for both the orthorhombic and tetragonal forms (table

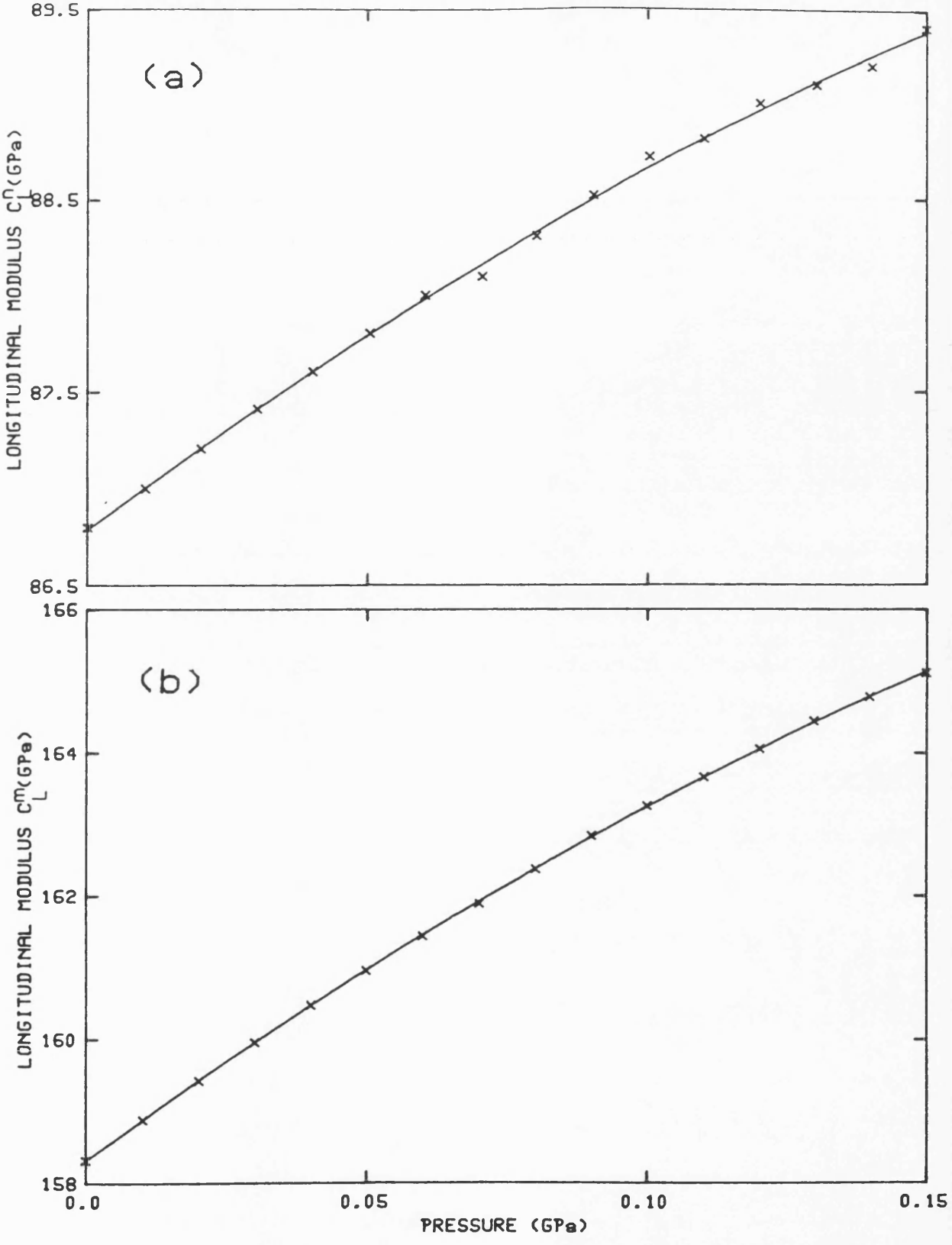

Figure 9.12
The hydrostatic pressure dependences of the longitudinal modulus (a) C_L^n (porous material) and (b) C_L^m (non-porous matrix) of orthorhombic $GdBa_2Cu_3O_{7-x}$ sample at 295K calculated from the experimental data and using equations (4.4) and (4.5). The solid lines are least square fits to the data.

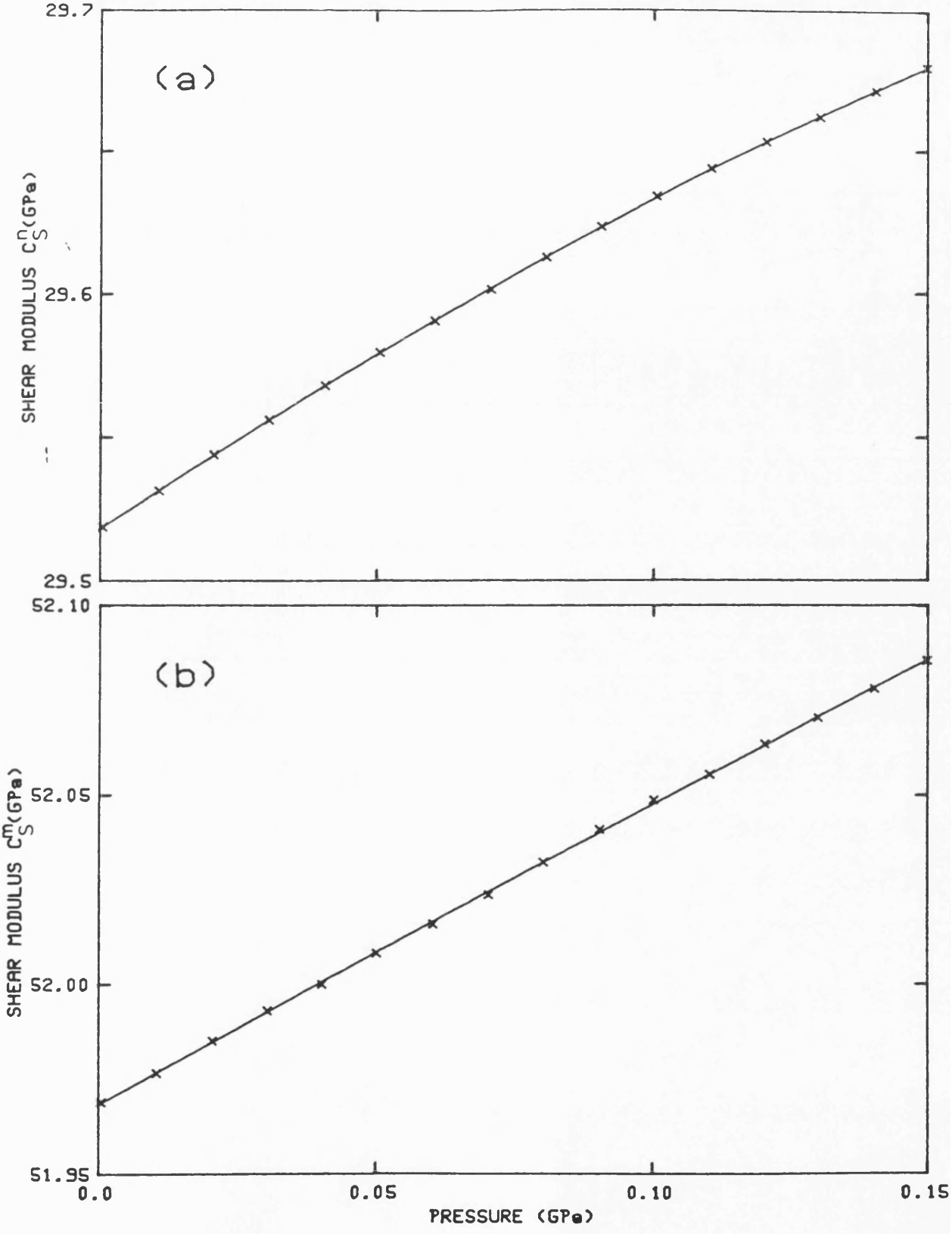

Figure 9.13
The hydrostatic pressure dependences of the shear modulus (a) C_S^n (porous material) and (b) C_S^m (non-porous matrix) of orthorhombic $GdBa_2Cu_3O_{7-x}$ sample at 295K calculated from the experimental data and using equations (4.4) and (4.5). The solid lines are least square fits to the data.

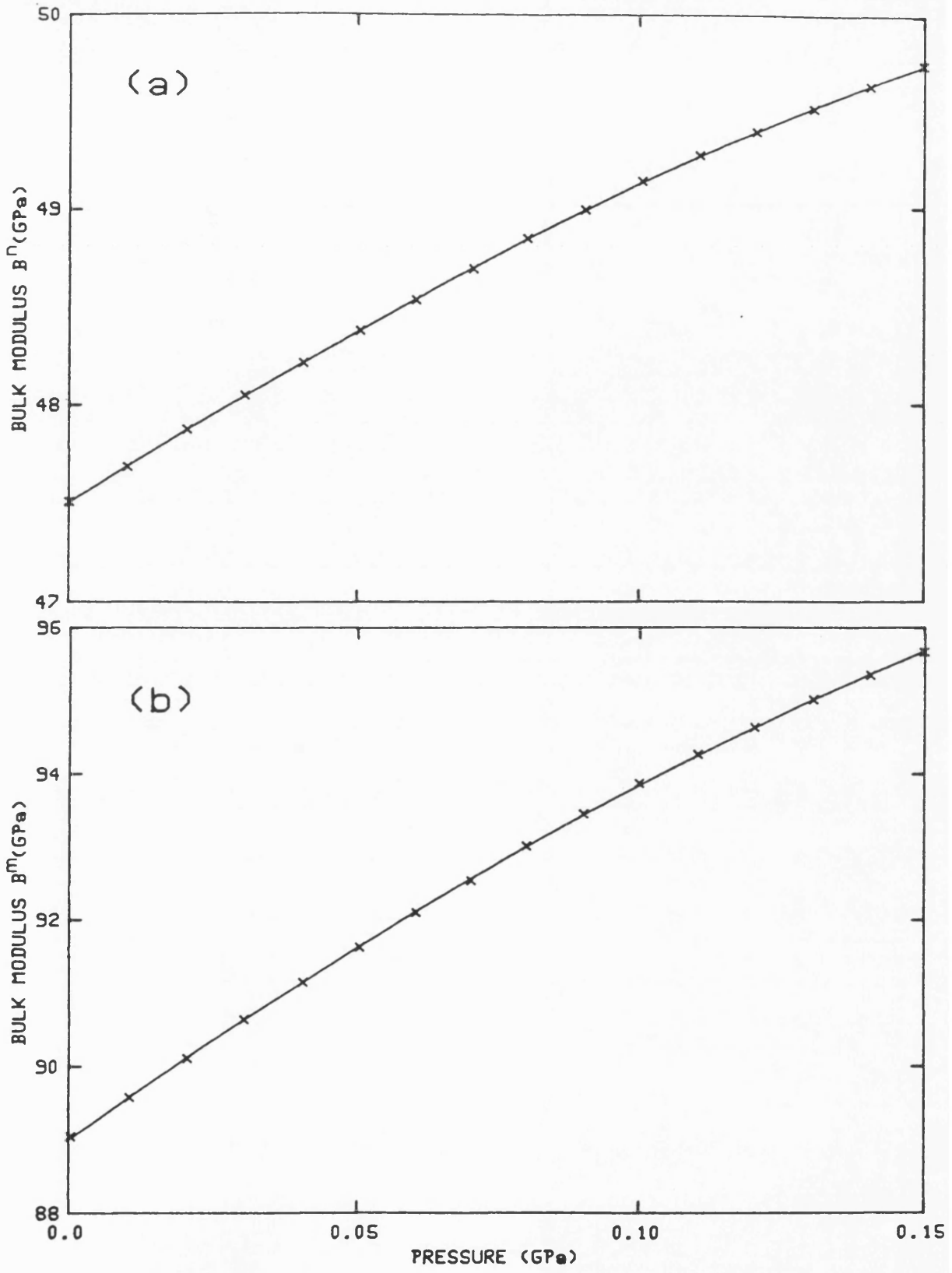

Figure 9.14
The hydrostatic pressure dependences of the bulk modulus (a) B^n (porous material) and (b) B^m (non-porous matrix) of orthorhombic $GdBa_2Cu_3O_{7-x}$ sample at 295K calculated from the experimental data and using equations (4.4) and (4.5). The solid lines are least square fits to the data.

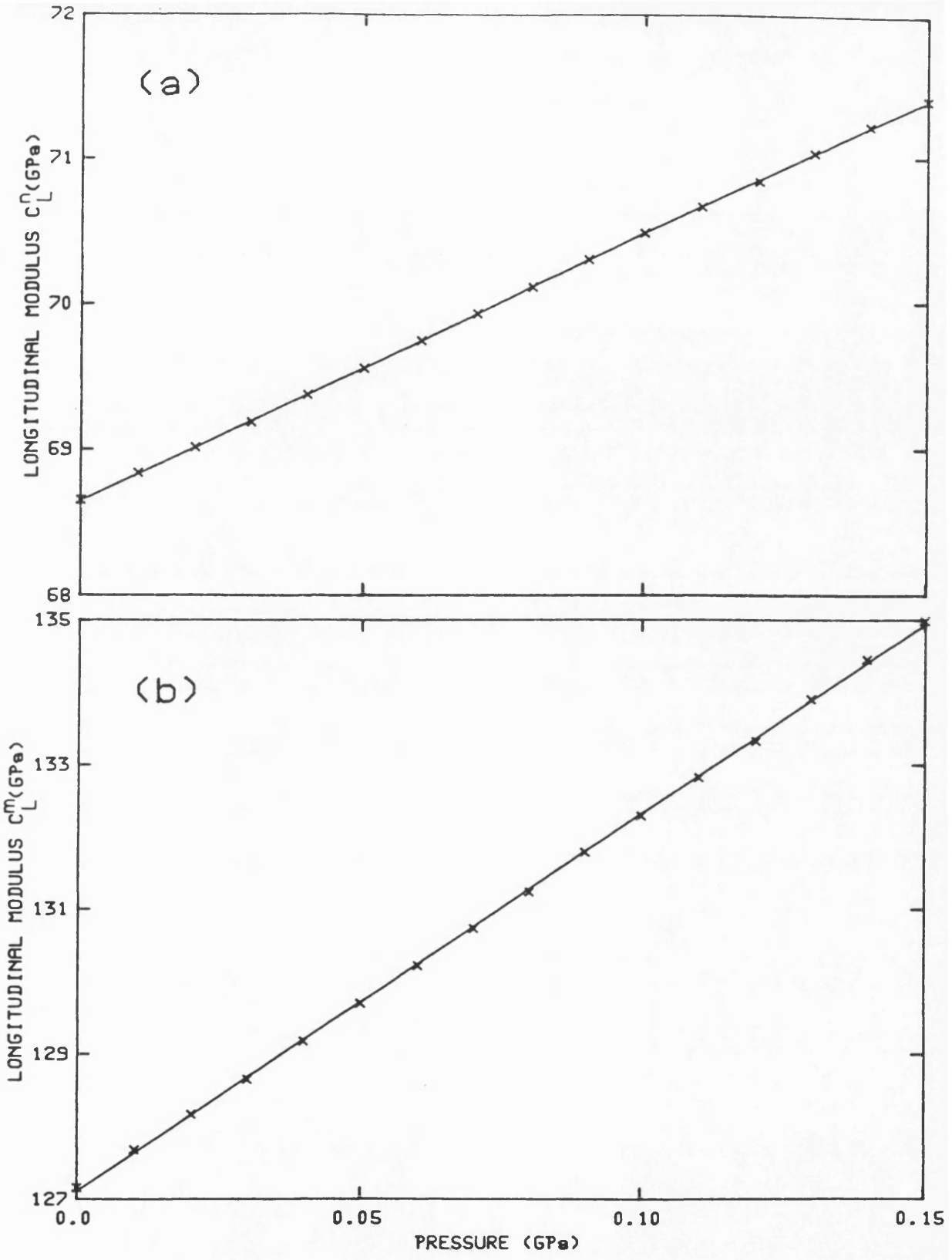

Figure 9.15
The hydrostatic pressure dependences of the longitudinal modulus (a) C_L^n (porous material) and (b) C_L^m (non-porous matrix) of tetragonal $GdBa_2Cu_3O_{7-x}$ sample at 295K calculated from the experimental data and using equations (4.4) and (4.5). The solid lines are least square fits to the data.

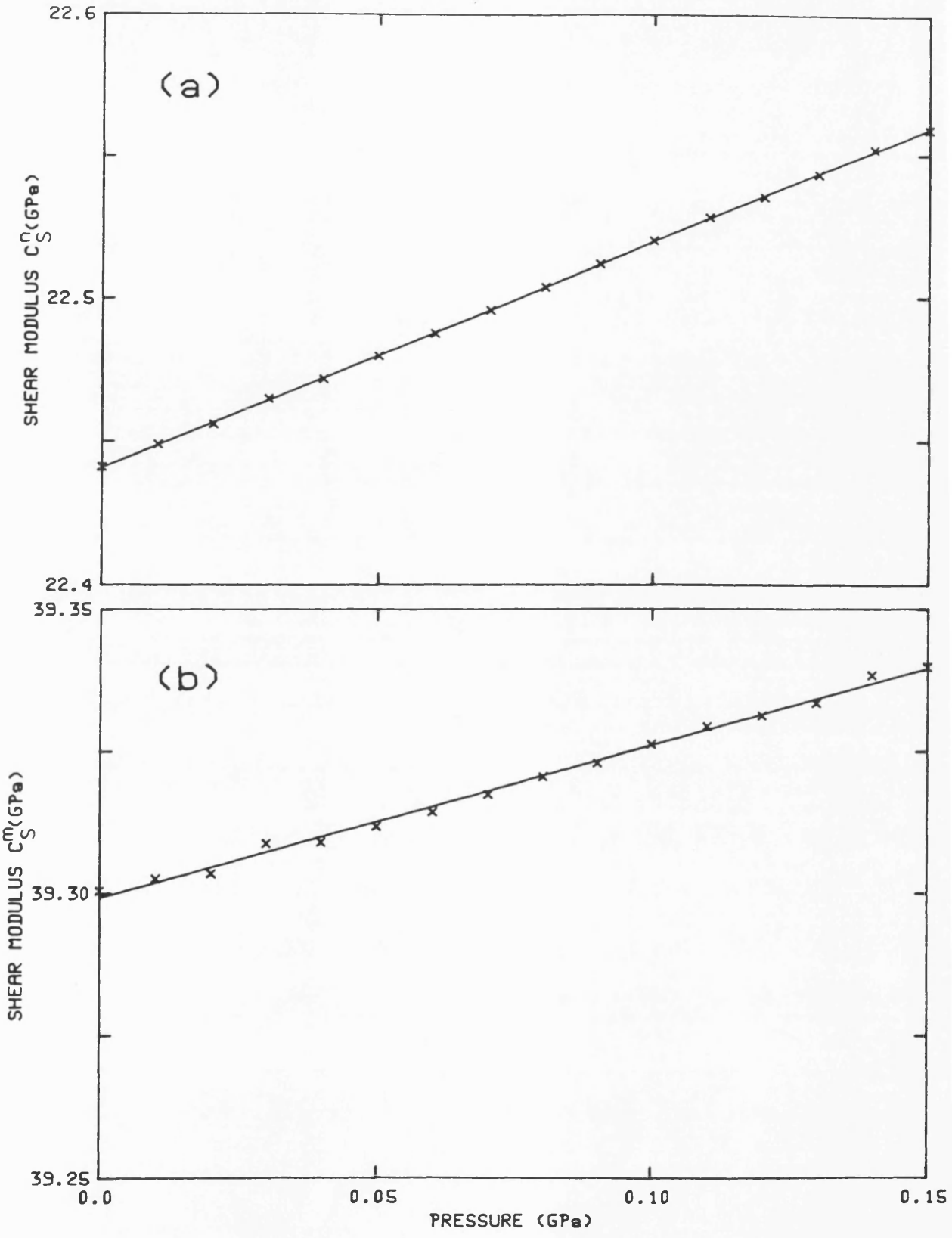

Figure 9.16
The hydrostatic pressure dependences of the shear modulus (a) C_S^n (porous material) and (b) C_S^m (non-porous matrix) of tetragonal $GdBa_2Cu_3O_{7-x}$ sample at 295K calculated from the experimental data and using equations (4.4) and (4.5). The solid lines are least square fits to the data.

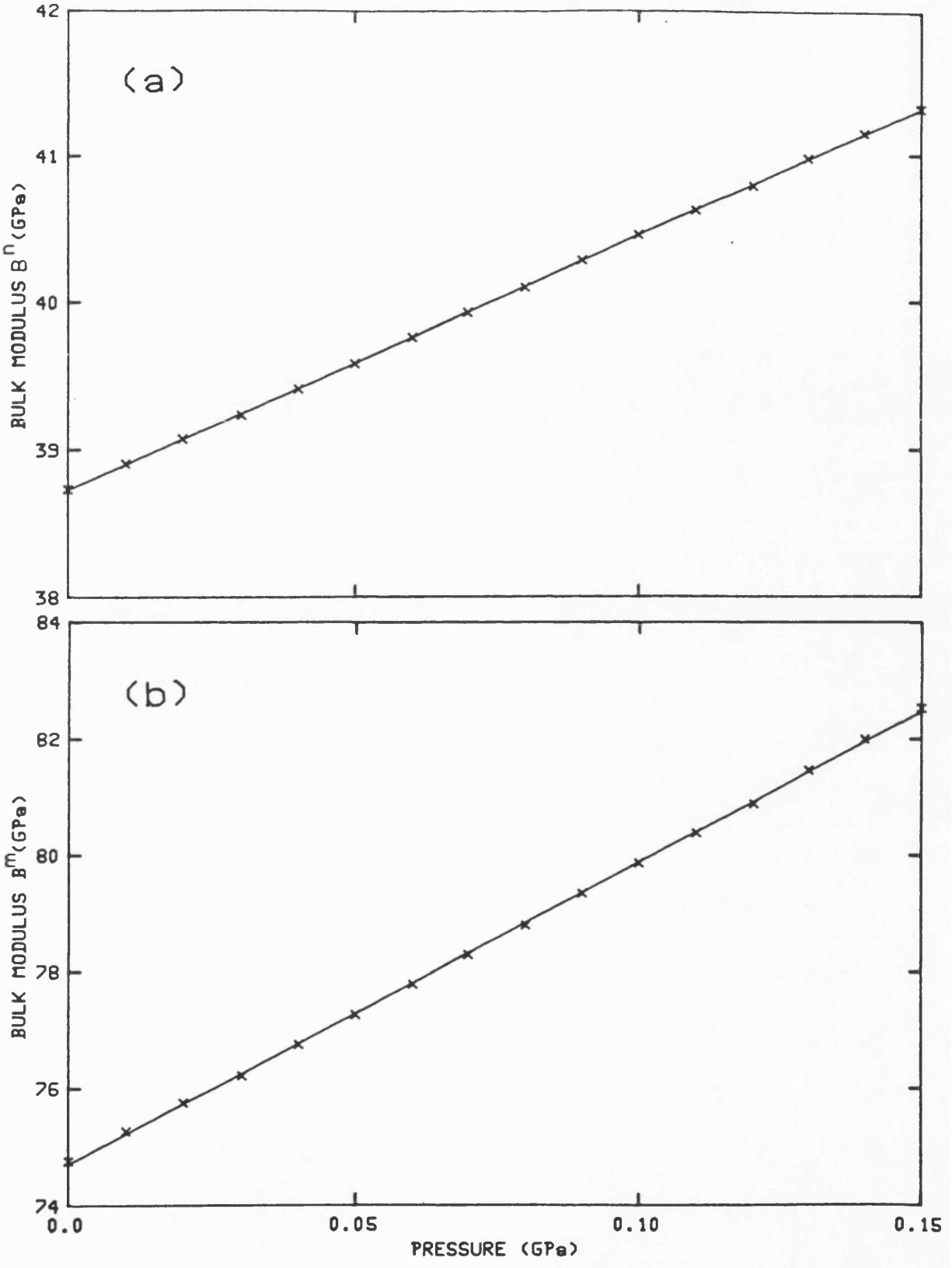

Figure 9.17
The hydrostatic pressure dependences of the bulk modulus (a) B^n (porous material) and (b) B^m (non-porous matrix) of tetragonal $GdBa_2Cu_3O_{7-x}$ sample at 295K calculated from the experimental data and using equations (4.4) and (4.5). The solid lines are least square fits to the data.

Table 9.4. The elastic properties of polycrystalline orthorhombic and tetragonal $GdBa_2Cu_3O_{7-X}$ at 295K. The raw experimental data for the porous ceramic are given in the first column in each case. Data for the non-porous matrix obtained by applying the equations (4.4) and (4.5) developed from wave scattering theory are given in the second column.

Property	ORTHORHOMBIC		TETRAGONAL	
	Porous	Non-Porous	Porous	Non-Porous
Density (kg/m^3)	5549	7138	5174	6700
Porosity	0.22	-	0.23	-
Ultrasonic wave velocity (ms^{-1})				
Longitudinal V_L	3955	4710	3642	4356
Shear V_S	2306	2700	2083	2422
C_L (GPa)	86.8	158	68.6	127
C_S (GPa)	29.5	52	22.4	39.3
Bulk modulus (GPa)	47.5	89	38.7	74.7
Young's modulus (GPa)	73	131	56	100
Poisson's ratio	0.242	0.255	0.257	0.276
$(\partial C_L/\partial P)_{P=0}$	22	56	18	52
$(\partial C_S/\partial P)_{P=0}$	1.5	0.8	0.79	0.27
$(\partial B/\partial P)_{P=0}$	20	55	17	52
Superconducting transition temperature T_C (K)	92	-	-	-

9.4). In contrast to the orthorhombic form there are no twins in the tetragonal structure, so neither the comparatively small B_o nor the large $(\partial B/\partial P)_{P=0}$ can be directly associated with twin boundary motion. Comparison between the elastic moduli as measured for the porous ceramics and those of the non-porous matrices (table 9.4) shows that the porosity does reduce the moduli considerably in the case of this highly porous material. The pressure derivative $(\partial B/\partial P)_{P=0}$ of bulk modulus is large for both phases even after the correction for porosity has been made. Removal of oxygen in making the tetragonal form increases the volume of the unit cell; this implies breaking of certain inter-ionic bonds, so softening the structure. This would be expected to lead to slower ultrasonic wave velocities and smaller elastic stiffnesses in the tetragonal form of $GdBa_2Cu_3O_{7-x}$, as found (table 9.4).

The results obtained for $GdBa_2Cu_3O_{7-x}$ compound in both orthorhombic and tetragonal forms will be compared and discussed with those obtained for other high temperature superconducting compounds in chapter eleven.

CHAPTER TEN

ELASTIC AND NON-LINEAR ACOUSTIC PROPERTIES OF BISMUTH-BASED COPPER-OXIDE SUPERCONDUCTORS

10.1 INTRODUCTION

The compound $Bi_2Sr_2Ca_{n-1}Cu_nO_{4+2n}$ has been investigated ultrasonically. The elastic behaviour of Bi(Pb)2223, Bi(Pb)2212 and lead free Bi2212 compounds have been studied as a function of hydrostatic pressure and temperature.

The samples studied here were prepared by the solid state reaction method as described in chapter four. In order to obtain single phase samples, a low oxygen partial pressure was used during the final annealing step. X-ray diffraction studies showed that the samples were pure single phase of Bi2212 and Bi2223, with no detectable impurity phases. Evidence for tendency to texture was found in the Bi(Pb)2223 samples from an X-ray diffractometry study which showed marked preferential reflection perpendicular to the basal plane: these samples have a preferred orientation of grains with the c-axis parallel to the direction of pressing. The lead-free samples had initial compositions of $Bi_2Sr_2Ca_1Cu_2O_8$ and $Bi_2Sr_2Ca_2Cu_3O_{10}$. The pellets were melted slightly during the final annealing. X-ray patterns showed that both samples are pure Bi2212 phase with no detectable impurity phases in

spite of different starting compositions. Table 10.1 summarizes the nominal compositions, density, porosity, the superconducting transition temperature T_c of the samples, and the temperatures T_{ac} and T_{aw} at which anomalous behaviour of ultrasonic velocity has been observed for cooling and warming cycles respectively (see section 10.3).

It is now recognized that the elastic stiffnesses of the cuprates which show superconductivity at high temperatures are unusually small. This is especially true for the bismuth-based cuprates. The objective of this chapter has been to shed further light on the elastic behaviour of a series of Bi-based cuprates, including the effects of lead-doping and quenching, by measuring the ultrasonic properties as a function of hydrostatic pressure and temperature.

A comparative study of the temperature dependence of ultrasonic wave velocity and attenuation in Bi(Pb)2223, Bi(Pb)2212 and lead-free Bi2212 samples should give some insight into the origin of anomalies and the elastic hysteresis observed in the range 200-240K. Therefore measurements have been made of the effects of temperature from 10K to 300K on the longitudinal and shear velocities

Table 10.1. The nominal compositions, density, porosity, superconducting transition temperature T_C (at which the zero resistance condition is achieved) of the $Bi_2Sr_2Ca_{n-1}Cu_nO_{4+2n}$ samples. T_{ac} and T_{aw} are the temperatures at which the elastic anomaly occurs for the cooling and warming cycles respectively.

Sample	Composition	Density (kg/m^3)	Porosity	T_C (K)	T_{ac} (K)	T_{aw} (K)
Bi(Pb)2223 (sample 1)	$Bi_{1.8}Pb_{0.3}Sr_2Ca_2Cu_3O_{10}$	4953	0.22	98	189	232
Bi(Pb)2223 (sample 2)	$Bi_{1.8}Pb_{0.3}Sr_2Ca_2Cu_3O_{10}$	4936	0.23	98	-	-
Bi(Pb)2212	$Bi_{1.8}Pb_{0.3}Sr_2CaCu_3O_8$	5110	0.23	70	no effect	no effect
Bi2212 (sample 1)	$Bi_2Sr_2Ca_2Cu_3O_8$	3230	0.50	64	204	231
Bi2212 (sample 2)	$Bi_2Sr_2Ca_2Cu_3O_8$	4433	0.32	62	198	226

and attenuation of 5 and 10MHz ultrasonic waves propagated through single phase Bi(Pb)2223, Bi(Pb)2212 and lead-free Bi2212 samples.

Measurements of ultrasonic wave velocities as a function of hydrostatic pressure on polycrystalline Bi(Pb)2223, Bi(Pb)2212 and Bi2212 samples may provide information about the origin of the extremely small bulk modulus of these materials. Since the ultrasonic properties of ceramics are sensitive to their porous structure, one must be careful in deciding whether a small bulk modulus is an intrinsic property of the compound or due to the rather porous nature of these particular materials.

This chapter includes results of measurements of the temperature dependence of electrical resistance. This have been carried out as part of the process of characterisation of specimens (as will be discussed in section 10.2) of Bi(Pb)2223, Bi(Pb)2212 and lead-free Bi2212. Section 10.3 will contain a discussion of the results obtained for the temperature dependences of ultrasonic wave velocities and attenuation in the Bi-based cuprates. The effects of quenching on the elastic moduli of lead-free Bi2212 samples will be analysed in section 10.4. The effects of hydrostatic pressure on the ultrasonic wave velocities in the Bi-based

cuprates will be presented in section 10.5. Finally, section 10.6 will discuss the effects of hydrostatic pressure on the elastic moduli of the Bi-based samples.

10.2 THE ELECTRICAL RESISTANCE MEASUREMENTS

The four-point *DC* technique with computerised data acquisition was employed to measure the electrical resistance. The Bi(Pb)2223 sample exhibits a sharp superconducting transition with onset at about 110K and zero resistance at 98K (figure 10.1). The resistance-temperature curve for Bi(Pb)2223 suggests a single-phase transition, since there is no resistance tail or shoulder below 100K.

For the Bi(Pb)2212 sample as first prepared, there was no superconducting transition down to 30K. After re-annealing at 840°*C* in air for two days, the Bi(Pb)2212 sample showed zero resistance at 70K (with little difference in the X-ray diffraction pattern compared with the previous one).

To ascertain whether the preparation method affects the resistive behaviour with temperature, two lead-free Bi2212 samples were prepared from two different starting compositions: $Bi_2Sr_2Ca_1Cu_2O_8$ and $Bi_2Sr_2Ca_2Cu_3O_{10}$. The pellets were melted slightly during the final annealing. X-ray patterns showed that both samples were nearly pure Bi2212 phase. Bi2212 sample 1 and Bi2212 sample 2 reached zero resistance at 64K and 62K respectively. Bi2212 (sample 2) was heated at 830°*C* in air for 25 hours and quenched with liquid nitrogen. It is found that this thermal treatment has a marked effect on the resistive behaviour (figure 10.2) [Fanggao et al

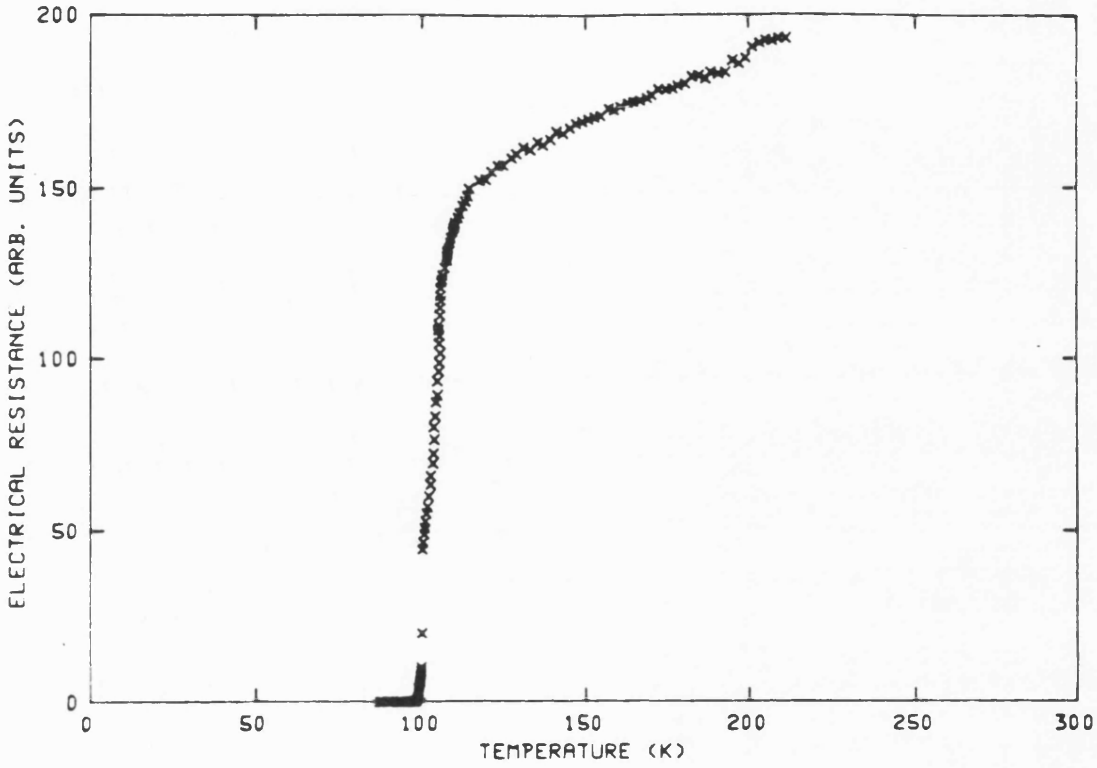

Figure 10.1
The temperature dependence of the electrical resistance for Bi(Pb)2223 (sample 1).

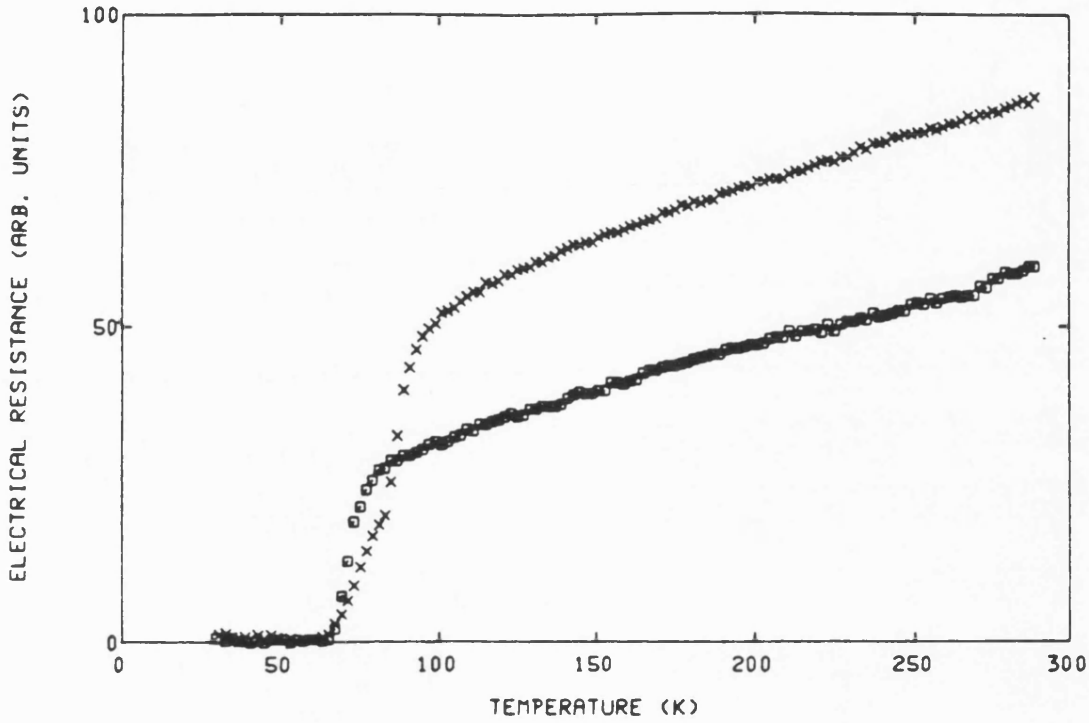

Figure 10.2
The effect of quenching from 830°C into liquid nitrogen on the temperature dependence of the electrical resistance of Bi2212 (sample 2). The squares refer to the measurements made before quenching and the crosses to those after quenching the sample.

(1990b)] as reported previously [Tallon et al (1988), Almond et al (1988), Namgung et al (1989)], but did not affect the specimen microstructure.

It has been established that the resistance-temperature relationship is very sensitive to the microstructure of the sample, especially to the grain-boundary regions. For example, shoulders in the resistance transition have been correlated to the presence of the lower-T_c phase at the grain-boundary, leading to a lack of inter-granular connectivity.

10.3 THE TEMPERATURE DEPENDENCES OF ULTRASONIC WAVE VELOCITY AND ATTENUATION IN BISMUTH-BASED CUPRATES

The effects of temperature on the longitudinal and shear ultrasonic wave velocities for Bi(Pb)2223 (sample 1), measured using Nonaq as a bonding material between the sample and the quartz transducer, are shown in figure 10.3 [Fanggao et al (1990b)]. The data obtained during both cooling and warming cycles are given. The room temperature ultrasonic wave velocities obtained for the sample studied here (sample 1) are in fairly good agreement with those obtained by Plechácek and Dominec (1990) but is much less from those obtained by Ledbetter et al (1989b) (see table 10.2 for comparison). The experimental results show no measurable effect within the limits of experimental resolution (1 part in 10^5) near T_c associated with the onset of superconductivity; this is true for all the samples studied. In fact the temperature dependence of the ultrasonic wave velocities below about 170K can be fitted by the conventional model of vibrational anharmonicity described by Lakkad (1971). There is a small peak at about 40K in the temperature dependences of both mode velocities; this has been observed in every Bi-based sample studied here independent of composition or thermal treatment. The most interesting feature is the step in the velocity and the associated hysteresis loop between

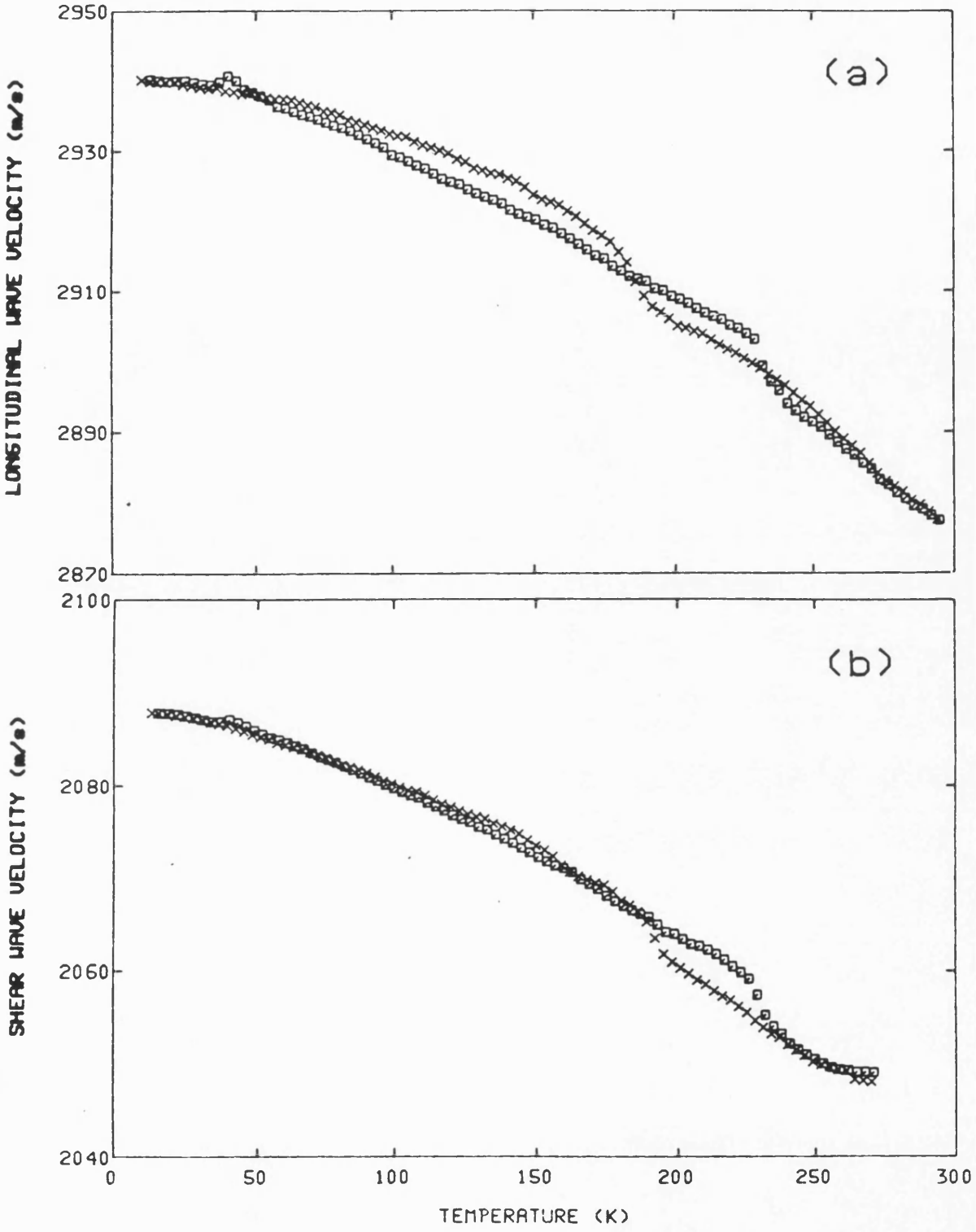

Figure 10.3
The temperature dependences of the velocities of 5MHz (a) longitudinal and (b) shear ultrasonic waves propagated in Bi(Pb)2223 (sample 1). The crosses correspond to measurements made with decreasing temperature and the squares to those as the temperature was increased.

Table 10.2. Comparison between the ultrasonic wave velocities for ceramic Bi-based compounds measured in this work with those obtained by other groups.

References	Ultrasonic wave velocities		Temperature (K)
	Longitudinal (m/s)	Shear (m/s)	
This work			
Bi(Pb)2223 (sample 1)	2879	2049	293
Bi(Pb)2223 (sample 2)	2953	2054	293
Bi(Pb)2212	2870	1919	293
Bi2212 (sample 1)	2220	1505	293
Bi2212 (sample 2)	2555	1508	293
Bi2212 (sample 2, quenched)	2444	1604	293
Choi et al (1989)		-	
Bi1112	2027		80
Ledbetter et al (1989)			
Bi(Pb)2223	3570	2310	293
Nes et al (1991)		-	
Bi2212	3100		300
Plechácek et al (1990)			
Bi(Pb)2223	2700	2030	293
Reddy and Ramana (1990)		-	
Bi2212	3060		300
Rodriguez et al (1991)		-	
Bi2212	2000		293

189 and 232K, which resembles that reported by Fukami et al (1989). However, it should be noted that these effects seen around 190-235K in Bi(Pb)2223 are much less pronounced than those observed in $YBa_2Cu_3O_{7-x}$ and $GdBa_2Cu_3O_{7-x}$ (figures 8.1, 8.2 and 9.3). The common structural feature of Bi(Pb)2223 and $YBa_2Cu_3O_{7-x}$ is the presence of Cu-O planes. However this type of elastic behaviour has been also observed in ceramic $BaPb_{1-x}Bi_xO_3$ (Horie et al 1987a); so it cannot be simply due to an effect in the Cu-O planes. [Fukami et al (1989)] has attributed this phenomenon to the creation of small nuclei of a new phase and their growth in a structural phase transition in which case the hysteresis would be due to a large potential barrier to nucleation of a new phase. An observation which indicates that the hysteresis effects do not reflect the porous structure of the ceramics is that a similar effect has been found for the C_{66} mode in a single crystal of Bi2212 [Wang et al (1989), Wu et al (1990)]. Although the presence of pores affects the absolute value of ultrasonic wave velocities, their influence on the temperature dependence should be much less. Ledbetter et al (1989b) reported a softening of the bulk modulus and Poisson's ratio of a Bi(Pb)2223 specimen in the temperature region below 215K indicating strong interatomic changes. Fukami et

al (1989) measured the temperature dependence of the frequency and the amplitude of mechanical resonances of continuous sound waves propagated through a Bi(Pb)2223 specimen having 50% of theoretical density. They observed hysteresis on curves of acoustic quantities versus temperature between 200 and 240K; this hysteretic behaviour has been ascribed to a structural phase transition.

The temperature dependence of ultrasonic attenuation in Bi(Pb)2223 (sample 1) (figure 10.4) shows no pronounced peaks which can be ascribed to relaxation effects like those in $GdBa_2Cu_3O_{7-x}$ [Almond et al (1989)]. However the attenuation, like the velocity data, does show elastic hysteresis effects between 190-235K [Fanggao et al (1990b)]. The ultrasonic wave velocity and attenuation data are similar to those reported by Fukami et al (1989), although the temperature range over which they observed the elastic hysteresis was about 10K higher.

Figure 10.5 shows the temperature dependences of the longitudinal and shear ultrasonic wave velocities in a Bi(Pb)2212 sample [Fanggao et al (1990b)]. The data for both modes show a continuous stiffening and softening when the sample was cooled and warmed respectively; the anomalous change in the velocity and the hysteretic behaviour found for Bi(Pb)2223 are absent.

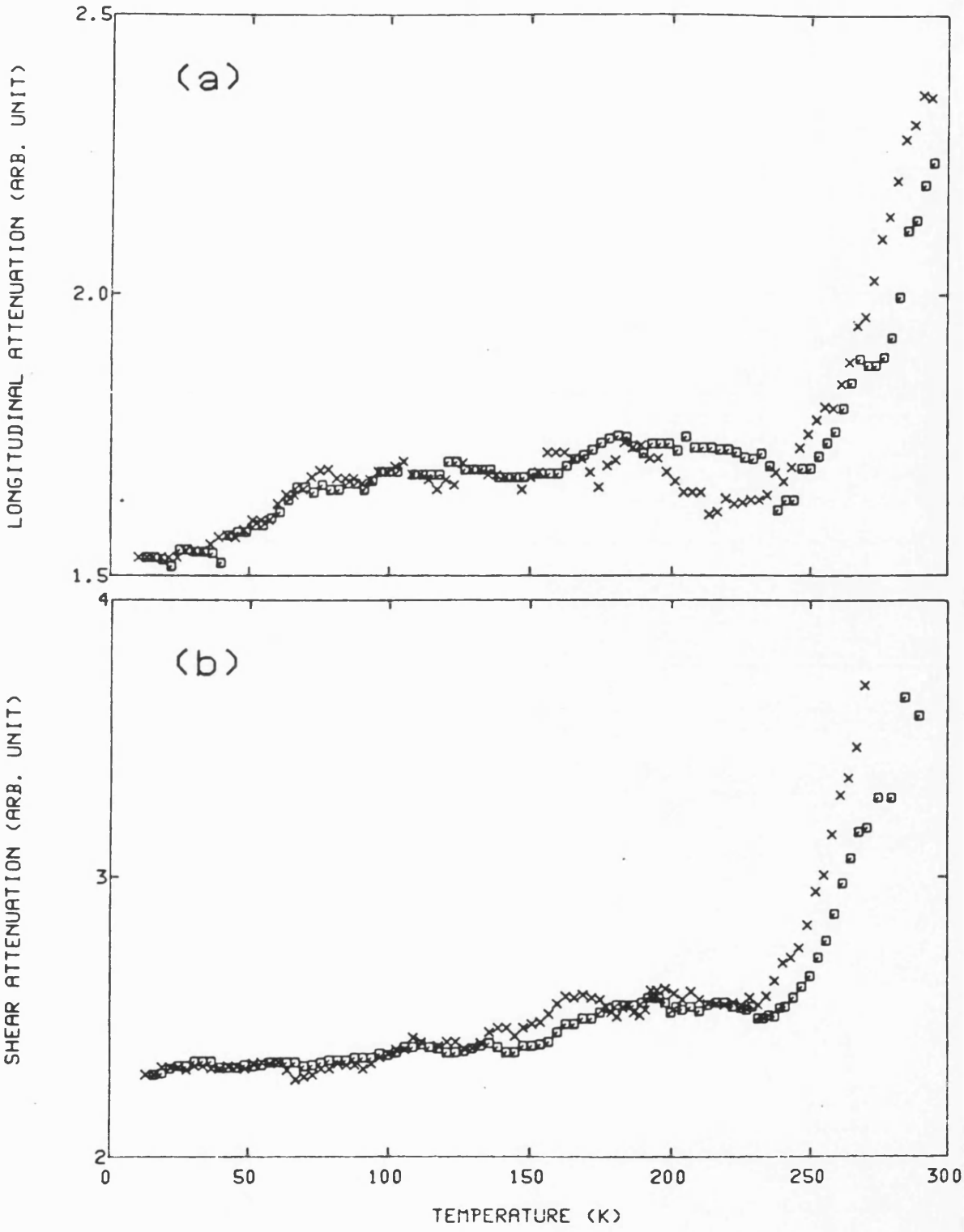

Figure 10.4
The temperature dependences of 5MHz (a) longitudinal and (b) shear ultrasonic waves attenuation propagated in Bi(Pb)2223 (sample 1). The crosses correspond to measurements made with decreasing temperature and the squares to those as the temperature was increased.

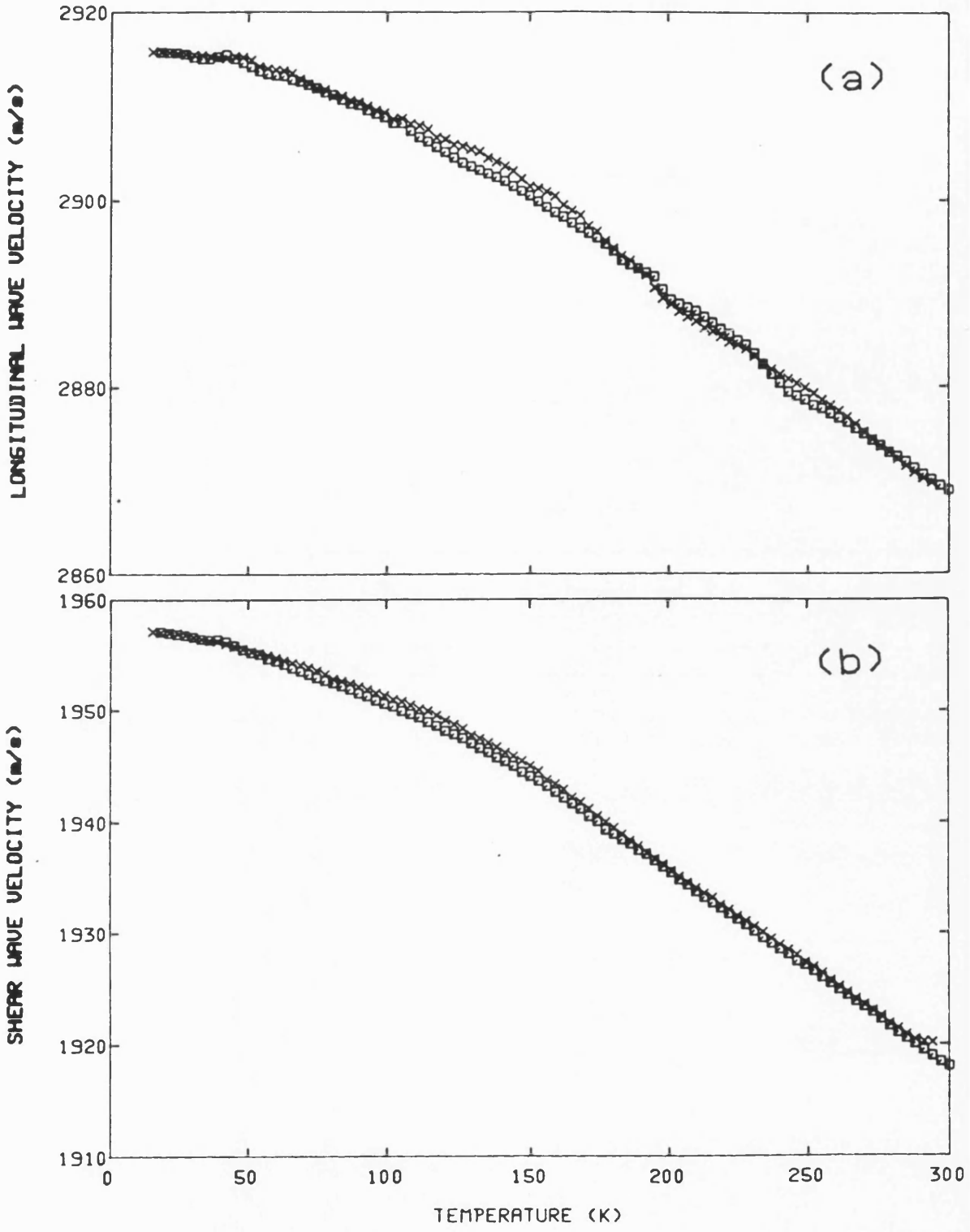

Figure 10.5
The temperature dependences of the velocities of 5MHz (a) longitudinal and (b) shear ultrasonic waves propagated in Bi(Pb)2212. The crosses correspond to measurements made with decreasing temperature and the squares to those as the temperature was increased.

The temperature dependences of both longitudinal and shear ultrasonic wave velocities in Bi2212 (sample 1) show the step at 204K and 231K in cooling and warming cycles respectively (figure 10.6) [Fanggao et al (1990b)]. The width of the hysteresis and the temperatures at which the steep changes occur are the same for both modes. Comparison between the velocity data for Bi(Pb)2212 (figure 10.5) and Bi2212 (sample 1) (figure 10.6) shows that Pb doping in the Bi2212 phase suppresses the anomalous change in ultrasonic wave velocity at 204K (cooling) and at 231K (warming), and hence the elastic hysteretic behaviour. This observation indicates that the anomalous changes in sound velocity at 204K and 231K may not be an inherent property of Bi-based cuprates, but depend on doping and/or sample preparation.

The effects of temperature on the velocities of 5MHz ultrasonic waves propagated in Bi2212 (sample 2), shown in figure 10.7 [Fanggao et al (1990b)], are rather different from those found in the much less dense Bi2212 (sample 1) (see table 10.3). On cooling there is a sudden, large jump in both mode velocities at 198K. Below this temperature, almost linear stiffening occurs down to about 135K where there is a change in gradient. The warming curve reveals a similar temperature dependence, but the steep change shifted up to 226K. Thus the data for both modes show well pronounced

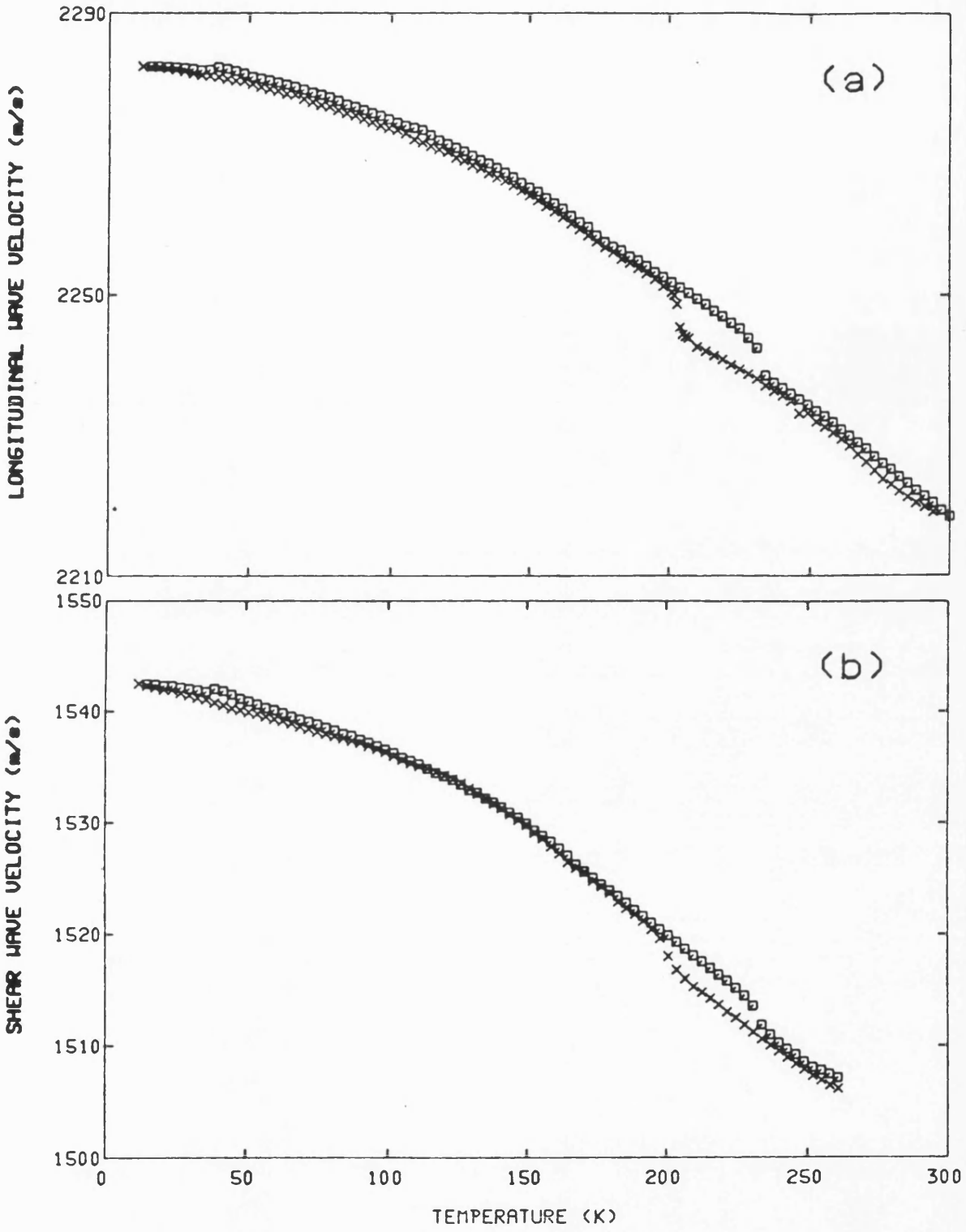

Figure 10.6
The temperature dependences of the velocities of 5MHz (a) longitudinal and (b) shear ultrasonic waves propagated in Bi2212 (sample 1). The crosses correspond to measurements made with decreasing temperature and the squares to those as the temperature was increased.

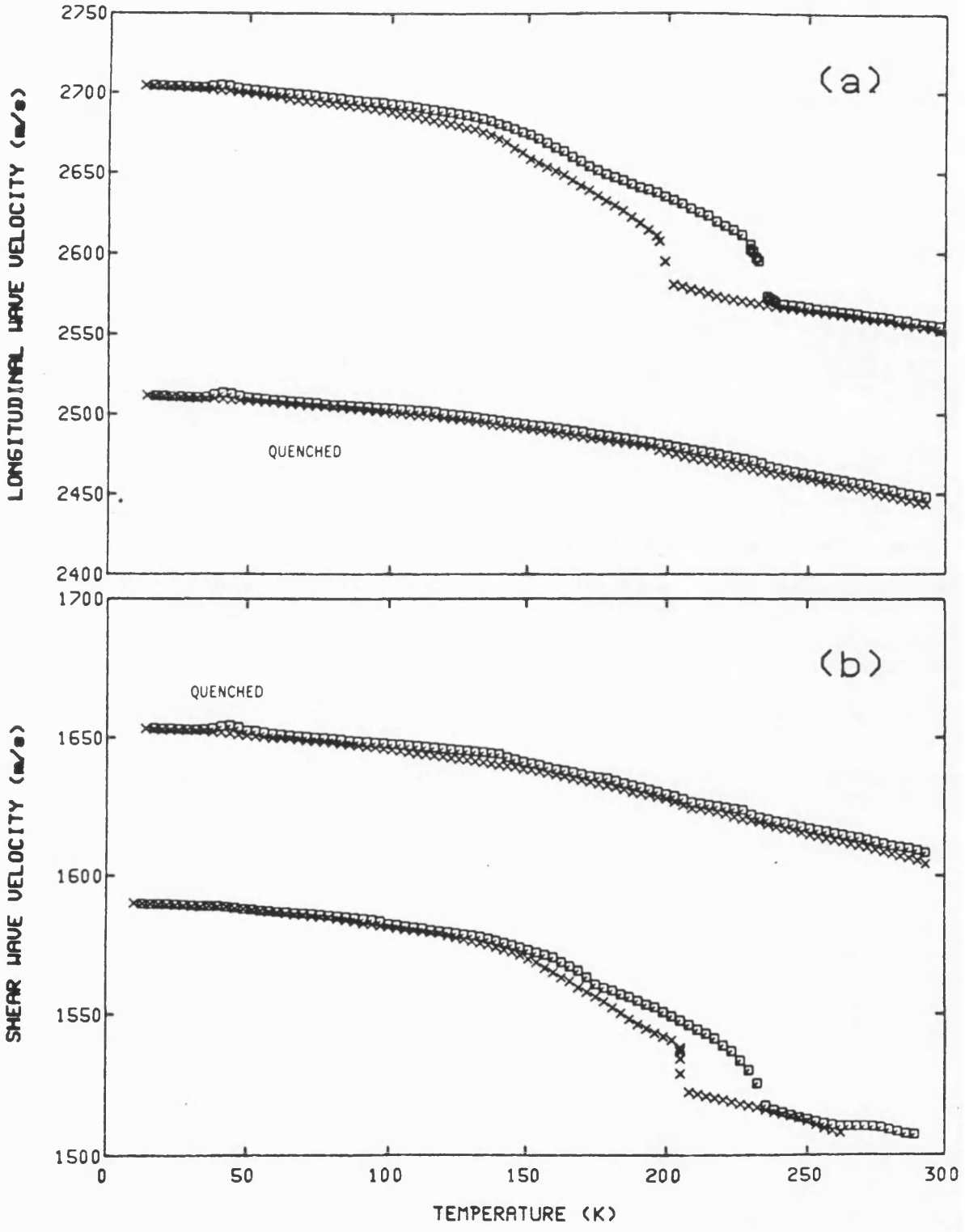

Figure 10.7
The effect of quenching on the velocity of 5MHz (a) longitudinal and (b) shear ultrasonic waves propagated in Bi2212 (sample 2). The crosses correspond to measurements made with decreasing temperature and the squares to those as the temperature was increased.

Table 10.3. The ultrasonic wave velocities, elastic properties and hydrostatic pressure derivatives of elastic moduli of polycrystalline Bi(Pb)2223, Bi(Pb)2212 and Bi2212 at 295K. Data for the non-porous matrix were obtained by correcting the measurements using wave scattering theory in a porous medium (see section 4.12).

Property	Bi(Pb)2223 (sample 1)		Bi(Pb)2223 (sample 2)		Bi(Pb)2212		Bi2212		
	Ceramic sample	Non-porous matrix	Ceramic sample	Non-porous matrix	Ceramic sample	Non-porous matrix	Ceramic Sample 1	Ceramic Sample 2	Ceramic Sample 2 (quenched)
Density (kg/m^3)	4953	6407	4936	6407	5110	6660	3230	4433	4407
Porosity (n)	0.22	-	0.23	-	0.23	-	0.50	0.32	0.33
Longitudinal wave velocity V_L (m/s)	2879	3343	2953	3469	2870	3342	2220	2555	2444
Shear wave velocity V_s (m/s)	2049	2483	2054	2520	1919	2325	1505	1508	1604
Longitudinal modulus C_L (GPa)	41.0	71.6	43.1	77.1	42.1	74.4	15.9	28.9	26.3
Shear modulus C_s (GPa)	20.8	39.5	20.8	40.7	18.8	36.0	7.3	10.1	11.3
Bulk modulus B_o (GPa)	13.3	18.9	15.3	22.9	17.0	26.4	6.2	15.4	11.2
Young's modulus E (GPa)	41.0	69.8	42.9	76.5	41.2	74.3	15.7	24.9	25.4
Poisson's ratio σ	-0.014	-0.116	0.031	-0.058	0.096	0.032	0.075	0.233	0.121
Acoustic Debye temperature θ_D^{ac} (K)	250	328	251	334	231	304	157	177	-
$(\partial C_L/\partial P)_{P=0}$	37	63	27.8	48.6	28.5	52	16	-	-
$(\partial C_s/\partial P)_{P=0}$	5.4	3.1	5.1	4.5	6.0	9.5	-	-	-
$(\partial B/\partial P)_{P=0}$	30	59	20.9	39.3	20.6	40	-	-	-

temperature hysteresis. No significant differences occurred on changing the carrier frequency from 5MHz to 10MHz. The measurements of longitudinal and shear mode attenuation (figure 10.8) revealed features closely related to those in the velocity data [Fanggao et al (1990b)]. For the shear mode in particular, peaks occur in the attenuation corresponding to the steps in the velocity on both the cooling and warming cycles. Keeping the temperature fixed at 160K for periods up to ten hours produced no appreciable shift in the velocity or attenuation. It can be concluded that the unusual temperature dependence of the elastic properties is very sample dependent for the Bi2212 phase and Pb doping of this phase results in disappearance of the hysteretic elastic behaviour with temperature.

The Bi2212 (sample 2) was then quenched from 830°*C* into liquid nitrogen and the ultrasonic velocity and attenuation were re-measured down to 10K. Quenching has considerable effects on the ultrasonic properties. The longitudinal velocity is substantially reduced (figure 10.7a) while that of the shear mode is increased (figure 10.7b). It also has the remarkable consequence of removing the elastic and anelastic anomalies (figure 10.7). Since the major effect of quenching is to alter the oxygen concentration [Tallon et al (1988), Almond et al (1988) and Namgung et al (1989)],

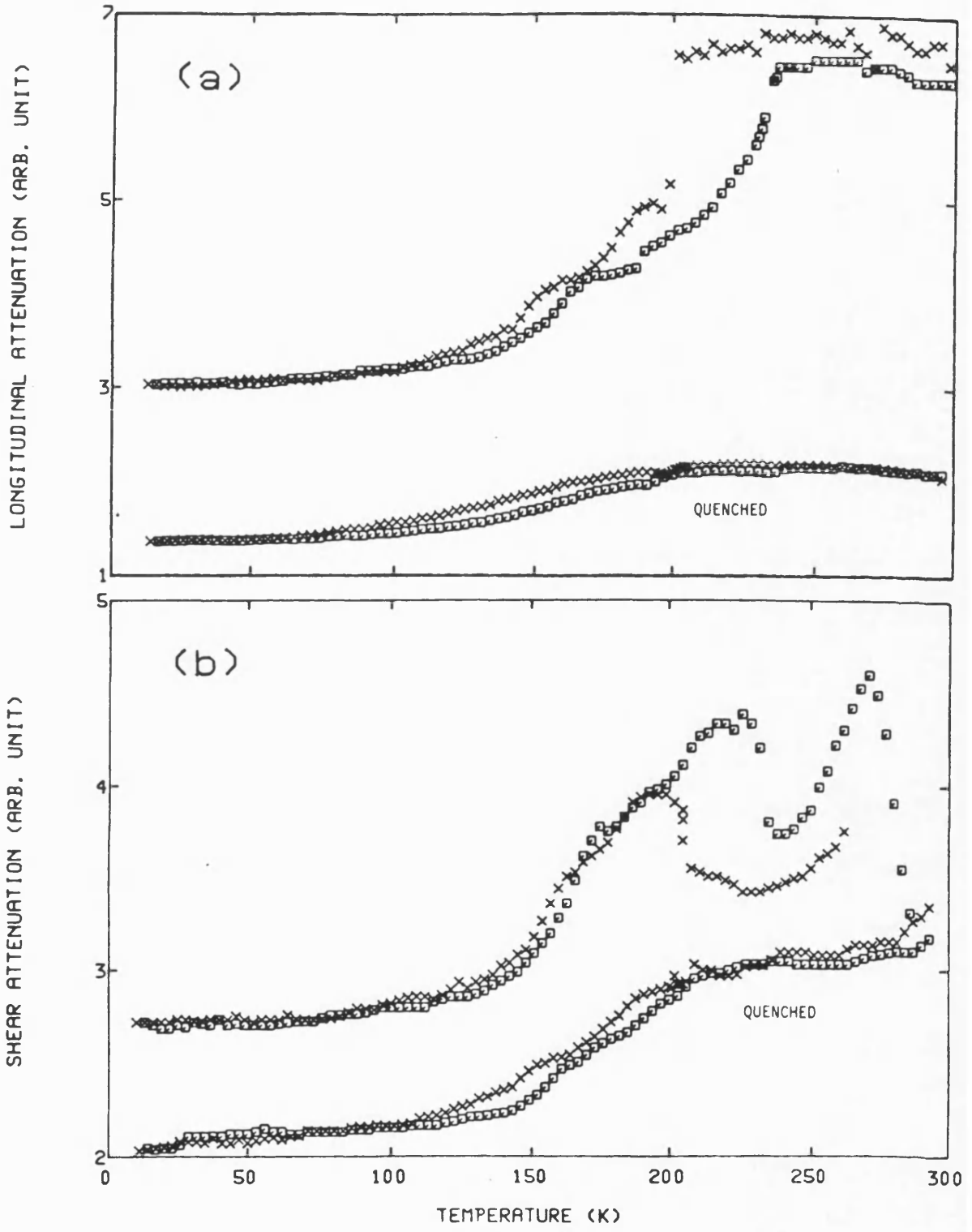

Figure 10.8
The effect of quenching on the attenuation of 5MHz (a) longitudinal and (b) shear ultrasonic waves propagated in Bi2212 (sample 2). The crosses correspond to measurements made with decreasing temperature and the squares to those as the temperature was increased.

it can be concluded that the anomalous behaviour is very sensitive to this parameter. In this context it is interesting to recall that the similar elastic anomalies around 200K-240K in orthorhombic $GdBa_2Cu_3O_{7-x}$ are also removed when it is quenched from 700°C to reduce the oxygen content and retain the tetragonal form [Almond et al (1989), Cankurtaran et al (1990a)]. However, it is important to note that the quenched Bi2212 (sample 2) which showed no elastic anomalies had better superconducting properties than it had shown previously following slow cooling (figure 10.2). This suggests that the 240K phenomena are not an intrinsic property of properly optimised material. It indicates that they are a property of Bi2212 that results as extra oxygen absorbed during slow cooling from sintering temperatures. Xiang et al (1989) measured the elastic properties of a single crystalline Bi2212 sample; the relative change of Young's and shear moduli with temperature showed monotomic behaviour and no remarkable change was observed at T_c by them. Sihan et al (1989) observed a broad hysteresis in the variation of the ultrasonic wave velocity in a Bi2212 sample with temperature and a softening of bulk modulus below 200K. For single crystal Bi2212, Saint-Paul et al (1990b) observed a large softening of the C_L longitudinal mode around T_c , but they argue that this cannot easily be related to the

superconducting transition. Recently Yusheng et al (1989) discussed the anomalous change of sound velocity with temperature at about 200K and interpreted this as an isothermal structural phase transition.

10.4 THE EFFECT OF QUENCHING ON THE ELASTIC MODULI OF THE Bi2212 PHASE

The pronounced effects of quenching on the elastic stiffnesses of Bi2212 (figure 10.9 and table 10.3) [Fanggao et al (1990b)] have been considered separately from the hysteresis effects which have just been considered in the previous section. The reduction of the longitudinal ultrasonic wave velocity (figure 10.7) shows that considerable long wavelength acoustic mode softening as well as enhancement of T_c is induced by the reduction of oxygen content produced by quenching. The large decrease in bulk modulus (figure 10.9a) and Poisson's ratio (figure 10.9c), which are induced by quenching of Bi2212 phase, indicate a considerable weakening in the interatomic binding forces. These effects can to some extent be related to small increase of the c-axis lattice parameter produced by quenching [Almond et al (1988)]; this implies a decrease in the BiO inter-layer binding force and the concomitant softening of the long wavelength longitudinal mode with propagation vector along c-axis. The room temperature value for Young's modulus for the quenched sample is larger than that before quenching (figure 10.9b and table 10.3).

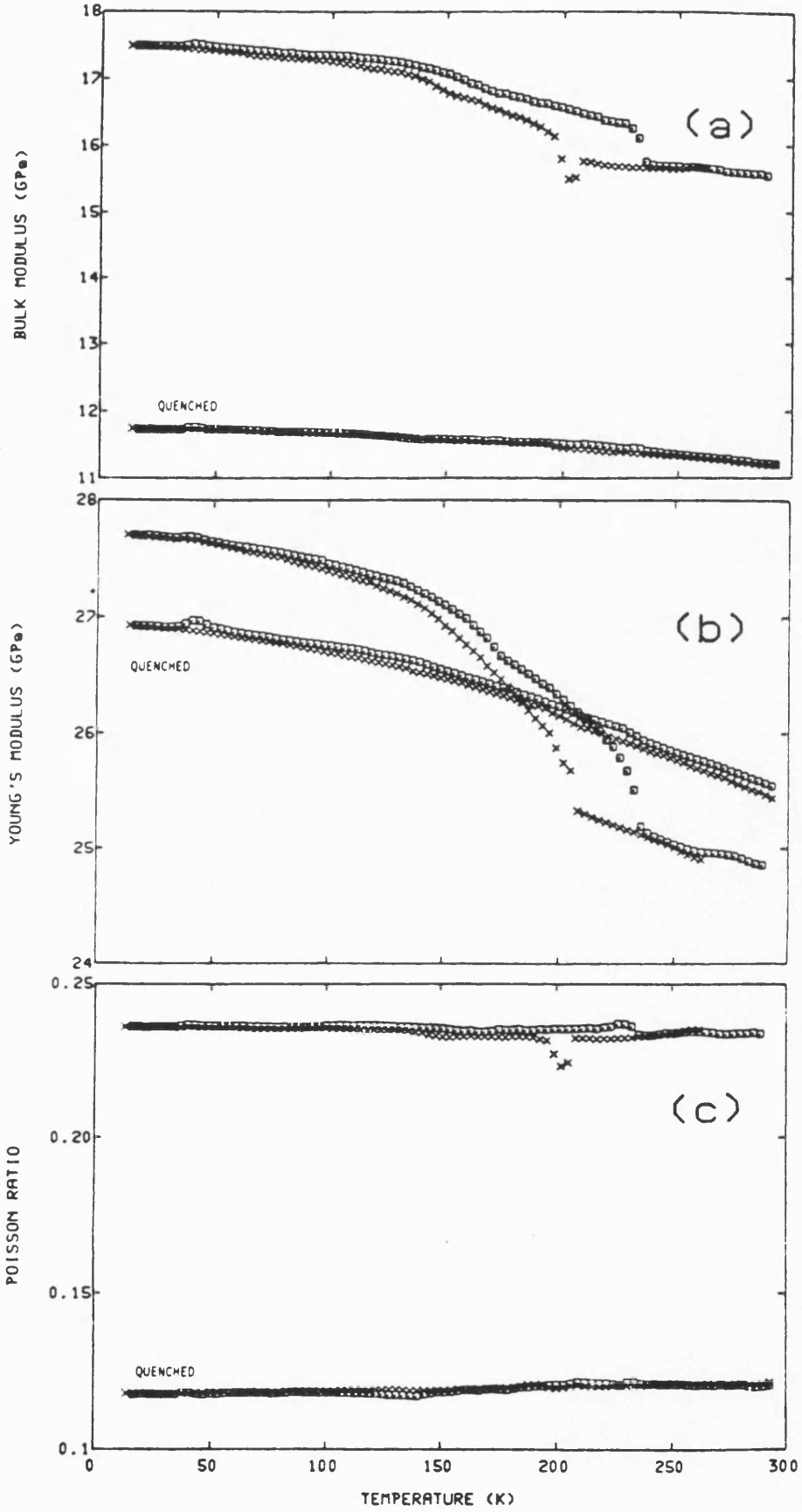

Figure 10.9
The effect of quenching on the temperature dependences of the technological moduli: (a) bulk modulus (b) Young's modulus and (c) Poisson's ratio in Bi2212 (sample 2). The crosses correspond to measurements made with decreasing temperature and the squares to those as the temperature was increased.

The major source of the longitudinal mode softening may be due to a change in the mean value of the intermediate valence of the copper ions produced by the alteration in oxygen content on quenching. The stoichiometry of the Bi2212 phase is very sensitive to the oxygen partial pressure [Namgung et al (1989)], the oxygen content becomes reduced by quenching [Tallon et al (1988), Almond et al (1988) and Namgung et al (1989)] and furthermore the superconducting behaviour depends strongly on the oxygen content. The critical temperature T_c varies considerably with oxygen content with a maximum occurring for y equal to 0.035±0.003 in $Bi_2Sr_2CaCu_2O_{8+y}$ [Namgung et al (1989)]. No structural change associated with the variations of oxygen content have been found. Changing the oxygen concentration alters the hole density [Groen et al (1990)]. Superconductivity does not occur at doping levels up to about 0.007 holes/Cu per CuO_2 plane. With increasing hole content T_c shows a broad maximum of about 90K at about 0.2 holes/Cu per CuO_2 plane. The copper ion valence of about +2.3 [Cheetham et al (1988)] depends upon the oxygen content. To account for the fact that oxygen depletion produces an increase in T_c , it has been suggested that there is an optimal value for the copper valency [Groen et al (1990), Koihe et al (1989) and Tang et al (1990)]. Fluctuating copper valence is characteristic feature of the

high T_c cuprates. Now a small, or even negative Poisson's ratio, and a small bulk modulus are characteristic features of compounds in intermediate valence state [Boppart et al (1981), Mook and Holtzberg (1981), Hailing et al (1984) and Yogurtcu et al (1985)]. Since higher valent ions are smaller than the lower valent ones, coupling to the lattice is strong for the longitudinal phonons which alter the unit cell volume. Hence the small bulk modulus and Poisson's ratio found here for the quenched Bi2212 phase consistent with changed fluctuating copper valence enhancing the longitudinal acoustic mode softening in the material with oxygen content optimised to increase T_c .

10.5 THE HYDROSTATIC PRESSURE DEPENDENCE OF ULTRASONIC WAVE VELOCITY

The results obtained for the effects of hydrostatic pressure on the velocities of longitudinal and shear 5MHz ultrasonic waves propagated at room temperature, using Resin as a bonding material between the sample and the quartz transducer, in the specimens of Bi(Pb)2223 (sample 1), Bi(Pb)2223 (sample 2), Bi(Pb)2212 and Bi2212 (sample 1) are shown in figures 10.10 to 10.13 respectively [Fanggao et al (1991b)]. In each case the measurements were reproducible and hysteresis was minimal under pressure cycling. The longitudinal mode velocity is much more pressure dependent than that of the shear waves. The pressure dependences of the longitudinal mode velocities of both Bi(Pb)2223 samples show a pronounced change of slope at about 0.03GPa; the shear mode velocities show a slight indication of the same effect at the same pressure (figures 10.10a, b and 10.11a, b). In Bi(Pb)2223 ceramic samples it seems that the first effect of pressure is to reduce the pore volume, close microcracks and increase the adhesion between the plate-like grains. Above the knee the slope of the pressure dependence is substantially smaller and has been used to determine the pressure derivatives of the elastic moduli intrinsic to Bi(Pb)2223 samples given in table 10.3. The effect of pressure

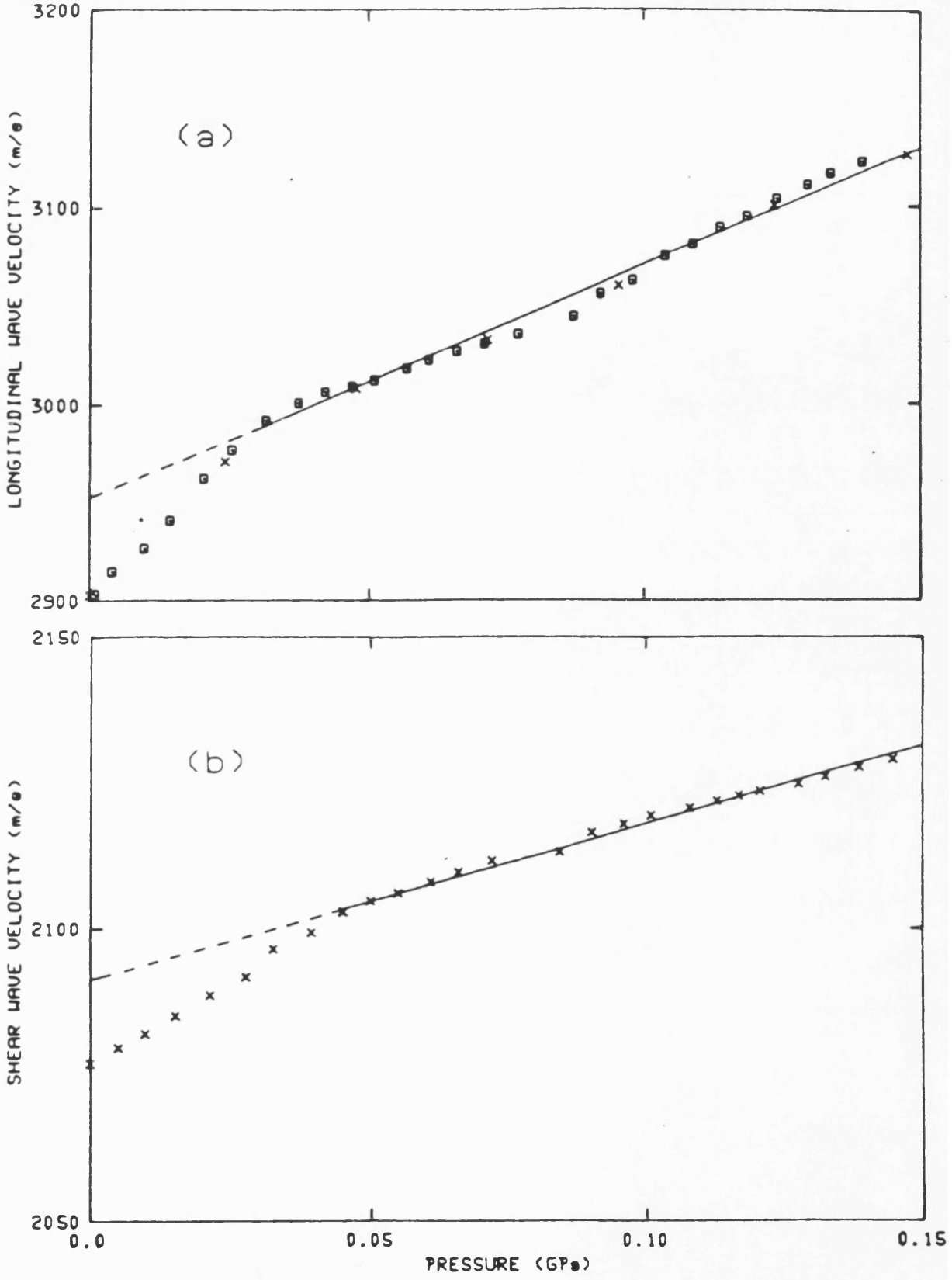

Figure 10.10
The hydrostatic pressure dependences of the velocities of 5MHz (a) longitudinal and (b) shear ultrasonic waves propagated in Bi(Pb)2223 (sample 1). The squares correspond to measurements made with decreasing pressure and the crosses to those obtained as the pressure was increased. The solid line is the least mean squares fit to the data obtained above the knee at about 0.03GPa which has been used to evaluate the pressure derivatives of the elastic moduli.

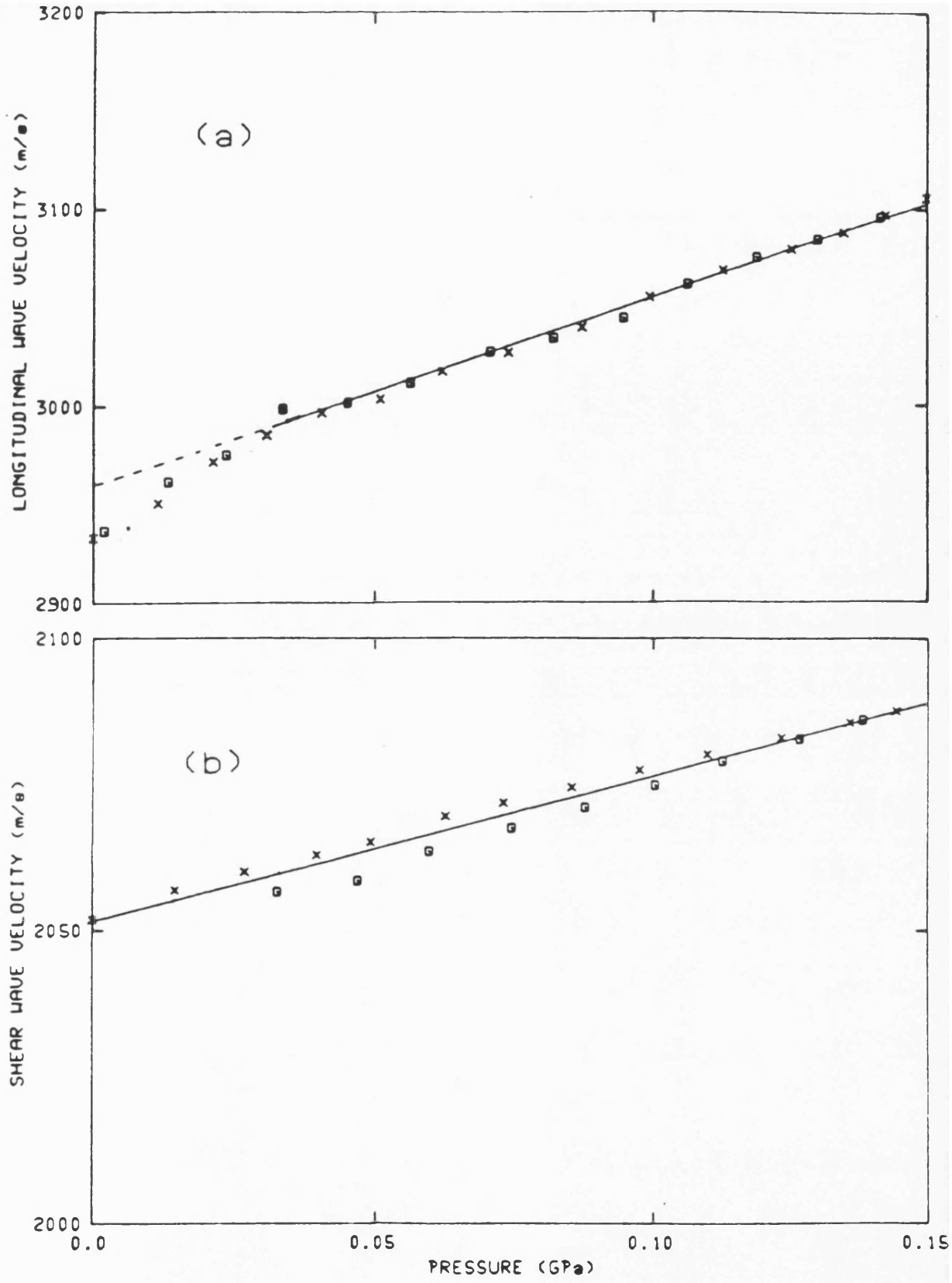

Figure 10.11
The hydrostatic pressure dependences of the velocities of 5MHz (a) longitudinal and (b) shear ultrasonic waves propagated in Bi(Pb)2223 (sample 2). The squares correspond to measurements made with decreasing pressure and the crosses to those obtained as the pressure was increased. The solid line is the least mean squares fit to the data.

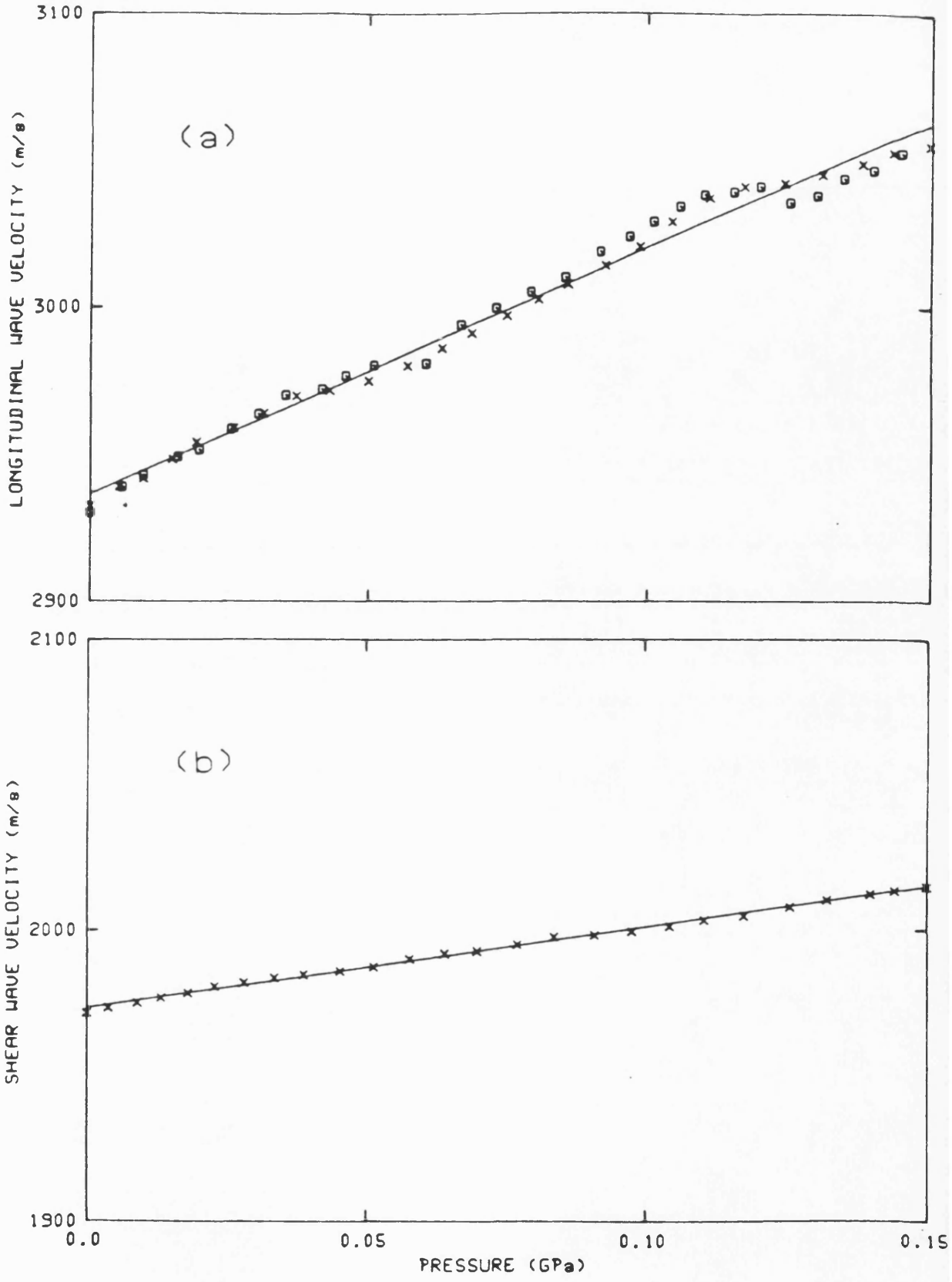

Figure 10.12
The hydrostatic pressure dependences of the velocities of 5MHz (a) longitudinal and (b) shear ultrasonic waves propagated in Bi(Pb)2212. The squares correspond to measurements made with decreasing pressure and the crosses to those obtained as the pressure was increased. The solid line is the least mean squares fit to the data.

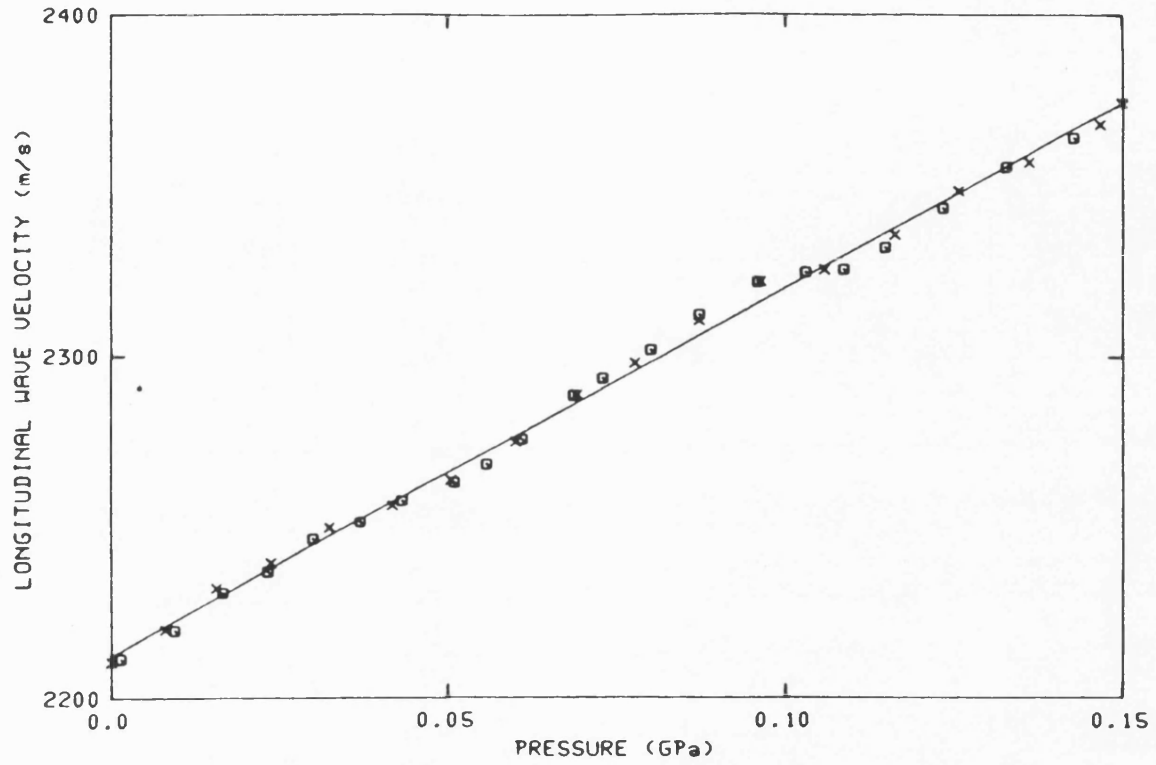

Figure 10.13
The hydrostatic pressure dependence of the velocity of 5MHz longitudinal ultrasonic waves propagated in Bi2212 (sample 1). The squares correspond to measurements made with decreasing pressure and the crosses to those as the pressure was increased. The solid line is the least mean squares fit to the data.

on ultrasonic velocity in the Bi(Pb)2212 phase samples does not show this change of slope at 0.03GPa (figure 10.12) possibly due to microstructural differences.

The velocities of longitudinal (V_L) and shear (V_S) ultrasonic waves propagated at room temperature in Bi(Pb)2223, Bi(Pb)2212 and Bi2212 samples are given in table 10.3. They confirm that the absolute values of both mode velocities in Bi-based copper oxide are considerably smaller than those found for $Nd_{1.85}Ce_{0.15}CuO_{4-y}$, $La_{1.8}Sr_{0.2}CuO_{4-y}$, $YBa_2Cu_3O_{7-x}$ and $GdBa_2Cu_3O_{7-x}$ (see chapters 6,7,8 and 9 respectively). The slowness of the velocities in polycrystalline Bi(Pb)2223 has been attributed to sample texture [Plechácek and Dominec (1990)] and this may play a role in the samples investigated here as well. It should be noted that the velocity V_L of the longitudinal mode generated in the basal plane of a single crystal Bi2212 was estimated to be about 5000ms^{-1} [Saint-Paul et al (1990b)].

10.6 THE ELASTIC CONSTANTS AND THEIR HYDROSTATIC PRESSURE DEPENDENCES FOR BISMUTH-BASED CUPRATES

From the velocity data and specimen density the two independent mean elastic constants C_L and C_S for an isotropic medium have been determined. The hydrostatic pressure dependences of the as measured (porous) C_L , C_S and the bulk modulus are shown respectively in part (a) of figures 10.14 to 10.16 for Bi(Pb)2223 (sample 1), part (a) of figures 10.17 to 10.19 for Bi(Pb)2223 (sample 2) and in part (a) of figures 10.20 to 10.22 for Bi(Pb)2212 sample. These elastic constants together with the bulk and Young's moduli, Poisson's ratio and the Debye temperature (Θ_D^{el}) are given in table 10.3. The results obtained confirm previous observations [Sihan et al (1989), Ledbetter et al (1989b), Plechácek and Dominec (1990) and Fanggao et al (1990b)] that these Bi-based copper-oxide superconductors are elastically much softer than $Nd_{1.85}Ce_{0.15}CuO_{4-y}$, $La_{1.8}Sr_{0.2}CuO_{4-y}$ $YBa_2Cu_3O_{7-x}$ and $GdBa_2Cu_3O_{7-x}$ (see chapters 6,7,8 and 9 respectively). The microstructure of these ceramics comprises thin platelets stacked, often loosely, upon each other. It is not a simple problem to establish with certainty for the Bi-based ceramics how much the open porous microstructure and specimen texture are responsible for the small elastic moduli.

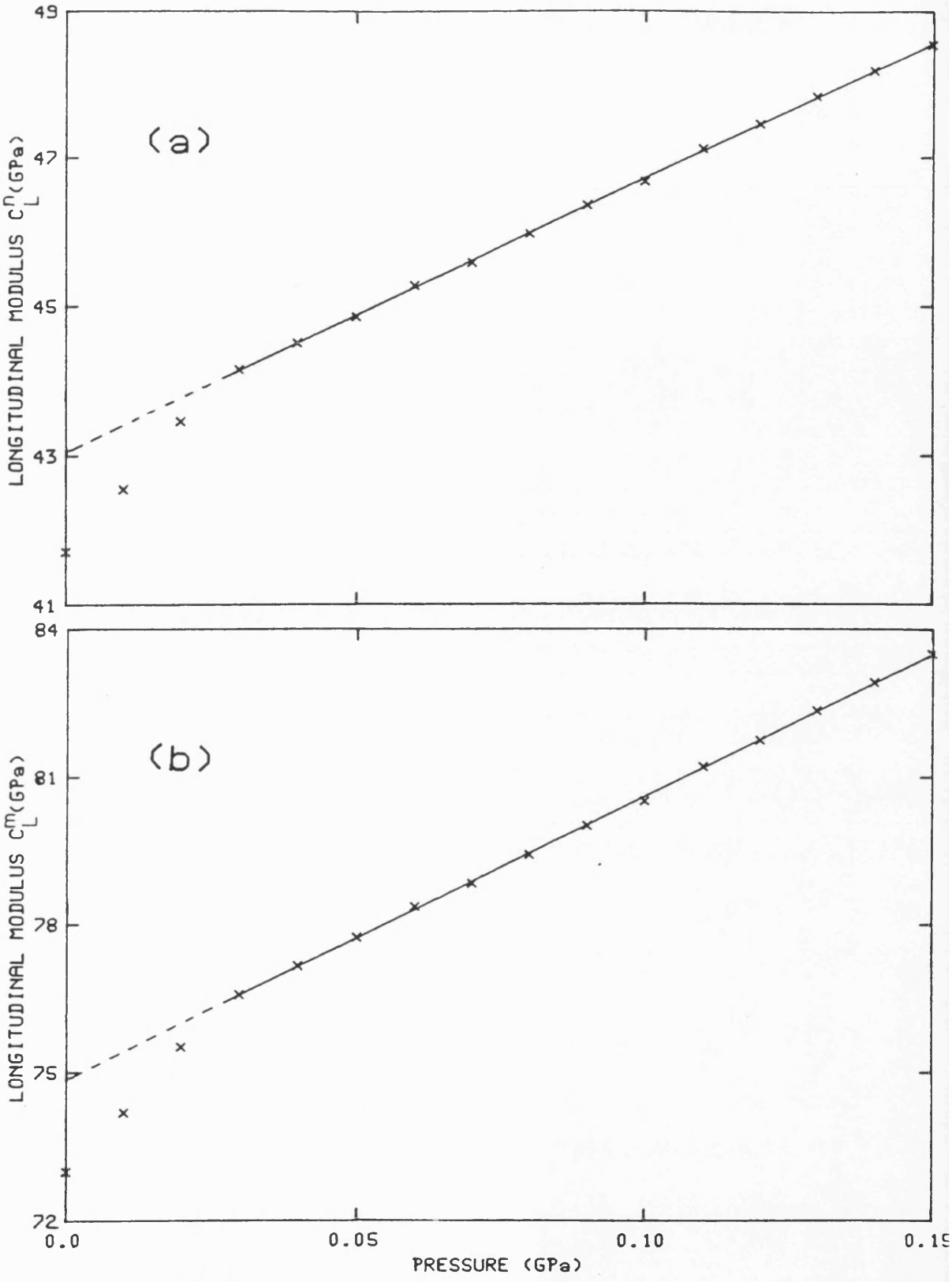

Figure 10.14
The hydrostatic pressure dependences of the longitudinal modulus (a) C_L^n (porous material) and (b) C_L^m (non-porous matrix) of Bi(Pb)2223 (sample 1) at 295K calculated from the experimental data and using equations (4.4) and (4.5). The solid line is the least mean squares fit to the data obtained above the knee at about 0.03GPa which has been used to evaluate the pressure dorivatives of the elastic moduli.

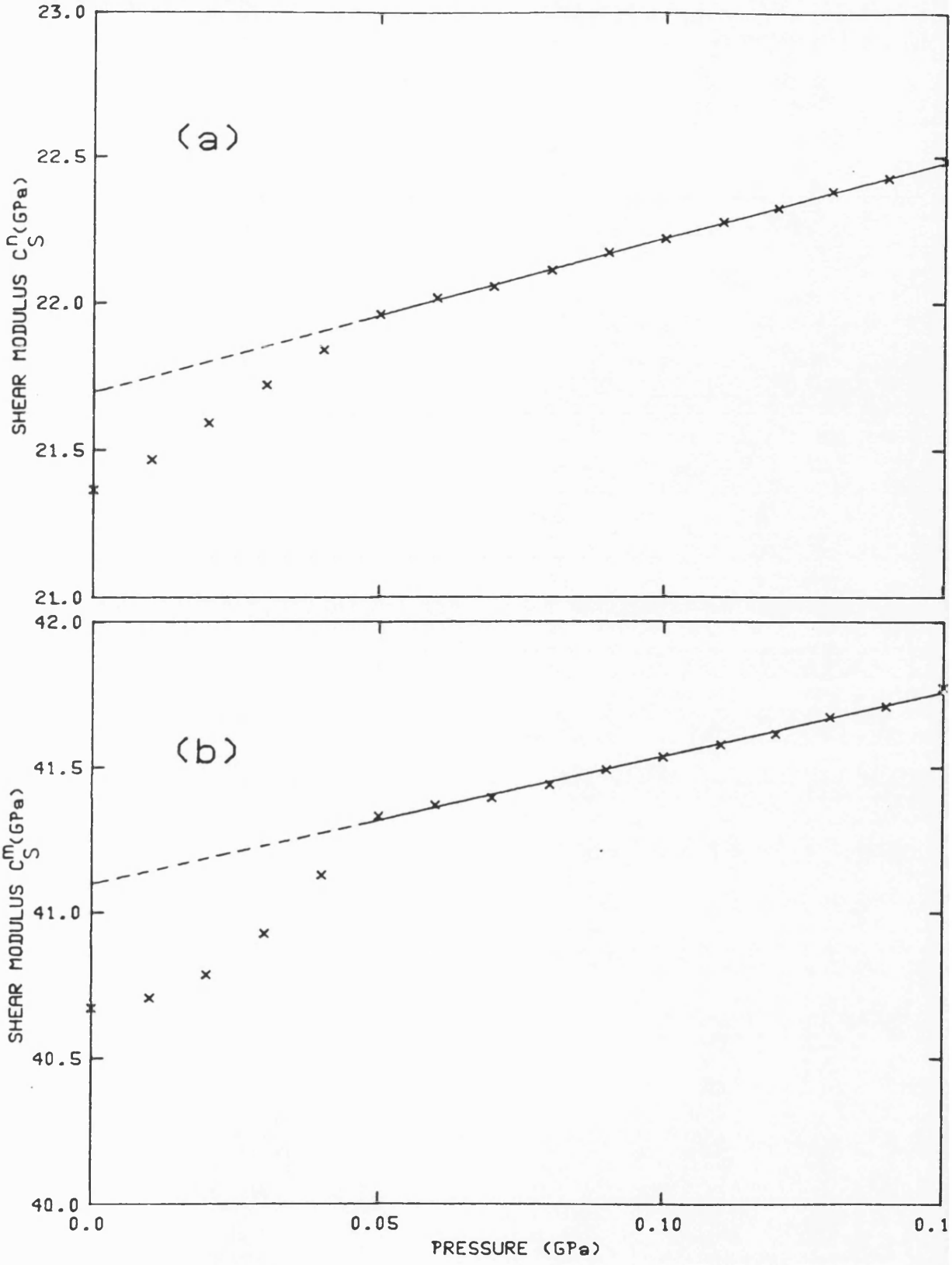

Figure 10.15
The hydrostatic pressure dependences of the shear modulus (a) C_S^n (porous material) and (b) C_S^m (non-porous matrix) of Bi(Pb)2223 (sample 1) at 295K calculated from the experimental data and using equations (4.4) and (4.5). The solid line is the least mean squares fit to the data obtained above the knee at about 0.05GPa which has been used to evaluate the pressure derivatives of the elastic moduli.

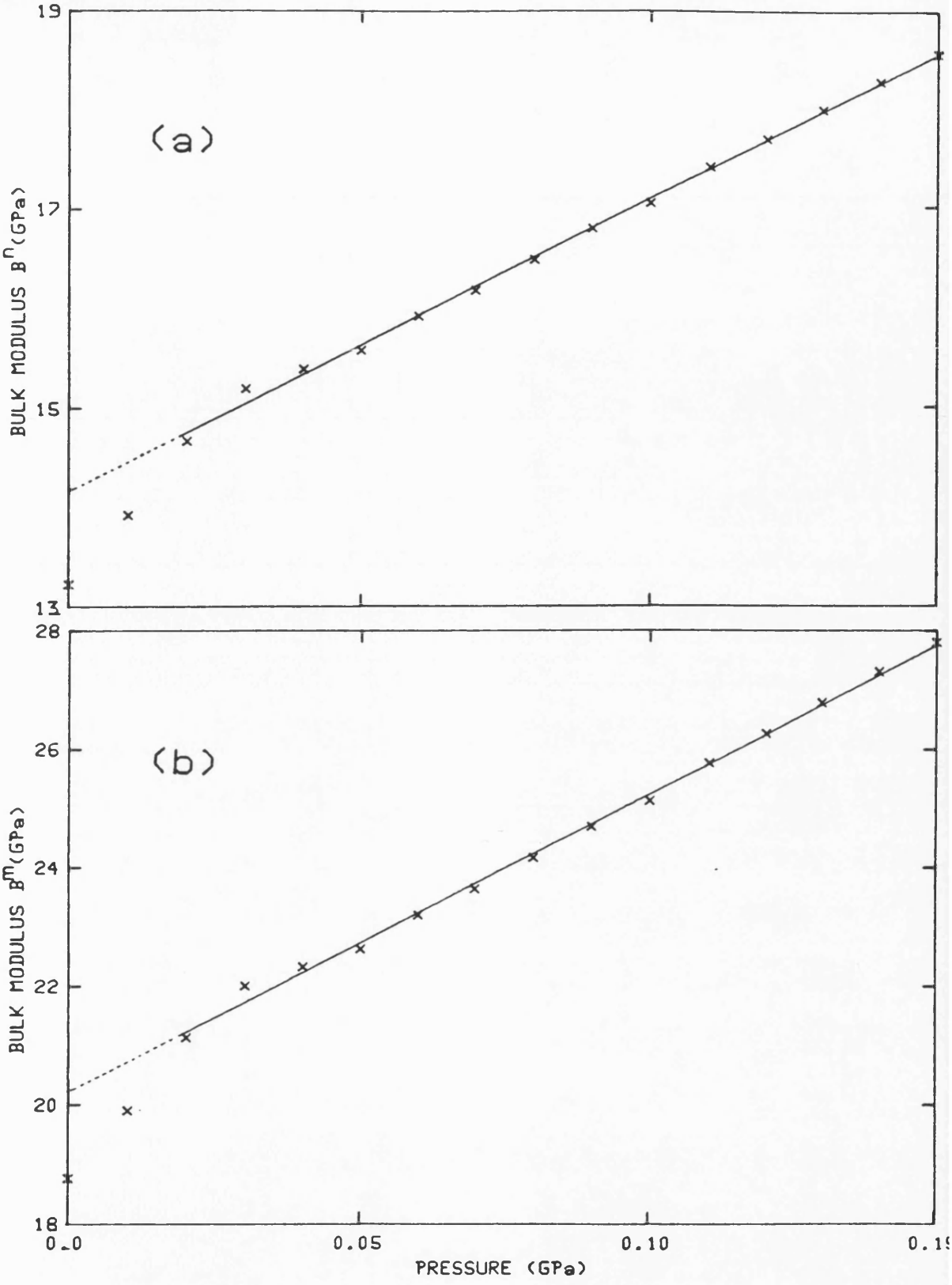

Figure 10.16
The hydrostatic pressure dependences of the bulk modulus (a) B^n (porous material) and (b) B^m (non-porous matrix) of Bi(Pb)2223 (sample 1) at 295K calculated from the experimental data and using equations (4.4) and (4.5). The solid line is the least mean squares fit to the data obtained above the knee at about 0.02GPa which has been used to evaluate the pressure derivatives of the elastic moduli.

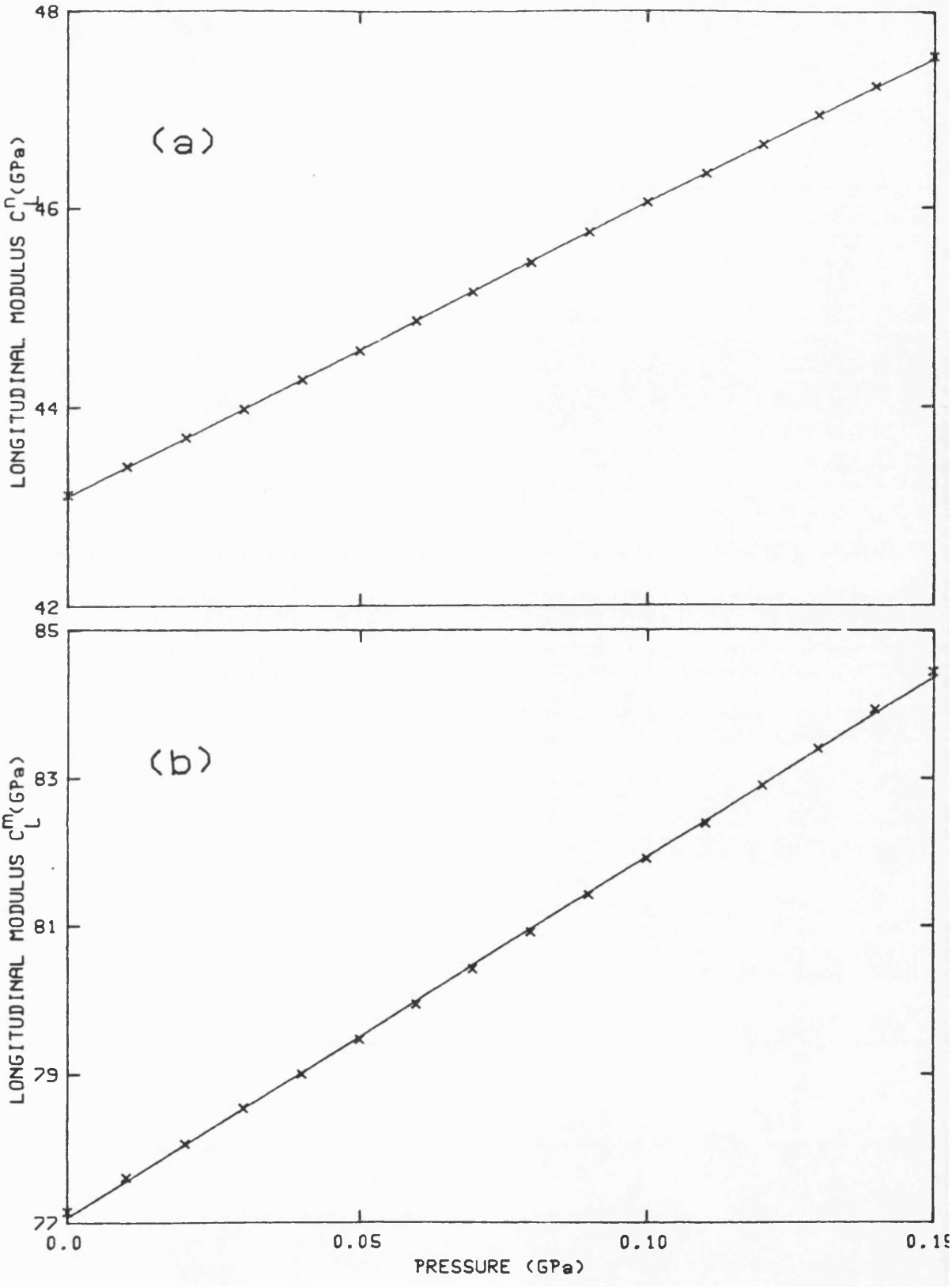

Figure 10.17
The hydrostatic pressure dependences of the longitudinal modulus (a) C_L^n (porous material) and (b) C_L^m (non-porous matrix) of Bi(Pb)2223 (sample 2) at 295K calculated from the experimental data and using equations (4.4) and (4.5). The solid lines are least square fits to the data.

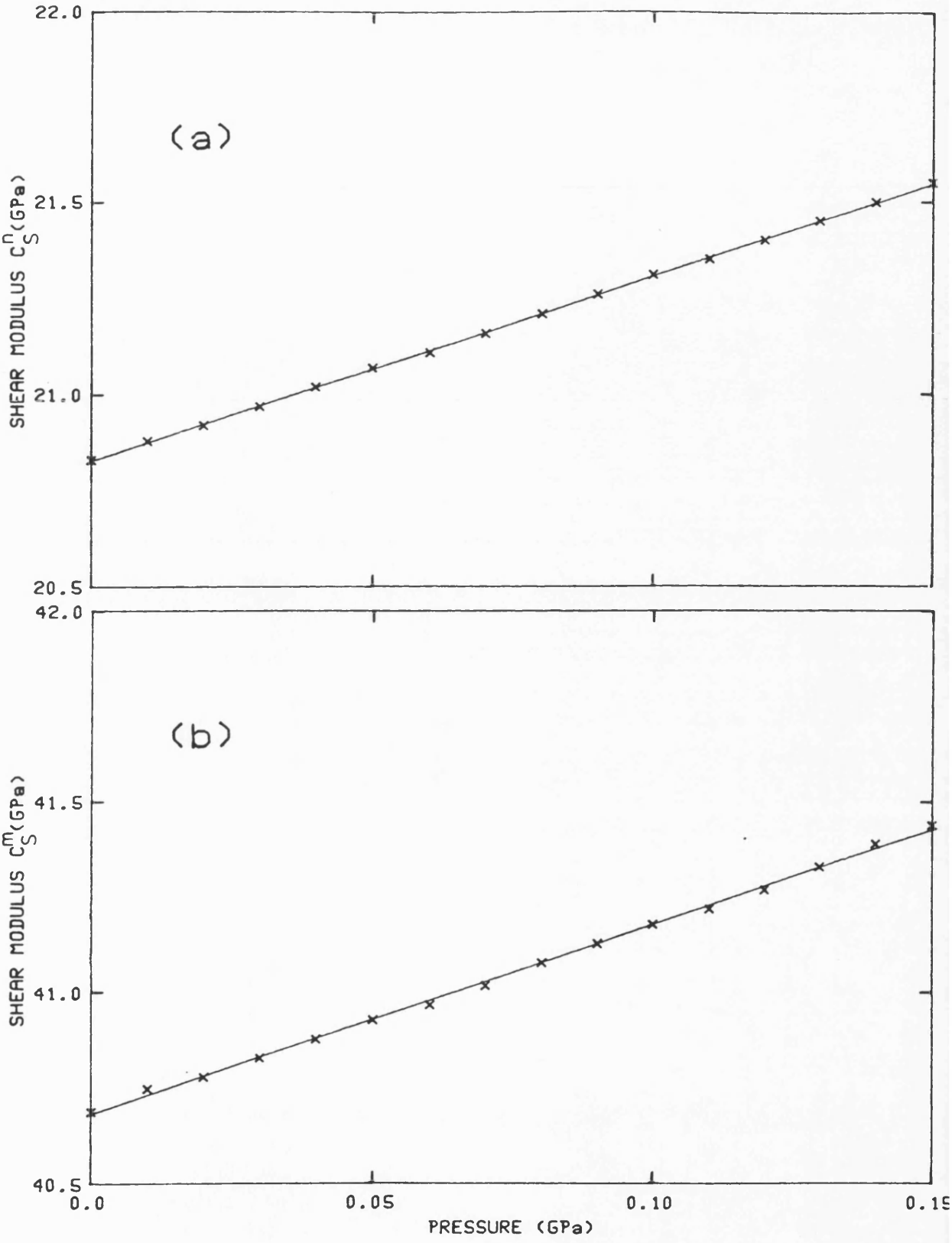

Figure 10.18
The hydrostatic pressure dependences of the shear modulus (a) C_S^n (porous material) and (b) C_S^m (non-porous matrix) of Bi(Pb)2223 (sample 2) at 295K calculated from the experimental data and using equations (4.4) and (4.5). The solid lines are least square fits to the data.

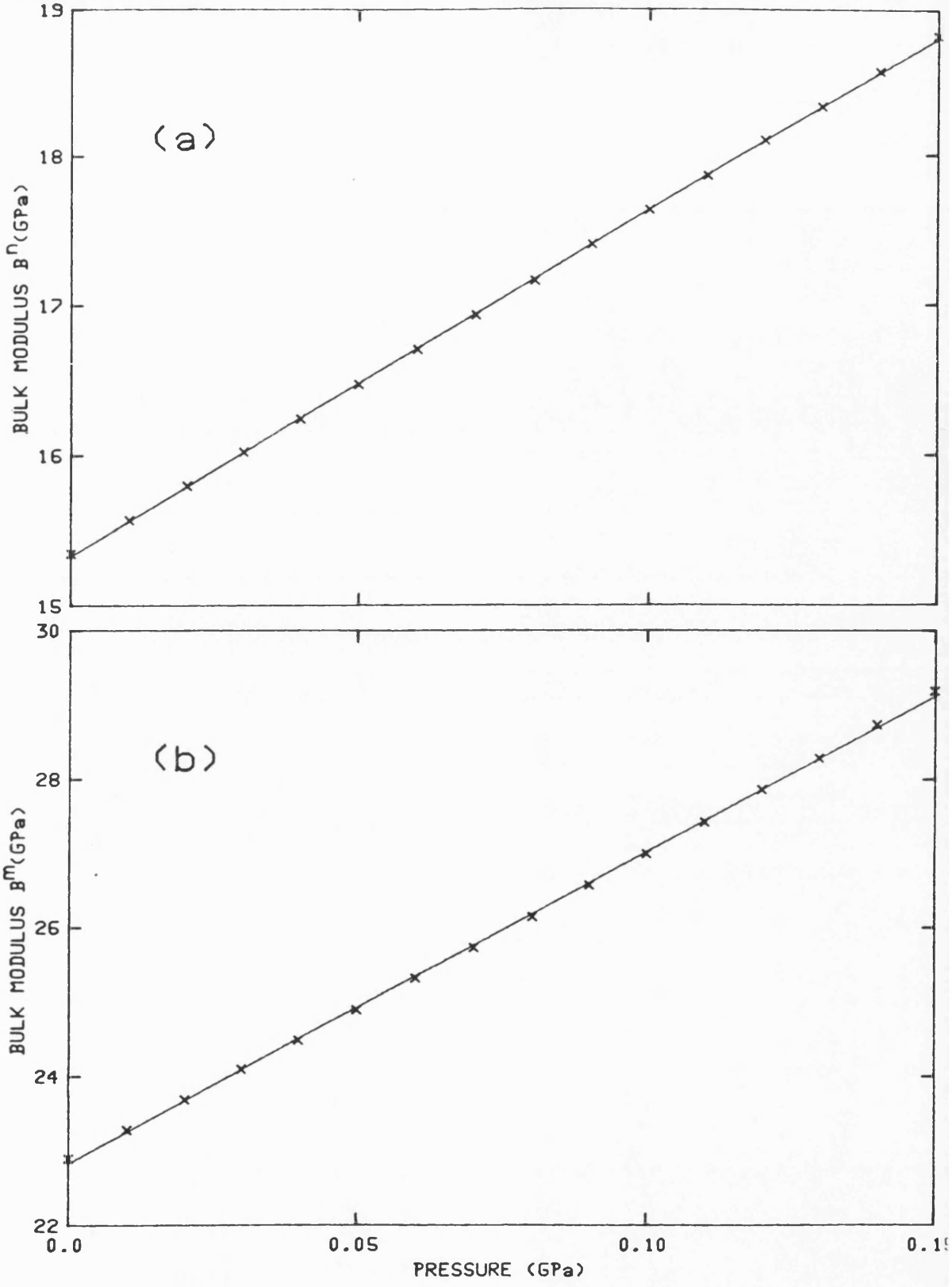

Figure 10.19
The hydrostatic pressure dependences of the bulk modulus (a) B^n (porous material) and (b) B^m (non-porous matrix) of Bi(Pb)2223 (sample 2) at 295K calculated from the experimental data and using equations (4.4) and (4.5). The solid lines are least square fits to the data.

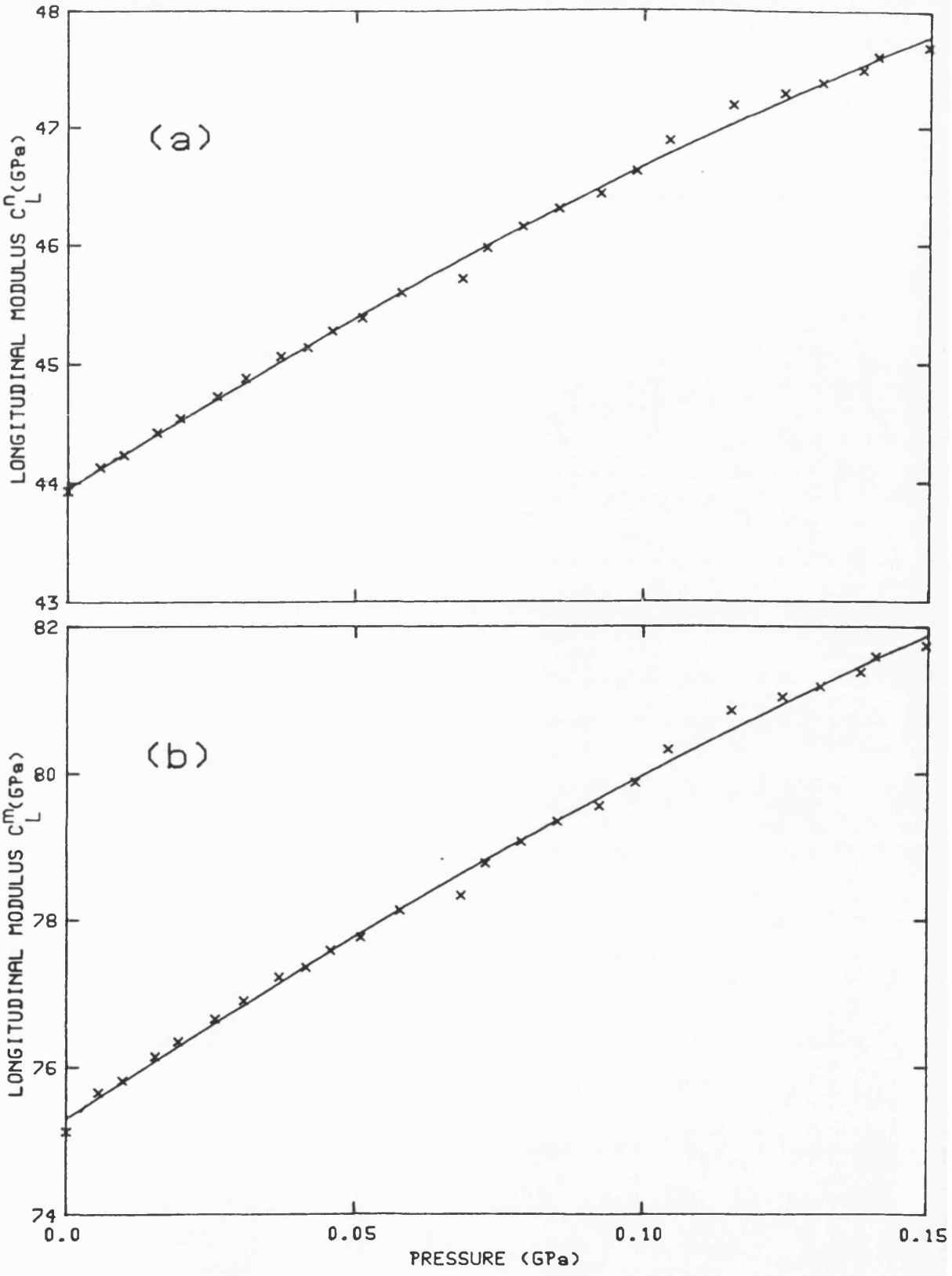

Figure 10.20
The hydrostatic pressure dependences of the longitudinal modulus (a) C_L^n (porous material) and (b) C_L^m (non-porous matrix) of Bi(Pb)2212 at 295K calculated from the experimental data and using equations (4.4) and (4.5). The solid lines are least square fits to the data.

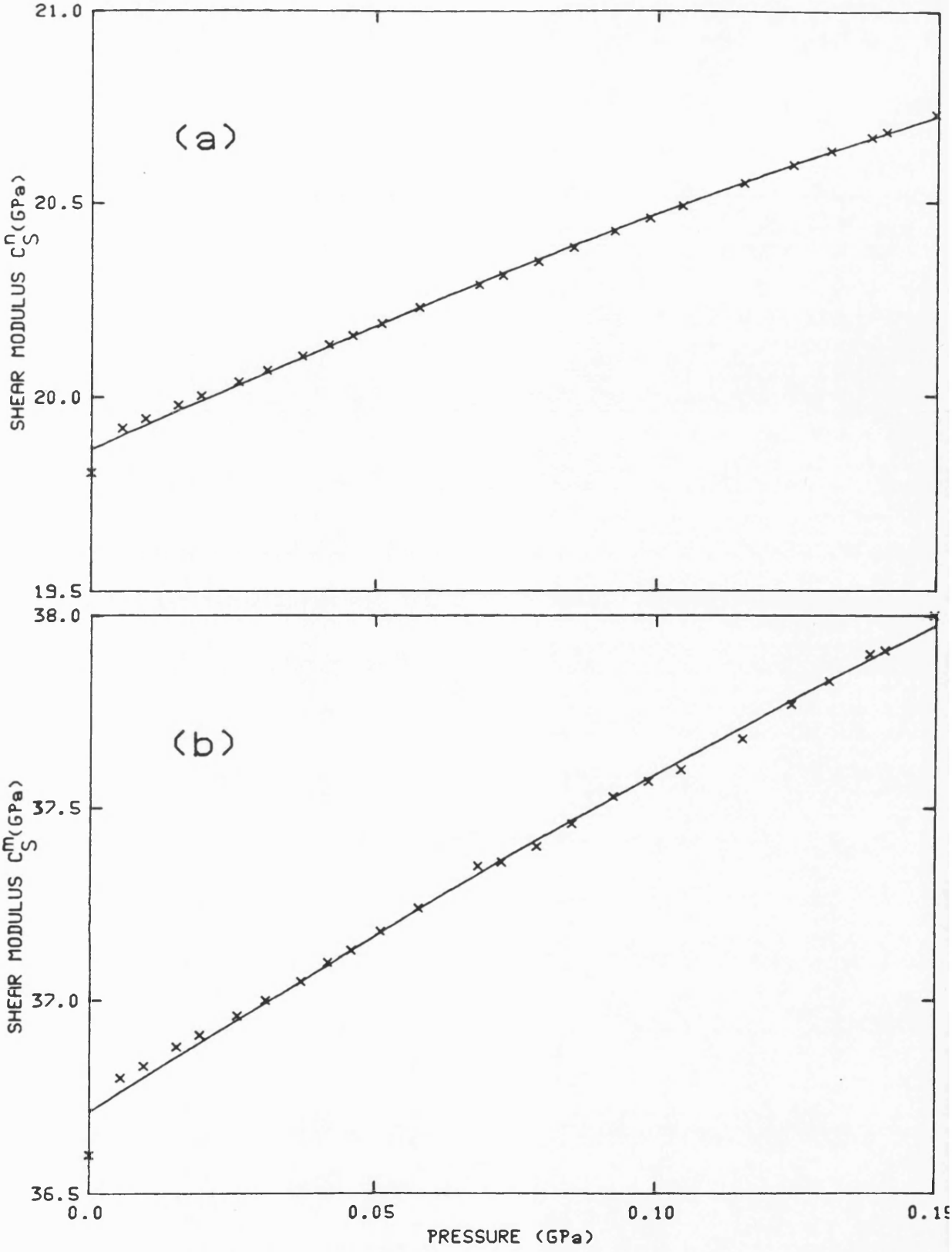

Figure 10.21
The hydrostatic pressure dependences of the shear modulus (a) C_S^n (porous material) and (b) C_S^m (non-porous matrix) of Bi(Pb)2212 at 295K calculated from the experimental data and using equations (4.4) and (4.5). The solid lines are least square fits to the data.

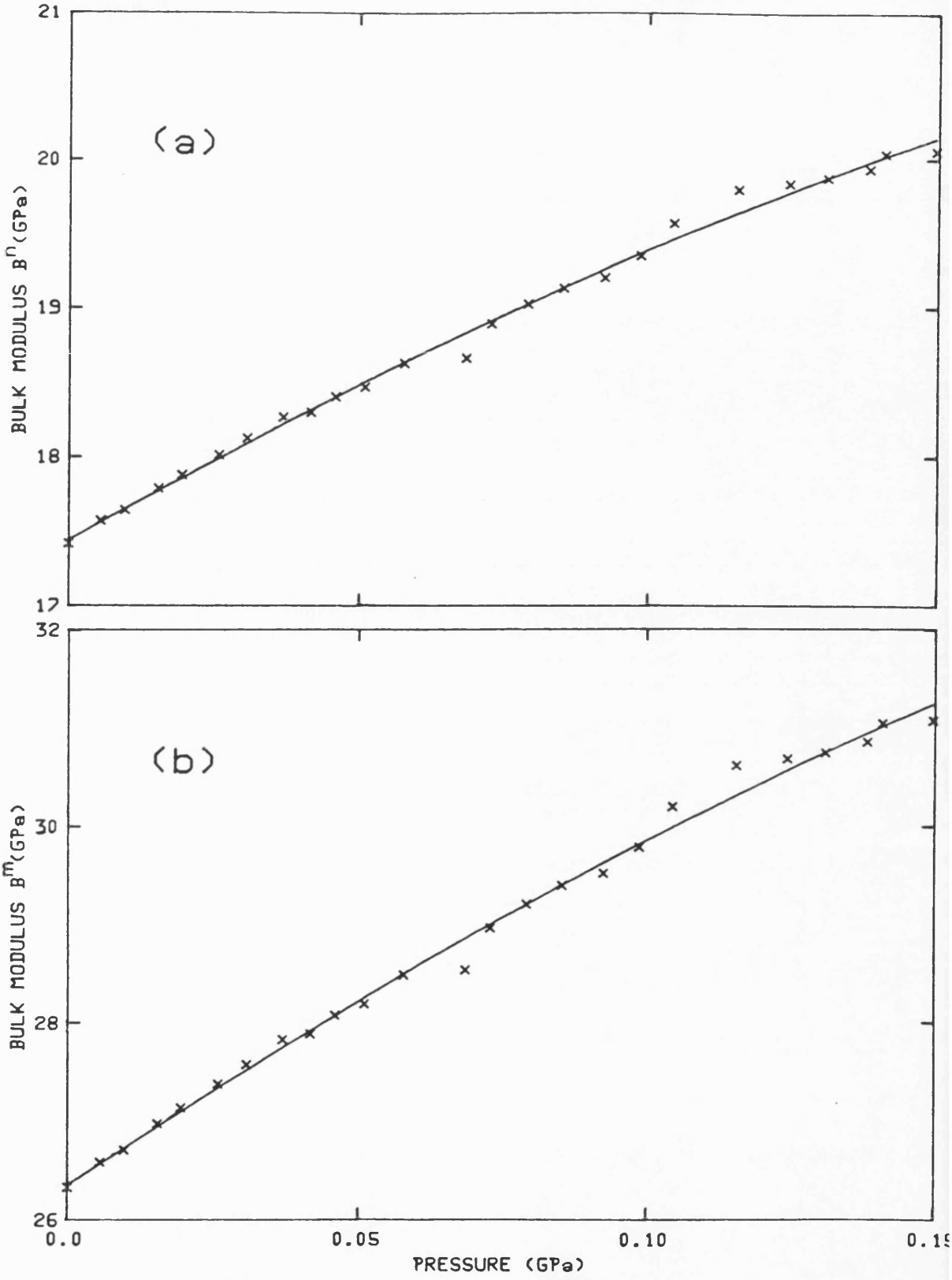

Figure 10.22
The hydrostatic pressure dependences of the bulk modulus (a) B^n (porous material) and (b) B^m (non-porous matrix) of Bi(Pb)2212 at 295K calculated from the experimental data and using equations (4.4) and (4.5). The solid lines are least square fits to the data.

The microstructure of the Bi-based cuprates is quite different in kind from that of $YBa_2Cu_3O_{7-x}$ which takes the form of a homogeneous polycrystalline matrix perforated by roughly spherical pores. The BISCO microstructural porosity comprises the gaps between the roughly stacked platelets and cannot be approximated by the relatively low density of spherical cavities required for the validity of the method of correction for porosity based on wave scattering in a medium containing a uniform distribution of interconnected pores which was developed for $YBa_2Cu_3O_{7-x}$ (see section 4.12). Nevertheless it is useful to make a rough assessment of the effects of porosity and that has been implemented using the wave scattering theory. The hydrostatic pressure dependences of the non-porous matrix C_L , C_S and the bulk modulus are shown respectively in part (b) of figures 10.14 to 10.16 for Bi(Pb)2223 (sample 1), part (b) of figures 10.17 to 10.19 for Bi(Pb)2223 (sample 2) and in part (b) of figures 10.20 to 10.22 for Bi(Pb)2212 sample. The comparison (table 10.3) between ultrasonic wave velocities and elastic moduli calculated for the non-porous matrices of Bi(Pb)2223 and Bi(Pb)2212 and the raw experimental data shows that the effect of porosity is to reduce the measured values of elastic stiffnesses. Even after alleviation for the effects of porosity the elastic moduli of Bi-based cuprates remain

extremely small. It is surprising to find that the elastic Debye temperatures obtained using ultrasonic wave velocities measured at 10K and corrected for porosity for these ceramic bismuth cuprate samples are substantially larger than those determined from low temperature specific heat data [217-256K for Bi2212 and 220-292K for Bi2223, unusually wide ranges of limiting Debye temperature Θ_D which may be due to differences in sample composition (Collocott and Driver (1990))].

The hydrostatic pressure derivatives $(\partial C_L/\partial P)_{P\text{-}O}$, $(\partial C_S/\partial P)_{P\text{-}O}$ and $(\partial B/\partial P)_{P\text{-}O}$ obtained for the Bi-based ceramic samples are given in table 10.3. For all these bismuth-cuprate ceramics the effect of porosity is to reduce $(\partial B/\partial P)_{P\text{-}O}$ as well as B_o . Although the microstructure of these bismuth cuprate ceramics is quite different in kind from those of the other high T_C superconductors, the values found for $(\partial B/\partial P)_{P\text{-}O}$ are similar in these various materials, which implies that the anomalously large values of this quantity are not solely a function of the microstructure. It can also be seen that $(\partial C_S/\partial P)_{P\text{-}O}$ is much smaller than $(\partial C_L/\partial P)_{P\text{-}O}$, another general feature of this series of cuprates (table 10.3). If the large values of $(\partial B/\partial P)_{P\text{-}O}$ and $(\partial C_L/\partial P)_{P\text{-}O}$ were solely a consequence of porosity, then $(\partial C_S/\partial P)_{P\text{-}O}$ would also be expected to be influenced by porosity and be quite large.

The main effect of application of hydrostatic pressure to a layer-like compound is to squeeze the widely spaced weakly bonded layers together, so the influence of the comparatively small repulsive forces which act between the pairs of BiO layers must play an especially important role in the behaviour of these $Bi_2Sr_2Ca_{n-1}Cu_nO_{4+2n}$ compounds under pressure. The work done against these forces requires that the velocity of the longitudinal mode propagated down the c-axis should increase substantially when pressure is applied. Therefore the corresponding mode Grüneisen parameter ($-\partial \ln \omega_i / \partial \ln P$) and the hydrostatic pressure derivatives of the mode velocity and elastic stiffness tensor component should be positive and much larger than those of other acoustic modes and constitute a major contribution to the large measured values of $(\partial B/\partial P)_{P=0}$. In accord with this the bulk modulus (73GPa) of the Bi2212 compound determined [Tajima et al (1989)] from X-ray measurements of the pressure dependence of the lattice parameters is also small. However that measured ultrasonically (=22 GPa) is very low indeed largely due to the particular microstructure and texture of the bismuth cuprate ceramics.

In addition to their layer-like nature there is a second feature of the BISCO compounds, namely the intermediate valence of the copper ions, which could in part lead to

their small elastic stiffnesses and large values of the pressure derivatives. In the Bi2212 phase the copper ion valence is about +2.3 [Cheetham et al (1988)]. *XPS* studies indicate that in the Bi2223 phase both the Cu and Bi ions are in mixed valence states: there are valence fluctuations between the ionic states (Cu^{2+} and Cu^{3+}) and also (Bi^{3+} and Bi^{5+}) [Schwarz (1990)]. Fluctuating copper valence is a characteristic feature of high T_c cuprates and may have pronounced effects on their elastic and nonlinear acoustic properties [Kim et al (1988b), Cankurtaran et al (1989) and Fanggao et al (1991b)]. As mentioned earlier: a small, or even negative Poisson's ratio, and a small bulk modulus are characteristic features of compounds in intermediate valence state [Boppart et al (1983), Mook and Holtzberg (1981), Hailing et al (1984) and Yogurtcu et al (1985)]. Since higher valent ions are smaller than the lower valent ones, coupling to the lattice is strong for the longitudinal phonons which alter the unit cell volume. This is not so for the shear modes. Furthermore the effects of pressure on the longitudinal mode velocity are necessarily large because the intermediate valence and ion size alter under compression. Therefore the effects expected of fluctuating valence are a large $(\partial C_L/\partial P)_{P\text{-}O}$ but a small $(\partial C_S/\partial P)_{P\text{-}O}$, as found experimentally for the bismuth cuprates (table 10.3). Hence

the small longitudinal C_L and bulk B_o moduli and their large pressure dependences are consistent with fluctuating valence softening the longitudinal acoustic modes. It is interesting that the BISCO compounds are the most elastically soft of all the high T_c cuprates examined to date yet have very high T_c's . The intriguing fundamental question remains: are the fluctuating valence, and possibly also the consequent longitudinal phonon softening, related to the superconducting pairing interaction?. In the next chapter (11), the results obtained for the Bi-based samples investigated here will be compared with the other high temperature superconducting compounds.

CHAPTER ELEVEN

DISCUSSIONS AND CONCLUSIONS

11.1 INTRODUCTION

In this chapter a comparison between the results obtained in this work for the different high temperature superconducting compounds will be presented. In section 11.2, the hydrostatic pressure and temperature dependences of ultrasonic wave velocities obtained for the different high temperature superconducting compounds will be compared. Emphasis will be placed in section 11.3 on the apparent difference between the bulk moduli $B^T(P)$ determined at high pressure (>1GPa) from X-ray measurements and B_o obtained from ultrasonic wave velocity measurements at atmospheric pressure. Grüneisen parameters obtained using ultrasonic velocity measurements for the different high temperature superconducting compounds under pressure will be compared in section 11.4. Finally, in section 11.5, the conclusions of this work will be presented.

11.2 HYDROSTATIC PRESSURE AND TEMPERATURE DEPENDENCES OF ULTRASONIC WAVE VELOCITIES

11.2A HYDROSTATIC PRESSURE EFFECTS

The effects of hydrostatic pressure on the velocities of longitudinal and shear ultrasonic waves propagated in high T_c superconducting compounds show two distinct features: (i) a linearity and (ii) a non-linearity.

(i) linear behaviour of the ultrasonic wave velocities as a function of pressure is found in $Nd_{1.85}Ce_{0.15}CuO_{4-y}$ (figure 6.11) and $La_{1.8}Sr_{0.2}CuO_{4-y}$ (figure 7.10) and their non-superconducting parent compounds Nd_2CuO_{4-y} (figure 6.12) and La_2CuO_{4-y} (figure 7.11). In each of these four compounds the measurements are reproducible and show no hysteresis effects. The ultrasonic wave velocities increase linearly with pressure, much more steeply for the longitudinal than for the shear mode.

(ii) In contrast, the pressure dependences of ultrasonic wave velocities in $YBa_2Cu_3O_{7-x}$ (sample Y1) show non-linear behaviour (figure 8.8). Even after re-annealing sample Y1 (to produce sample Y1A), non-linear behaviour is still observed in sample Y1A (figure 8.9). The non-linearity is more pronounced in sample Y1A than that of sample Y1, and the shear wave velocity changes less in sample Y1A than that in sample Y1 as the pressure changes. Hysteresis effects

are found in the hydrostatic pressure dependences of ultrasonic wave velocities in a coarse grained, more dense sample of $YBa_2Cu_3O_{7-x}$ (sample Y2) (figure 8.10) but not in a large grained sample of $YBa_2Cu_3O_{7-x}$, prepared by the halide flux method, for which a linear behaviour with pressure is found for the longitudinal wave velocity (figure 8.26a).

Both longitudinal and shear ultrasonic wave velocities for orthorhombic $GdBa_2Cu_3O_{7-x}$ show the unusual feature of a non-linear pressure dependence (figure 9.10), although the non-linearity of ultrasonic wave velocities is not so pronounced as found for $YBa_2Cu_3O_{7-x}$ samples Y1 and Y1A (figures 8.8 and 8.9). It is interesting to note that the pressure dependences of the ultrasonic wave velocities in the tetragonal form of $GdBa_2Cu_3O_{7-x}$ (figure 9.11) are almost linear: the vibrational anharmonicity of the long wavelength phonons is much less than that of the orthorhombic form.

Another interesting feature in the pressure dependences of ultrasonic wave velocities is found in two different samples of the Bi(Pb)2223 compound. The pressure dependences of the longitudinal mode velocities of both Bi(Pb)2223 samples show a pronounced change of slope at about 0.03GPa; the shear mode velocities show a slight indication of the same effect at the same pressure (figures 10.10a, b and 10.11a, b). Above the knee the slope of the pressure

dependence is substantially smaller. The effects of pressure on ultrasonic velocities in the Pb doped (figure 10.12) and the undoped (figure 10.13) Bi2212 samples does not show this change of slope at 0.03GPa, in contrast these materials show a good linear behaviour similar to that found in $Nd_{1.85}Ce_{0.15}CuO_{4-y}$ (figure 6.11), Nd_2CuO_{4-y} (figure 6.12), $La_{1.8}Sr_{0.2}CuO_{4-y}$ (figure 7.10) and La_2CuO_{4-y} (figure 7.11) compounds.

11.2B TEMPERATURE EFFECTS

Different behaviours of the ultrasonic wave velocities as a function of temperature are found for different materials. The temperature dependences of longitudinal and shear ultrasonic wave velocities in the electron doped $Nd_{1.85}Ce_{0.15}CuO_{4-y}$ superconductor and its parent Nd_2CuO_{4-y} compound showed continuous increase as the temperature was reduced (figures 6.5 and 6.6). There was no reduction in the velocity, as the temperature was reduced below 170K, of the type found in $La_{1.8}Sr_{0.2}CuO_{4-y}$ (figure 7.3) which has been attributed to mode softening associated with the orthorhombic-tetragonal phase transition. However, the temperature dependence of the longitudinal wave velocity of $Nd_{1.85}Ce_{0.15}CuO_{4-y}$ shows a change of gradient near 220K. This is also observed, but is much less marked, in the shear wave velocity (figure 6.6). The temperature dependences of the

ultrasonic wave velocities for La_2CuO_{4-y} (figure 7.4) do not show the same softening of the doped compound sample: the softening is a feature of the doped La_2CuO_{4-y} structure. However, inspection of the low temperature data for La_2CuO_{4-y} reveals that a minimum in the ultrasound velocity also occurs in a temperature region similar to that present in the data for $La_{1.8}Sr_{0.2}CuO_{4-y}$.

The temperature dependences of ultrasonic wave velocities obtained for $YBa_2Cu_3O_{7-x}$ (sample Y1) (figure 8.1) show a marked thermal hysteresis in the temperature range 200-240K which has been attributed [Toulouse et al (1990)] to an order-disorder phase transition involving the oxygen ions in the copper-oxygen planes. The thermal hysteresis and the step-like behaviour contrast markedly with the elastic behaviour of $Nd_{2-x}Ce_xCuO_{4-y}$ and $La_{2-x}Sr_xCuO_{4-y}$ compounds (figures 6.5, 6.6 and 7.3) where no thermal hysteresis is found for either material. The temperature dependences of ultrasonic wave velocities measured in $YBa_2Cu_3O_{7-x}$ (sample Y2) (figure 8.2) show a distinct dip in sound velocity at about 80K. Above this temperature there are significant differences between data obtained on cooling and those obtained on warming. In the temperature region below the superconducting transition temperature (92K), the ultrasonic wave velocities

exhibit little elastic hysteresis. At much higher temperatures (170-180K) a markedly increasing velocity for both longitudinal and shear waves was consistently observed during cooling. By comparing figures 8.1 and 8.2 it can be seen that in both samples (Y1 and Y2) the ultrasonic wave velocities increase with decreasing temperature and that both samples exhibit a large thermal hysteresis but in different temperature regions. The velocity of longitudinal ultrasonic waves propagated in the large grained, halide flux grown $YBa_2Cu_3O_{7-x}$ specimen (figure 8.25) increases as the temperature is reduced from room temperature down to about 140K where the velocity decreases as the temperature is decreased, then it starts increasing sharply as the temperature is decreased below T_c . Below 140K the data obtained on cooling fall almost on the data obtained on warming. However, there is a marked hysteresis in the temperature range 140-300K. This behaviour contrasts with that found for samples Y1 and Y2 (figures 8.1 and 8.2) indicating the effects of the microstructure and the grain size on the elastic properties of the $YBa_2Cu_3O_{7-x}$ compound.

The results obtained for the ultrasonic wave velocities as a function of temperature for both the orthorhombic and the tetragonal forms of $GdBa_2Cu_3O_{7-x}$ (figure 9.3) show that the annealing process, to obtain the tetragonal phase,

reduces the velocity in the sample; i.e. the ultrasonic wave velocities in the tetragonal sample are slower than those in the orthorhombic form. A striking feature of the velocity data for the sample in the orthorhombic structure is the large warming versus cooling hysteresis over the whole temperature range from 300K down to 10K. This thermal hysteresis was absent in the tetragonal form. The data obtained for the orthorhombic sample (figure 9.3) is almost the same to that obtained for $YBa_2Cu_3O_{7-x}$ sample Y1 (figure 8.1).

The effects of temperature on the longitudinal and shear ultrasonic wave velocities for Bi(Pb)2223 (sample 1) (figure 10.3), show that both mode velocities increase as the temperature is decreased with a small peak at about 40K. The most interesting feature is the steep change in the velocity and the associated hysteresis loop between 189 and 232K. However, it should be noted that these effects seen around 190-235K in Bi(Pb)2223 are much less pronounced than those observed in $YBa_2Cu_3O_{7-x}$ and $GdBa_2Cu_3O_{7-x}$ (figures 8.1, 8.2 and 9.3).

The temperature dependences of ultrasonic wave velocities in a Bi(Pb)2212 sample (figure 10.5) show continuous stiffening with a small peak at 40K similar to that found in Bi(Pb)2223. However, the anomalous change in the velocity

and the hysteretic behaviour found for Bi(Pb)2223 are absent in the Bi(Pb)2212 sample. The temperature dependences of both longitudinal and shear ultrasonic wave velocities in the undoped Bi2212 (sample 1) show a clear hysteretic behaviour in the temperature region 200K-240K with a small peak at around 40K (figure 10.6). Comparison between the velocity data for Bi(Pb)2212 (figure 10.5) and Bi2212 (sample 1) (figure 10.6) shows that Pb doping in the Bi2212 phase suppresses the anomalous change in ultrasonic wave velocity, and hence the elastic hysteretic behaviour.

The effects of temperature on the velocities of ultrasonic waves propagated in Bi2212 (sample 2) (figure 10.7) are rather different from those found in the much less dense Bi2212 (sample 1) (figure 10.6). On cooling there is a sudden, large jump in both mode velocities at 198K. Below this temperature, almost linear stiffening occurs down to about 135K where there is a change in gradient. The data for both modes show pronounced temperature hysteresis. Quenching Bi2212 (sample 2) has considerable effects on the ultrasonic properties. The longitudinal velocity is substantially reduced (figure 10.7a) while that of the shear mode is increased (figure 10.7b). It also has the remarkable consequence of removing the elastic and anelastic anomalies (figure 10.7). It is interesting to recall that the similar

elastic anomalies around 200K-240K in orthorhombic $GdBa_2Cu_3O_{7-X}$ were also removed when it was quenched to reduce the oxygen content and retain the tetragonal form.

11.3 COMPARISON BETWEEN THE BULK MODULUS B_o OBTAINED FROM ULTRASONIC WAVE VELOCITY MEASUREMENTS AND $B^T(P)$ DETERMINED AT HIGH PRESSURE (>1GPa) FROM X-RAY MEASUREMENTS

The predominant feature of the high temperature superconducting compounds studied here is that the bulk modulus measured ultrasonically is found to be small when compared with the value determined at high pressure from X-ray measurements. One major objective of the present study was to make ultrasonic velocity measurements on superconducting ceramic materials to find out whether a small bulk modulus and a large pressure dependence are general characteristics of these mixed oxides based on copper.

The adiabatic bulk modulus B_o^n obtained from ultrasonic wave velocity measurements together with the values corrected for porosity B_o^m , using equations 4.4 and 4.5, are given in table 11.1. The Bi-based cuprates studied here have very small bulk modulus B_o compared with the other high temperature superconducting compounds even after correction for the effect of porosity. This has been attributed to the open microstructure of the bismuth cuprate ceramics [Hewat et al (1988)].

An important development in the present context has been the measurement of the elastic constants of single crystal

Table 11.1. The bulk moduli (in units of GPa) B_o at atmospheric pressure [B_o^n before and B_o^m after correction for the effects of porosity] and $B(P)$ at pressure P (in units of GPa) obtained from ultrasonic experiments for the non-porous matrices of the mixed oxides. $B(P)$ has been calculated taking P as the approximate lower pressure limit used in the high pressure experiments (the references are given in brackets); in the case of $Nd_{1.85}Ce_{0.15}CuO_{4-y}$ and its parent compound Nd_2CuO_{4-y}, P has been taken to be 2.5GPa. The isothermal bulk modulus $B^T(P)$ data are those determined at high pressures from X-ray measurements of lattice parameters using diamond cell technology.

Material	B_o^n	B_o^m	P	$B(P)$	$B^T(P)$
La_2CuO_4 (single crystal)	112 [Migliori et al (1990)]				-
(polycrystalline)	122 [Kim et al (1990)]				168 [Akthar et al (1988)]
(polycrystalline)	72	87	2	142	185 [Fietz et al (1989)]
$La_{1.8}Sr_{0.2}CuO_4$	65	93	2.5	183	180 [Wijngaarden and Griessen (1989)]
$YBa_2Cu_3O_{7-X}$	42	64	1.2	197	180 [Fietz et al (1987)] 157 [Olsen et al (1988)]
$GdBa_2Cu_3O_{7-X}$ (orthorhombic)	47.5	89	1	144	155 [Ecke et al (1988)]
(tetragonal)	38.7	75	1	127	-
Nd_2CuO_{4-y}	77	110	2.5	183	-
$Nd_{1.85}Ce_{0.15}CuO_{4-y}$	72	93	2.5	132	-
Bi(Pb)2223 (sample 1)	13.3	18.9	1	78	73 [Yoneda et al (1990)]
Bi(Pb)2223 (sample 2)	15.3	22.9	1	62	
Bi(Pb)2212	17	26.4	1	66.4	61 [Yoneda et al (1990)] 73 [Tajima et al (1989)]

La_2CuO_4 [Migliori et al (1990)]. These data enable a comparison between the bulk modulus of monocrystalline and polycrystalline specimens of the same compound and thus make a direct check that the ultrasonic measurements do indeed give the correct bulk modulus for at least one of these ceramic materials. The ultrasonic wave velocities and bulk modulus B_o measured in the polycrystalline La_2CuO_{4-y} sample [V_L = 4906 m/s, V_S = 2978 m/s and B_o^m = 87GPa] are in reasonable agreement with those determined from elastic constant measurements in single crystal La_2CuO_{4-y} [V_L = 5050 m/s, V_S = 3260 m/s and B_o^m = 112GPa]. This observation lends strong support to the suggestion that for these mixed oxide ceramics the true bulk modulus at atmospheric pressure is the one B_o derived from ultrasonic measurements rather than that $B^T(P)$ obtained from X-ray experiments at very high pressures.

The apparent discrepancy between B_o and $B^T(P)$ is found to be a common characteristic of all these materials and can be resolved by taking the contribution of $(\partial B/\partial P)_{P=O}$ to the high pressure bulk modulus into account in $B^T(P)$. To reconcile $B^T(P)$ with B_o , the values for B_o and $(\partial B/\partial P)_{P=O}$ determined ultrasonically have been used to estimate the bulk modulus $B(P)$ at pressure P which can be written as

$$B(P) = B_o + P(\partial B/\partial P)_{P=O} \qquad (11.1)$$

to a first approximation. To make this estimation, the pressure P has been used as an approximate lower limit of the pressures employed in the corresponding high pressure diamond cell studies (table 11.1). There is reasonable agreement between the calculated values of $B(P)$ and the data for $B^T(P)$ inferred from the X-ray measurements of the pressure dependence of the lattice parameters (table 11.1). This reinforces the suggestion [Cankurtaran et al (1989a)] that the substantial differences between B_o and $B^T(P)$ arise from the large pressure derivative $(\partial B/\partial P)_{P=0}$. At the high pressures involved in the diamond cell experiments the unit cell volume is substantially reduced: the bulk moduli $B^T(P)$ reported by Fietz et al (1987, 1989), Jaya et al (1988), Aleksandrov et al (1988), Ecke et al (1988), Akhtar et al (1988), Wijngaarden and Griessen (1989) and Olsen et al (1988) correspond to values for the material under high compression, which enhances the bulk moduli and in addition causes $(\partial B/\partial P)$ to be a pressure dependent quantity, decreasing with pressure as measurements of $(\partial^2 B/\partial P^2)$ showed [Cankurtaran et al (1989a, b)]. Furthermore the lattice parameter measurements are independent of porosity. Hence the accord found between $B(P)$ and $B^T(P)$ obtained by the two entirely different experimental methods adds further support to: (i) the use of equations (4.4) and (4.5), and the theory on which they are based

[Cankurtaran et al (1989a)], to take into account the effects of porosity in the determinations of the elastic properties under pressure, (ii) the suggestion that ultrasonic measurements do give the true bulk modulus at atmospheric pressure for these mixed oxides. Further support comes from a theoretical calculation [Ramakrishnan and Krishnamurthy (1991)] of the elastic stiffness moduli which predicts similar sound wave velocities for polycrystalline $YBa_2Cu_3O_{7-x}$. For single-crystal $YBa_2Cu_3O_{7-x}$ a comparable value for an average longitudinal wave velocity of $4460ms^{-1}$ was obtained [Fanggao et al (1991a)] from published data [Kim et al (1990)]; the single-crystal ultrasonic wave velocity measurements of Saint-Paul et al (1991) are in accord with this. These observations evidence that the ultrasonic technique measures correct sound wave velocities for the ceramics.

The hydrostatic pressure derivative $(\partial B/\partial P)_{P=0}$ (=15.6) at room temperature for the non-porous matrix of $Nd_{1.85}Ce_{0.15}CuO_{4-y}$ was found to be substantially smaller than those of other mixed oxide ceramics including $YBa_2Cu_3O_{7-x}$ and $GdBa_2Cu_3O_{7-x}$ (table 11.2). This could be due to:

(a) $YBa_2Cu_3O_{7-x}$ and $GdBa_2Cu_3O_{7-x}$ are defect structure compounds having low anion/cation ratios for perovskite-like materials: they contain O_{7-x} rather than the O_9 in AB_3O_9. Such

Table 11.2. The ultrasonic wave velocities, the elastic constants and their hydrostatic pressure derivatives for the high temperature superconducting compounds studied in this work. All data are corrected for the effects of porosity using equations 4.4 and 4.5, with the exception of the data obtained for the $YBa_2Cu_3O_{7-X}$ sample prepared by the halide flux technique.

Material	Density (kg/m^3)	Porosity (%)	Ultrasonic wave velocities (m/s)		B_o (GPa)	C_L (GPa)	C_S (GPa)	E (GPa)	σ	$\left(\frac{\partial B}{\partial P}\right)_{P=0}$	$\left(\frac{\partial C_L}{\partial P}\right)_{P=0}$	$\left(\frac{\partial C_S}{\partial P}\right)_{P=0}$
			longitudinal	shear								
$YBa_2Cu_3O_{7-X}$ (Y2)	5985	0.056	4658	2986	62	138	57	130	0.151	118	162	33
$YBa_2Cu_3O_{7-X}$ (Y1)	5199	0.18	4564	2837	64	132	51	121	0.185	111	136	19
$YBa_2Cu_3O_{7-X}$ (halide flux grown sample)	5720	0.097	4354	-	-	108	-	-	-	-	40	-
$GdBa_2Cu_3O_{7-X}$ (orthorhombic)	5549	0.22	4710	2700	89	158	52	131	0.255	55	56	0.8
$GdBa_2Cu_3O_{7-X}$ (tetragonal)	5174	0.23	4356	2422	74.7	127	39.3	100	0.276	52	52	0.3
$Nd_{1.85}Ce_{0.15}CuO_{4-y}$	6481	0.12	5010	3045	93	184	68	164	0.207	15.6	18.3	1.9
Nd_2CuO_{4-y}	6425	0.13	5069	2824	110	189	59	150	0.275	29.1	36	4.0
$La_{1.8}Sr_{0.2}CuO_{4-y}$	6000	0.16	5206	3245	93	193	75	177	0.182	36	37	0.9
La_2CuO_{4-y}	6495	0.09	4906	2978	87	171	63	152	0.210	28.7	32	2.7
Bi(Pb)2223 (sample 1)	4953	0.22	3343	2483	18.9	71.6	39.5	70	-0.116	59	63	3.1
Bi(Pb)2223 (sample 2)	4936	0.23	3469	2520	22.9	77.1	40.7	76.5	-0.058	39.3	48.6	4.5
Bi(Pb)2212	5110	0.23	3342	2325	26.4	74.4	36	74.3	0.032	40	52	9.5

sited vacancy compounds tend to have a reduced bulk modulus [Saunders and Seddon (1976)] and an enhanced $(\partial B/\partial P)_{P=0}$ [Tu Hailing et al (1982)]. The measured bulk moduli B_o of $Nd_{1.85}Ce_{0.15}CuO_{4-y}$ and Nd_2CuO_{4-y} are larger than those of $YBa_2Cu_3O_{7-x}$ and $GdBa_2Cu_3O_{7-x}$ (table 11.1). This feature and the substantially smaller $(\partial B/\partial P)_{P=0}$ are consistent with the fact that $Nd_{1.85}Ce_{0.15}CuO_{4-y}$ and Nd_2CuO_{4-y} are not sited vacancy compounds in the sense that $YBa_2Cu_3O_{7-x}$ and $GdBa_2Cu_3O_{7-x}$ are. Furthermore the concentration of oxygen vacancies in $Nd_{1.85}Ce_{0.15}CuO_{4-y}$ is small. The presence of the cerium dopant makes the structure less inclined to oxygen deficiency than Nd_2CuO_{4-y}, the deficiency y in $Nd_{1.85}Ce_{0.15}CuO_{4-y}$ being only about 0.04 [Takagi et al (1989)]. This feature could be in part responsible for the difference between the values of $(\partial B/\partial P)_{P=0}$ obtained for $Nd_{1.85}Ce_{0.15}CuO_{4-y}$ and Nd_2CuO_{4-y} (table 11.2).

(b) Application of pressure to these cuprates can alter Cu ion valence and affect $(\partial B/\partial P)_{P=0}$. For $YBa_2Cu_3O_{7-x}$ the copper has an average valence of 2.33+ and in the oxygen deficient $YBa_2Cu_3O_{7-x}$ it has a value of (7-2x)/3; application of pressure leads to an increase in copper valence and a decrease in copper ion size - enhancing $(\partial B/\partial P)_{P=0}$. However, in the case of $Nd_{2-x}Ce_xCuO_{4-y}$ doping with Ce^{4+} introduces electrons which fill the 3d holes on the Cu atoms, thus converting some Cu^{2+} ions to Cu^{+} [for full discussion see Fanggao et al (1990a)].

Application of pressure forces the intermediate valence Ce^{3+z} in the direction of Ce^{4+} (thus reducing the mean Ce ion size) taking more Cu^{2+} ions to Cu^{+}. Thus volume reduction due to an increasing valence of Ce will be compensated by a volume increase of the Cu ions. Hence any enhancement of $(\partial B/\partial P)_{P-O}$ due to pressure induced increase in the Ce^{3+z} ion intermediate valence may well be partially cancelled out for $Nd_{1.85}Ce_{0.15}CuO_{4-y}$ and may account to some extent for its much smaller $(\partial B/\partial P)_{P-O}$ than that of $YBa_2Cu_3O_{7-x}$.

The Smaller value for $(\partial B/\partial P)_{P-O}$ in $Nd_{1.85}Ce_{0.15}CuO_{4-y}$ (table 11.2) reinforces the proposal that very large values of $(\partial B/\partial P)_{P-O}$ are intrinsic properties of $YBa_2Cu_3O_{7-x}$ and $GdBa_2Cu_3O_{7-x}$ rather than merely being a result of the application of pressure to a porous ceramic. Further confirmation comes from measurements in a very large grained sample of $YBa_2Cu_3O_{7-x}$ (grown by the eutectic KCl-NaCl flux technique) of the longitudinal ultrasonic wave velocity and its pressure dependence giving values of 108GPa for C_L and 40 for $(\partial C_L/\partial P)_{P-O}$-in the same range as those for ceramic materials (table 11.2). Further support for the suggestion that a large value of $(\partial B/\partial P)_{P-O}$ is an intrinsic property of $YBa_2Cu_3O_{7-x}$ comes from the measurements of the ultrasonic wave velocities as a function of hydrostatic pressure in a very dense sample of this compound (having a porosity of 0.042) [Cankurtaran

et al (1992)]. The ultrasonic wave velocities and the elastic constants derived from them for this dense, comparatively small-grained $YBa_2Cu_3O_{7-x}$ ceramic sample at room temperature fall within the range of values measured on both coarse-grained (sample Y2) and fine-grained (sample Y1) ceramic materials and a very large-grained halide flux-grown specimen.

For the $La_{1.8}Sr_{0.2}CuO_{4-y}$ sample studied in this work, $(\partial B/\partial P)_{P-0}$ is higher than that of $Nd_{1.85}Ce_{0.15}CuO_{4-y}$ but much smaller than that of $YBa_2Cu_3O_{7-x}$ and $GdBa_2Cu_3O_{7-x}$ (table 11.2). An explanation of the physical origin of the comparatively large $(\partial B/\partial P)_{P-0}$ for the $La_{1.8}Sr_{0.2}CuO_{4-y}$ compound could be based on the fact that the apical Cu-O bond length was shown to be sensitive on application of pressure. Pei et al (1990) observed a monotonic decrease of the apical Cu-O bond with pressure (in the range 0-0.53GPa) in $La_{1.85}Sr_{0.15}CuO_4$. The rate of decrease was found to be roughly twice as large as the cell compression along the same direction (c-axis). The observation that the compression of this bond is significantly larger than the corresponding cell compression suggests that the applied pressure may indeed induce a redistribution of charge. A shorter bond indicates an increase of the mean valence of the copper ions. Since the higher valent ions should be smaller than the lower valent ones, coupling to

the lattice can be expected to be strong for longitudinal phonon modes, which alter the unit cell volume but not for shear modes. Hence if pressure dependent valence is involved in $La_{1.8}Sr_{0.2}CuO_4$, then $(\partial C_L/\partial P)_{P\text{-}0}$ [and hence also $(\partial B/\partial P)_{P\text{-}0}$] would be expected to be much larger than $(\partial C_S/\partial P)_{P\text{-}0}$, and they are (table 11.2). The bulk modulus B_o of $La_{1.8}Sr_{0.2}CuO_4$ is rather small (table 11.1) (compared for example with that (139.4GPa) of $BaTiO_3$ [Ishidate and Sasaki (1989)]): this material shows the feature common to intermediate valence materials [Yogurtcu et al (1985)] of being highly compressible. Thus the volume changes in $La_{1.8}Sr_{0.2}CuO_4$ under pressure as measured by the bulk modulus and its pressure derivative (table 11.2) are consistent with pressure dependent intermediate valence Cu^{2+z} associated with Cu 3d electrons.

Tetragonal $GdBa_2Cu_3O_{7-x}$ has a smaller bulk modulus than that of the orthorhombic phase (table 11.1). A neutron diffraction investigation of $YBa_2Cu_3O_{7-x}$ at high pressure [Glazkov et al (1988)] showed a strong increase in the compression along the c-axis as a result of loss of oxygen from the tetragonal phase. This was attributed to a preferential weakening of the oxygen bonds along the c-axis; this is in agreement with an increase in the c-axis parameter [Tokura et al (1989)] on transformation from the orthorhombic

to the tetragonal form. It is also reported that the compressibility is strongly dependent on the oxygen content, and the compressibility of tetragonal form is higher than that of orthorhombic phase; a result which implies a smaller bulk modulus in the tetragonal phase than that in the orthorhombic phase as found here for $GdBa_2Cu_3O_{7-x}$ (table 11.1). The open nature of the oxygen framework has a dominant influence on the compressibility of oxide superconductors.

For the Bi-based cuprates samples, the ultrasonically determined bulk modulus even after correction (B_o^m) is also smaller than $B^T(P)$ determined at high pressure X-ray experiments. This can, in large extent, be attributed to the open microstructure of the bismuth cuprate ceramics. The bulk modulus B_o^m of the Bi(Pb)2212 ceramic (=26.4GPa) is much smaller than that ($B^T(P)$ =73GPa) determined [Tajima et al (1989)] from X-ray measurements of the pressure dependence of the lattice parameters. To reconcile $B^T(P)$ with B_o, the ultrasonically determined values for B_o and $(\partial B/\partial P)_{P-0}$ were used to estimate the bulk modulus $B(P)$ at pressure P using equation 11.1. Inserting 1.00GPa, as an approximate lower limit of the pressures employed in the high pressure diamond cell studies, into that equation gives 66GPa for $B(P)$ which is in reasonable agreement with the value of $B^T(P)$ (=73GPa) inferred from the X-ray measurements of the pressure

dependence of the lattice parameters [Tajima et al (1989)]. Hence the substantial differences between B_o and $B^T(P)$ result from the large magnitude of the pressure derivative $(\partial B/\partial P)_{P=0}$.

In addition to their layer-like nature there is a second feature of the Bi-based cuprates, namely the intermediate valence of the copper ions, which could in part lead to their small elastic stiffnesses and large values of the pressure derivatives. In the Bi2212 phase the copper ion valence is about +2.3 [Cheetham et al (1988)]. X-ray powder spectra studies indicate that in the Bi2223 phase both the Cu and Bi ions are in mixed valence states: there are valence fluctuations between the ionic states (Cu^{2+} and Cu^{3+}) and also (Bi^{3+} and Bi^{5+}) [Schwarz (1990)]. Fluctuating copper valence is a characteristic feature of all the high T_c cuprates and may have pronounced effects on their elastic and nonlinear acoustic properties [Kim et al (1988b)]. A small, or even negative Poisson's ratio, and a small bulk modulus are characteristic features of compounds in intermediate valence state [Boppart et al (1983), Mook and Holtzberg (1981), Hailing et al (1984) and Yogurtcu et al (1985)]. As mentioned earlier, since higher valent ions are smaller than the lower valent ones, coupling to the lattice is strong for the longitudinal phonons which alter the unit

cell volume. This is not so for the shear modes. Furthermore the effects of pressure on the longitudinal mode velocity are necessarily large because both the intermediate valence and ion size alter under compression. Therefore the effects expected from fluctuating valence are a large $(\partial C_L/\partial P)_{P\text{-}O}$ but a small $(\partial C_S/\partial P)_{P\text{-}O}$, as found experimentally for the bismuth cuprates and for the other related materials (table 11.2). Hence the small longitudinal and bulk moduli and their large pressure dependences are consistent with that fluctuating valence leads to softening the longitudinal acoustic modes. It is interesting that the Bi-based compounds are the most elastically soft of all the high T_c cuprates examined to date yet have very high T_c's . The intriguing fundamental question remains: are the fluctuating valence, and possibly also the consequent longitudinal phonon softening, related to the superconducting pairing interaction?

There are inconsistencies between the bulk modulus values obtained by the X-ray method for $YBa_2Cu_3O_{7-x}$. From experiments made up to a comparatively low pressure of 6GPa for diamond cell X-ray work, Jaya et al (1988) obtained the value of 95GPa for $B^T(P)$. Aleksandrov et al (1988) report a value of 115GPa for monocrystalline $YBa_2Cu_3O_{7-x}$ up to 20GPa. Fietz et al (1987) give 180GPa from measurements up to 14GPa. These differences between the X-ray bulk modulus data may be

experimental in origin or they could be real and reflect the highly pressure dependent nature of the bulk modulus. Hence the question as to whether the true bulk modulus of $YBa_2Cu_3O_{7-x}$, and also of the other mixed oxide ceramics, is the smaller value determined from ultrasonic data at atmospheric pressure or the much larger one obtained from high pressure lattice parameter data remains unresolved and its answer requires further investigation.

Finally, a very important review of the bulk modulus and its pressure derivative obtained by different groups for the high temperature superconducting compounds were presented by Fietz et al (1992). They discussed the discrepancies between the results obtained from ultrasonic techniques with those obtained by high pressure diamond cell. They concluded that the correct bulk moduli of these high temperature superconducting compounds are not known, but a higher oxygen content seems to give a higher bulk modulus. They attributed the discrepancies between the results to non-hydrostatic pressure components, errors in the pressure calibration, errors in interpreting the complex spectra of these materials, oxygen ordering effects or problems with the sample quality.

11.4 GRÜNEISEN PARAMETERS AND THE VIBRATIONAL ANHARMONICITY OF THE LONG WAVELENGTH ACOUSTIC MODES IN HIGH TEMPERATURE SUPERCONDUCTING COMPOUNDS

Vibrational anharmonicity is responsible for physical phenomena, which depend upon atomic motion, such as nonlinear acoustic properties, including phonon-phonon interactions and thermal expansion. In the context of *BCS* theory, Müller (1990) has pointed out that anharmonic motion of ions could generate a large electron-phonon coupling constant and that this is possible for $YBa_2Cu_3O_{7-x}$ via anharmonic coupling of pyramidal apex oxygen O(1) motion along the c-axis direction. In addition to being responsible for a large anharmonicity of the corresponding optic modes, such motion would affect the acoustic modes. The measurements of the pressure derivatives of the elastic constants enable an assessment of the magnitudes of the anharmonicities associated with the long wavelength acoustic modes.

There is strong evidence for pronounced vibrational anharmonicity of the long wavelength acoustic phonons in the high T_c cuprates [Cankurtaran et al (1989a, b and 1990b), Jiang and Breazeale (1990), Fanggao et al (1990a)]. In each of these materials, with the exception of $Nd_{1.85}Ce_{0.15}CuO_{4-y}$, the anharmonicity of the longitudinal modes is large, particularly for $YBa_2Cu_3O_{7-x}$.

The nonlinear acoustic properties of a solid are usually expressed in terms of higher order elastic constants which quantify the coefficients $(\partial^3 U(\eta)/\partial\eta_{ab}\partial\eta_{cd}\partial\eta_{ef})_{\eta=0}$ of the cubic term in the expansion of the strain energy density $U(\eta)$ with respect to the Lagrangian strain η and thus the leading term in the vibrational anharmonicity of the long wavelength acoustic phonons [Barron et al (1980)]. If these polycrystalline ceramics are treated as isotropic bodies, the two independent measurements of the pressure dependences of the velocities of longitudinal and shear ultrasonic waves provide two combinations of the third order elastic constants. These can be written in the form

$$(\partial C_S/\partial P)_{P=0} = -\frac{(C_L + 2C_{12} + C_S + C_{144} + 2C_{166})}{(C_L + 2C_{12})} \qquad (11.2)$$

$$(\partial B/\partial P)_{P=0} = -\frac{(C_{111} + 6C_{112} + 2C_{123})}{9B} \qquad (11.3)$$

These third order elastic constant combinations and the data used to calculate them are collected in table 11.3. Although the fine and coarse grained ceramic $YBa_2Cu_3O_{7-x}$ materials have widely different porosities, 0.18 and 0.056 respectively, after correction for the effects of this porosity the elastic properties and their behaviour under pressure are very similar for their non-porous matrices: this provides further

striking evidence for the validity of the model [Cankurtaran et al (1989a)] used to describe wave propagation in these porous media. The combination $(C_{111}+6C_{112}+2C_{123})$ is much larger than $(C_{144}+2C_{166})$ reflecting the much greater effect of pressure on the longitudinal than on the shear wave velocity in all of these materials. The value of $(C_{111}+6C_{112}+2C_{123})$ is much greater for $YBa_2Cu_3O_{7-x}$, and to a somewhat lesser extent for $GdBa_2Cu_3O_{7-x}$, than for the other oxides. In fact it is interesting to note the trend for the superconductors that there is a tendency that the greater the vibrational anharmonicity the higher is T_c in line with Müller's comment [Müller (1990)] that anharmonic motion could generate a large coupling constant.

In addition to being responsible for the nonlinear elastic behaviour of a solid under finite strain, the anharmonicity of lattice vibrations also causes thermal expansion. The thermal and acoustic properties of these materials can be linked by the Grüneisen parameter approach. The Grüneisen parameters for the longitudinal (γ_L) and shear (γ_S) acoustic modes in the long wavelength limit have been calculated from the elastic constants and their hydrostatic pressure derivatives using

$$\gamma_L = -\frac{B_o}{6C_L}\left[3-\left(\frac{2C_{12}}{B_o}\right)-3\left(\frac{dB}{dP}\right)-4\left(\frac{dC_S}{dP}\right)\right] \quad (11.4)$$

$$\gamma_S = -\frac{1}{6C_S}\left[2C_S-3B_o\left(\frac{dC_S}{dP}\right)-\frac{3}{2B_o}+\frac{3}{2}C_{12}\right] \quad (11.5)$$

The results, together with those for the mean long wavelength acoustic mode Grüneisen parameter

$$\gamma^{el} = \frac{(\gamma_L + 2\gamma_S)}{3} \quad (11.6)$$

are collected in table 11.3. The mean long wavelength acoustic mode Grüneisen parameter ranges between 2.2 and 3.8 for the non-porous forms of $Nd_{1.85}Ce_{0.15}CuO_{4-y}$, $La_{1.8}Sr_{0.2}CuO_{4-y}$, La_2CuO_{4-y} and Bi(Pb)2223. These values lie in the normal range for crystalline solids in contrast to those for γ^{el} of both fine and coarse grained samples of $YBa_2Cu_3O_{7-x}$ (table 11.3). In the case of $GdBa_2Cu_3O_{7-x}$, although its $(\partial B/\partial P)_{P-0}$ and $(\partial C_L/\partial P)_{P-0}$ are also large [Cankurtaran et al (1989b)], γ^{el} (=5.5) is substantially smaller than that of $YBa_2Cu_3O_{7-x}$. Hence the relatively small (and "normal") magnitudes of γ^{th} do not always concur with the proposition [Swenson et al (1989)] that the elastic constants for ceramic specimen have a normal pressure dependence. Nevertheless the difference between γ^{el} and γ^{th} found for $YBa_2Cu_3O_{7-x}$ remains unexplained [Swenson et al (1989)]. However there is mounting evidence for pronounced

Table 11.3. Comparison for the mixed oxide materials between the vibrational anharmonicities of long wavelength acoustic modes expressed in terms of third order elastic constants combinations and Grüneisen parameters.

Material	B_o (GPa)	C_L (GPa)	C_S (GPa)	C_{12} (GPa)	$\left(\frac{\partial B}{\partial P}\right)_{P=0}$	$\left(\frac{\partial C_S}{\partial P}\right)_{P=0}$	$(C_{111}+6C_{112}+2C_{123})$	$(C_{144}+2C_{166})$	γ_L	γ_S	γ'
$YBa_2Cu_3O_{7-X}$ (Y2)	62	138	57	24	118	33	-65844	-6381	36.2	17.8	23.9
$YBa_2Cu_3O_{7-X}$ (Y1)	64	132	51	30	111	19	-63936	-3891	32.9	11.7	18.8
$GdBa_2Cu_3O_{7-X}$ (orthorhombic)	89	158	52	54	55	0.8	-44055	-531	15.6	0.5	5.5
$GdBa_2Cu_3O_{7-X}$ (tetragonal)	75	127	39.3	48.4	52	0.3	-34960	-323	15.2	0.10	5.1
$Nd_{1.85}Ce_{0.15}CuO_{4-y}$	93	184	68	48	15.6	1.9	-13057	-880	4.7	1.13	2.3
Nd_2CuO_{4-y}	110	189	59	73	29.1	4.0	-28809	-1734	9.9	3.5	5.6
$La_{1.8}Sr_{0.2}CuO_{4-y}$	93	193	75	44	36	0.9	-30132	-609	8.8	0.4	3.2
La_2CuO_{4-y}	87	171	63	45	28.7	2.7	-22472	-1029	8.0	1.7	3.8
Bi(Pb)2223 (sample 1)	18.9	71.6	39.5	-7.4	59	3.1	-10036	-272	8.2	0.6	3.1
Bi(Pb)2223 (sample 2)	22.9	77.1	40.7	-4.3	39.3	4.5	-8100	-417	6.6	0.6	2.6
Bi(Pb)2212	26.4	74.4	36	2.2	40	9.5	-9504	-863	9.2	3.3	5.3

vibrational anharmonicity in $YBa_2Cu_3O_{7-x}$, and there have been many reports of phonon mode softening [Marsh et al (1988), Williams et al (1988), Genzel et al (1989), Vass et al (1990)].

From a joint X-ray/neutron study of the $YBa_2Cu_3O_{7-x}$ structure it has been found that the Ba, Cu(2) and O(2) ions have large and nearly equal values of the thermal Grüneisen parameter along the c-axis, suggesting that there could be a high degree of concerted motion of these ions, possibly as a low frequency optic mode [Williams et al (1988)]. Thus it appears that in $YBa_2Cu_3O_{7-x}$ the vibrational anharmonicity of certain optic and long wavelength acoustic phonons is large; this could be due to optic phonon-acoustic phonon interactions. A large $(\partial B/\partial P)_{P\text{-}O}$ is consistent with such lattice dynamical properties. Certainly it can be anticipated that the pronounced phonon anharmonicity must have a substantial influence on the individual mode Grüneisen parameters.

11.5 CONCLUSIONS

[I] The hydrostatic pressure dependences of the ultrasonic wave velocities in the fine grained sample of $YBa_2Cu_3O_{7-x}$ show a non-linear behaviour while the behaviour is linear in the halide flux grown sample of $YBa_2Cu_3O_{7-x}$ indicating the effects of the microstructure on the elastic properties of these compounds. The hydrostatic pressure dependences of the ultrasonic wave velocities in the orthorhombic fine grained sample of $GdBa_2Cu_3O_{7-x}$ show a non-linear behaviour while the behaviour is linear in the tetragonal phase. This might be due to the effect of removing an oxygen atom to produce the tetragonal phase which indicates the importance of the effects of this factor (removing of the oxygen atoms) on the elastic properties of these compounds. In contrast to the non-linear behaviour found in orthorhombic fine grained samples of $YBa_2Cu_3O_{7-x}$ and $GdBa_2Cu_3O_{7-x}$, the pressure dependences of the ultrasonic wave velocities in $Nd_{1.85}Ce_{0.15}CuO_{4-y}$ and $La_{1.8}Sr_{0.2}CuO_{4-y}$ are found to be linear indicating that the higher order vibrational anharmonicity associated with multi-phonon processes of the long wavelength phonons is much less. Another behaviour in the pressure dependences of the ultrasonic wave velocities have been observed in the

Bi(Pb)2223 compound where a discontinuity in the slope is found at around 0.03GPa. It seems that the first effect of pressure is to reduce the pore volume and increase the adhesion between the plate-like grains. This change in slope was not found in the Pb doped and undoped samples of Bi2212 compound, possibly due to microstructural differences.

[II] Thermal hysteresis has been found in the temperature dependences of ultrasonic wave velocities of $YBa_2Cu_3O_{7-x}$ samples. However, this thermal hysteresis has been found in different temperature ranges for different samples. Thermal hysteresis is also been observed in orthorhombic $GdBa_2Cu_3O_{7-x}$ sample but it is absent in the tetragonal phase which again indicates the importance of the oxygen stoichiometry in the determination of the elastic behaviour of these compounds. This is also true for the Bi2212 sample 2 where quenching the sample supresses the thermal hysteresis found in the sample before quenching. The thermal hysteresis observed in the Bi2212 samples is absent in the Pb doped phase of that compound. This observation indicates that the anomalous hysteretic behaviour may not be an inherent property of Bi-based cuprates, but rather may depend on doping and/or sample preparation. Measurements of

the behaviour of the ultrasonic wave velocities of $Nd_{1.85}Ce_{0.15}CuO_{4-y}$ with temperature show no thermal hysteresis. The change in gradient near 220K is attributed to the intermediate valence state of the cerium ion. The parent Nd_2CuO_{4-y} sample does not show the pronounced change in slope in ultrasonic wave velocity around 220K; however, it does show quite marked hysteresis in the temperature range 200-290K. Another compound investigated here having a fascinating ultrasonic behaviour is $La_{1.8}Sr_{0.2}CuO_{4-y}$. This compound shows extreme acoustic mode softening below room temperature with no thermal hysteresis in the temperature range 10-300K. However, the parent compound La_2CuO_{4-y} does not show this elastic softening in the temperature dependences of the ultrasonic wave velocities. The thermal hysteresis found in these compounds has been attributed to a structural phase transition.

[III] A theoretical model to correct the experimental results for the effects of porosity has been developed and used extensively throughout this work. The results obtained for all the compounds studied here have been corrected for the effect of porosity using this model. It has been found that the effect of porosity is to reduce the ultrasonic wave velocities and therefore the elastic

constants. One important experimental proof for the validity of this theoretical model comes from the measurements of the elastic constants in single crystal La_2CuO_4 by Migliori et al (1990) which are in good agreement with those obtained here for the ceramic sample of La_2CuO_4. This confirms that the ultrasonic wave velocity measurements after corrections for the effects of porosity do give correct data for the second order elastic stiffnesses including the bulk modulus for ceramic specimens. That this is also true for $YBa_2Cu_3O_{7-x}$ is strongly suggested by the agreement found for this material at low temperatures between the Debye temperatures (Θ_D^{el}) and (Θ_D) obtained respectively from the ultrasonic measurements and from the specific heat data [Swenson et al (1989) and Collocot et al (1987)]. Further support for this is provided by the finding that the value of C_L for the large grained alkali halide flux grown $YBa_2Cu_3O_{7-x}$ and the average longitudinal velocity of single crystal $YBa_2Cu_3O_{7-x}$ are comparable with those of ceramic materials (table 11.2). Hence it has been considered that the true bulk modulus for these materials is closer to that (B_o) determined at

atmospheric pressure from ultrasonic wave velocity measurements rather than that ($B^T(P)$) obtained at very high pressures using diamond cell techniques.

[IV] $YBa_2Cu_3O_{7-x}$ and $GdBa_2Cu_3O_{7-x}$ compounds have been found to be softer than $Nd_{1.85}Ce_{0.15}CuO_{4-y}$ and $La_{1.8}Sr_{0.2}CuO_{4-y}$ compounds (by comparing the elastic constants obtained for these compounds in table 11.2). However, the hydrostatic pressure derivatives of the elastic constants in $YBa_2Cu_3O_{7-x}$ and $GdBa_2Cu_3O_{7-x}$ are larger than those of $Nd_{1.85}Ce_{0.15}CuO_{4-y}$ and $La_{1.8}Sr_{0.2}CuO_{4-y}$. On the other hand, Bi-based cuprates are found to be softer than all the other high T_c superconducting compounds studied here. However, the hydrostatic pressure derivatives of their elastic constants are similar to those of $YBa_2Cu_3O_{7-x}$ and $GdBa_2Cu_3O_{7-x}$ and larger than those of $Nd_{1.85}Ce_{0.15}CuO_{4-y}$ and $La_{1.8}Sr_{0.2}CuO_{4-y}$.

[V] The apparent discrepancy between B_o and $B^T(P)$ is found to be a common characteristic of all these mixed oxide materials and has been resolved by taking the contribution of $(\partial B/\partial P)_{P\text{-}O}$ to the high pressure bulk modulus into account (table 11.1).

[VI] As for the other mixed oxides based on copper, which show high T_c superconductivity, the hydrostatic pressure derivatives $(\partial C_L/\partial P)_{P\text{-}O}$ and $(\partial B/\partial P)_{P\text{-}O}$ of the bismuth

cuprates are large, partially due to their open microstructure on the macroscopic level. However these large effects also have an intrinsic origin indicating pronounced vibrational anharmonicity associated with long wavelength longitudinal acoustic phonons due in part to (i) the rather open layer-like structure of the Bi-based cuprates with weak inter-layer binding forces and (ii) the intermediate valence state of the copper ions.

[VII] The hydrostatic pressure derivatives $(\partial B/\partial P)_{P=0}$ (=15.6) and $(\partial C_L/\partial P)_{P=0}$ (=18.3) at room temperature for the non-porous matrix of $Nd_{1.85}Ce_{0.15}CuO_{4-y}$ are found to be substantially smaller than those of other mixed oxide ceramics, showing that large values of these quantities are not simply a result of porosity. Hence the very large values of $(\partial B/\partial P)_{P=0}$ and $(\partial C_L/\partial P)_{P=0}$ found for $YBa_2Cu_3O_{7-x}$ and $GdBa_2Cu_3O_{7-x}$ are probably intrinsic properties rather than being just a result of the application of pressure to a porous ceramic. Strong evidence in support of this proposal is provided by the finding of a large value of $(\partial C_L/\partial P)_{P=0}$ for the large grained, alkali halide flux grown $YBa_2Cu_3O_{7-x}$ (table 11.2).

[VII I] **In all the high T_c superconducting compounds studied here, with the exception of $Nd_{1.85}Ce_{0.15}CuO_{4-y}$, the vibrational anharmonicity of the long wavelength longitudinal acoustic phonons is large, particularly for $YBa_2Cu_3O_{7-x}$.**

REFERENCES

1 Akhtar M J, Catlow C R A, Clark S M and Temmerman W M (1988), J. Phys. C: Solid State Phys. *21*, L917.

2 Akhtar M J, Akhtar Z N and Catlow (1990), J. Phys.: Condens. Matter *2*, 3231.

3 Aleksandrov I V, Goncharov A F and Stishov S (1988), JETP Lett. *47*, 428.

4 Allan N L and Mackrodt W C (1988), Phil. Mag. *A58*, 555.

5 Allan N L, Lawton J M and Mackrodt W C (1989), Phil. Mag. *B59*, 191.

6 Almond D P, Lambson E, Saunders G A and Hong W (1987), J. Phys. F: Met. Phys. *17*, L221.

7 Almond D P, Chapman B and Saunders G A (1988), Supercond. Sci. Technol. *1*, 123.

8 Almond D P, Wang Q, Freestone J, Lambson E F, Chapman B and Saunders G A (1989), J. Phys. Condens. Matter *1*, 6853.

9 Almond D P, Fanggao C, Ford P J and Saunders G A (1990), Supercond. Sci. Technol. *3*, 583.

10 Axe J D, Moudden A H, Hohlwein D, Cox D E, Mohanty K M, Moodenbaugh A R and Xu Y (1989), Phys. Rev. Lett. *62*, 2751.

11 Baetzold R C (1990), Phys. Rev. *B42*, 56.

12 Bardeen J, Cooper L N and Schrieffer J R (1957), Phys. Rev. *108*, 1175.

13 Barron T H K, Collins J G and White G K (1980), Adv. Phys. *29*, 609.

14 Bateman T B (1966), J. Acous. Soc. Amer. *41*, 1011.

15 Bednorz J G and Müller K A (1986), Z. Phys. *B64*, 189.

16 Bhattacharya S, Higgins M J, Johnston D C, Jacobson A J, Stokes J P, Goshorn D P and Lewandowski J T (1988), Phys. Rev. Lett. *60*, 1181.

17 Bishop D J, Gammel P L, Ramirez A P, Cava R J, Batlogg B and Rietman E A (1987a), Phys. Rev. *B35*, 8788.

18 Bishop D J, Ramirez A P, Gammel P L, Batlogg B, Rietman E A, Cava R J and Millis A J (1987b), Phys. Rev. *B36*, 2408.

19 Block S, Piermarini G J, Munro R G and Wong-Ng W (1987), Advanced Ceramic Materials *2*, 601.

20 Boppart H, Rehwald W, Kaldis E and Wachter P (1983), Physica *B+C 117-118*, 564.

21 Bordet P, Capponi J J, Chaillout C, Chenavas J, Hewat A W, Hewat E A, Hodeau J L, Marezio M, Tholence J L and Tranqui D (1988), Physica *C156*, 189.

22 Bourne L C, Zettl A, Chang K J, Cohen M L, Stacy A M and Ham W K (1987), Phys. Rev. *B35*, 8785.

23 Bradley C C (1969), High Pressure Methods in Solid State Research, (Butterworth, London).

24 Brassington M P (1982), Ph.D. Thesis, University of Bath.

25 Bridgman P W (1911), Proc. Amer. Acad. Arts Sci. *47*, 321.

26 Bridgman P W (1958), The Physics of High Pressure, (Bell and Sons, London).

27 Brown S E, Migliori A and Fisk Z (1988), Solid State Commun. *65*, 483.

28 Cankurtaran M, Saunders G A, Willis J R, Al-khef-faji A and Almond D P (1989a), Phys. Rev. *B39*, 2872.

29 Cankurtaran M, Saunders G A, Almond D P, Al-Khef-faji A, Lambson E F and Draper R C J (1989b) J. Phys: Condensed Matter *1*, 9067.

30 Cankurtaran M, Saunders G A, Almond D P, Al-Khef-faji A Freestone J, Wang Q and Lambson E F (1990a), Physics and Materials Science of High Temperature Superconductors, edited by Kossowsky R, Methfessel S and Wholleben D (Kluwer Academic, Dordrecht), 627.

31 Cankurtaran M, Al-Kheffaji A, Saunders G A, Almond D P, Freestone J (1990b), Supercond. Sci. Technol. *3*, 76.

32 Cankurtaran M, Saunders G A, Goretta K C and Poeppel R B (1992), to be published in Phys. Rev. B.

33 Cannelli G, Cantelli R and Cordero F (1988), Phys. Rev. *B38*, 7200.

34 Cava R J, Van Dover R B, Batlogg B and Rietman (1987a), Phys. Rev. Lett. *58*, 408.

35 Cava R J, Battlog B, Vandover R B, Murphy D N, Sunshine S, Siegrist T, Remeika J P, Rietman E A, Zahurak S and Espinosa G R (1987b), Phys. Rev. Lett. *58*, 1676.

36 Cava R J (1987c), Intern. J. Mode. Phys. *B1*, 813.

37 Cava R J (1990), Science *247*, 656.

38 Chaplot S L (1990), Phys. Rev. *B42*, 2149.

39 Cheetham A K, Chippindale A M and Hibble S J (1988), Nature *333*, 21.

40 Cheng X, Sun L, Wang Y, Shen H and Yu Z (1988), J. Phys. C: Solid State Phys. *21*, 4603.

41 Cheong S W, Thompson J D and Fisk Z (1989), Physica *C158*, 109.

42 Choi P K, Koizumi H, Takagi K and Suzuki T (1989), Solid State Commun. *70*, 1175.

43 Chu C W, Hor P H, Meng R L, Gao L, Huang Z L and Wang Y Q (1987), Phys. Rev. Lett. *58*, 405.

44 Collocott S J, White G K, Dou S X and Williams R K (1987), Phys. Rev. *B36*, 5684.

45 Collocott S J and Driver R (1990), Physica *C167*, 598.

46 Cooper J R, Zhou L W, Dunn B, Chu C T, Alavi B and Grüner (1987), Solid State Commun. *64*, 253.

47 Decroux M, Junod A, Bezinge A, Cattani D, Cors J, Jorda J L, Stettler A, Francois M, Yvon K, Fischer O and Muller J (1987), Europhys. Lett. *3*, 1035.

48 Del Moral A, Ibarra M R, Arnaudas J I, Algarabel P A, Marquina C, Morán E and Alario M A (1988), J. Magne. and Magnetic Mater. *76&77*, 612.

49 Dietrich M R, Fietz W H, Ecke J and Politis C (1987a), Jap. J. Appl. Phys. *26*, 1113.

50 Dietrich M R, Fietz W H, Ecke J, Obst B and Politis C (1987b), Z. Phys. *B66*, 283.

51 Dominec J (1989), Supercond. Sci. Technol. *2*, 91.

52 Durán C, Esquinazi P, Fainstein C and Regueiro N (1988), Solid State Commun. *65*, 957.

53 Ecke J, Fietz W H, Dietrich M R, Wassilew C A, Wühl H and Flükinger R (1988), Physica *C153-155*, 954.

54 Emery V J (1989), Nature *337*, 306.

55 Esquinazi P, Luzuriaga J, Duran C, Esparza D A and D'Ovidio C (1987), Phys. Rev. *B36*, 2316.

56 Fanggao C, Al-kheffaji A, Ford P J, Ladds D A, Freestone J, Chapman B, Mañosa Li, Almond D P and Saunders G A (1990a), Supercond. Sci. Technol. *3*, 422.

57 Fanggao C, Cankurtaran M, Saunders G A, Almond D P, Ford P J and Al-Kheffaji A (1990b), Supercond. Sci. Technol. *3*, 546.

58 Fanggao C, Cankurtaran M, Saunders G A, Al-Kheffaji A, Almond D P, Ford P J and Ladds D A (1991a), Phys. Rev. *B43*, 5526.

59 Fanggao C, Cankurtaran M, Saunders G A, Al-Kheffaji A, Almond D P, Ford P J (1991b), Supercond. Sci. Technol. *4*, 13.

60 Favrot D, Déchamps and Revcolevschi (1991), Phil. Mag. Lett. *64*, 147.

61 Fietz W H, Dietrich M R and Ecke J (1987), Z. Phys. *B69*, 17.

62 Fietz W H, Wassilew C A, Ewert D, Dietrich M R, Wüehl H, Hochheimer D and Fisk Z (1989), Phys. Lett. *A142*, 300.

63 Fietz W H, Ludwig H A, Wanger B P, Grube K, Benischke and Wühl H (1992), to appear in the proceeding of the NATO ARW on "Frontiers of High Pressure Research".

64 Fossheim K, Laegreid T, Sandvold E, Vassenden F, Müller K A and Bednorz J G (1987), Solid State Commun. *63*, 531.

65 Francois M, Jundo A, Yvon K, Hewat A W, Capponi J J, strobel P, Marezio M and Fischer P (1988), Solid State commun. *66*, 1117.

66 Freestone J (1990), MPhil. Thesis, University of Bath.

67 Freitas P P and Plaskett T S (1987), Phys. Rev. *B36*, 5723.

68 Fröhlich H (1950), Phys. Rev. *79*, 845.

69 Fukami T, Yousef A A A, Horie Y and Mase S (1989), Physica *C161*, 34.

70 Ganguly P and Rao C N R (1973), Mater. Res. Bull. *8*, 405.

71 Gavaler J R (1973), Appl. Phys. Lett. *23*, 480.

72 Genzel L, Wittlin A, Bauer M, Cardona M, Schönherr E and Simon A (1989), Phys. Rev. *B40*, 2170.

73 Glazkov V P, Goncharenko I N and Somenkov V A (1988), Sov. Phys. Solid State *30*, 2127.

74 Gopalakrishnan I K, Yakhmi J V, Vaidya M A and Iyer R M (1987a), Appl. Phys. Lett. *51* (17), 1367.

75 Gopalakrishnan I K, Umarji A M, Yakhmi J V, Gupta L C, Iyer R M and Vijayaraghavan (1987b), Mater. Lett. *5*, 165.

76 Grant P M, Parkin S S P, Lee Y V, Engler E M, Ramirez M L, Vazquez J E, Lim G, Jacowitz R D and Greene R L (1987), Phys. Rev. Lett. *58*, 2482.

77 Groen W A, de Leeuw D M and Feiner L F (1990), Physica *C165*, 55.

78 Hailing Tu, Saunders G A and Lambson W A (1982), Phys. Rev. *B26*, 5786.

79 Hailing Tu, Saunders G A, Yogurtcu Y K, Bach H and Methfessel S (1984), J. Phys. C: Solid State Physics *17*, 4559.

80 Hardy G E and Hulm J K (1954), Phys. Rev. *93*, 1004.

81 Hazen R M (1988), Scientific American *258*, 52.

82 Heremans J, Morelli D T, Smith G W and Stire III S C (1988), Phys. Rev. *B37*, 1604.

83 Hewat E A, Dupuy M, Bourret A, Capponi J J and Marezio M (1987), Nature *327*, 400.

84 Hewat E A, Dupuy M, Bordet P, Capponi J J, Chaillout C, Hodeau J L and Marezio M (1988), Nature *333*, 53.

85 Hidaka Y and Suzuki M (1989), Nature *338*, 635.

86 Hoen S, Bourne L C, Kim C M and Zettl A (1988), Phys. Rev. *B38*, 11949.

87 Hor P H, Meng R L, Wang Y Q, Gao L, Haung Z J, Bechtold J, Forster K and Chu C W (1987), Phys. Rev. Lett. *58*, 1891.

88 Horie Y, Fukami T and Mase S (1987a), Solid State Commun. *62*, 471.

89 Horie Y, Fukami T and Mase S (1987b), Solid State Commun. *63*, 653.

90 Horie Y and Mase S (1989), Solid State Commun. *69*, 535.

91 Horie Y, Terashi Y, Fukami T and Mase S (1990), Physica *C166*, 87.

92 Howard C J, Nelmes R J and Vettier C (1989) Solid State Commun. *69*, 261.

93 Ihara H, Sugise R, Hirabayashi M, Terada N, Jo M, Hayashi K, Negishi A, Tokumoto M, Kimura Y and Shimomura T (1988), Nature *334*, 518.

94 Ishidate T and Sasaki S (1989), Phys. Rev. Lett. *62*, 67.

95 Ivanov A G and Tsymbal L T (1990), Phys. Lett. *A148*, 131.

96 Izumi F, Jorgensen J D, Lightfoot P, Pei S, Yamada Y, Takayama M E and Matsumoto T (1990), Physica *C172*, 166.

97 Jaya N V, Natarajan S and Rao G V S (1988), Solid State Commun. *67*, 51.

98 Jayaraman A (1979), Handbook on Physics and Chemistry of Rare Earths, ed. Gschneider K A and Eyring L, (Amsterdam, North Holland), 575.

99 Jericho J M, Simpson A M, Tarascon J M, Green L H, McKinnon R and Hall G (1988), Solid State Commun. *65*, 987.

100 Jiang W J and Breazeale M A (1990), Frontiers of nonlinear acoustics: Proceeding of 12th ISNA, edited by Hamilton M F and Blackstock D T (Elsvier Science Publishers Ltd., London), 541.

101 Johnston D C, Stokes J P, Goshorn D P and Lewandowski J T (1987), Phys. Rev *B36*, 4007.

102 Jorgensen J D, Schüttler H -B, Hinks D G, Capone D W, Zhang K, Brodsky M B and Scalapino D J (1987a), Phys. Rev. Lett. *58*, 1024.

103 Jorgensen J D, Beno M A, Hinks D G, Soderholm L, Volin K J, Hitterman R L, Grace J D, Schuller I K, Segre C U, Zhang K and Kleefisch M S (1987b), Phys. Rev. *B36*, 3608.

104 Kanai T, Kamo T and Matsuda S (1989), Jap. J. Appl. Phys. *28*, L551.

105 Kaneko T, Yoshida H, Syono Y, Morita H, Abe S, Noto K and fujimori H (1987), Physica *B148*, 494.

106 Kim H J and Moret R (1988a), Physica *C156*, 363.

107 Kim T J, Lüthi B, Schwarz M, Kühnberger H, Wolf B, Hampel G, Nikl D and Grill W (1988b), J. Magn. Magnetic Mater. *76&77*, 604.

108 Kim T J, Kowalewski J, Assmus W and Grill W (1990), Z. Phys. *B78*, 207.

109 Kittinger E (1977), Ultrasonics *15*, 30.

110 Kishida S, Tokutaka H, Nishimori K, Ishihara N, Watanabe Y and Noishiki Y (1988), Jap. J. Appl. Phys. *27*, 325.

111 Koihe Y, Iwabuchi Y, Hosoya S, Kobayashi N and Fukase T (1989), Physica *C159*, 105.

112 Komatsu T, Imai K, Sato R, Matusita K and Yamashita T (1988), Jap. J. Appl. Phys. *27*, 533.

113 Kusz B and Murawski L (1988), Solid State Commun. *67*, 435.

114 Laegreid T and Fossheim K (1988a), Europhys. Lett. *6*, 81.

115 Laegreid T, Fossheim K, Vassenden F (1988b), Physica *C153-155*, 1096.

116 Laegreid T, Ting W, Nes O -M, Slaski E, Eidem E, Samuelsen E J, Fossheim K and Hidaka Y (1990), Advances in Superconductivity II, Proceeding of the second symposium on superconductivity (ISS'89), Tsukuba, Japan 14-17 Nov. 1989, (Tokyo, Japan: Springer-Verlag 1990), 595.

117 Lakkad S C (1971), J. Appl. Phys. *42*, 4277.

118 Lang M, Steglich F, Schefzyk R, Lachner T, Spille H, Rietschel H, Goldacker W and Renker B (1987), Europhys. Lett. *4*, 1145.

119 Lang M, Lechner T, Riegel S, Steglich F, Weber G, Kim T J, Lüthi B, Wolf B, Rietschel H and Wilhelm M (1988), Z. Phys. *B69*, 459.

120 Lang M, Höhr A, Spille H, Steglich F, Rietschel H, Roth G, Hidaka Y and Murakami T (1989), Z. Phys. *B74*, 3.

121 Ledbetter H M and Kim S A (1988), Phys. Rev. *B38*, 11857.

122 Ledbetter H, Kim S A, Violet C E and Thompson J D (1989a), Physica *C162-164*, 460.

123 Ledbetter H M, Kim S A, Goldfarb R B and Togano K (1989b), Phys. Rev. *B39*, 9689.

124 Lemmens P, Stellmach F, Ewert S, Guo S, Wynants J, Arlt G, Comberg A, Passing H and Marbach G (1988), Physica *C153-155*, 294.

125 Liang J K, Xu X T, Rao G H, Xie S S, Shao X Y and Duan Z G (1987), J. Phys. D: Appl. Phys. *20*, 1324.

126 Lim Z S, Han K H, Lee S I, Jeong Y H, Salk S H, Song Y S and Park Y W, (1989) Phys. Rev. *B40*, 7310.

127 London F (1961), Superfluids Volume *1*, New York Dover, 34.

128 López-Morales M E, Savoy R J and Grant P M (1989), Solid State Commun. *71*, 1079.

129 Lüthi B, Wolf B, Kim T and Grill W (1987), Jap. J. Appl. Phys. *26 Suppl. 3*, 1127.

130 Maeda H, Tanaka Y, Fukutomi M and Asano T (1988), Jap. J. Appl. Phys. *27*, L209.

131 Marsh P, Siegrist T, Fleming R M, Schneemeyer L S and Waszczak J V (1988), Phys. Rev. *B38*, 874.

132 Mase S (1989), Studies of High Temperature Superconductors Vol.*2*, Edit. Narlikar A, Nova Science Publisher, 129.

133 Mason W P (1964), Piezoelectric Crystals and Their Application to Ultrasonics, D. Van Nostrand Company.

134 Matsuda M, Kikuchi A, Maeda T, Ishii M, Iwai Y, Takata M and Yamashita T (1988), Jap. J. Appl. Phys. *27*, L529.

135 Matthhias B T, Geballe T H, Geller S and Corenzwit E (1954), Phys. Rev. *95*, 1435.

136 Matthias B T, Geballe T H, Longinotti L D, Corenzwit E, Hull G W Jr. and Maita J P (1967), Science *156*, 645.

137 Maxwell E (1950), Phys. Rev. *78*, 477.

138 May Jr. J E (1958), IRE Natl. Conv. Rec. *6*, 2, 134.

139 Mazaki H, Takano M, Takada J, Oda K, Kitaguchi H, Imura Y, Ikeda Y, Tomii Y and Kubozoe T (1988), Jap. J. Appl. Phys. *27*, L1639.

140 Migliori A, Chen T, Alavi B and Grüner G (1987), Solid State Commun. *63*, 827.

141 Migliori A, Visscher W M, Brown S E, Fisk Z, Cheong S W, Atlen B, Ahrens E T, Kubat-Martin K A, Maynard J D, Haung Y, Kirk D R, Gillis K A, Kim H K and Chan M H W (1990), Phys. Rev. *B41*, 2098.

142 Mizuno M, Endo H, Tsuchiya J, Kijima N, Sumiyama A and Oguri Y (1988), Jap. J. Appl. Phys. *27*, L1225.

143 Mook H A and Holtzberg F (1981), Valence Fluctations in Solids ed. Falicov L M, Hanke W and Maple M B, (Amsterdam: North-Holland), 117.

144 Mott N F and Davis E A (1979), Electronic Processes in Non-crystalline Materials, second edition, Oxford University Press, 111.

145 Müller-Buschbaum H and Wollschlager W (1975), Z. Anorg. Allg. Chem. *414*, 76.

146 Müller J. (1980), Rep. Prog. Phys. *43*, 641.

147 Muller V, Maurer D, Roth C, Hucho C, Winau D, de Groot K, Eickenbusch H and Schöllhorn R (1988), Physica *C153-155*, 280.

148 Müller K A (1990), Z. Phys. *B80*, 193.

149 Murayama N, Sudo E, Awano M, Kani K and Torii Y (1988), Jap. J. Appl. Phys. *27*, L1629.

150 Murayama C, Mori N, Yomo S, Takagi H, Uchida S and Toitura Y (1989), Nature *339*, 293.

151 Murnaghan F D (1944), Proc. Natn. Acad. Sci. USA *30*, 244.

152 Namgung C, Irvine J T S, Binks J H, Lachowski E E and West A R (1989), Supercond. Sci. Technol. *2*, 181.

153 Nes O -M, Castro M, Slaski M, Laeggreid T, Fossheim K, Motohira N and Kitazawa K (1991), Supercond. Sci. Technol. *4*, S388.

154 Nobumasa H, Shimizu K, Kitano Y and Kawai T (1988), Jap. J. Appl. Phys. *27*, L1669.

155 Oh-Ishi K., Kikuchi M., Syono Y., Kobayashi N., Sasaoka T., Matsuhir T., Muto Y. and Yamauchi H. (1988), Jap. J. Appl. Phys. *27*, L1449.

156 Olsen J S, Steenstrup S, Johannsen I and Gerward L (1988), Z. Phys. *B72*, 165.

157 Ono A (1987), Jap. J. Appl. Phys. *26*, L1223.

158 Pace N G, Saunders G A and Sümengen Z (1970), J. Phys. Chem. Solids *31*, 1467.

159 Papadakis E P (1964), J. Appl. Phys. *35*, 1474.

160 Papadakis E P (1966), J. Acous. Soc. Amer. *40*, 863.

161 Papadakis E P (1967), J. Acous. Soc. Amer. *42*, 1045.

162 Paul D McK, Balakrishnan G, Bernhoeft N R, David W I F and Harrison W T A (1987), Phys. Rev. Lett. *58*, 1976.

163 Pei S, Jorgensen J D, Hinks D G, Dabrowski B, Lightfoot P and Richards D R (1990), Physica *C169*, 179.

164 Peng J L, Shelton R N and Radousky H B (1990), Phys. Rev. *B41*, 187.

165 Plechácek V and Dominec J (1990), Solid State Commun. *74*, 633.

166 Ramachandran V, Ramadass G A and Srinivasan R (1988), Physica *C153-155*, 278.

167 Ramakrishnan C and Krishnamurthy N (1991), Solid State Commun. *79*, 363.

168 Rao C N R (1988), chemical and structural aspects of high temperature superconductors, Edit Rao C N R (World Scientific), 1.

169 Reddy P V and Ramana Y V (1990), Solid State Commun. *74*, 377.

170 Rodriguez E, Luzuriaga J, Regueiro M N and Fainstein (1991), Solid State Commun. *77*, 777.

171 Rice T M (1987), Z. Phys. *B67*, 141.

172 Rice T M (1989) Nature *337*, 686.

173 Robinson J M (1979), Phys. Reports *51*, 1.

174 Saint-Paul M, Tholence J L, Noël H, Levet J C and Gougeon P P (1989a), Solid State Commun. *69*, 1161.

175 Saint-Paul M and Henry J Y (1989b), Solid State Commun. *72*, 685.

176 Saint-Paul M, Tholence J L, Piñol S, Obradors X, Melville R J and Palmer S B (1990a), Solid State Commun. *76*, 1257.

177 Saint-Paul M, Tholence J-L, Noël H, Levet J C, Potel M and Gougeon P (1990b), Physica *C166*, 405.

178 Saint-Paul M, Noel H, Levet J C, Potel M and Gougeon P (1991), Physica *C180*, 394.

179 Salleh M D M (1988), PhD. Thesis, University of Bath.

180 Salomons E, Hemmes H, Scholtz J J, Koeman N, Brouwer R, Driessen A, De Groot D G and Griessen R (1987), Physica *B145*, 253.

181 Samara G A and Giardini A A (1964), Rev. Sci. Instrum. *35*, 989.

182 Saunders G A (1969), Engineering *21*, 555.

183 Saunders G A and Seddon T (1976), J. Phys. Chem. Solids *37*, 873.

184 Schuller I K, Hinks D G, Beno M A, Capone D W, Soderholm L, Locquet J P, Bruynseraede Y, Segre C U and Zhang K (1987), Solid State Commun. *63*, 385.

185 Schwarz M (1989), NATO ASI, Physics and Materials Science of High Temperature Superconductors (13-26 Aug. 1989, Bad Windsheim, Germany) ed. Kossowsky R et al (Deventer:Kluwer).

186 Shaplygin I S, Kakhan B G and Lazerev V B (1979), Russ. J. Inorg. Chem. *24*, 820.

187 Shi X D, Yu R C, Wang Z Z, Ong N P and Chaikin P M (1989), Phys. Rev. *B39*, 827.

188 Sihan L, Yusheng H, Chongde W and Zhaohui S (1989), Supercond. Sci. Technol. *2*, 145.

189 Skanthakumar S, Zhang H, Clinton T W, Li W H, Lynn J W, Fisk Z and Cheong S W (1989), Physica *C160*, 124.

190 Slaski M, Steinsvoll O, Samuelsen E J, Nes O-M, Ting W, Laegreid T, Fosshheim K and Hidaka Y I (1991), Solid State Commun. *77*, 945.

191 Srinivasan R (1988a), Studies of High Temperature Superconductors Vol.*1*, Edit. Narlikar A, Nova Science Publisher, 267.

192 Srinivasan R, Girirajan K S, Ganesan V, Radhakrishnan V and Rao G V S (1988b), Phys. Rev. *B38*, 889.

193 Sudhakar N, Pillai M K, Banerjee A, Bahadur D, Das A, Gupta K P, Sharma S V and Majumdar A K (1991), Solid State Commun. *77*, 529.

194 Sun K J, Winfree W P, Xu M F, Samra B K, Levy M, Caton R and Selim R (1988), Phys. Rev. *B38*, 11988.

195 Suzuki M, Okuda Y, Iwasa I, Ikushima A J, Takabatake T, Nakazawa Y and Ishikawa M (1988), Physica *C153-155*, 266.

196 Swenson C A, McCallum R W and No K (1989), Phys. Rev. *B40*, 8861.

197 Tajima Y, Hikita M, Suzuki M and Hidaka Y (1989), Physica *C158*, 237.

198 Takagi H, Uchida S and Tokura Y (1989), Phys. Rev. Lett. *62*, 1197.

199 Takahashi H, Murayama C, Yomo S, Mori N, Kishio K, Kitazawa K and Fueki K (1987a), Jap. J. Appl. Phys. *26*, L504.

200 Takahashi H, Murayama C, Yomo S, Mori N, Ustumi W and Yagi T (1987b), Jap. J. Appl. Phys. *26*, 1109.

201 Takano M, Takada J, Oda K, Kitaguchi H, Miura Y, Ikeda Y, Tomii Y and Mazaki H (1988), Jap. J. Appl. Phys. *27*, L1041.

202 Tallon J L, Buckley R G, Gilberd P W, Presland M R, Brown I W M, Bowden M E, Christian L A and Goguel R (1988), Nature *333*, 153.

203 Tang I M, Eaiprasertsak K, Chitaree R and Winotai P (1990), Physica *C167*, 491.

204 Tarascon J M, McKinnon W R, Greene L H, Hull G W and Vogel E M (1987), Phys. Rev. *B36*, 226.

205 Taylor K N R, Russell G L, Bosi S, Matthews D N, Cochrane J, Town S, Hunter B, Puzzer T, Bailey A and Vaile R A (1990), Physics and Materials Science of High Temperature Superconductors, ed. Kossowsky R et al (Deventer:Kluwer), 245.

206 van Tendezoo G, Zanbergen H W and Amelinckx S (1987), Solid State Commun. *63*, 389.

207 Terada N, Ihara H, Hirakayashi M, Senzaki K, Kimura Y, Murata K, Tokumoto M, Shimonura O and Kikegawa T (1987), Jap. J. Appl. Phys. *26*, L510.

208 Testardi R L (1973), Physical Acoustics *10*, 193.

209 Tokura Y, Takagi H and Uchida S (1989), Nature *337*, 345.

210 Toulouse J, Wang X M and Hong D J L (1988), Phys. Rev. *B38*, 7077.

211 Toulouse J, Wang X M and Hong D J L (1990), Phase Transition *23*, 35.

212 Truell R, Elbaum C and Chick B B (1969), Ultrasonic Methods in Solid State Physics (Academic Press, New York).

213 Varma C M (1976), Rev. Mod. Phys *48*, 219.

214 Vass H, Pawley G S and Saunders G A (1990), J. Mat. Sci. Letts. *9*, 535.

215 Uchida S, Takagi H, Kitazawa K and Tanaka S (1987), Jap. J. Appl. Phys. Lett. *26*, L1.

216 Wang C Y (1967), Rev. Sci. Inst. *38*, 24.

217 Wang Y, Wu J, Zhu J, Shen H and Zhang J (1989), Phys. Lett. *A142*, 289.

218 Wang Y, Sun L, Wu J and Gu M (1990), Solid State Commun. *75*, 495.

219 Wentorf R H (1962), Modern Very High Pressure Techniques, Butterworths: London.

220 Wijngaarden R J and Griessen (1989), Studies of High Temperature Superconductors Vol.*2*, Edit. Narlikar A, Nova Science Publisher, 29.

221 Williams A, Kwei G H, Von Dreele R B, Larsen A C, Raistrick I D and Bish D L (1988), Phys. Rev. *B37*, 7960.

222 Wolf B, Kim T J, Kühnberger H, Palme W, Krimmel A, Xanthopoulos I, Grill W, Lüthi B and Schwarz M (1988), Physica *C153-155*, 284.

223 Wu M K, Ashburn J R, Torng C J, Hor P H, Meng R L, Gao L, Huang Z J, Wang Y Q and Chu C W (1987), Phys. Rev. Lett. *58*, 908.

224 Wu J, Wang Y, Shen H, Zhu J, Yan Y and Zhao Z (1990), Phys. Lett. *A148*, 127.

225 Xiang X -D, Brill J W, Delong L E, Bourne L C, Zettl A, Jones J C and Rice L A (1988), Solid State Commun. *65*, 1073.

226 Xiang X D, Chung M, Brill J W, Hoen S, Pinsukanjana P and Zetl A (1989), Solid State Commun. *69*, 833.

227 Xiaorong Z Changguo Q, Changming G, Zhongnan L, Shiyuan Z, Hao W, Ningsheng Z, Zijun W and Qiang M (1987), Intern. J. Mode. Phys. *B1*, 495.

228 Xu X T, Liang J K, Xie S S, Che G C, Shao X Y, Duan Z G and Cui C G (1987), Solid State Commun. *63*, 649.

229 Xu M-F, Baum H-P, Schenstrom A, Sarma B K, Levy M, Sun K J, Toth L E, Wolf S A and Gubser D U (1988), Phys. Rev. *B37*, 3675.

230 Yanagisawa E, Dietderich D R, Kamakara H, Togano K, Maeda H and Takahashi K (1988), Jap. J. Appl. Phys. *27*, L1460.

231 Yening W, Huimin S, Jinsong Z, Ziran X, Min G, Zhongmin N and Zhifang Z (1987), J. Phys. C: Solid State Phys. *20*, L665.

232 Yogurtcu Y K, Tu Hailing, Saunders G A, Bach H and Methfessel S (1985), J. Mater. Sci. Lett. *4*, 230.

233 Yu R C, Naughton M J, Yan X, Chaikin P M, Holtzberg F, Greene R L, Stuart J and Davies P (1988), Phys. Rev. *B37*, 7963.

234 Yusheng H, Baiwen Z, Sihan L, Jiong X, Yongming L and Haoming C (1987), J. Phys. F: Met. Phys. *17*, L243.

235 Yusheng H, Jiong X, Xin W, Aisheng H, Jincang Z and Fanggao C (1989), Phys. Rev. *B40*, 7384.

236 **Zandbergen H M, Groen P, van Tendeloo G, van Landuyt J and Amelinckx S (1988), Solid State Commun. *66*, 397.**

REFERENCES

1 Akhtar M J, Catlow C R A, Clark S M and Temmerman W M (1988), J. Phys. C: Solid State Phys. *21*, L917.

2 Akhtar M J, Akhtar Z N and Catlow (1990), J. Phys.: Condens. Matter *2*, 3231.

3 Aleksandrov I V, Goncharov A F and Stishov S (1988), JETP Lett. *47*, 428.

4 Allan N L and Mackrodt W C (1988), Phil. Mag. *A58*, 555.

5 Allan N L, Lawton J M and Mackrodt W C (1989), Phil. Mag. *B59*, 191.

6 Almond D P, Lambson E, Saunders G A and Hong W (1987), J. Phys. F: Met. Phys. *17*, L221.

7 Almond D P, Chapman B and Saunders G A (1988), Supercond. Sci. Technol. *1*, 123.

8 Almond D P, Wang Q, Freestone J, Lambson E F, Chapman B and Saunders G A (1989), J. Phys. Condens. Matter *1*, 6853.

9 Almond D P, Fanggao C, Ford P J and Saunders G A (1990), Supercond. Sci. Technol. *3*, 583.

10 Axe J D, Moudden A H, Hohlwein D, Cox D E, Mohanty K M, Moodenbaugh A R and Xu Y (1989), Phys. Rev. Lett. *62*, 2751.

11 Baetzold R C (1990), Phys. Rev. *B42*, 56.

12 Bardeen J, Cooper L N and Schrieffer J R (1957), Phys. Rev. *108*, 1175.

13 Barron T H K, Collins J G and White G K (1980), Adv. Phys. *29*, 609.

14 Bateman T B (1966), J. Acous. Soc. Amer. *41*, 1011.

15 Bednorz J G and Müller K A (1986), Z. Phys. *B64*, 189.

16 Bhattacharya S, Higgins M J, Johnston D C, Jacobson A J, Stokes J P, Goshorn D P and Lewandowski J T (1988), Phys. Rev. Lett. *60*, 1181.

17 Bishop D J, Gammel P L, Ramirez A P, Cava R J, Batlogg B and Rietman E A (1987a), Phys. Rev. *B35*, 8788.

18 Bishop D J, Ramirez A P, Gammel P L, Batlogg B, Rietman E A, Cava R J and Millis A J (1987b), Phys. Rev. *B36*, 2408.

19 Block S, Piermarini G J, Munro R G and Wong-Ng W (1987), Advanced Ceramic Materials *2*, 601.

20 Boppart H, Rehwald W, Kaldis E and Wachter P (1983), Physica *B+C 117-118*, 564.

21 Bordet P, Capponi J J, Chaillout C, Chenavas J, Hewat A W, Hewat E A, Hodeau J L, Marezio M, Tholence J L and Tranqui D (1988), Physica *C156*, 189.

22 Bourne L C, Zettl A, Chang K J, Cohen M L, Stacy A M and Ham W K (1987), Phys. Rev. *B35*, 8785.

23 Bradley C C (1969), High Pressure Methods in Solid State Research, (Butterworth, London).

24 Brassington M P (1982), Ph.D. Thesis, University of Bath.

25 Bridgman P W (1911), Proc. Amer. Acad. Arts Sci. *47*, 321.

26 Bridgman P W (1958), The Physics of High Pressure, (Bell and Sons, London).

27 Brown S E, Migliori A and Fisk Z (1988), Solid State Commun. *65*, 483.

28 Cankurtaran M, Saunders G A, Willis J R, Al-khef-faji A and Almond D P (1989a), Phys. Rev. *B39*, 2872.

29 Cankurtaran M, Saunders G A, Almond D P, Al-Khef-faji A, Lambson E F and Draper R C J (1989b) J. Phys: Condensed Matter *1*, 9067.

30 Cankurtaran M, Saunders G A, Almond D P, Al-Khef-faji A Freestone J, Wang Q and Lambson E F (1990a), Physics and Materials Science of High Temperature Superconductors, edited by Kossowsky R, Methfessel S and Wholleben D (Kluwer Academic, Dordrecht), 627.

31 Cankurtaran M, Al-Kheffaji A, Saunders G A, Almond D P, Freestone J (1990b), Supercond. Sci. Technol. *3*, 76.

32 Cankurtaran M, Saunders G A, Goretta K C and Poeppel R B (1992), to be published in Phys. Rev. B.

33 Cannelli G, Cantelli R and Cordero F (1988), Phys. Rev. *B38*, 7200.

34 Cava R J, Van Dover R B, Batlogg B and Rietman (1987a), Phys. Rev. Lett. *58*, 408.

35 Cava R J, Battlog B, Vandover R B, Murphy D N, Sunshine S, Siegrist T, Remeika J P, Rietman E A, Zahurak S and Espinosa G R (1987b), Phys. Rev. Lett. *58*, 1676.

36 Cava R J (1987c), Intern. J. Mode. Phys. *B1*, 813.

37 Cava R J (1990), Science *247*, 656.

38 Chaplot S L (1990), Phys. Rev. *B42*, 2149.

39 Cheetham A K, Chippindale A M and Hibble S J (1988), Nature *333*, 21.

40 Cheng X, Sun L, Wang Y, Shen H and Yu Z (1988), J. Phys. C: Solid State Phys. *21*, 4603.

41 Cheong S W, Thompson J D and Fisk Z (1989), Physica *C158*, 109.

42 Choi P K, Koizumi H, Takagi K and Suzuki T (1989), Solid State Commun. *70*, 1175.

43 Chu C W, Hor P H, Meng R L, Gao L, Huang Z L and Wang Y Q (1987), Phys. Rev. Lett. *58*, 405.

44 Collocott S J, White G K, Dou S X and Williams R K (1987), Phys. Rev. *B36*, 5684.

45 Collocott S J and Driver R (1990), Physica *C167*, 598.

46 Cooper J R, Zhou L W, Dunn B, Chu C T, Alavi B and Grüner (1987), Solid State Commun. *64*, 253.

47 Decroux M, Junod A, Bezinge A, Cattani D, Cors J, Jorda J L, Stettler A, Francois M, Yvon K, Fischer O and Muller J (1987), Europhys. Lett. *3*, 1035.

48 Del Moral A, Ibarra M R, Arnaudas J I, Algarabel P A, Marquina C, Morán E and Alario M A (1988), J. Magne. and Magnetic Mater. *76&77*, 612.

49 Dietrich M R, Fietz W H, Ecke J and Politis C (1987a), Jap. J. Appl. Phys. *26*, 1113.

50 Dietrich M R, Fietz W H, Ecke J, Obst B and Politis C (1987b), Z. Phys. *B66*, 283.

51 Dominec J (1989), Supercond. Sci. Technol. *2*, 91.

52 Durán C, Esquinazi P, Fainstein C and Regueiro N (1988), Solid State Commun. *65*, 957.

53 Ecke J, Fietz W H, Dietrich M R, Wassilew C A, Wühl H and Flükinger R (1988), Physica *C153-155*, 954.

54 Emery V J (1989), Nature *337*, 306.

55 Esquinazi P, Luzuriaga J, Duran C, Esparza D A and D'Ovidio C (1987), Phys. Rev. *B36*, 2316.

56 Fanggao C, Al-kheffaji A, Ford P J, Ladds D A, Freestone J, Chapman B, Mañosa Li, Almond D P and Saunders G A (1990a), Supercond. Sci. Technol. *3*, 422.

57 Fanggao C, Cankurtaran M, Saunders G A, Almond D P, Ford P J and Al-Kheffaji A (1990b), Supercond. Sci. Technol. *3*, 546.

58 Fanggao C, Cankurtaran M, Saunders G A, Al-Kheffaji A, Almond D P, Ford P J and Ladds D A (1991a), Phys. Rev. *B43*, 5526.

59 Fanggao C, Cankurtaran M, Saunders G A, Al-Kheffaji A, Almond D P, Ford P J (1991b), Supercond. Sci. Technol. *4*, 13.

60 Favrot D, Déchamps and Revcolevschi (1991), Phil. Mag. Lett. *64*, 147.

61 Fietz W H, Dietrich M R and Ecke J (1987), Z. Phys. *B69*, 17.

62 Fietz W H, Wassilew C A, Ewert D, Dietrich M R, Wüehl H, Hochheimer D and Fisk Z (1989), Phys. Lett. *A142*, 300.

63 Fietz W H, Ludwig H A, Wanger B P, Grube K, Benischke and Wühl H (1992), to appear in the proceeding of the NATO ARW on "Frontiers of High Pressure Research".

64 Fossheim K, Laegreid T, Sandvold E, Vassenden F, Müller K A and Bednorz J G (1987), Solid State Commun. *63*, 531.

65 Francois M, Jundo A, Yvon K, Hewat A W, Capponi J J, strobel P, Marezio M and Fischer P (1988), Solid State commun. *66*, 1117.

66 Freestone J (1990), MPhil. Thesis, University of Bath.

67 Freitas P P and Plaskett T S (1987), Phys. Rev. *B36*, 5723.

68 Fröhlich H (1950), Phys. Rev. *79*, 845.

69 Fukami T, Yousef A A A, Horie Y and Mase S (1989), Physica *C161*, 34.

70 Ganguly P and Rao C N R (1973), Mater. Res. Bull. *8*, 405.

71 Gavaler J R (1973), Appl. Phys. Lett. *23*, 480.

72 Genzel L, Wittlin A, Bauer M, Cardona M, Schönherr E and Simon A (1989), Phys. Rev. *B40*, 2170.

73 Glazkov V P, Goncharenko I N and Somenkov V A (1988), Sov. Phys. Solid State *30*, 2127.

74 Gopalakrishnan I K, Yakhmi J V, Vaidya M A and Iyer R M (1987a), Appl. Phys. Lett. *51* (17), 1367.

75 Gopalakrishnan I K, Umarji A M, Yakhmi J V, Gupta L C, Iyer R M and Vijayaraghavan (1987b), Mater. Lett. *5*, 165.

76 Grant P M, Parkin S S P, Lee Y V, Engler E M, Ramirez M L, Vazquez J E, Lim G, Jacowitz R D and Greene R L (1987), Phys. Rev. Lett. *58*, 2482.

77 Groen W A, de Leeuw D M and Feiner L F (1990), Physica *C165*, 55.

78 Hailing Tu, Saunders G A and Lambson W A (1982), Phys. Rev. *B26*, 5786.

79 Hailing Tu, Saunders G A, Yogurtcu Y K, Bach H and Methfessel S (1984), J. Phys. C: Solid State Physics *17*, 4559.

80 Hardy G E and Hulm J K (1954), Phys. Rev. *93*, 1004.

81 Hazen R M (1988), Scientific American *258*, 52.

82 Heremans J, Morelli D T, Smith G W and Stire III S C (1988), Phys. Rev. *B37*, 1604.

83 Hewat E A, Dupuy M, Bourret A, Capponi J J and Marezio M (1987), Nature *327*, 400.

84 Hewat E A, Dupuy M, Bordet P, Capponi J J, Chaillout C, Hodeau J L and Marezio M (1988), Nature *333*, 53.

85 Hidaka Y and Suzuki M (1989), Nature *338*, 635.

86 Hoen S, Bourne L C, Kim C M and Zettl A (1988), Phys. Rev. *B38*, 11949.

87 Hor P H, Meng R L, Wang Y Q, Gao L, Haung Z J, Bechtold J, Forster K and Chu C W (1987), Phys. Rev. Lett. *58*, 1891.

88 Horie Y, Fukami T and Mase S (1987a), Solid State Commun. *62*, 471.

89 Horie Y, Fukami T and Mase S (1987b), Solid State Commun. *63*, 653.

90 Horie Y and Mase S (1989), Solid State Commun. *69*, 535.

91 Horie Y, Terashi Y, Fukami T and Mase S (1990), Physica *C166*, 87.

92 Howard C J, Nelmes R J and Vettier C (1989) Solid State Commun. *69*, 261.

93 Ihara H, Sugise R, Hirabayashi M, Terada N, Jo M, Hayashi K, Negishi A, Tokumoto M, Kimura Y and Shimomura T (1988), Nature *334*, 518.

94 Ishidate T and Sasaki S (1989), Phys. Rev. Lett. *62*, 67.

95 Ivanov A G and Tsymbal L T (1990), Phys. Lett. *A148*, 131.

96 Izumi F, Jorgensen J D, Lightfoot P, Pei S, Yamada Y, Takayama M E and Matsumoto T (1990), Physica *C172*, 166.

97 Jaya N V, Natarajan S and Rao G V S (1988), Solid State Commun. *67*, 51.

98 Jayaraman A (1979), Handbook on Physics and Chemistry of Rare Earths, ed. Gschneider K A and Eyring L, (Amsterdam, North Holland), 575.

99 Jericho J M, Simpson A M, Tarascon J M, Green L H, McKinnon R and Hall G (1988), Solid State Commun. *65*, 987.

100 Jiang W J and Breazeale M A (1990), Frontiers of nonlinear acoustics: Proceeding of 12th ISNA, edited by Hamilton M F and Blackstock D T (Elsvier Science Publishers Ltd., London), 541.

101 Johnston D C, Stokes J P, Goshorn D P and Lewandowski J T (1987), Phys. Rev *B36*, 4007.

102 Jorgensen J D, Schüttler H -B, Hinks D G, Capone D W, Zhang K, Brodsky M B and Scalapino D J (1987a), Phys. Rev. Lett. *58*, 1024.

103 Jorgensen J D, Beno M A, Hinks D G, Soderholm L, Volin K J, Hitterman R L, Grace J D, Schuller I K, Segre C U, Zhang K and Kleefisch M S (1987b), Phys. Rev. *B36*, 3608.

104 Kanai T, Kamo T and Matsuda S (1989), Jap. J. Appl. Phys. *28*, L551.

105 Kaneko T, Yoshida H, Syono Y, Morita H, Abe S, Noto K and fujimori H (1987), Physica *B148*, 494.

106 Kim H J and Moret R (1988a), Physica *C156*, 363.

107 Kim T J, Lüthi B, Schwarz M, Kühnberger H, Wolf B, Hampel G, Nikl D and Grill W (1988b), J. Magn. Magnetic Mater. *76&77*, 604.

108 Kim T J, Kowalewski J, Assmus W and Grill W (1990), Z. Phys. *B78*, 207.

109 Kittinger E (1977), Ultrasonics *15*, 30.

110 Kishida S, Tokutaka H, Nishimori K, Ishihara N, Watanabe Y and Noishiki Y (1988), Jap. J. Appl. Phys. *27*, 325.

111 Koihe Y, Iwabuchi Y, Hosoya S, Kobayashi N and Fukase T (1989), Physica *C159*, 105.

112 Komatsu T, Imai K, Sato R, Matusita K and Yamashita T (1988), Jap. J. Appl. Phys. *27*, 533.

113 Kusz B and Murawski L (1988), Solid State Commun. *67*, 435.

114 Laegreid T and Fossheim K (1988a), Europhys. Lett. *6*, 81.

115 Laegreid T, Fossheim K, Vassenden F (1988b), Physica *C153-155*, 1096.

116 Laegreid T, Ting W, Nes O -M, Slaski E, Eidem E, Samuelsen E J, Fossheim K and Hidaka Y (1990), Advances in Superconductivity II, Proceeding of the second symposium on superconductivity (ISS'89), Tsukuba, Japan 14-17 Nov. 1989, (Tokyo, Japan: Springer-Verlag 1990), 595.

117 Lakkad S C (1971), J. Appl. Phys. *42*, 4277.

118 Lang M, Steglich F, Schefzyk R, Lachner T, Spille H, Rietschel H, Goldacker W and Renker B (1987), Europhys. Lett. *4*, 1145.

119 Lang M, Lechner T, Riegel S, Steglich F, Weber G, Kim T J, Lüthi B, Wolf B, Rietschel H and Wilhelm M (1988), Z. Phys. *B69*, 459.

120 Lang M, Höhr A, Spille H, Steglich F, Rietschel H, Roth G, Hidaka Y and Murakami T (1989), Z. Phys. *B74*, 3.

121 Ledbetter H M and Kim S A (1988), Phys. Rev. *B38*, 11857.

122 Ledbetter H, Kim S A, Violet C E and Thompson J D (1989a), Physica *C162-164*, 460.

123 Ledbetter H M, Kim S A, Goldfarb R B and Togano K (1989b), Phys. Rev. *B39*, 9689.

124 Lemmens P, Stellmach F, Ewert S, Guo S, Wynants J, Arlt G, Comberg A, Passing H and Marbach G (1988), Physica *C153-155*, 294.

125 Liang J K, Xu X T, Rao G H, Xie S S, Shao X Y and Duan Z G (1987), J. Phys. D: Appl. Phys. *20*, 1324.

126 Lim Z S, Han K H, Lee S I, Jeong Y H, Salk S H, Song Y S and Park Y W, (1989) Phys. Rev. *B40*, 7310.

127 London F (1961), Superfluids Volume *1*, New York Dover, 34.

128 López-Morales M E, Savoy R J and Grant P M (1989), Solid State Commun. *71*, 1079.

129 Lüthi B, Wolf B, Kim T and Grill W (1987), Jap. J. Appl. Phys. *26 Suppl. 3*, 1127.

130 Maeda H, Tanaka Y, Fukutomi M and Asano T (1988), Jap. J. Appl. Phys. *27*, L209.

131 Marsh P, Siegrist T, Fleming R M, Schneemeyer L S and Waszczak J V (1988), Phys. Rev. *B38*, 874.

132 Mase S (1989), Studies of High Temperature Superconductors Vol.*2*, Edit. Narlikar A, Nova Science Publisher, 129.

133 Mason W P (1964), Piezoelectric Crystals and Their Application to Ultrasonics, D. Van Nostrand Company.

134 Matsuda M, Kikuchi A, Maeda T, Ishii M, Iwai Y, Takata M and Yamashita T (1988), Jap. J. Appl. Phys. *27*, L529.

135 Matthhias B T, Geballe T H, Geller S and Corenzwit E (1954), Phys. Rev. *95*, 1435.

136 Matthias B T, Geballe T H, Longinotti L D, Corenzwit E, Hull G W Jr. and Maita J P (1967), Science *156*, 645.

137 Maxwell E (1950), Phys. Rev. *78*, 477.

138 May Jr. J E (1958), IRE Natl. Conv. Rec. *6*, 2, 134.

139 Mazaki H, Takano M, Takada J, Oda K, Kitaguchi H, Imura Y, Ikeda Y, Tomii Y and Kubozoe T (1988), Jap. J. Appl. Phys. *27*, L1639.

140 Migliori A, Chen T, Alavi B and Grüner G (1987), Solid State Commun. *63*, 827.

141 Migliori A, Visscher W M, Brown S E, Fisk Z, Cheong S W, Atlen B, Ahrens E T, Kubat-Martin K A, Maynard J D, Haung Y, Kirk D R, Gillis K A, Kim H K and Chan M H W (1990), Phys. Rev. *B41*, 2098.

142 Mizuno M, Endo H, Tsuchiya J, Kijima N, Sumiyama A and Oguri Y (1988), Jap. J. Appl. Phys. *27*, L1225.

143 Mook H A and Holtzberg F (1981), Valence Fluctations in Solids ed. Falicov L M, Hanke W and Maple M B, (Amsterdam: North-Holland), 117.

144 Mott N F and Davis E A (1979), Electronic Processes in Non-crystalline Materials, second edition, Oxford University Press, 111.

145 Müller-Buschbaum H and Wollschlager W (1975), Z. Anorg. Allg. Chem. *414*, 76.

146 Müller J. (1980), Rep. Prog. Phys. *43*, 641.

147 Muller V, Maurer D, Roth C, Hucho C, Winau D, de Groot K, Eickenbusch H and Schöllhorn R (1988), Physica *C153-155*, 280.

148 Müller K A (1990), Z. Phys. *B80*, 193.

149 Murayama N, Sudo E, Awano M, Kani K and Torii Y (1988), Jap. J. Appl. Phys. *27*, L1629.

150 Murayama C, Mori N, Yomo S, Takagi H, Uchida S and Toitura Y (1989), Nature *339*, 293.

151 Murnaghan F D (1944), Proc. Natn. Acad. Sci. USA *30*, 244.

152 Namgung C, Irvine J T S, Binks J H, Lachowski E E and West A R (1989), Supercond. Sci. Technol. *2*, 181.

153 Nes O -M, Castro M, Slaski M, Laeggreid T, Fossheim K, Motohira N and Kitazawa K (1991), Supercond. Sci. Technol. *4*, S388.

154 Nobumasa H, Shimizu K, Kitano Y and Kawai T (1988), Jap. J. Appl. Phys. *27*, L1669.

155 Oh-Ishi K., Kikuchi M., Syono Y., Kobayashi N., Sasaoka T., Matsuhir T., Muto Y. and Yamauchi H. (1988), Jap. J. Appl. Phys. *27*, L1449.

156 Olsen J S, Steenstrup S, Johannsen I and Gerward L (1988), Z. Phys. *B72*, 165.

157 Ono A (1987), Jap. J. Appl. Phys. *26*, L1223.

158 Pace N G, Saunders G A and Sümengen Z (1970), J. Phys. Chem. Solids *31*, 1467.

159 Papadakis E P (1964), J. Appl. Phys. *35*, 1474.

160 Papadakis E P (1966), J. Acous. Soc. Amer. *40*, 863.

161 Papadakis E P (1967), J. Acous. Soc. Amer. *42*, 1045.

162 Paul D McK, Balakrishnan G, Bernhoeft N R, David W I F and Harrison W T A (1987), Phys. Rev. Lett. *58*, 1976.

163 Pei S, Jorgensen J D, Hinks D G, Dabrowski B, Lightfoot P and Richards D R (1990), Physica *C169*, 179.

164 Peng J L, Shelton R N and Radousky H B (1990), Phys. Rev. *B41*, 187.

165 Plechácek V and Dominec J (1990), Solid State Commun. *74*, 633.

166 Ramachandran V, Ramadass G A and Srinivasan R (1988), Physica *C153-155*, 278.

167 Ramakrishnan C and Krishnamurthy N (1991), Solid State Commun. *79*, 363.

168 Rao C N R (1988), chemical and structural aspects of high temperature superconductors, Edit Rao C N R (World Scientific), 1.

169 Reddy P V and Ramana Y V (1990), Solid State Commun. *74*, 377.

170 Rodriguez E, Luzuriaga J, Regueiro M N and Fainstein (1991), Solid State Commun. *77*, 777.

171 Rice T M (1987), Z. Phys. *B67*, 141.

172 Rice T M (1989) Nature *337*, 686.

173 Robinson J M (1979), Phys. Reports *51*, 1.

174 Saint-Paul M, Tholence J L, Noël H, Levet J C and Gougeon P P (1989a), Solid State Commun. *69*, 1161.

175 Saint-Paul M and Henry J Y (1989b), Solid State Commun. *72*, 685.

176 Saint-Paul M, Tholence J L, Piñol S, Obradors X, Melville R J and Palmer S B (1990a), Solid State Commun. *76*, 1257.

177 Saint-Paul M, Tholence J-L, Noël H, Levet J C, Potel M and Gougeon P (1990b), Physica *C166*, 405.

178 Saint-Paul M, Noel H, Levet J C, Potel M and Gougeon P (1991), Physica *C180*, 394.

179 Salleh M D M (1988), PhD. Thesis, University of Bath.

180 Salomons E, Hemmes H, Scholtz J J, Koeman N, Brouwer R, Driessen A, De Groot D G and Griessen R (1987), Physica *B145*, 253.

181 Samara G A and Giardini A A (1964), Rev. Sci. Instrum. *35*, 989.

182 Saunders G A (1969), Engineering *21*, 555.

183 Saunders G A and Seddon T (1976), J. Phys. Chem. Solids *37*, 873.

184 Schuller I K, Hinks D G, Beno M A, Capone D W, Soderholm L, Locquet J P, Bruynseraede Y, Segre C U and Zhang K (1987), Solid State Commun. *63*, 385.

185 Schwarz M (1989), NATO ASI, Physics and Materials Science of High Temperature Superconductors (13-26 Aug. 1989, Bad Windsheim, Germany) ed. Kossowsky R et al (Deventer:Kluwer).

186 Shaplygin I S, Kakhan B G and Lazerev V B (1979), Russ. J. Inorg. Chem. *24*, 820.

187 Shi X D, Yu R C, Wang Z Z, Ong N P and Chaikin P M (1989), Phys. Rev. *B39*, 827.

188 Sihan L, Yusheng H, Chongde W and Zhaohui S (1989), Supercond. Sci. Technol. *2*, 145.

189 Skanthakumar S, Zhang H, Clinton T W, Li W H, Lynn J W, Fisk Z and Cheong S W (1989), Physica *C160*, 124.

190 Slaski M, Steinsvoll O, Samuelsen E J, Nes O-M, Ting W, Laegreid T, Fosshheim K and Hidaka Y I (1991), Solid State Commun. *77*, 945.

191 Srinivasan R (1988a), Studies of High Temperature Superconductors Vol.*1*, Edit. Narlikar A, Nova Science Publisher, 267.

192 Srinivasan R, Girirajan K S, Ganesan V, Radhakrishnan V and Rao G V S (1988b), Phys. Rev. *B38*, 889.

193 Sudhakar N, Pillai M K, Banerjee A, Bahadur D, Das A, Gupta K P, Sharma S V and Majumdar A K (1991), Solid State Commun. *77*, 529.

194 Sun K J, Winfree W P, Xu M F, Samra B K, Levy M, Caton R and Selim R (1988), Phys. Rev. *B38*, 11988.

195 Suzuki M, Okuda Y, Iwasa I, Ikushima A J, Takabatake T, Nakazawa Y and Ishikawa M (1988), Physica *C153-155*, 266.

196 Swenson C A, McCallum R W and No K (1989), Phys. Rev. *B40*, 8861.

197 Tajima Y, Hikita M, Suzuki M and Hidaka Y (1989), Physica *C158*, 237.

198 Takagi H, Uchida S and Tokura Y (1989), Phys. Rev. Lett. *62*, 1197.

199 Takahashi H, Murayama C, Yomo S, Mori N, Kishio K, Kitazawa K and Fueki K (1987a), Jap. J. Appl. Phys. *26*, L504.

200 Takahashi H, Murayama C, Yomo S, Mori N, Ustumi W and Yagi T (1987b), Jap. J. Appl. Phys. *26*, 1109.

201 Takano M, Takada J, Oda K, Kitaguchi H, Miura Y, Ikeda Y, Tomii Y and Mazaki H (1988), Jap. J. Appl. Phys. *27*, L1041.

202 Tallon J L, Buckley R G, Gilberd P W, Presland M R, Brown I W M, Bowden M E, Christian L A and Goguel R (1988), Nature *333*, 153.

203 Tang I M, Eaiprasertsak K, Chitaree R and Winotai P (1990), Physica *C167*, 491.

204 Tarascon J M, McKinnon W R, Greene L H, Hull G W and Vogel E M (1987), Phys. Rev. *B36*, 226.

205 Taylor K N R, Russell G L, Bosi S, Matthews D N, Cochrane J, Town S, Hunter B, Puzzer T, Bailey A and Vaile R A (1990), Physics and Materials Science of High Temperature Superconductors, ed. Kossowsky R et al (Deventer:Kluwer), 245.

206 van Tendezoo G, Zanbergen H W and Amelinckx S (1987), Solid State Commun. *63*, 389.

207 Terada N, Ihara H, Hirakayashi M, Senzaki K, Kimura Y, Murata K, Tokumoto M, Shimonura O and Kikegawa T (1987), Jap. J. Appl. Phys. *26*, L510.

208 Testardi R L (1973), Physical Acoustics *10*, 193.

209 Tokura Y, Takagi H and Uchida S (1989), Nature *337*, 345.

210 Toulouse J, Wang X M and Hong D J L (1988), Phys. Rev. *B38*, 7077.

211 Toulouse J, Wang X M and Hong D J L (1990), Phase Transition *23*, 35.

212 Truell R, Elbaum C and Chick B B (1969), Ultrasonic Methods in Solid State Physics (Academic Press, New York).

213 Varma C M (1976), Rev. Mod. Phys *48*, 219.

214 Vass H, Pawley G S and Saunders G A (1990), J. Mat. Sci. Letts. *9*, 535.

215 Uchida S, Takagi H, Kitazawa K and Tanaka S (1987), Jap. J. Appl. Phys. Lett. *26*, L1.

216 Wang C Y (1967), Rev. Sci. Inst. *38*, 24.

217 Wang Y, Wu J, Zhu J, Shen H and Zhang J (1989), Phys. Lett. *A142*, 289.

218 Wang Y, Sun L, Wu J and Gu M (1990), Solid State Commun. *75*, 495.

219 Wentorf R H (1962), Modern Very High Pressure Techniques, Butterworths: London.

220 Wijngaarden R J and Griessen (1989), Studies of High Temperature Superconductors Vol.*2*, Edit. Narlikar A, Nova Science Publisher, 29.

221 Williams A, Kwei G H, Von Dreele R B, Larsen A C, Raistrick I D and Bish D L (1988), Phys. Rev. *B37*, 7960.

222 Wolf B, Kim T J, Kühnberger H, Palme W, Krimmel A, Xanthopoulos I, Grill W, Lüthi B and Schwarz M (1988), Physica *C153-155*, 284.

223 Wu M K, Ashburn J R, Torng C J, Hor P H, Meng R L, Gao L, Huang Z J, Wang Y Q and Chu C W (1987), Phys. Rev. Lett. *58*, 908.

224 Wu J, Wang Y, Shen H, Zhu J, Yan Y and Zhao Z (1990), Phys. Lett. *A148*, 127.

225 Xiang X -D, Brill J W, Delong L E, Bourne L C, Zettl A, Jones J C and Rice L A (1988), Solid State Commun. *65*, 1073.

226 Xiang X D, Chung M, Brill J W, Hoen S, Pinsukanjana P and Zetl A (1989), Solid State Commun. *69*, 833.

227 Xiaorong Z Changguo Q, Changming G, Zhongnan L, Shiyuan Z, Hao W, Ningsheng Z, Zijun W and Qiang M (1987), Intern. J. Mode. Phys. *B1*, 495.

228 Xu X T, Liang J K, Xie S S, Che G C, Shao X Y, Duan Z G and Cui C G (1987), Solid State Commun. *63*, 649.

229 Xu M-F, Baum H-P, Schenstrom A, Sarma B K, Levy M, Sun K J, Toth L E, Wolf S A and Gubser D U (1988), Phys. Rev. *B37*, 3675.

230 Yanagisawa E, Dietderich D R, Kamakara H, Togano K, Maeda H and Takahashi K (1988), Jap. J. Appl. Phys. *27*, L1460.

231 Yening W, Huimin S, Jinsong Z, Ziran X, Min G, Zhongmin N and Zhifang Z (1987), J. Phys. C: Solid State Phys. *20*, L665.

232 Yogurtcu Y K, Tu Hailing, Saunders G A, Bach H and Methfessel S (1985), J. Mater. Sci. Lett. *4*, 230.

233 Yu R C, Naughton M J, Yan X, Chaikin P M, Holtzberg F, Greene R L, Stuart J and Davies P (1988), Phys. Rev. *B37*, 7963.

234 Yusheng H, Baiwen Z, Sihan L, Jiong X, Yongming L and Haoming C (1987), J. Phys. F: Met. Phys. *17*, L243.

235 Yusheng H, Jiong X, Xin W, Aisheng H, Jincang Z and Fanggao C (1989), Phys. Rev. *B40*, 7384.

236 **Zandbergen H M, Groen P, van Tendeloo G, van Landuyt J and Amelinckx S (1988), Solid State Commun. *66*, 397.**

PUBLICATIONS

1. Bulk modulus and its pressure derivative of $YBa_2Cu_3O_{7-x}$.

   M. Cankurtaran, G.A. Saunders, J.R. Willis, A. Al-Kheffaji and D.P. Almond. Phys. Rev. B. 39, 2872-5 (1989).

2. Elastic behaviour under pressure of high-T_c superconductors $RBa_2Cu_3O_{7-x}$ (R = Y, Gd and Eu).

   A. Al-Kheffaji, M. Cankurtaran, G.A. Saunders, D.P. Almond, E.F. Lambson and R.C.J. Draper. Phil. Mag. B. 59, 487-97 (1989).

3. A comparison of the ultrasonic evidence for mode softening in $La_{1.8}Sr_{0.2}CuO_4$ and the electron-doped superconductor $Nd_{1.85}Ce_{0.15}CuO_{4-y}$.

   A. Al-Kheffaji, J. Freestone, D.P. Almond, G.A. Saunders and Jing Wang. J. Phys.: Condens. Matter 1, 5993-6 (1989).

4. The effect of hydrostatic pressure on the elastic behaviour of $GdBa_2Cu_3O_{7-x}$.

   M. Cankurtaran, G.A. Saunders, D.P. Almond, A. Al-Kheffaji, E.F. Lambson and R.C.J. Draper. J. Phys. Condensed Matter 1, 9067-76 (1989).

5. The effect of hydrostatic pressure on the elastic behaviour of orthorhombic and tetragonal $GdBa_2Cu_3O_{7-x}$.
M. Cankurtaran, A. Al-Kheffaji, G.A. Saunders, D.P. Almond and J. Freestone. Superconductor Science and Technology 3, 76-80 (1990).

6. Elastic and anelastic effects in the orthorhombic and tetragonal forms of $GdBa_2Cu_3O_{7-x}$ as a function of pressure and temperature.
M. Cankurtaran, G.A. Saunders, D.P. Almond, A. Al-Kheffaji, J. Freestone, Qingxian Wang, and E.F. Lambson. Physics and Materials Science of High Temperature Superconductors, edited Ram Kossowsky, Siegfried Methfessel and Dieter Wohlleben, Kluwer Academic Publishers (1990) pages 627-37.

7. A comparative study of the high T_c superconductor $Nd_{1.85}Ce_{0.15}CuO_{4-y}$ and its parent compound Nd_2CuO_{4-y}.
Chang Fanggao, A. Al-Kheffaji, P.J. Ford, D.A. Ladds, J. Freestone, B. Chapman, Ll. Mañosa, D.P. Almond and G.A. Saunders. Superconductor Science and Technology 3, 422-8 (1990).

8. The effects of quenching and lead substitution on the ultrasonic wave velocity and attenuation in bismuth cuprate high T_c superconductors.

Chang Fanggao, M. Cankurtaran, G.A. Saunders, D.P. Almond, P.J. Ford and A. Al-Kheffaji. Superconductor Science and Technology 3, 546-55 (1990).

9. Ultrasonic evidence of low bulk modulus and large vibrational anharmonicity in the bismuth cuprate high $T_c$superconductors.

Chang Fanggao, M. Cankurtaran, G.A. Saunders, A. Al-Kheffaji, D.P. Almond and P.J. Ford. Superconductor Science and Technology 4, 13-20 (1991).

10. Elastic behaviour of the high T_c superconductors $Nd_{1.85}Ce_{0.15}CuO_{4-y}$ and Nd_2CuO_{4-y}.

Chang Fanggao, A. Al-Kheffaji, P.J. Ford, D.P. Almond, B. Chapman, J. Freestone, D.A. Ladds, Ll. Mañosa, M. Cankurtaran and G.A. Saunders. Proc. LT 19 Satellite Meeting on High T_c Superconductivity, Queens' College, Cambridge. Superconductor Science and Technology 4, S199-201 (1991).

11. Ultrasonic evidence of strong vibrational anharmonicity in high T_c superconductors and its effect on determination of their elastic properties.

Chang Fanggao, M. Cankurtaran, G.A. Saunders, A. Al-Kheffaji, D.P. Almond, P.J. Ford and D.A. Ladds. Phys. Rev. B43, 5526-37 (1991).

PAPERS PRESENTED AT PROFESSIONAL MEETINGS AND CONFERENCES

1. **Ultrasonic studies of high T_c superconductors.**
   D.P. Almond, A. Al-Kheffaji, M. Cankurtaran, E.F. Lambson and G.A. Saunders. Review of Progress in Physical Acoustics and Ultrasonics, Institutes of Physics and Acoustics, 27th September 1988, University of Keele.

2. **Ultrasonic studies of high T_c superconductors.**
   D.P. Almond, A. Al-Kheffaji, M. Cankurtaran, E.F. Lambson and G.A. Saunders. Ceramic Superconductors, Imperial College London, 19-21 September, 1988.

3. **Elastic and anelastic effects in the orthorhombic and tetragonal forms of $GdBa_2Cu_3O_{7-x}$ as a function in pressure and temperature.**
   M. Cankurtaran, G.A. Saunders, D.P. Almond, A. Al-Kheffaji, J. Freestone, Wang Qingxian and E.F. Lambson. High Temperature Superconductors Physics and Materials Sciences, NATO Advanced Study Institute, Bad Windsheim, F.R.G., 13-26 August, 1989.

4. **Ultrasonics studies of high T_c superconductors.**
   D.P. Almond, G.A. Saunders, A. Al-Kheffaji, J. Freestone and Qingxian Wang. High Temperature Superconductors, University of Birmingham, 19-21 September 1989.

5. Elastic and anelastic effects in the orthorhombic and tetragonal forms of $GdBa_2Cu_3O_{7-x}$.
   A. Al-Kheffaji, J. Freestone, D.P. Almond, G.A. Saunders, Qingxian Wang, P.J. Ford, E.F. Lambson and M. Cankurtaran. Solid State Physics Conference 1989, University of Warwick, 19-21 December, 1989.
6. A comparison of the temperature and pressure dependence of the ultrasonic characteristics of $La_{1.8}Sr_{0.2}CuO_4$ and the electron doped superconductor $Nd_{1.85}Ce_{0.15}CuO_{4-y}$.
   A. Al-Kheffaji, J. Freestone, D.P. Almond and G.A. Saunders. Solid State Physics Conference 1989, University of Warwick, 19-21 December, 1989.
7. Investigation of $Nd_{1.85}Ce_{0.15}CuO_{4-y}$ and Nd_2CuO_{4-y}.
   Chang Fanggao, A. Al-Kheffaji, P.J. Ford, D.P. Almond, B. Chapman, J. Freestone, D.A. Ladds, Ll. Mañosa, M. Cankurtaran and G.A. Saunders. LT-19 Satellite Conference on High Temperature Superconductivity, 13-15 August 1990, Queens' College, Cambridge.
8. Ultrasonic Characteristics of High T_c Superconductors.
   Chang Fanggao, M. Cankurtaran, A. Al-Kheffaji, D.P. Almond, G.A. Saunders, P.J. Ford, Qingxian Wang and J. Freestone. High Temperature Superconductors Polar Solids Discussion Group, Royal Society of Chemistry, 17-19 September 1990, University of Bath.

9. **Ultrasonic studies of high T_c superconductors. Chang Fanggao, M. Cankurtaran, P.J. Ford, G.A. Saunders, A. Al-Kheffaji and D.P. Almond. 11th General Conf. of the Condensed Matter Division (EPS) University of Exeter, 8-11 April 1991.**